AD-A094 297   GENERAL ELECTRIC CO CINCINNATI OH AIRCRAFT ENGINE GROUP   F/G 20/1
HIGH VELOCITY JET NOISE SOURCE LOCATION AND REDUCTION. TASK 5. --ETC(U)
JAN 79 N BAUMGARDT, J F BRAUSCH, W S CLAPPER   DOT-OS-30034
UNCLASSIFIED R78AEG628   FAA-RD-76-79-5   NL

1 OF 3
AD
A094297

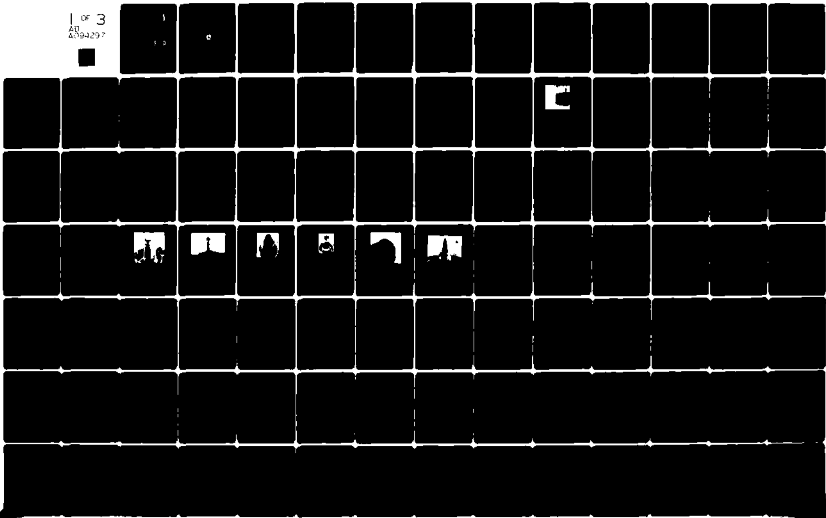

PHOTOGRAPH THIS SHEET

AD A094297

DTIC ACCESSION NUMBER

III

LEVEL

INVENTORY

GENERAL ELECTRIC CO CINCINNATI OHIO AIRCRAFT ENGINE GROUP
HIGH VELOCITY JET NOISE SOURCE LOCATION AND REDUCTION. TASK 5. INVESTIGATION OF "IN-FLIGHT" AEROACOUSTIC EFFECTS ON SUPPRESSED EXHAUSTS. FINAL REPT., JAN.'79
REPT. NO. R78AEG628 CONTRACT DOT-OS-30034 FAA-RD-76-79-5.

DISTRIBUTION STATEMENT A
Approved for public release;
Distribution Unlimited

DISTRIBUTION STATEMENT

ACCESSION FOR		
NTIS	GRA&I	X
DTIC	TAB	☐
UNANNOUNCED		☐
JUSTIFICATION		
BY		
DISTRIBUTION /		
AVAILABILITY CODES		
DIST	AVAIL AND/OR SPECIAL	
A		

DISTRIBUTION STAMP

DTIC
S ELECTE D
JAN 29 1981
D

DATE ACCESSIONED

SEE ALSO TASK 4, AD-A041 849

81 1 27 003

DATE RECEIVED IN DTIC

PHOTOGRAPH THIS SHEET AND RETURN TO DTIC-DDA-2

DTIC FORM OCT 79 70A

DOCUMENT PROCESSING SHEET

REPORT NO. FAA-RD-76-79, V

R78AEG628

HIGH VELOCITY JET NOISE SOURCE LOCATION AND REDUCTION

TASK 5 - INVESTIGATION OF "IN-FLIGHT" AEROACOUSTIC EFFECTS ON SUPPRESSED EXHAUSTS

TECHNICAL CONTRIBUTORS:

N. Baumgardt R. Mani P. Vogt

J.F. Brausch E.J. Stringas R. Whittaker

W.S. Clapper

GENERAL ELECTRIC COMPANY
AIRCRAFT ENGINE GROUP
CINCINNATI, OHIO 45215

DEPARTMENT OF TRANSPORTATION ★ UNITED STATES OF AMERICA ★

JANUARY 1979

FINAL REPORT

Document is available to the U.S. public through the National Technical Information Service, Springfield, Virginia 22161.

Prepared for

U.S. DEPARTMENT OF TRANSPORTATION
FEDERAL AVIATION ADMINISTRATION
Systems Research & Development Service
Washington, D.C. 20590

1. Report No.	2. Government Accession No.	3. Recipient's Catalog No.
FAA-RD-76-79, V		

4. Title and Subtitle
High Velocity Jet Noise Source Location and Reduction
Task 5 - Investigation of "In-Flight" Aero-Acoustic Effects on Suppressed Exhausts

5. Report Date
January 1979

6. Performing Organization Code

7. Author(s)
W.S. Clapper (Task 5 Technical Director and Editor), et al.
E.J. Stringas (Technical Project Manager)

8. Performing Organization Report No.
R78AEG628

9. Performing Organization Name and Address
General Electric Company
Advanced Engineering and Technology Programs Department
Aircraft Engine Group
Cincinnati, Ohio 45215

10. Work Unit No.

11. Contract or Grant No.
DOT-OS-30034

12. Sponsoring Agency Name and Address
U.S. Department of Transportation
Federal Aviation Administration
Systems Research and Development Services
Washington, D.C. 20590

13. Type of Report and Period Covered
Task 5 Final Report
Dec. 1976 - July 1978

14. Sponsoring Agency Code
ARD-550

15. Supplementary Notes This report is in partial fulfillment of the subject program. Related documents to be issued in the course of the program include final reports of the following tasks: Task 1 - Activation of Facilities and Validation of Source Location Techniques; Task 2 - Theoretical Developments and Basic Experiments; Task 3 - Experimental Investigation of Suppression Principles; Task 4 - Development/Evaluation of Techniques for Inflight Investigation; Task 6 - Noise Abatement Nozzle Design Guide. FAA Program Monitor R.S. Zuckerman.

16. Abstract

The flight noise characteristics in terms of peak noise, directivity and spectra were projected for five suppressor nozzle designs. Static and flight suppression levels are established using conical nozzle data as a reference. The noise characteristics were determined by testing each nozzle design in the anechoic free jet facility and then applying a transformation to account for dynamic effects. The transformation process is described and a computer program with instructions is presented.

Each of the five suppressor nozzles was selected by balancing suppression level, performance loss, and mechanical complexity. Weight estimates and performance estimates are presented. An assessment is made on how these suppressors affect the noise versus performance trades for typical variable cycle engine (VCE) operating conditions.

Suppressors are found to have minimal peak noise suppression loss in flight at high velocities. As mass average velocity decreases, the flight peak noise suppression levels are less than those measured statically from 0 to 5 PNdB. In all cases, the suppressors were quieter than the conical nozzle in flight. In the forward quadrant, multielement suppressors are effective in reducing shock noise; also, the forward quadrant noise for a suppressor is not amplified to the same degree as a conical nozzle. Overall, suppression characteristics measured statically are different than in-flight and are function of the specific suppressor design.

17. Key Words (Suggested by Author(s))

18. Distribution Statement

Document is available to the U.S. public through the National Technical Information Service, Springfield, Virginia 22161.

19. Security Classif. (of this report)	20. Security Classif. (of this page)	21. No. of Pages	22. Price*
UNCLASSIFIED	UNCLASSIFIED	174	

* For sale by the National Technical Information Service, Springfield, Virginia 22151

NASA-C-168 (Rev. 6-71)

METRIC CONVERSION FACTORS

Approximate Conversions to Metric Measures

Symbol	When You Know	Multiply by	To Find	Symbol
		LENGTH		
in	inches	*2.5	centimeters	cm
ft	feet	30	centimeters	cm
yd	yards	0.9	meters	m
mi	miles	1.6	kilometers	km
		AREA		
in^2	square inches	6.5	square centimeters	cm^2
ft^2	square feet	0.09	square meters	m^2
yd^2	square yards	0.8	square meters	m^2
mi^2	square miles	2.6	square kilometers	km^2
	acres	0.4	hectares	ha
		MASS (weight)		
oz	ounces	28	grams	g
lb	pounds	0.45	kilograms	kg
	short tons (2000 lb)	0.9	tonnes	t
		VOLUME		
tsp	teaspoons	5	milliliters	ml
Tbsp	tablespoons	15	milliliters	ml
fl oz	fluid ounces	30	milliliters	ml
c	cups	0.24	liters	l
pt	pints	0.47	liters	l
qt	quarts	0.95	liters	l
gal	gallons	3.8	liters	l
ft^3	cubic feet	0.03	cubic meters	m^3
yd^3	cubic yards	0.76	cubic meters	m^3
		TEMPERATURE (exact)		
°F	Fahrenheit temperature	5/9 (after subtracting 32)	Celsius temperature	°C

*1 in ≡ 2.54 (exactly). For other exact conversions and more detailed tables, see NBS Misc. Publ. 286, Units of Weights and Measures, Price $2.25, SD Catalog No. C13.10:286.

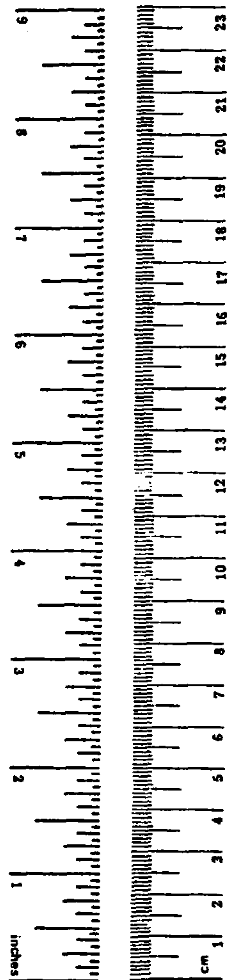

Approximate Conversions from Metric Measures

Symbol	When You Know	Multiply by	To Find	Symbol
		LENGTH		
mm	millimeters	0.04	inches	in
cm	centimeters	0.4	inches	in
m	meters	3.3	feet	ft
m	meters	1.1	yards	yd
km	kilometers	0.6	miles	mi
		AREA		
cm^2	square centimeters	0.16	square inches	in^2
m^2	square meters	1.2	square yards	yd^2
km^2	square kilometers	0.4	square miles	mi^2
ha	hectares (10,000 m^2)	2.5	acres	
		MASS (weight)		
g	grams	0.035	ounces	oz
kg	kilograms	2.2	pounds	lb
t	tonnes (1000 kg)	1.1	short tons	
		VOLUME		
ml	milliliters	0.03	fluid ounces	fl oz
l	liters	2.1	pints	pt
l	liters	1.06	quarts	qt
l	liters	0.26	gallons	gal
m^3	cubic meters	35	cubic feet	ft^3
m^3	cubic meters	1.3	cubic yards	yd^3
		TEMPERATURE (exact)		
°C	Celsius temperature	9/5 (then add 32)	Fahrenheit temperature	°F

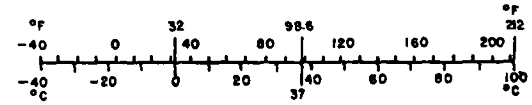

PREFACE

This report describes the work performed under Task 5 of the DOT/FAA High Velocity Jet Noise Source Location and Reduction Program (Contract DOT-OS-30034). The objectives of the contract were:

- Investigation of the aerodynamic and acoustic mechanisms of various jet noise suppressors, including scaling effects.
- Analytical and experimental studies of the acoustic source distribution in such suppressors, including identification of source location, nature and strength, and noise reduction potential.
- Investigation of in-flight effects on the aerodynamic and acoustic performance of these suppressors.

The results of these investigations have led to the preparation of a design guide report predicting the overall characteristics of suppressor concepts from models to full-scale static, to in-flight conditions, as well as a quantitative and qualitative prediction of the phenomena involved.

The work effort in this program was organized under the following major tasks, each of which is reported in a separate Final Report:

Task 1 -- Activation of Facilities and Validation of Source Location Techniques

Task 2 -- Theoretical Developments and Basic Experiments

Task 3 -- Experimental Investigation of Suppression Principles

Task 4 -- Development and Evaluation of Techniques for "In-flight" Investigation

Task 5 -- Investigation of "In-flight" Aeroacoustic Effects on Suppressed Exhausts

Task 6 -- Preparation of Noise Abatement Nozzle Design Guide Report

Task 1 was an investigative and survey effort designed to identify acoustic facilities and test methods best suited to jet noise studies. Task 2 was a theoretical effort complemented by theory verification experiments which extended across the entire contract period of performance. Task 3 represented a substantial contract effort to gather various test data on a wide range of High Velocity Jet Nozzle suppressors. These data, intended to help identify several "optimum" nozzles for "in-flight" testing under Task 5, provide an extensive high quality data bank useful to preparation of the Task 6 design guide, as well as to future studies.

Task 4 was similar to Task 1, except that it dealt with the specific test facility requirements, measurement techniques and analytical methods necessary to evaluate the "in-flight" noise characteristics of simple and complex suppressor nozzles. This effort provided the capability to conduct the "flight" effects test program Task 5, which is the subject of the present report (FAA-RD-76-79,V).

TABLE OF CONTENTS

TABLE OF CONTENTS (Concluded)

LIST OF ILLUSTRATIONS

LIST OF ILLUSTRATIONS (Continued)

LIST OF ILLUSTRATIONS (Continued)

LIST OF ILLUSTRATIONS (Continued)

LIST OF ILLUSTRATIONS (Continued)

LIST OF TABLES

1.0 SUMMARY

The High Velocity Jet Noise Source Location and Reduction Program (Contract DOT-OS-30034) was conceived to bring analytical and experimental knowledge to bear on understanding the fundamentals of jet noise for simple and complex suppressors.

Task 5, the subject of this report, was formulated to establish the static and flight noise characteristics of five optimum suppressor nozzle designs from different families which are considered applicable to advance propulsion systems to aid these systems in complying with noise regulations. The nozzles evaluated include a single flow, area ratio (AR) = 2.1, 32-chute design, and four dual flow suppressor nozzles: 40-shallow-chute - $(AR)_o$ = 1.75, 36-chute - $(AR)_o$ = 2.0, 36-chute with a treated ejector and 54-element coplanar mixer nozzle. Each scale model nozzle was subjected to static and free jet testing in the General Electric Anechoic Free Jet Facility. Free jet velocities ranged from 0 to 360 ft/sec. The flight noise was established based on transforming and scaling measured free jet data. The transformation was carried out by extracting the static directivity after correcting for refraction, turbulent scattering and absorption effects, and then employing a suitable multipole source decomposition to evaluate the proper dynamic effect.

The main result of this program has been to establish the static and flight suppression characteristics for the five suppressor nozzle designs in terms of peak noise characteristics, directivity, and spectra as a function of flight Mach number. Overall, flight effects for suppressors were demonstrated to be less favorable than for baseline nozzle configurations.

Suppressing only the outer stream of dual flow nozzles was found to be slightly less effective than suppressing the entire stream on a single flow nozzle. The loss in suppression effectiveness is between 1 and 2 PNdB for the same mass averaged velocity.

The effect of flight on the peak noise characteristics of suppressors was found to vary as a function of mass average velocity. At high velocities, for example, suppressors actually realize more peak noise reduction than a conical nozzle. However, at mass average velocities below 2000 ft/sec, suppressors generally lost 0 to 5 PNdB suppression in flight. In all cases, the noise level in flight for these suppressors was still lower than for the static case. On a directivity basis, flight reduces the noise in the aft quadrant, causes a modest change at 90°, and causes only slight changes relative to static in the forward quadrant. Spectrum changes are dependent on frequency, angle, and flight velocity. Overall, no reduction of high frequency noise occurred, even in the aft quadrant, except for the 54-element coplanar mixer nozzle. The flight effect on this configuration resembles more closely that on a conical nozzle.

The addition of a mechanical suppressor increases weight, reduces performance, and has a less favorable peak noise flight effect. Nevertheless,

for a given gross aircraft takeoff weight, payload, and specified noise goal, a suppressor allows the use of a smaller engine, which generally results in a range advantage over an unsuppressed system, because adding a suppressor less costly than reducing noise by upsizing the engine to reduce jet velocity. Overall, suppression characteristics measured statically are different than in flight and a function of the specific suppressor design.

2.0 INTRODUCTION

Extensive static testing has been conducted during the past two decades to establish the suppression characteristics of complex exhaust nozzle configurations[1,2,3]. Measured jet noise suppression levels in excess of 12 PNdB have been demonstrated, and performance test results have demonstrated that these levels may be achieved with a gross thrust loss in flight of 6 to 7%.[3] Actual flight test experience using some typical designs has provided inconclusive results[3,4,5]. Some suppressors are effective in flight, others become ineffective, and may cause a noise increase. It has, therefore, been established that static test data are inadequate to establish the flight noise signature of suppressor nozzles.

Several methods have been evaluated during the pase five years to establish the flight noise signature of complex suppressor nozzles without conducting costly and relatively inaccurate actual flight tests[6,7,8]. The methods include moving frame techniques and fixed frame techniques. The free jet method was selected and validated under Task 4 of the current program.[6]

The objective of the present Task 5 study was to establish the static and flight noise characteristics of five optimum suppressor nozzle designs which are considered to be applicable to advanced propulsion systems and which will aid these systems in complying with proposed noise regulations. The tests were conducted in the General Electric Anechoic Free Jet Facility. The present report includes a description of the free jet and a discussion of the facility validation results (Section 3), a presentation of the models (Section 4), and a definition of the test matrices (Section 5). The data acquisition and reduction procedures are discussed in Section 6. Section 7 presents the static and flight acoustic characteristics of the five optimum suppressor nozzle designs.

Static and flight suppression levels are established by comparison to conical nozzle data from References 9 and 10. Section 8 presents aerodynamic performance and weight assessments for each of the five nozzles for an advanced variable cycle engine.

Select thermodynamic and acoustic test data are tabulated in Appendix A, and Appendix B is a user's guide describing the mechanics of using the flight transformation program.

3.0 DESCRIPTION AND VALIDATION OF THE ANECHOIC FREE JET FACILITY

The General Electric Anechoic Facility (11) was modified to permit simulated wind-on testing via the Free Jet Technique which was evaluated and verified in Task 4 of the program (6). Free jet design criteria followed those evolved during an earlier free jet setup on General Electric's Jet Engine Noise Outdoor Test Site (JENOTS) (a free jet to nozzle area ratio of nominally between 40 to 50 to 1, a modest facility-nozzle contraction ratio yielding free jet longitudinal turbulence levels of 3 to 4 percent, and a velocity uniformity across the free jet of less than 4 percent).

Validation of the free jet was accomplished in early 1977 and comprised a number of acoustic and aerodynamic studies both in the upstream ducting and in the anechoic chamber proper. This section describes the key tertiary (free jet) flow facility components and the pertinent acoustic and aerodynamic data taken to validate the facility.

3.1 DESCRIPTION OF FACILITY

The tertiary system consists of a large electric motor-driven fan and associated ducting to surround model test nozzles with free jet airflow to provide external flow in order to simulate forward flight. The basic dual flow jet noise anechoic facility is described in detail in Reference 11. A schematic of the jet noise anechoic facility showing the tertiary flow arrangement is presented in Figure 3-1.

The tertiary air system consists of a 250,000 scfm (50 in. H2O static pressure) fan and 3500 hp electric motor. Transition duct work and a silencer section route the air from the fan discharge to the tertiary plenum room. The silencer reduces the noise level 30-50 dB. Air supply to the fan is pulled into the fan room outside ambient through an existing inlet silencer. A plenum room (14 ft x 12 ft x 10 ft) for the tertiary air is located just below the test deck. Three walls and the floor are covered with acoustic treatment (4-inch thick fiberglass pillows covered with fiberglass cloth and perforated plate). The coannular plenum chamber for model nozzle air supplies is located within the tertiary plenum chamber room. Tertiary air enters a 7 ft 4-inch-diameter x 6 ft long cylindrical test section mounted on top of the test deck. This cylindrical duct contains a flow straightening screen and honeycomb section (10-inch length x 1/4-inch Hexagonal cells). The duct is then smoothly transitioned to the 4-ft-diameter tertiary discharge nozzle on its upper-most end resulting in a free jet to jet nozzle flow area ratio of about 63 (based on 6-inch equivalent diameter nozzle). Maximum tertiary flow of about 310 lb/sec permits simulation of Mach numbers in excess of 0.30. Mach number variation is obtained by simply varying the fan inlet vanes thereby changing the tertiary air flow rate. A Mach number of approximately 0.41 is obtained with the vanes wide open. Entrained chamber flow enters from the outside through a silencer and enters the anechoic chamber

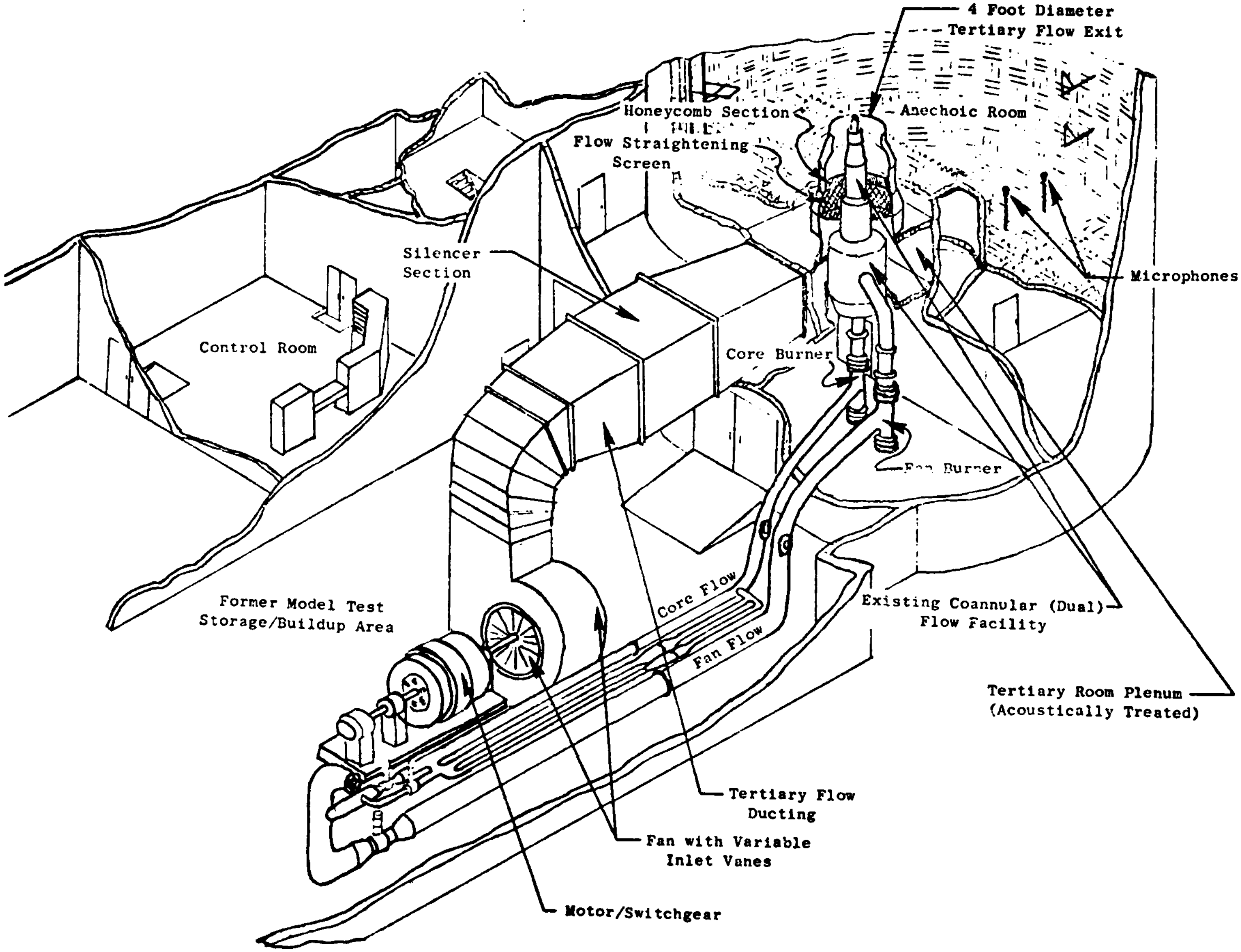

Figure 3-1. General Electric Anechoic Free Jet/Jet Noise Facility Schematic.

between acoustic wedges in the floor. All airflow exits through a "T" exhaust stack in the ceiling of the chamber directly over the nozzles.

Tufts for visual checking and thermocouples were located on the exhausts and thermocouples and microphones were located on the ceiling to verify that no apparent chamber recirculation exists. Wind-meter readings at the 130° microphone location indicate entrained flow velocities less than 1 ft/sec.

The converging section of the tertiary nozzle is treated with a 1/2-inch layer of Scottfelt (without a faceplate) to further reduce the high frequency noise content of the free jet flow. This treatment can be removed whenever it isn't needed. All validation and test results presented in this report were obtained with the acoustically treated tertiary nozzle.

Data acquisition of acoustic signals when the free jet is in operation is similar to previous static tests (11). Only the location of the microphones is slightly modified to accommodate the free jet plenum (described below).

Acoustic and LV/hot wire (HW) measurements were taken over a range of tertiary flow conditions for checkout as summarized below.

3.2 ACOUSTIC VALIDATION TESTS

A combination schematic and photograph of the anechoic jet noise facility showing the tertiary flow arrangement and microphone locations is presented in Figure 3-2. The locations of the 40, 50, 140, 150, and 160° microphones and their radial distances from the jet nozzle exit/centerline are included on Figure 3-2. A coannular-coplanar jet nozzle with both streams operating at identical thermodynamic conditions was used for the facility validation tests. Two (2) test series were conducted: a) an inverse square law (ISL) test without flow, and b) a background noise level test with flow.

The inverse square law (ISL) lossless test results at the 90° microphone position are shown in Figure 3-3. A speaker was used as the sound source for frequencies from 160 Hz to 630 Hz and an airball was used from 1000 Hz to 80 kHz. The procedure followed is detailed in Reference 11. A microphone was traversed from a position five feet from the noise source to a position near the far wall acoustic wedges. Data recorded at the various positions along the traverse are shown in Figure 3-3. The data trend follows the 6 dB per doubling of distance line quite well after correcting for atmospheric absorption. The standard deviation from the ISL tests for four (4) angles is shown in Figure 3-4 (see Reference 11 for procedure). The high points in the 50° lossless data are primarily attributed to the influence of the acoustic wedges surrounding the tertiary nozzle. The lossless data are comparable to the basic (static) facility validation results as documented in Reference 11.

The effect of the tertiary flow on the facility background noise level is shown in Figures 3-5 through 3-7 for 50, 90, and 150° microphones, respectively. Only data above the facility design cut-off frequency (220 Hz) are

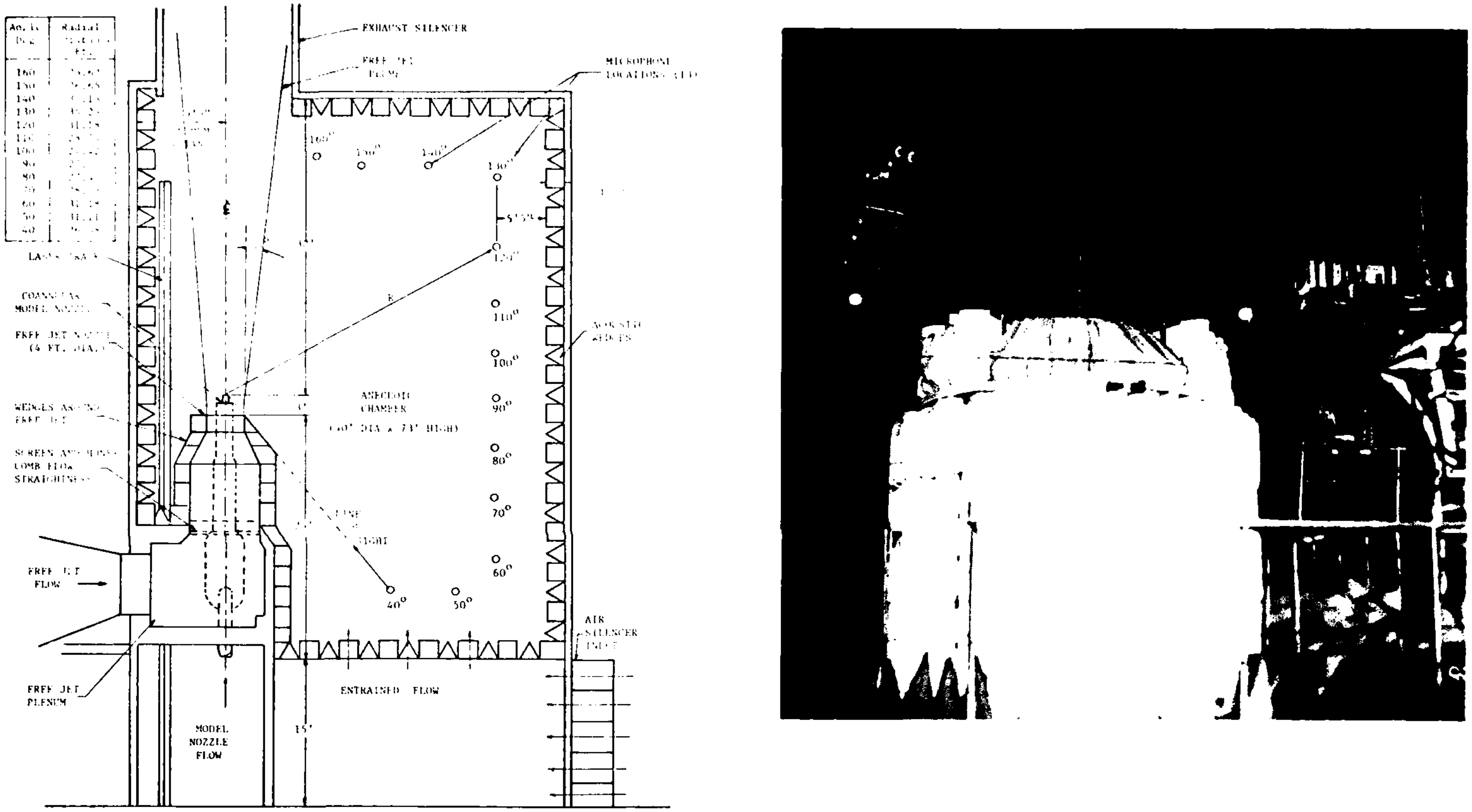

(a) Schematic

(b) Photo

Figure 3-2. Free Jet Arrangement in Anechoic Facility.

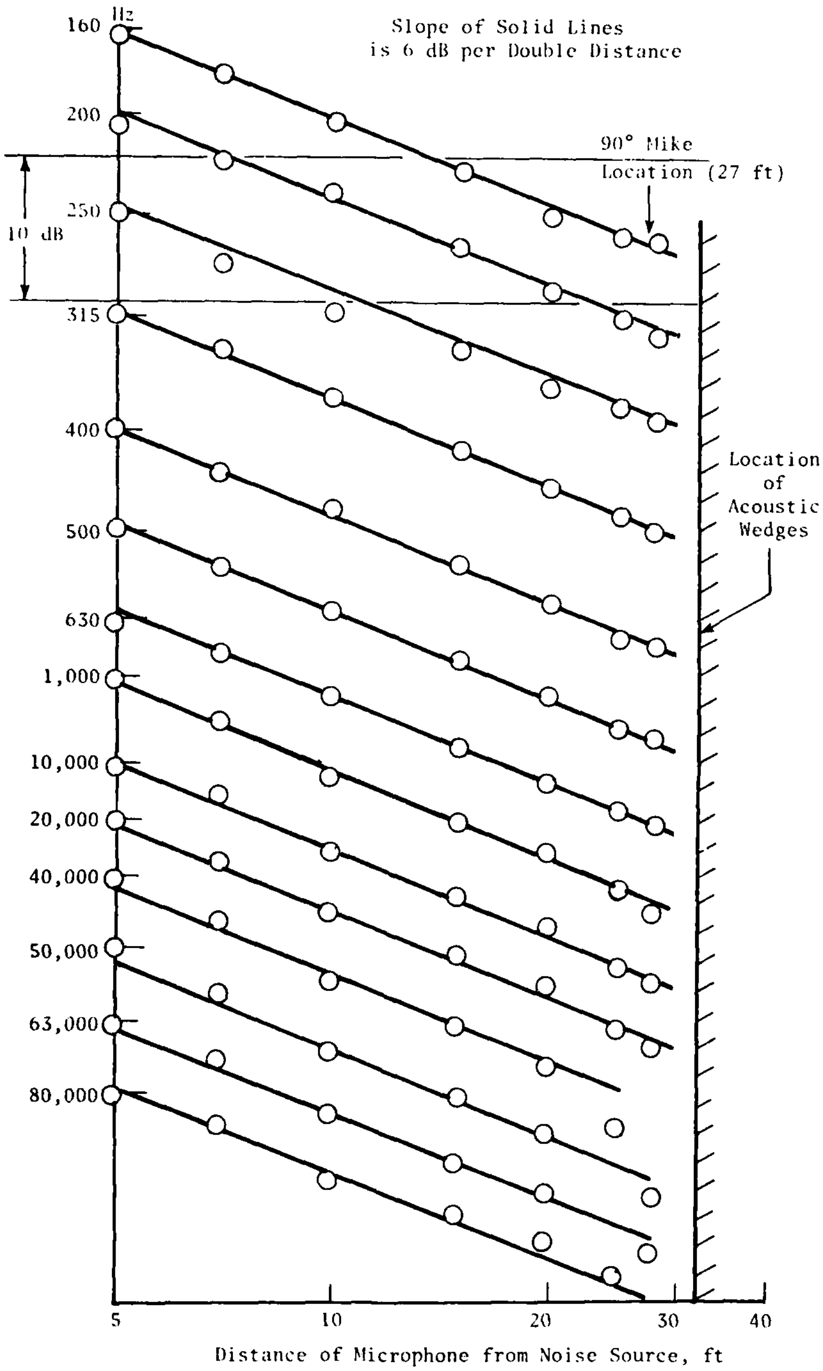

Figure 3-3. **Inverse Square Law Test at 90° with Tertiary and Coannular Nozzle Hardware (Bass, Bauer and Evans Atmospheric Correction Included), Lossless for 160 Hz < f < 630 Hz, Used Speaker for 1000 Hz < f < 80 kHz, Used Air Ball.**

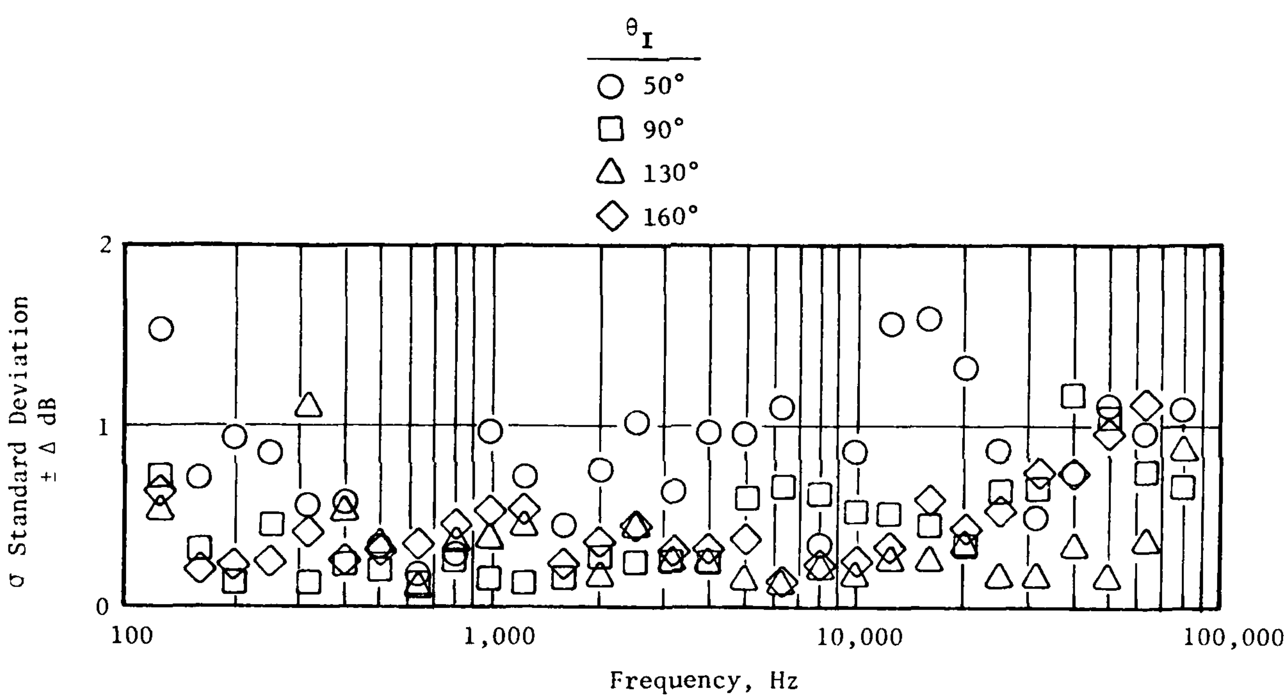

Figure 3-4. Standard Deviation of Inverse Square Law Tests with Tertiary and Co-annular Nozzle Hardware.

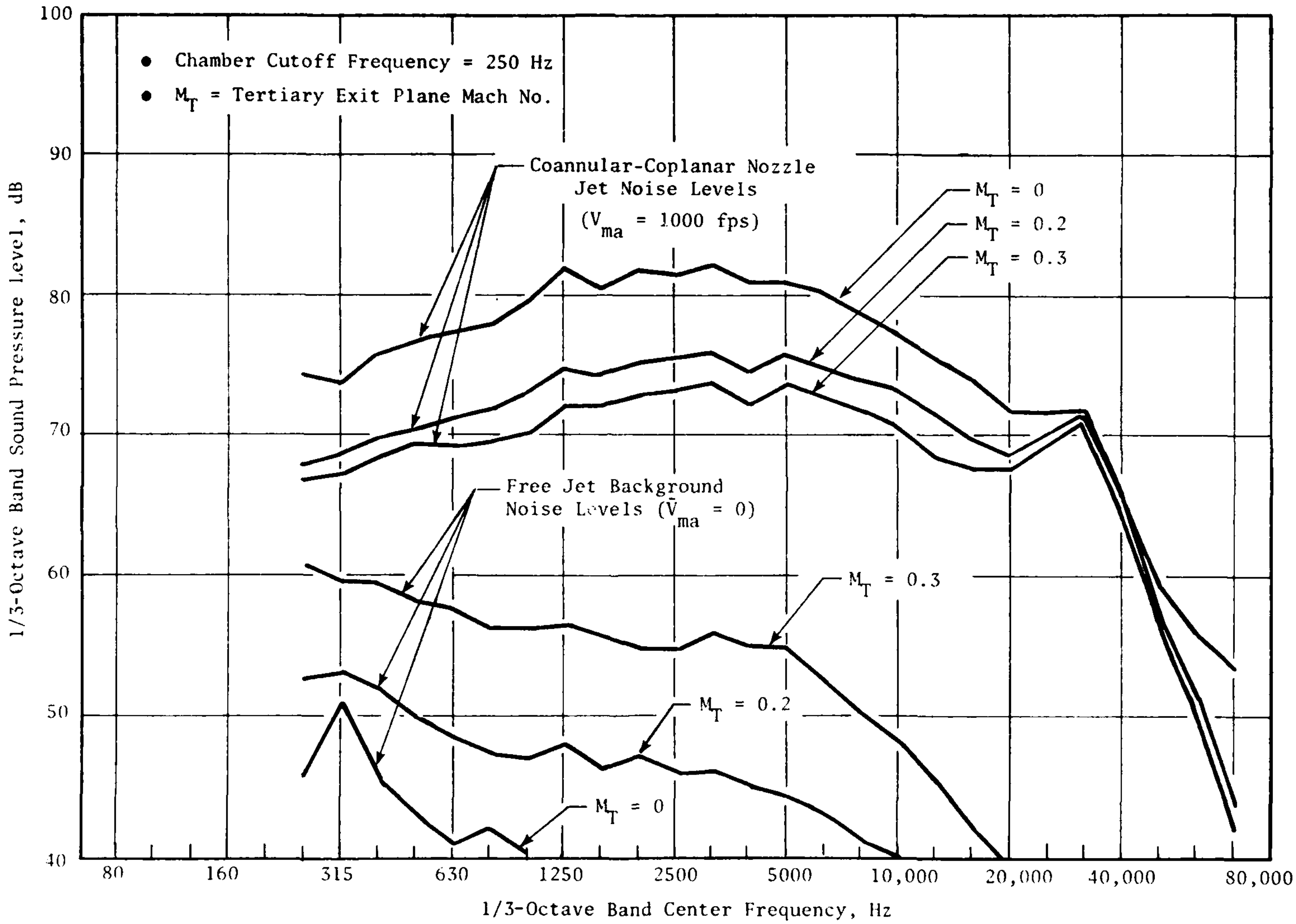

Figure 3-5. Comparison of Coannular-Coplanar Nozzle Spectra with Tertiary (Background) Spectra 40-ft Arc Data, $\theta_I = 50°$.

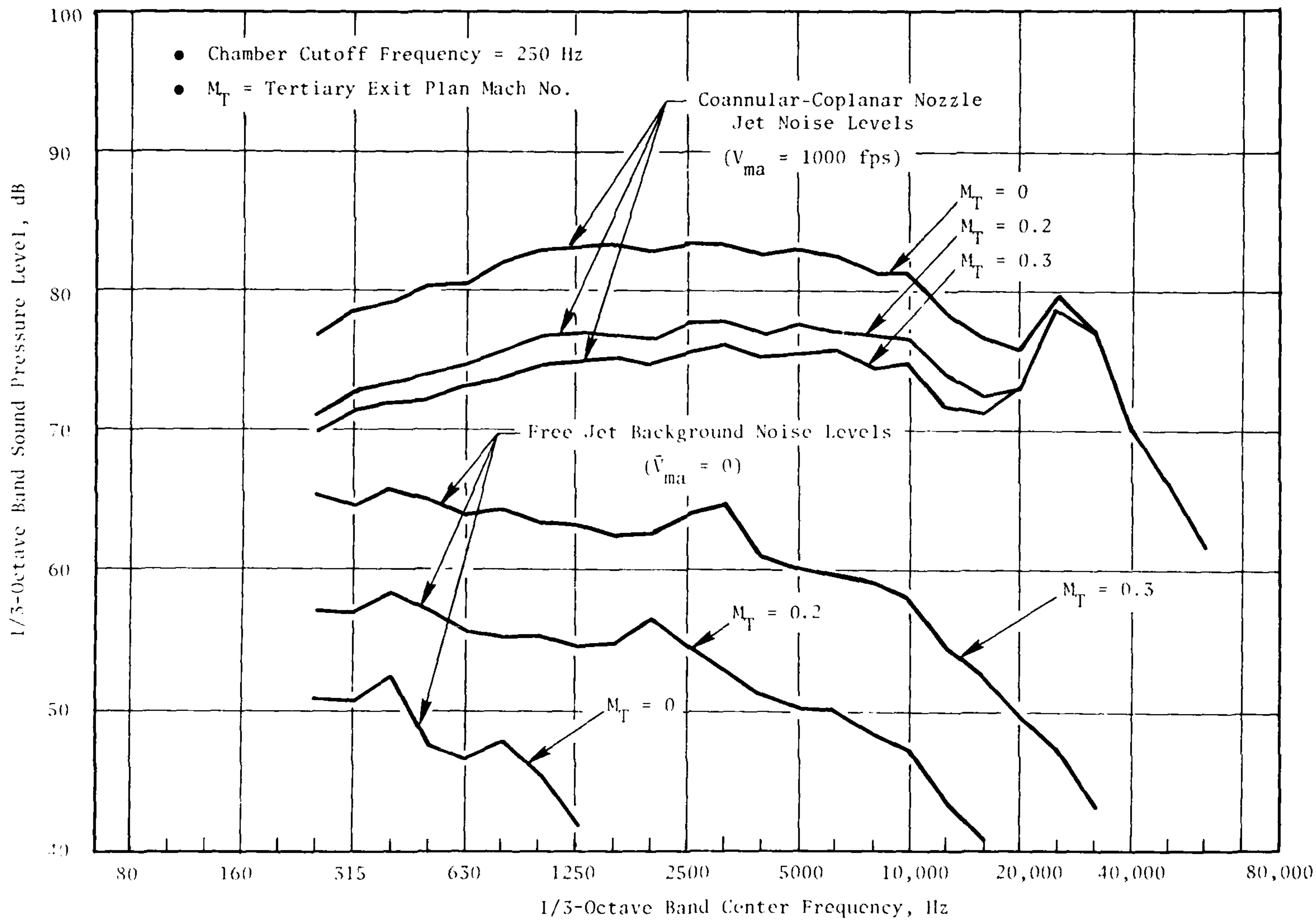

Figure 3-6. Comparison of Coannular-Coplanar Nozzle Spectra with Tertiary (Background) Spectra 40-ft Arc Data, θ_I = 90°.

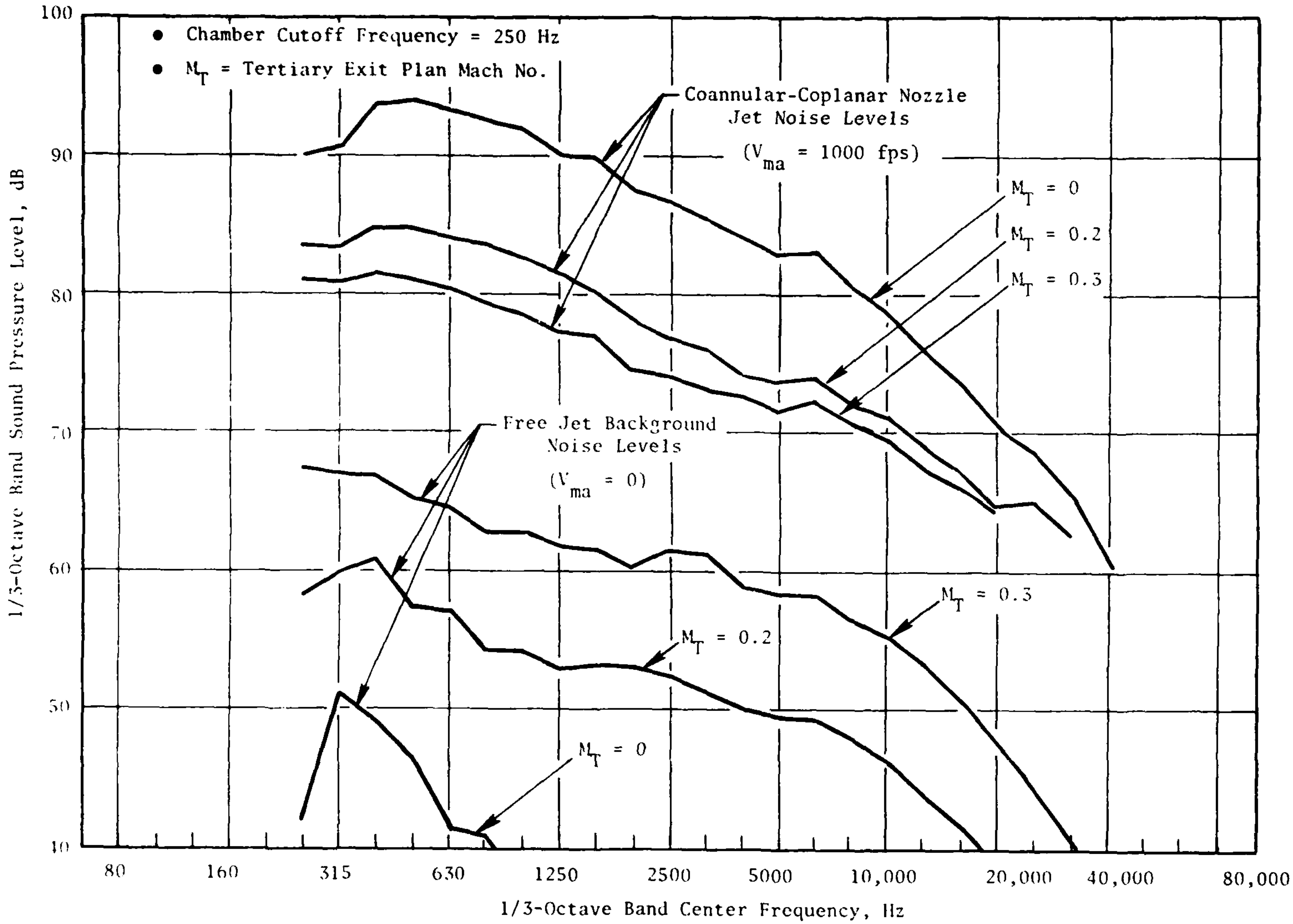

Figure 3-7. Comparison of Coannular-Coplanar Nozzle Spectra with Tertiary (Background) Spectra 40-ft Arc Data, $\theta_I = 150°$.

respectively. Only data above the facility design cut-off frequency (220 Hz) are shown. Typical spectra for the coannular/coplanar nozzle with both inner and outer flows at 1000 ft/sec ($V_{ma} \simeq 1000$ ft/sec) are shown with and without the tertiary. The jet noise levels are considerably above the noise levels of the free jet alone. At the lowest jet noise level ($V_{ma} \simeq 1000$ ft/sec and $M_T \simeq 0.3$ spectra compared with $V_{ma} \simeq 0$ ft/sec with $M_T \simeq 0.3$ spectra) the jet noise is approximately 10 dB above the tertiary alone noise. Background noise from the tertiary flow is not expected, therefore, to influence the jet noise levels or spectra for jet velocities above 1000 ft/sec. The tertiary flow does affect the low frequency noise somewhat, at jet velocities between 800 and 900 ft/sec.

3.3 AERODYNAMIC CHECKOUT TESTS

Measurements were made of the mean velocity and axial turbulence intensity distribution at the tertiary exit plane and at various downstream locations in the free jet. The development of the free jet (tertiary) plume was also studied. A schematic of the free jet aerodynamic test setup (with a 5-inch conical nozzle) is shown in Figure 3-8. For most tests the conical nozzle (or inner jet) was flowing air at the nominal free jet condition in order to prevent any "dead" flow regions. The North (N), South (S), East (E), and West (W) directions are shown around the tertiary exit for future reference to traverse direction. Laser Velocimeter (LV) and hot wire (HW) measurements were made at stations A, B, C, and D as shown in Figure 3-8. Measurements were made at several tertiary exit Mach numbers (M_T), however for purposes of illustrating facility aerodynamic characteristics most of the results are presented at near AST takeoff conditions (e.g. $M_T \simeq 0.30$).

The radial variation of the mean velocity as recorded with the Laser Velocimeter is shown in Figure 3-9 for two axial positions. Examination of Figure 3-9 reveals the following:

- The radial mean velocity profile at the free jet exit plane ($X/D = 0$) is relatively uniform (less than 4% velocity variation) for both traverse directions.

- The mean velocity at the test (conical) nozzle exit plane location decays slightly from its value at $X/D = 0$. The radial mean velocity profile is uniform at this location, except near the conical nozzle wall and in the free jet mixing (shear) layer.

The axial variation of mean velocity for two radial positions is shown in Figure 3-10. The centerline trace (i.e. $r/r_o = 0$ position), which is indicative of the free jet potential core, extends to at least five (5) diameters. Hence, the test nozzle detects little or no velocity decay in the free jet flow in these five tertiary flow diameters (or 17 ft downstream of the conical nozzle). The complete extent of the potential core has not been mapped due to a limit of the laser velocimeter track system in the facility. However, beyond $X/D \simeq 5 \rightarrow 6$ the velocity should decay at the rate $(X)^{-1}$, as

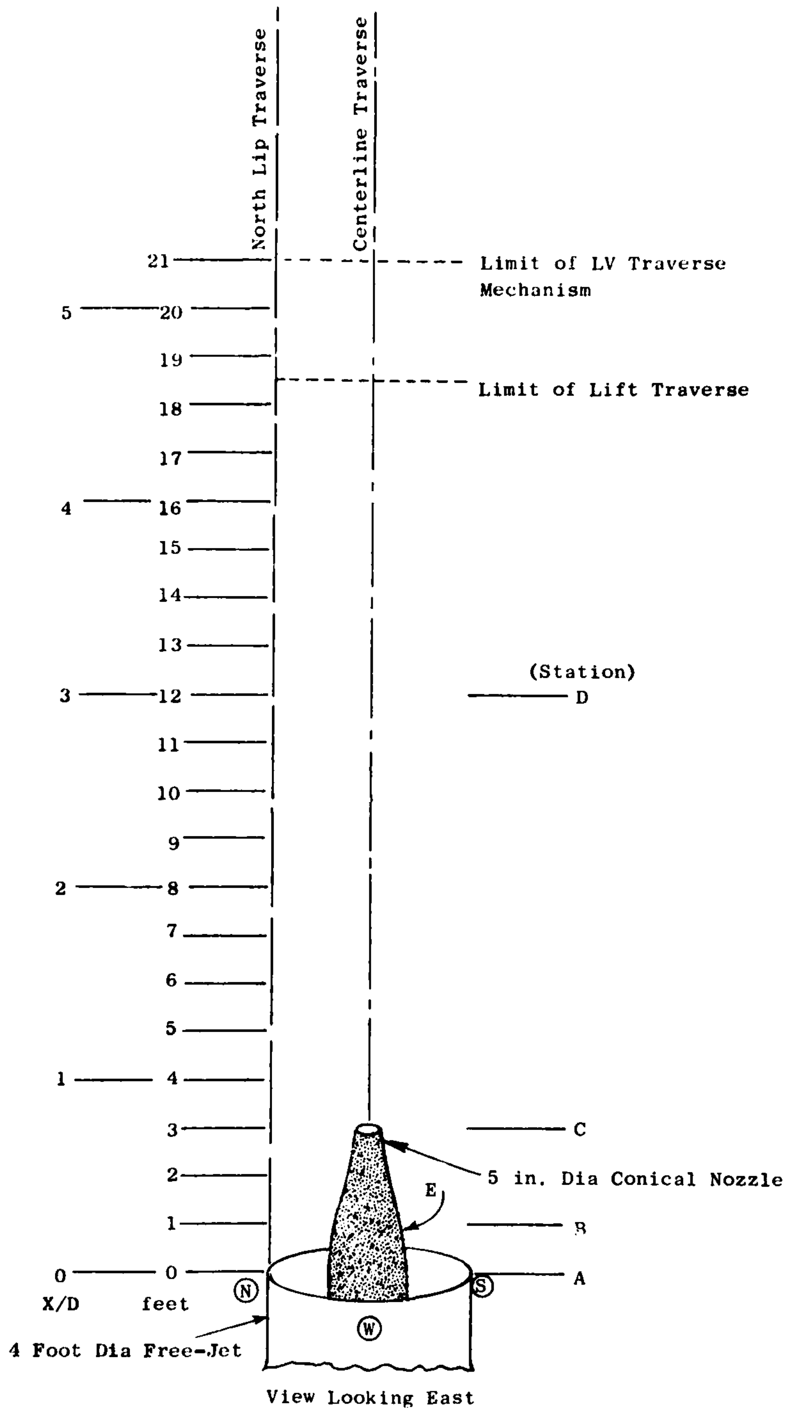

Figure 3-8. Schematic of Free-Jet Test Arrangement.

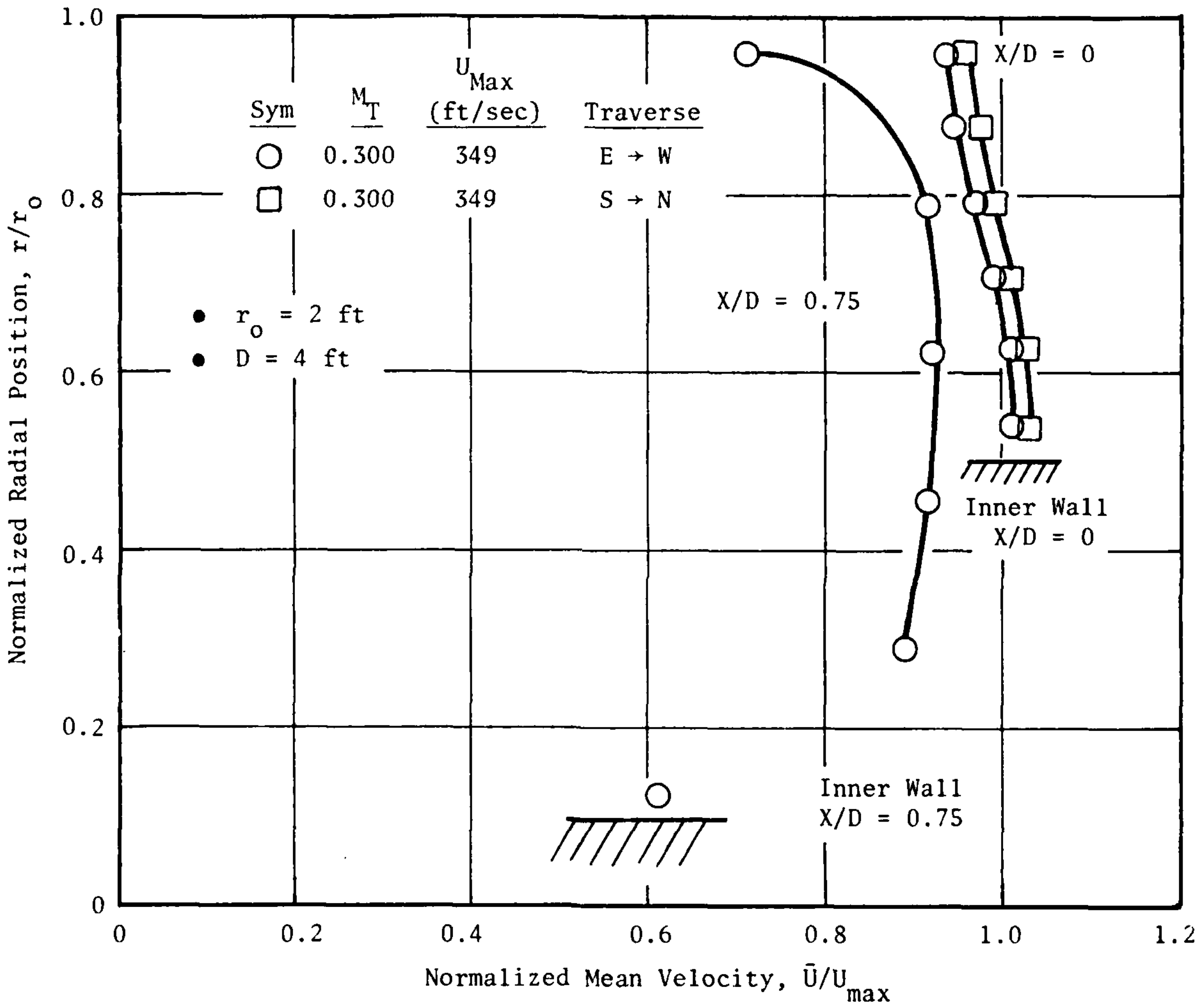

Figure 3-9. Radial Variation of Mean Velocity (Laser Velocimeter Data).

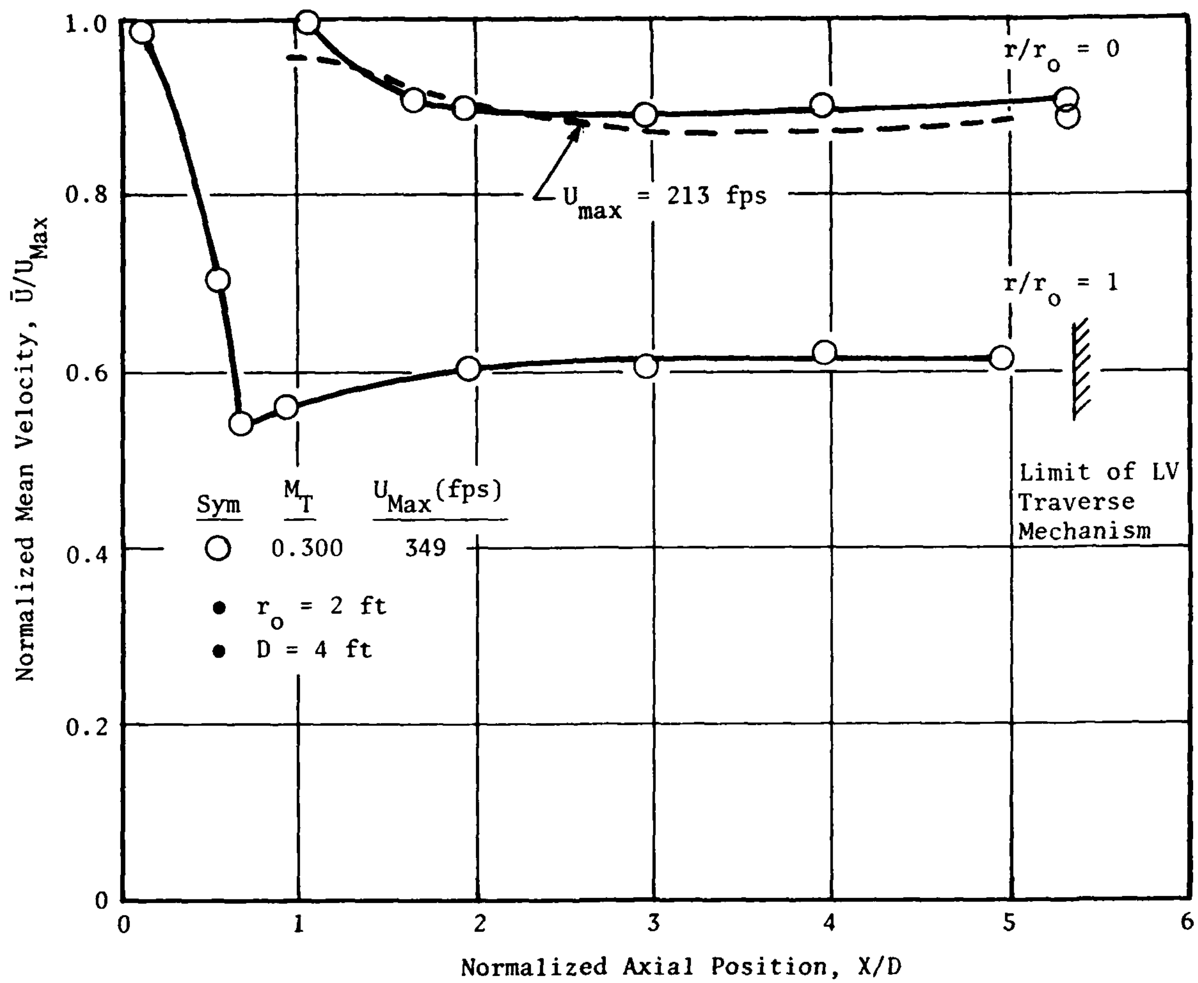

Figure 3-10. Axial Variation of Mean Velocity (Laser Velocimeter Data).

shown in Reference 12. The axial variation at $r/r_o = 1$ in Figure 3-10 shows a typical decay of mean velocity to approximately 60% of its maximum value, and thereafter a uniform value of X/D from 2 to 5. This region of uniformity suggests a similarity of tertiary mean velocity profile throughout the traversing range. Figure 3-10 also includes the centerline axial variation at $U_{max} = 213$ ft/sec.

The free jet (tertiary) velocity decay characteristics are further illustrated by the montage of Figure 3-11 which was constructed using laser velocimeter (LV) and hot wire (HW) radial traverses. The velocity profiles at X/D = 0, 0.27, and 0.75 are taken from LV point histogram data with the conical (inner) jet at approximately $M_j \approx 0.30$. The velocity profiles at X/D = 0.75, 1.53, and 2.30 are from HW traverse data with the conical (inner) jet at approximately $M_j \approx 0$. The profiles at X/D = 0.75 are identical for the LV and HW except for the near centerline region which is governed by the conical (inner) jet exit velocity.

The HW profiles were extrapolated to zero velocity (shown by the dashed line) to provide an indication of the free jet spreading angle. This angle was actually determined to be ~ 5.5° by studying two separate HW traces for each location. Further discussion on spreading angle determination is presented later.

The peak value of $\bar{U}/U_{max}$ at X/D = 0.75 in Figure 3-11 is approximately 10% lower than the value at X/D = 0 and remains essentially constant to at least 5 tertiary diameters (see Figure 3-10). This initial velocity decay is a result of free jet flow expansion caused by the decrease in outer diameter of the inner jet between stations A and C. The amount of reduction will depend on the nozzle configuration under evaluation. Figure 3-12 shows the variation in tertiary mean velocity as a function of tertiary area increase. It varies from practically zero for a JENOTS type test configuration (where inner jet outer diameter remained constant from the free jet exit plane to the jet nozzle exit), to about 10% for the previously discussed checkout nozzle (which corresponds to about 30% increase in effective tertiary flow area). Figure 3-12 also shows a point at almost 8% reduction in tertiary velocity based on suppressor LV measurements made in these Task 5 in-flight effects tests. Figure 3-12 can be utilized in a test to compensate for the tertiary mean velocity defect (at Station C) during a test by simply increasing the tertiary mean velocity at Station C. In the event test data are already acquired, Figure 3-12 can be used to reduce the tertiary mean velocity value at Station C during the flight transformation phase of the data reduction process.

Figure 3-13 depicts the radial variation of axial turbulence intensity measured with the LV at the free jet exit plane (Station A, or X/D = 0) and the conical (test) nozzle exit plane (Station C, or X/D = 0.75). The turbulence intensity is not significantly affected by tertiary exit velocity, as shown by dashed line in Figure 3-13 for $U_{max} \approx 213$ ft/sec. General conclusions can be drawn from Figure 3-13:

- Turbulence levels at the free jet exit plane are about 2.5% in the center of the free jet flow region.

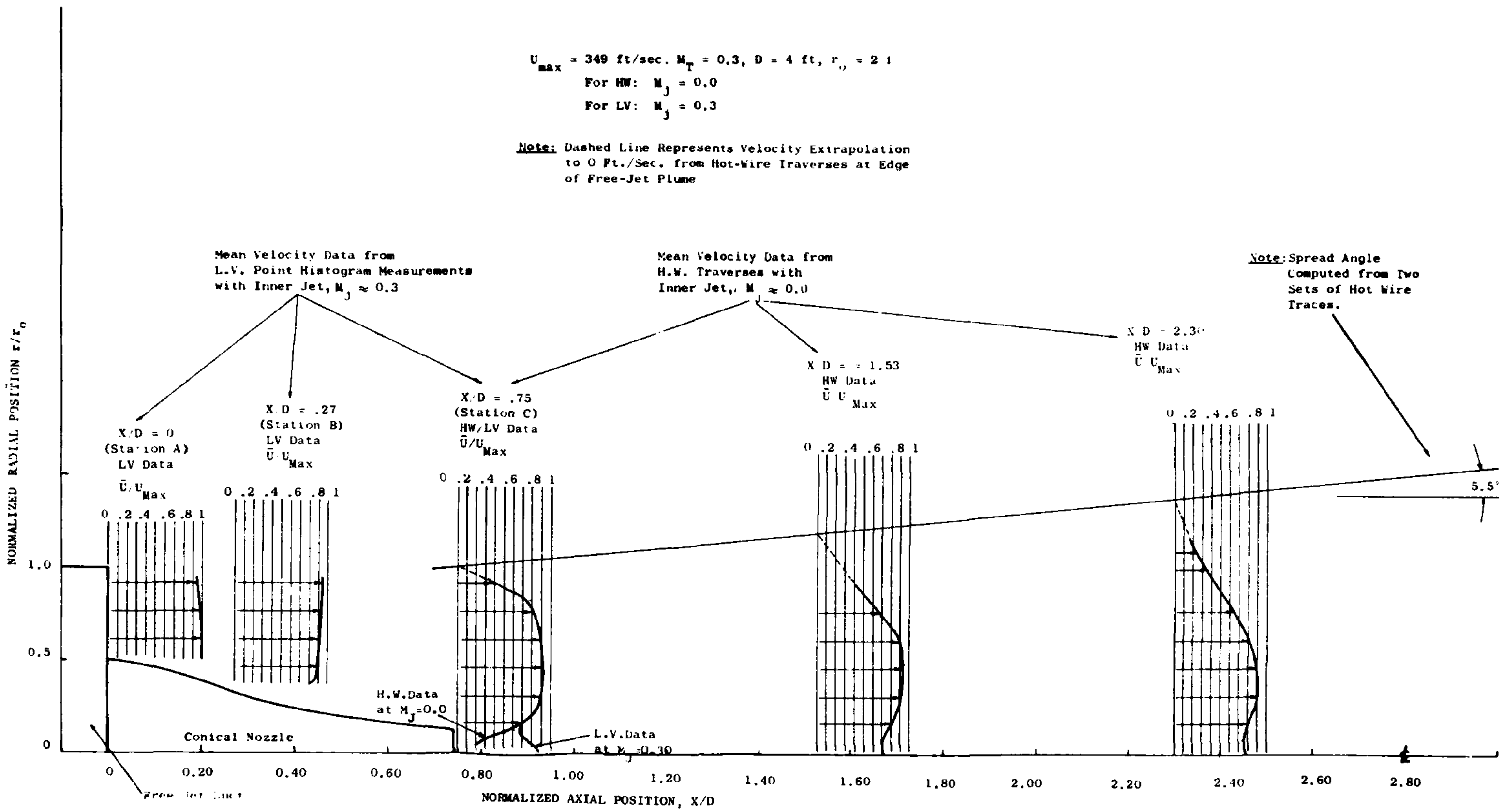

Figure 3-11. Axial Variation of Free Jet Mean Velocity HW/LV Data.

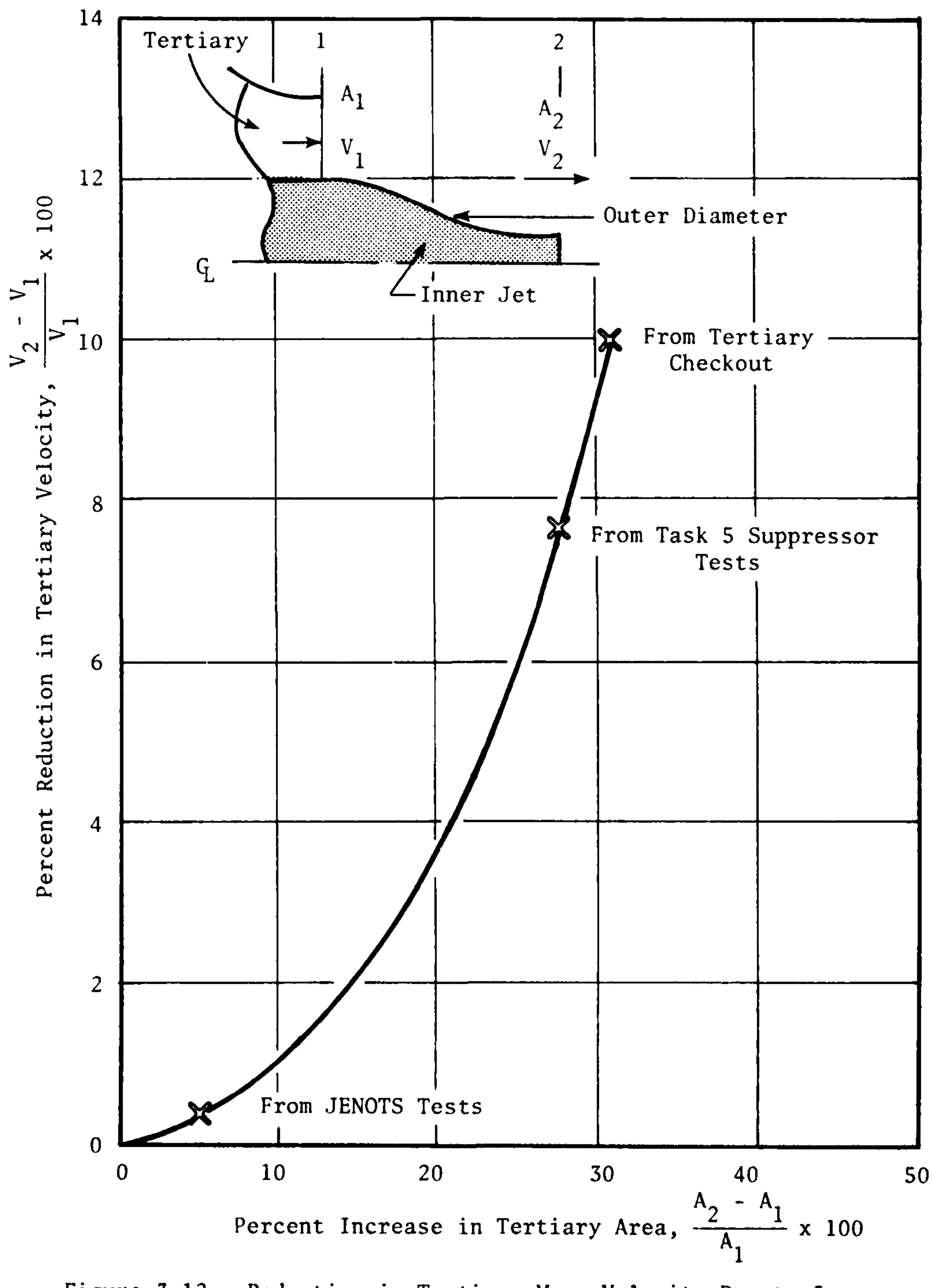

Figure 3-12. Reduction in Tertiary Mean Velocity Due to Increase in Tertiary Area.

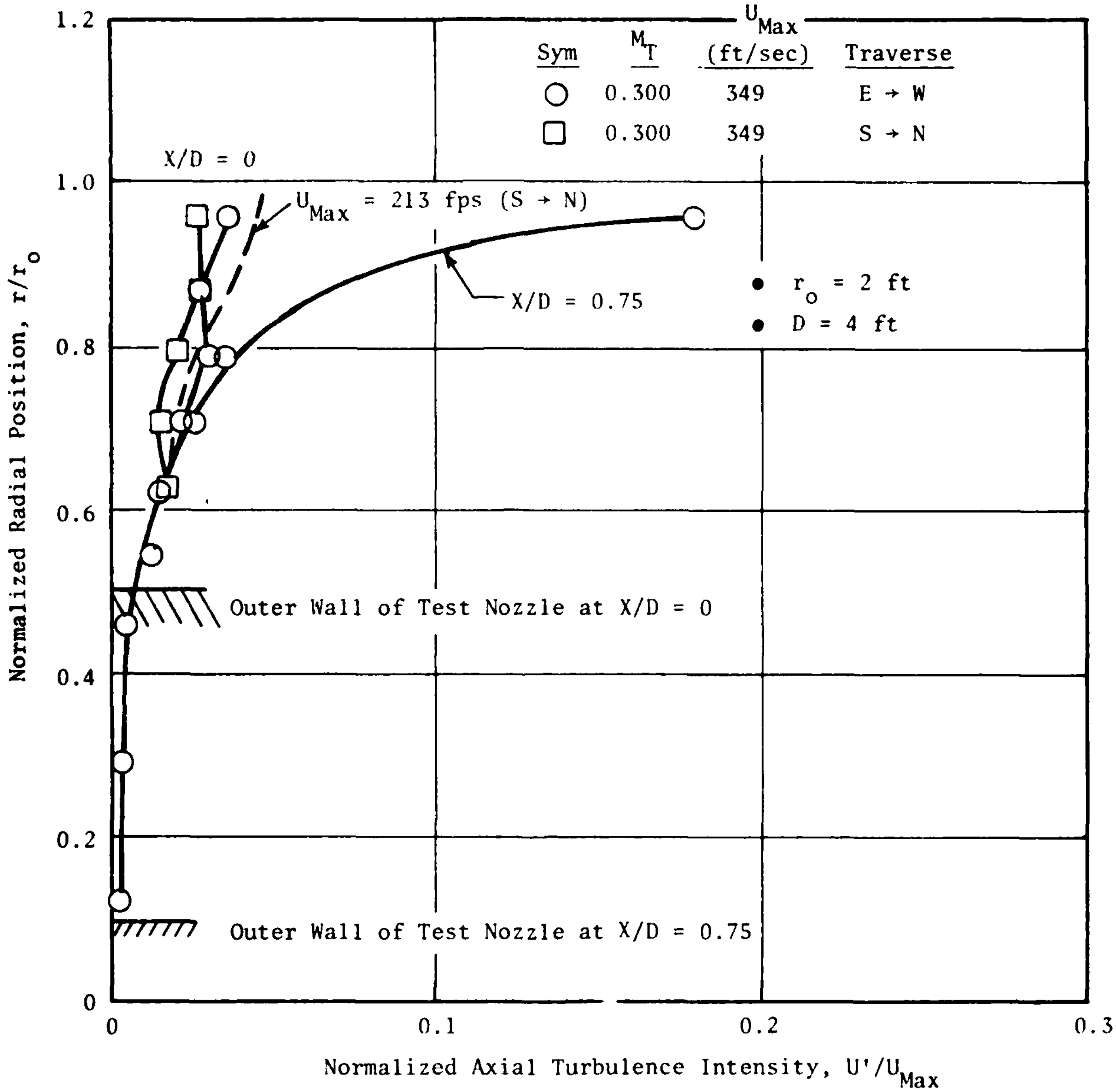

Figure 3-13. Radial Variation of Axial Turbulence (Laser Velocimeter Data).

- At the conical (test) nozzle exit plane, the turbulence level is on the order of 0.5%.

The axial variation of axial turbulence at U_{max} = 349 ft/sec is shown in Figure 3-14 for radial positions corresponding to r/r_o = 0 and r/r_o = 1. This general distribution for the free jet is similar to that previously observed in scale model subsonic test results (12).

The azimuthal variation of the mean velocity at the tertiary (free jet) exit (X/D = 0) for M_T = 0.3 is shown in Figure 3-15. Hot wire (HW) data taken every 30° are shown for three radial insertions (r/r_o = 0.625, 0.75, and 0.875). Laser Velocimeter (LV) data were taken for only North (N) and West (W) traverses. The HW and LV data show good agreement. The M_T = 0.30 HW data show that velocity uniformity at the tertiary exit plane is 2.6%, which compares favorably with the limited LV results (2.2%).

The azimuthal variation of turbulence intensity at M_T = 0.30 is shown in Figure 3-16 for the same three radial insertions described above. This again is a typical plot showing the similarity with radial position. Average azimuthal turbulence intensities are calculated to be between 1.8% (HW) and 2.3% (LV). In general, the results of Figure 3-15 and 3-16 illustrate that the free jet is reasonably symmetric in mean velocity and turbulence levels.

The following table summarizes the free jet HW and LV results based on the exit flow symmetry tests and compares them to those established from the JENOTS free jet during Task 4 Validation Tests (6) which were used as the design target for the anechoic free jet.

Free Jet Velocity	Mean Velocity Uniformity	Turbulence Intensity
• JENOTS - Task 4 Validation	<4%	3 - 4%
• Anechoic		
- U_{max} = 349 ft/sec	~ 2.4%	~ 2.0%
- U_{max} = 213 ft/sec	~ 2.9%	~ 2.7%

At Free Jet Exit Plane (Station A, X/D = 0). These results show the free jet flow quality equivalency of the JENOTS and Anechoic Facilities.

Results of a hot wire measurement study of the free jet plume spreading characteristic at M_T = 0.3 are shown in Figure 3-17. A total of eight hot wire traverses were made at three axial locations across the free jet nozzle exhaust. The data show that the tertiary plume does not start spreading appreciably until it reaches the <u>test nozzle exit plane</u>. It then spreads at an angle of approximately 5.5°. This spreading is assumed to be true for all

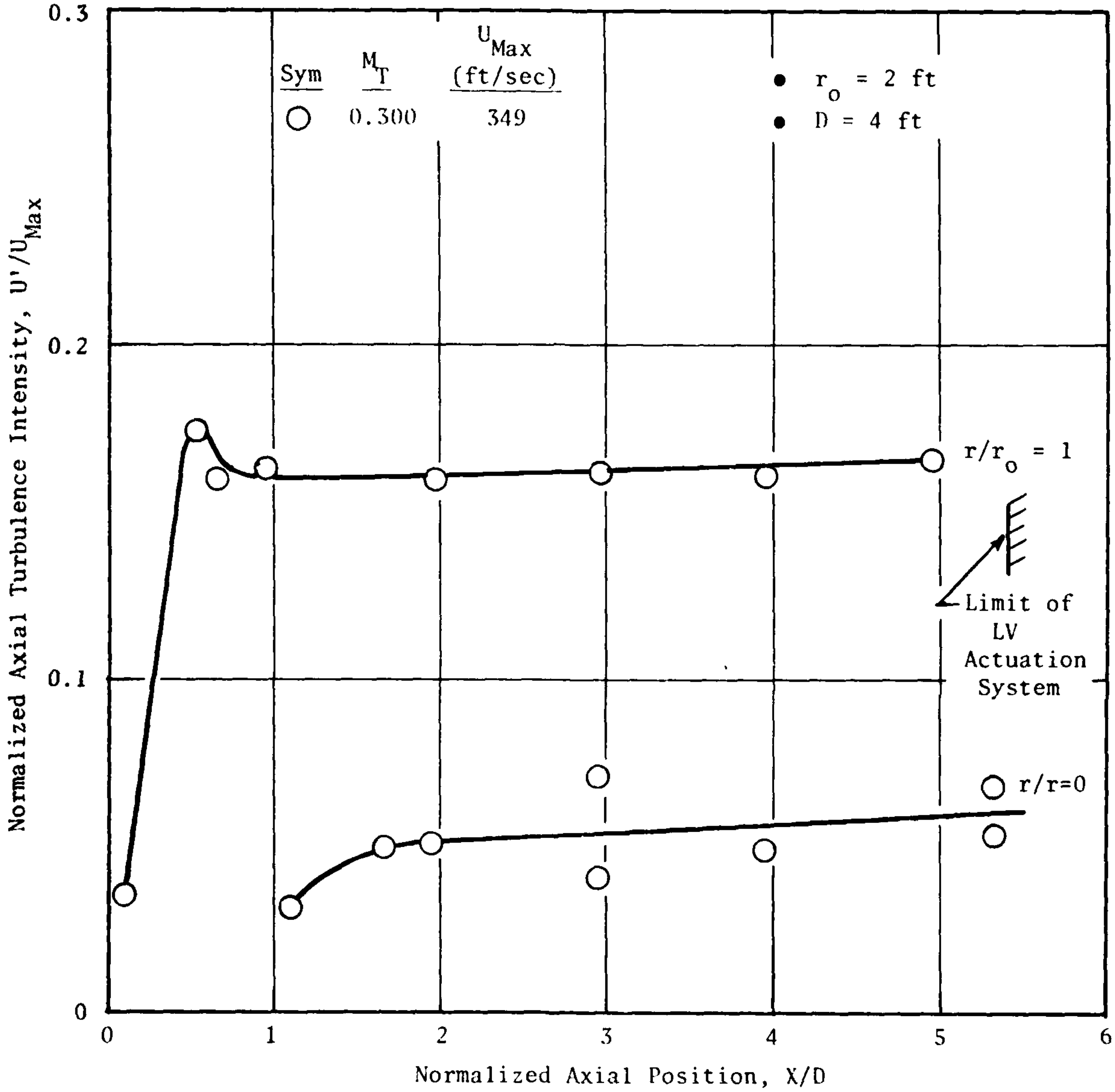

Figure 3-14. Axial Variation of Axial Turbulence (Laser Velocimeter Data).

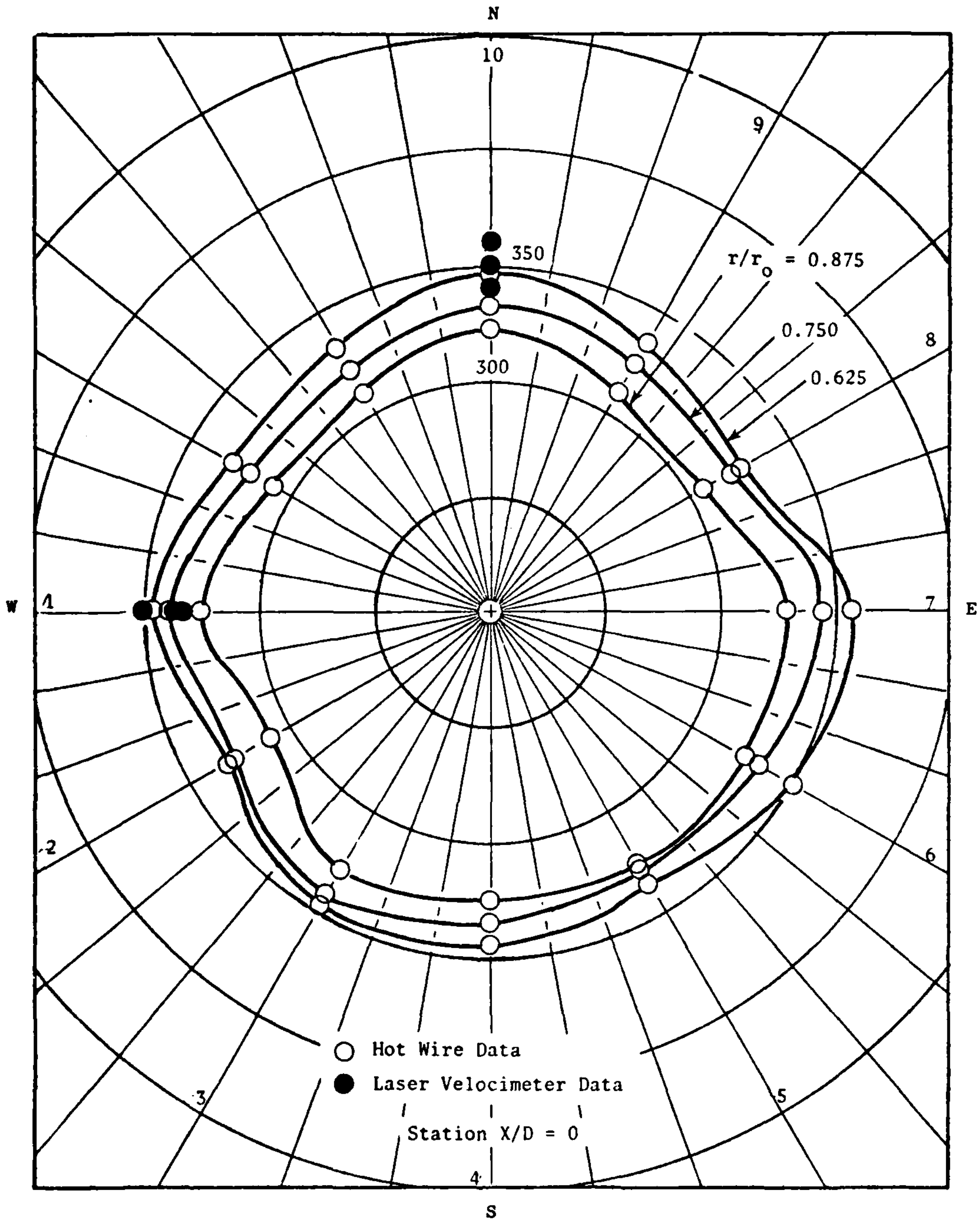

Figure 3-15. Azimuthal Variation of Mean Velocity at $M_T = 0.3$ (Laser Velocimeter/Hot Wire Data).

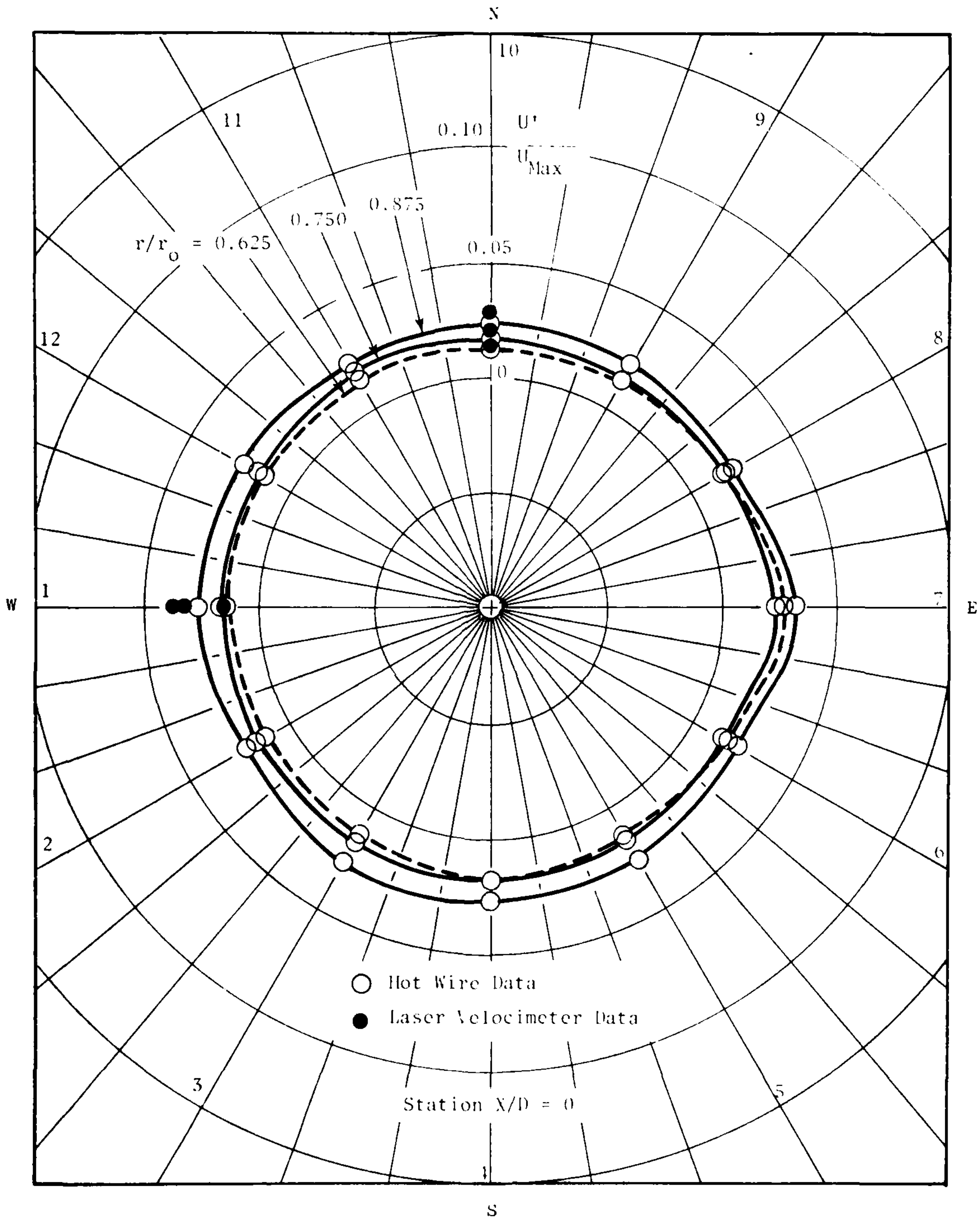

Figure 3-16. Azimuthal Variation of Turbulence Intensity at $M_T = 0.3$ (Laser Velocimeter/Hot Wire Data).

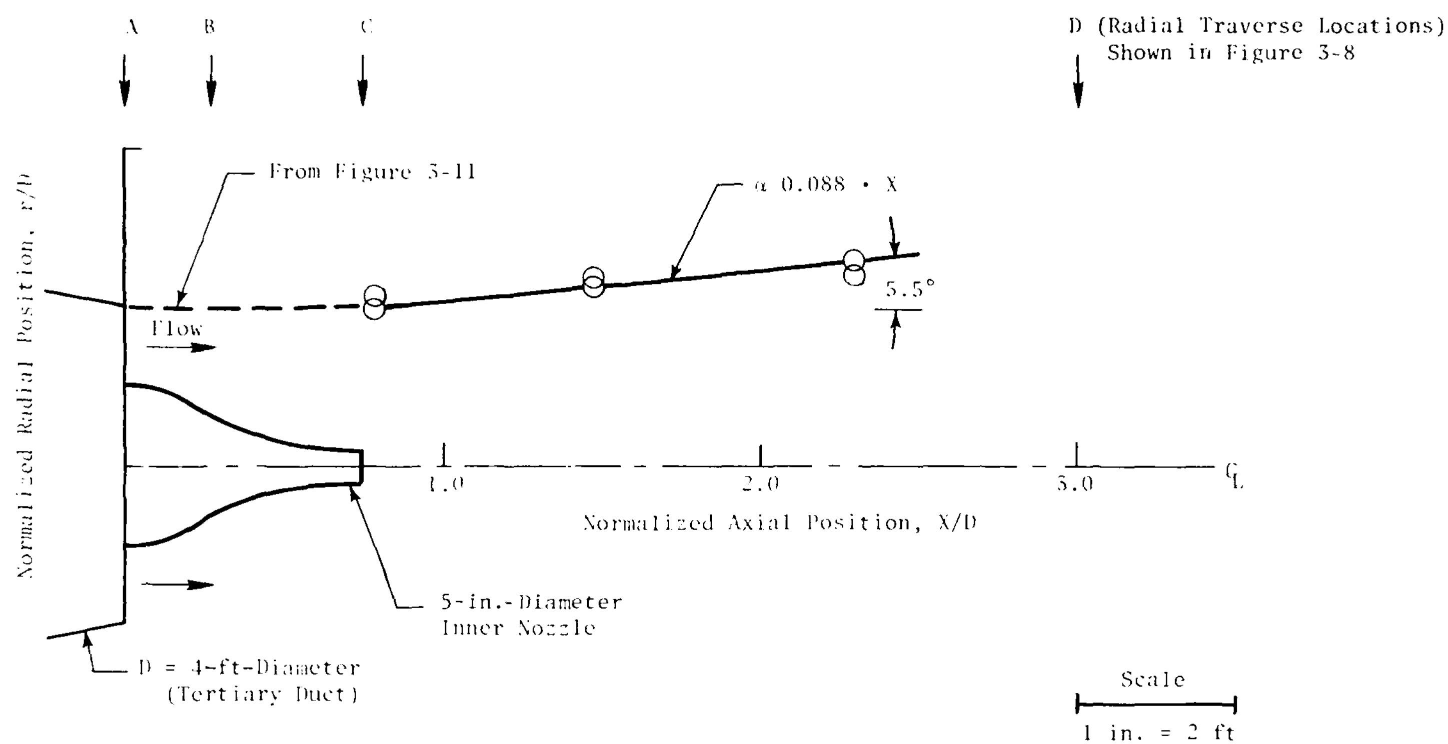

Figure 3-17. Study of Plume Spreading (Hot Wire Data).

azimuthal positions as was the case for the mean velocity and turbulence shown in Figure 3-15 and 3-16. This spreading rate of the plume is reasonably close to classical spreading (~7°).

The preceeding paragraphs have shown that the free jet design criteria evolved in the course of Task 4 (Reference 6) and adopted in the Anechoic Facility setup (Reference 11) produced good tertiary flow aerodynamics which, in turn, was reflected in the high quality of acoustic results taken during the verification tests.

4.0 MODEL SELECTION AND DESCRIPTION

Five suppressor nozzles and one unsuppressed nozzle were tested in the General Electric Anechoic Free Jet Facility. The six configurations were:

Model No.	Description	Figure No.
(1)	32-chute, AR = 2.1 - Single Flow Nozzle - $R_r = 0.62$	4-1
(2)	40-Shallow-Chute, $(AR)_o = 1.75$ Dual Flow Nozzle - $R_r^\circ = 0.717$	4-2
(3)	36-CD Chute, $(AR)_o = 2.0$ Dual Flow Nozzle - $R_r^\circ = 0.716$	4-3
(4)	Configuration 3 with a treated ejector - Dual Flow Nozzle - $R_r^\circ = 0.716$	4-4
(5)	54-Element Coplanar Mixer Dual Flow Nozzle	4-5
(6)	Coplanar - Coannular Nozzle - $R_r^\circ = 0.598$	4-6

Photographs and schematics defining each of the nozzle designs are summarized on Figures 4-1 through 4-6. Each of the five suppressor nozzle configurations was selected by evaluating and balancing suppression levels, performance loss, and mechanical complexity. Emphasis was placed on having variety of configurations in order that detailed flight noise characteristics could be projected for several suppressor nozzle families. This approach was considered appropriate because of the extremely limited data available to optimize the acoustic characteristics of suppressor designs in flight, especially for dual flow nozzle configurations as previously discussed in Section 3.0 of Reference 3. Conical nozzle data previously taken from the free jet and Aerotrain Test Series (References 6, 9, & 10) are used for comparing all the static and flight noise results from the above scale model nozzles.

A detailed description of the suppressors and the optimum nozzle selection process are included in Reference 3. Highlights from this study (Reference 3) are, however, included in the next few paragraphs for completeness of presentation.

Model 1, 32-chute AR=2.1 nozzle, was selected to be representative of suppressor nozzles which were applicable to single flow exhaust systems. This 32-chute nozzle was evaluated as result of the parametric test series described in Reference 1. The selection of this configuration was also justified by the

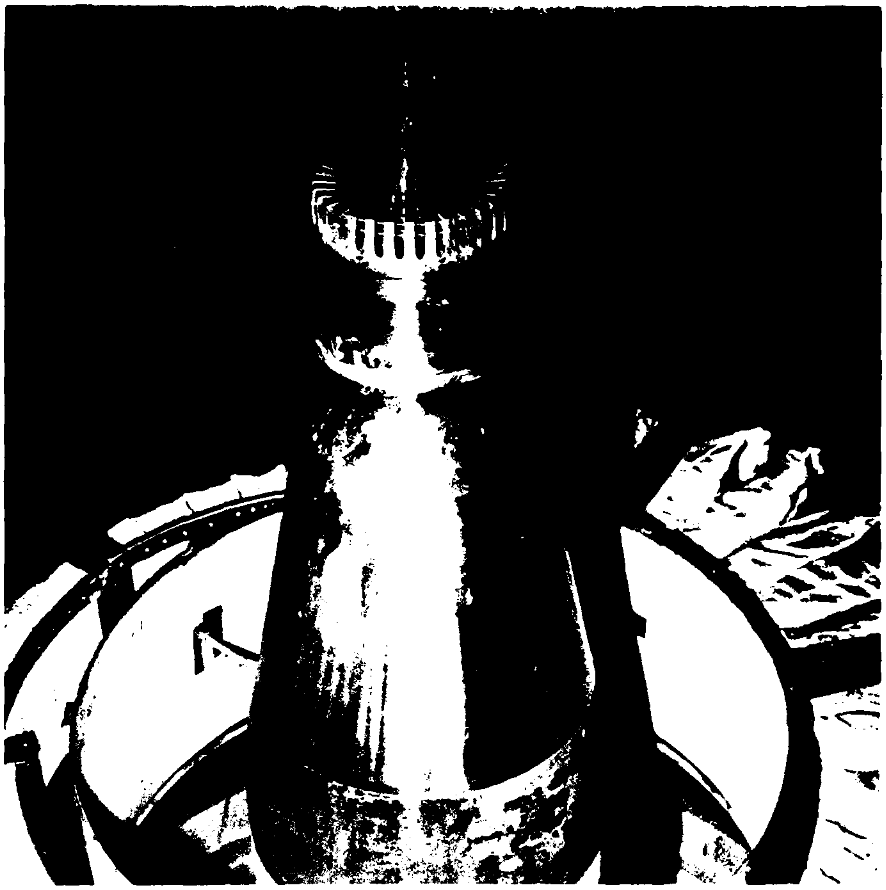

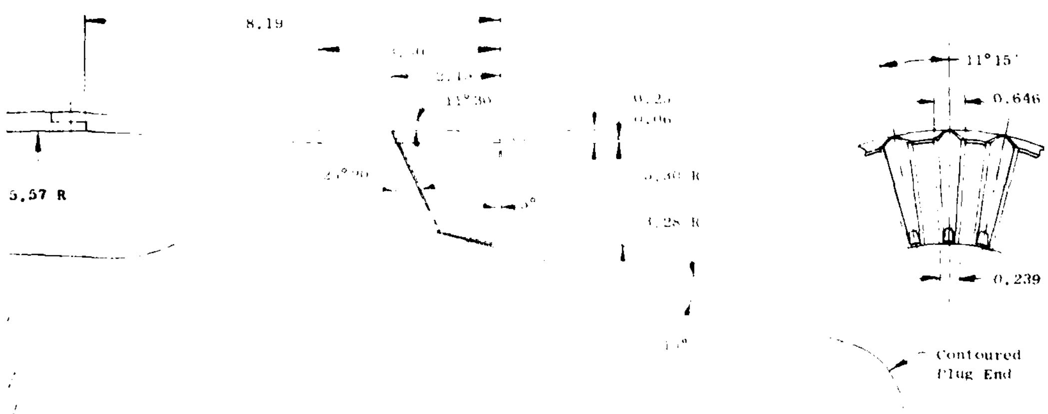

Figure 4-1. 32-Chute, AR = 2.1, R_r = 0.62 Turbojet Suppressor.

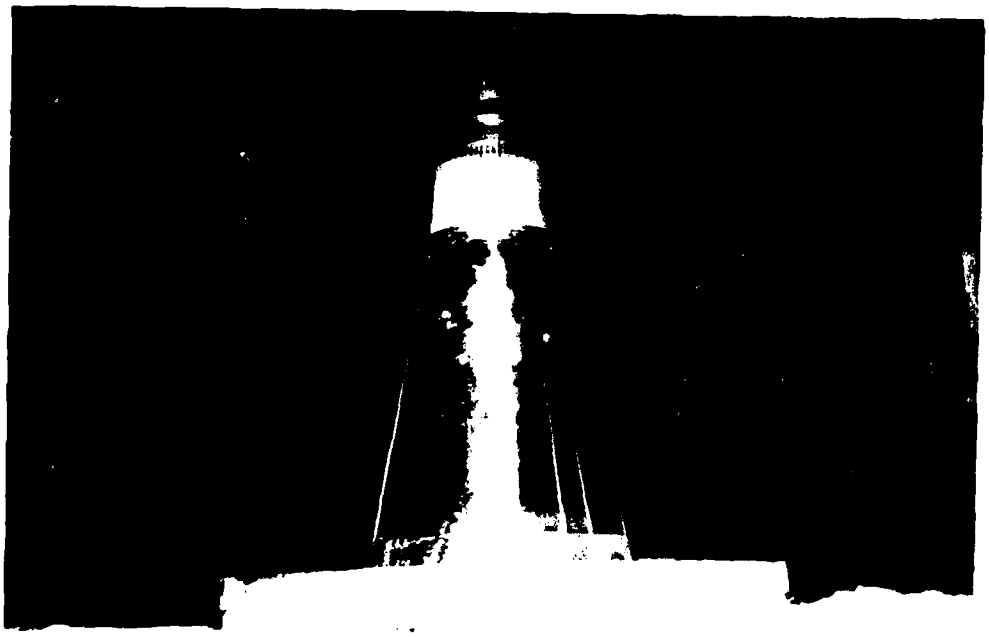

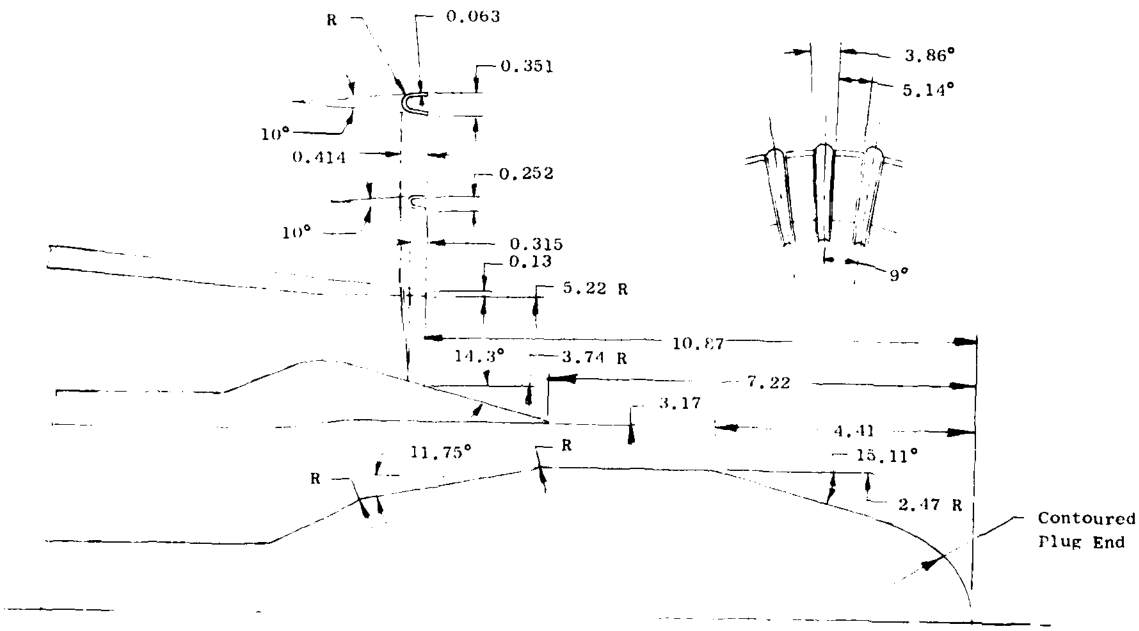

Figure 4-2. 40-Shallow Chute, $(AR)_o = 1.75$, $R_r^o = 0.717$ Duct Suppressor, $A_o/A_i = 1.92$, $R_r^i = 0.779$ Core Plug, In-Line.

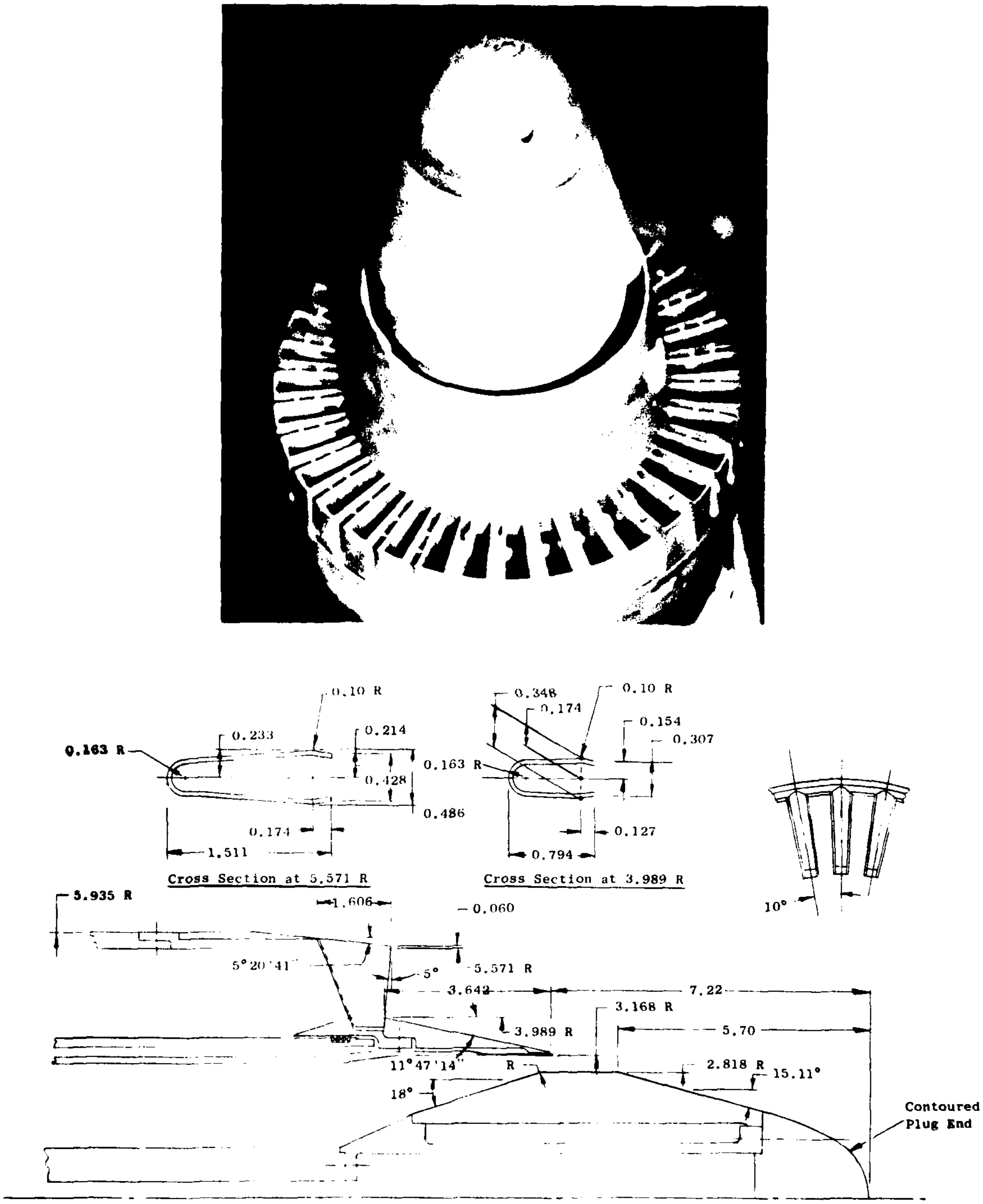

Figure 4-3. 36-Convergent-Divergent Chutes, $(AR)_o = 2.0$, $R_r^o = 0.716$ Duct Suppressor, $A_o/A_i = 3.62$, $R_r^i = 0.889$ Core Plug, In-Line

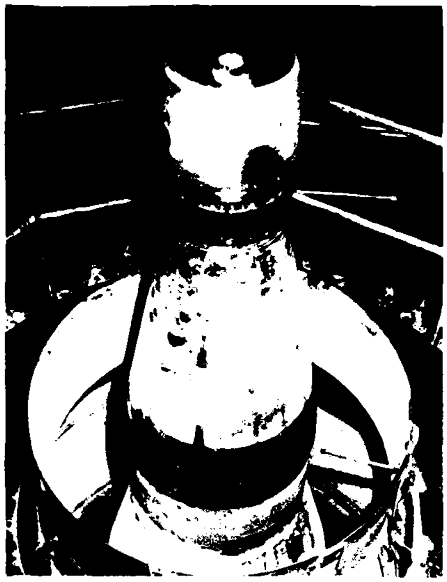

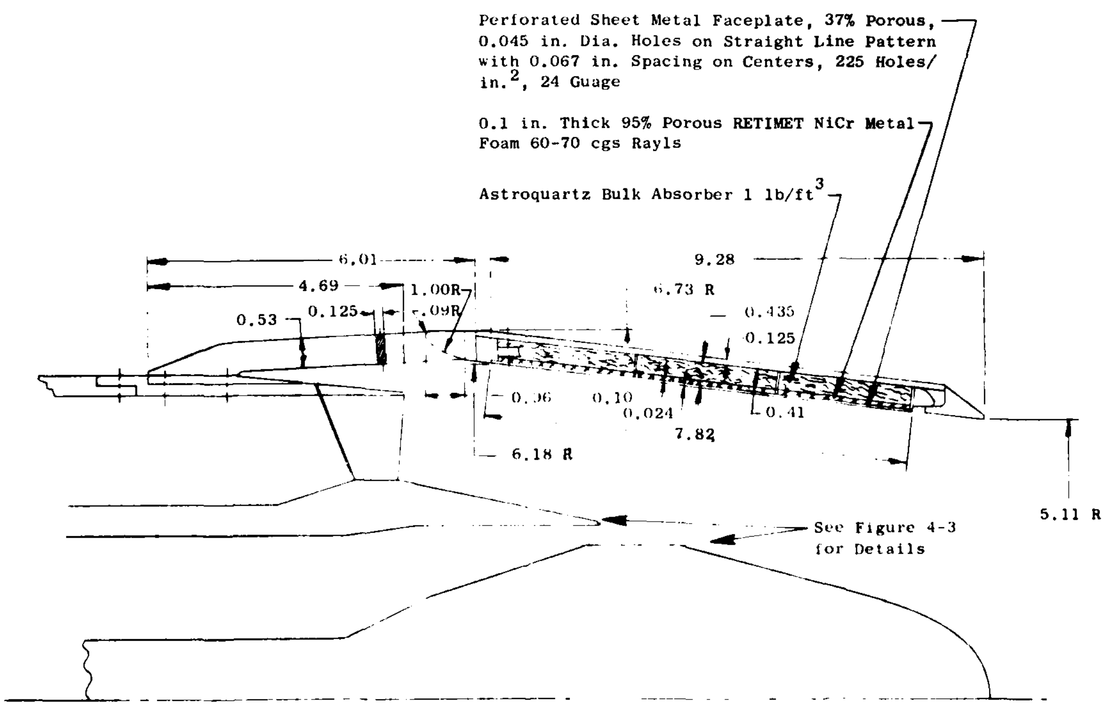

Figure 4-4. 36-Convergent-Divergent Chute Duct Suppressor (Figure 4-3) with Acoustically Treated Secondary Ejector.

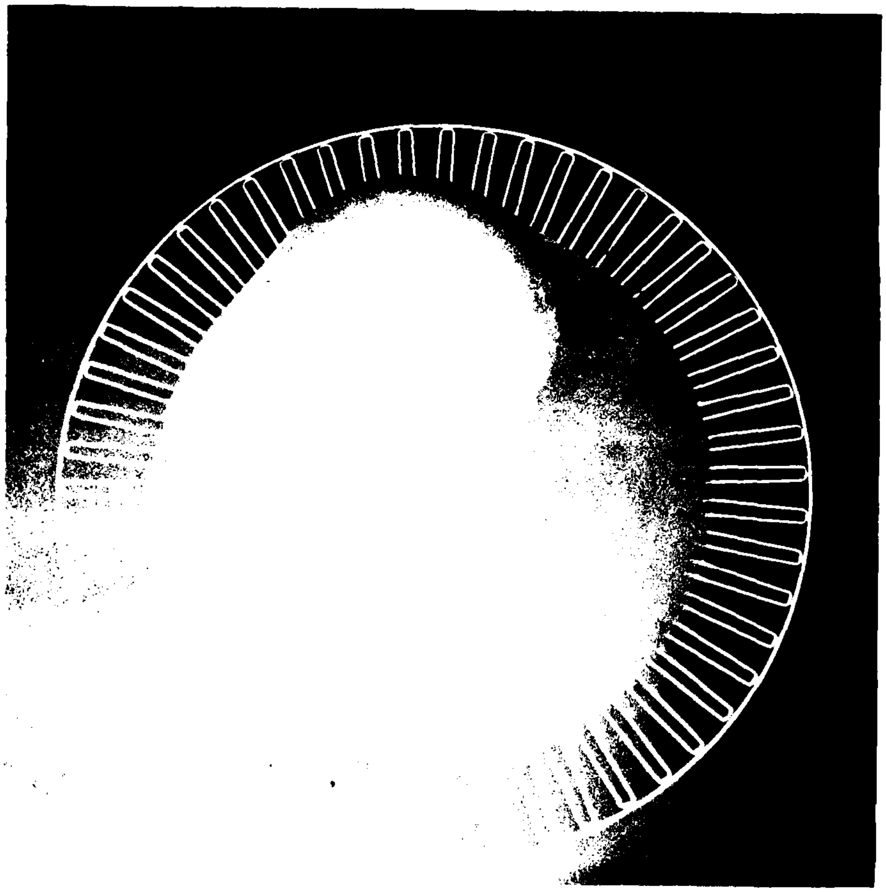

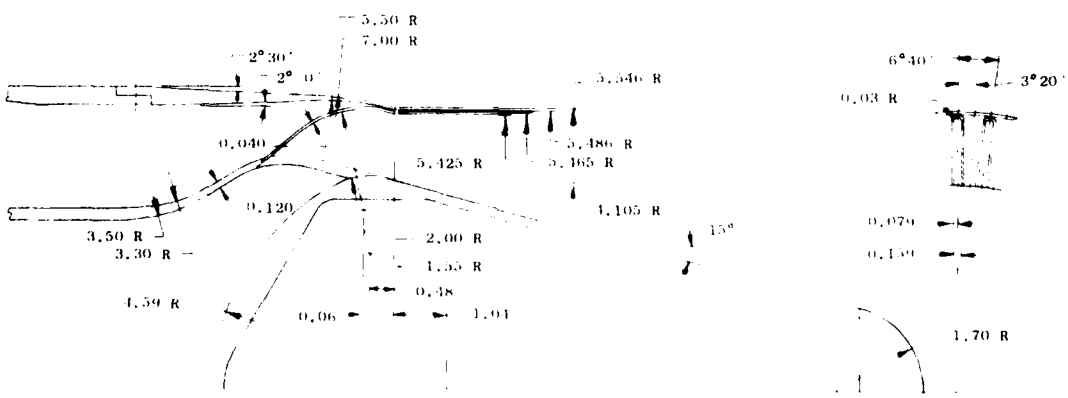

Figure 4-5. 54 Element Coplanar Mixer.

Figure 4-6. Coannular Coplanar, $A_o/A_i = 2.0$.

results of the aircraft integration studies described in Reference 3. The mechanical design studies indicated that the area ratio of 2.1 does fall within the range of acceptability. The static and flight aerodynamic performance of this nozzle was documented based on wind-tunnel testing data. Three other turbojet suppressors were also considered and evaluated in the aircraft integration study described in Reference 3. This may at first seem to be a limited group of nozzles, but in actuality, it represents a substantial portion of the suppressor nozzle work performed during the past 25 years. The 32-chute nozzle and 57-tube plus ejector nozzle are configurations which were evolved after extensive study conducted by General Electric and The Boeing Company after cancellation of the SST. These nozzles were evolved based on limited analytical, and extensive experimental studies conducted by the respective companies and described in References 1 and 2. The 36-chute nozzle area ratios 2.0 and 2.5 were configurations evolved for parametric testing during this current program and are more representative of the type of mechanical suppressors which could be implemented on a high radius ratio plug nozzle. Selection of the optimum nozzle Model 1 was based on maximum range attainable in order to meet current FAR36 (i.e., EPNL=108) noise levels.

The remaining four optimum nozzles were selected from the dual flow family. The second model was chosen to be $(AR)_0$=1.75 40-shallow chute nozzle with a modified core-plug geometry. This configuration was evolved as a result of the experimental data presented in References 3 and 10. The experimental results show that a modification to the core-plug geometry of the 40-shallow chute nozzle would result in a 1.5 PNdB improvement in suppression with essentially no change in exhaust system performance or weight. This configuration, based on the Task 3 experimental data, has the potential for maintaining suppression in flight. This projection is made based on the experimental observation that in flight, a significant low frequency reduction occurs for the suppressor, whereas, little or no change occurs in the high frequency portion of the spectra. The 40-shallow chute, when compared to the other shallow chute configurations, exibited the lowest high frequency noise levels and should, therefore, perform best in the flight environment.

Model 3 was selected to be an $(AR)_0$=2.0 36-chute nozzle and incorporated several unique design features. A nozzle area ratio of 2.0 was selected because it represents the best compromise from a suppression and weight point of view over a wide range of velocities (Reference 3). The core plug geometry of this configuration was designed based on the flow management studies described in Reference 10. The small step height was selected to provide a higher outer-to-inner-stream flow area ratio variation. The element number was selected based on the engineering correlation studies which indicated very little improvement in suppression with increasing element number, and 36 was selected based on performance data availability and the adverse effect that increasing element number has on performance.

The chute design itself was unique in that it incorporated a convergent-divergent flowpath to reduce the shock noise signature of the suppressor. The need for this design was predicted on test data presented in Volume II.

The influence of shock noise on the directivity and spectra characteristics of a suppressor is illustrated by the following example. Consider the AR = 2.0 turbojet nozzle (Reference 10) operating at two test conditions as a means of illustrating the importance of shock noise. The pressure ratio was held constant at approximately 3.3 and two temperature conditions were evaluated. These were 730° R and 1630° R, which result in velocities of 1600 and 2380 ft/sec, respectively. Previous results would indicate a significant decrease in PNL level as velocity is decreased. This trend was observed at acoustic angles of 90° and in the aft noise quadrant. In the forward quadrant, the PNL levels are equivalent even though there is a difference of 780 ft/sec in velocity. Examination of spectral results reveals that the high frequency portion of the spectra are equivalent in level whereas the low frequency levels are lower as expected. This insensitivity of high frequency noise is generally characteristic of shock noise. If the shock noise were reduced, a significant decrease in PNL levels should occur. Therefore, a convergent-divergent chute design was incorporated into this configuration.

Model 3 with an ejector was selected as optimum nozzle No. 4. An ejector was chosen to be representative of a high suppression nozzle from a different family of exhaust nozzles. The ejector design incorporated a length-to-diameter ratio of 1 and utilized the design criterion that flow area be held constant throughout the annulus. These are the design criteria for good aerodynamic performance at takeoff conditions. The ejector treatment utilized was a broadband bulk absorber, Astroquartz. The addition of a treated ejector to Model 3 is projected to increase PNdB suppression 2 to 4 PNdB (Reference 3).

Model 5 is a coplanar mixer plug nozzle (alternate hot and cold flow elements), which was evolved because of its aero performance and suppression considerations. This model configuration was selected from the application of the theoretical concepts developed in Task 2. Extensive diagnostic studies on multichute nozzles were carried out in Task 2. From these studies, a nozzle concept was developed which attempts to capitalize on the identified mechanisms of jet noise suppression. The first concept employed was that of injecting low velocity flow between the "chutes", which would provide several benefits: (1) reduce the shear, and hence the higher frequency noise, in the chute premerged zone, (2) eliminate the dependency of chute mixing on ambient air entrainment, and (3) improve the relative velocity effect in the flight condition. The velocity flow between the chutes could be supplied by the bypass bypass stream on an engine system application.

The second concept employed from Task 2 involved injecting low velocity flow between the chutes as a bypass stream, rather than through an inner core nozzle or base-bleed step. The plume should decay more rapidly with axial distance, because the bypass stream does not "fill up" the center of the plume. Instead, it is mixed with the ambient air along with the primary stream. This should produce lower convection Mach numbers, and hence reduce the convection amplification effects at aft angles.

The employment of chutes for flow-splitting was deemed desirable from the standpoint of reducing shock-cell broadband noise. By using a 54-chute configuration, hydraulic diameter can be minimized, thus greatly shortening

the shock structure and pushing the peak frequency of the shock noise component high enough to render it inaudible or highly vulnerable to air attenuation. The shock cell noise may also be controllable by properly matching primary and secondary stream pressure ratios. Finally, because the secondary (bypass) flow replaces the chute "base area", the aerodynamic performance of this concept over a conventional chute nozzle should be much improved.

Appendix A summarizes the pertinent flow areas for each of the optimum suppressors described herein.

5.0 DEFINITION OF TEST MATRICES

The test matrices utilized in this program varied as a function configuration. In general, cycle conditions along a typical variable cycle engine operating line were chosen to establish suppression characteristics as a function of mass average velocity, free jet velocity, weight flow ratio (W_i/W_o), and velocity ratio (V_i/V_o). A summary of the thermodynamic conditions for the data points obtained for each of the configurations is presented in Appendix A. Table 5-1 is an overview of the test matrices which defines the combination of data points which may be utilized to examine a specific variable.

Table 5-1. Overview of Test Matrices.

Model Numbers (Reference Section 4)	Data Points Numbers (Reference Appendix A)	Comments
1	1-7,11-20	Typical engine operating line
1	8-10	Isothermal points for shock noise studies
2	1-6	No inner flow
3	1-6,49-52	No inner flow
2,3,4	7-12	Weight flow ratio (W_i/W_o) held constant
2,3,4	13-28	Evaluation of inverted dual flow cycles with the inner stream velocities held constant at 1000, 1200, 1300 and 1400 ft/sec.
2,3,4	29-36	Typical AST/VCE cycle
3,4	37-48, 53-55	Outer stream pressure ratio was held constant $(P_T/P_o)_o = 3.0$
5	1,2,4-10,13, 15-17,21,29, 30	Evaluation of inverted dual flow cycles with bypass/inner stream velocities held constant at 1000,1200, 1300 and 1400 ft/sec.
5	3,11,14,22, 27,28	Weight flow ratio (W_i/W_o) held constant
5	12,18-20, 23-26	Typical AST/VCE cycle
5	31-50	Inner Stream variations at constant outer stream conditions(static test matrix only)

6.0 DATA ACQUISITION AND DATA REDUCTION PROCEDURES

A flow chart of the acoustic data acquisition and reduction system is shown in Figure 6-1. This system has been optimized for obtaining the acoustic data up through the 80 kHz 1/3-octave center frequency. The microphone type used to obtain f = 80 kHz data is the B&K 4135, 0.064 cm, condenser microphone for farfield measurements. All testing is conducted with microphone grid caps removed to obtain the best frequency response. The cathode followers used in the chamber are transistorized B&K 2619's for optimum frequency response and lower inherent system noise characteristics relative to the 2615 cathode follower. All systems utilize the B&K 2801 power supply operated in the direct mode.

The output of power supply is connected to a line driver adding 10 dB of amplification of the signal as well as adding "pre-emphasis" to the high frequency portion of the spectrum. The net effect of this amplifier is a 10 dB gain at all frequencies, plus an additional 3 dB at 40 kHz and 6 dB at 80 kHz due to pre-emphasis, increasing the ability to measure low amplitude high frequency data. The pre-emphasis starts at 10 kHz and follows a straight line ramp to 80 kHz as shown in the circled schematic of Figure 6-1.

In order to remove low frequency ambient noise, high-bypass filters with attenuations of 26 dB at 12.5 Hz linearly decreasing to 0 dB at 200 Hz, were installed in the system.

The tape recorder amplifiers have a variable gain from -10 dB to +60 dB in 10 dB steps and a gain trim capability for normalizing in. ming signals. The signal is then split to provide for both an unfiltered and filtered flowpath.

High-pass filters are incorporated in the acoustic data acquisition system to enhance high frequency data previously lost in the tape recorder electronic noise floor for microphones from 110° - 160°. The microphone signal below the 20 kHz 1/3-octave band is filtered out, and the gain is increased to boost the "signal-to-noise" ratio of the remaining high frequency signal. Both the unfiltered and filtered signals are recorded on tape.

The system used for recording acoustic data is a Sangamo/Sabre IV, 23-track FM recorder. The system was set up for Wideband Group I (intermediate band double extended) at 120 in./sec tape speed. Operating at 120 in./sec tape spedd provided improved dynamic range necessary for obtaining the high frequency/low amplitude portion of the acoustic signal. The tape recorder was set up for ±40% carrier deviation with a recording level of 8 volts peak-to-peak. During recording, the signal is displayed on a calibrated master oscilloscope, and signal gain is adjusted to maximum without exceeding the 8 volt peak-to-peak level.

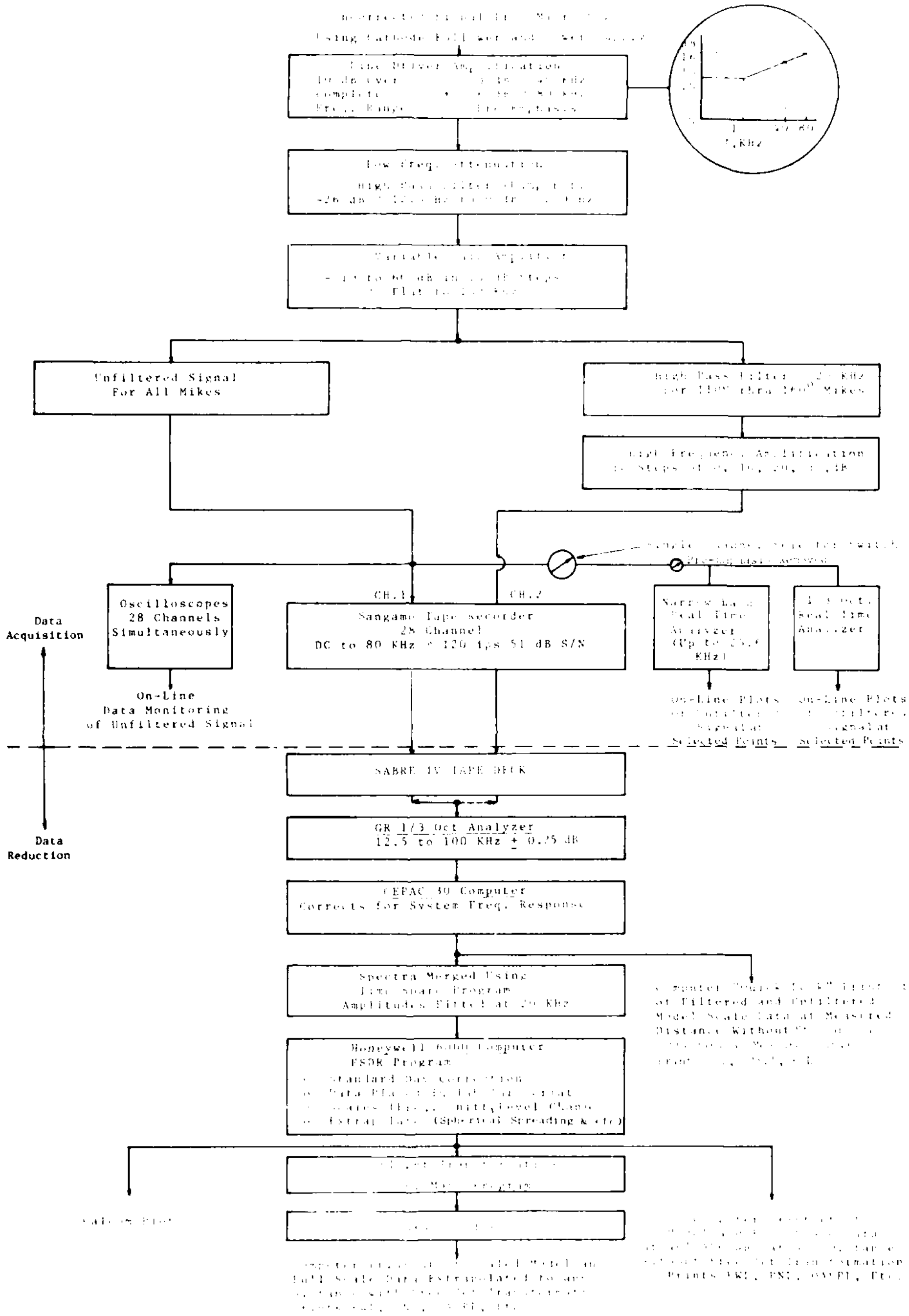

Figure 6-1. Acoustic Data Acquisition and Reduction Flow Chart.

Individual monitor scopes are used for observing signal characteristics during operation. On-line data monitoring of the unfiltered signal is available using 1/3-octave and narrow band real time analyzers for one angle at any given time. The analyzer outputs can be displayed on scopes or hard copy via an X-Y plotter.

Standard data reduction is conducted in the General Electric AEG Instrumentation and Data Room (IDR). The data tapes are played back on a CEC3700B tape deck with electronics capable of reproducing signal characteristics within the specifications indicated for Wideband Group I. An automatic shuttling control is incorporated in the system. In normal operation, a tone is inserted on the recorder in the time slot designed for data analysis. Tape control automatically shuttles the tape, initiating an integration start signal to the analyzer at the tone as the tape moves in its forward motion. This motion continues until an "integration complete" is received from the analyzer, at which time the tape direction is reversed and at the tone the tape restarts in the forward direction advancing the channel to be analyzed until all the channels have been processed. A time code generator is also utilized to signal the tape position of the readings as directed by the computer program control. After each total reading is completed, the number of tape channels at each point is advanced to the next reading.

All 1/3-octave analysis is performed on a General Radio 1921 1/3-octave analyzer. Normal integration time is set for 32 seconds to ensure good integration for the low frequency content. The analyzer has 1/3-octave filters set from 12.5 Hz to 100 kHz, and has a rated accuracy of $\pm 1/4$ dB in each band. Each data channel is passed through an interface to the GEPAC 30 computer where the data is corrected for the frequency response of the microphone and the data acquisition system and processed to calculate the perceived noise level and OASPL from the spectra.

At this point a computer quick-look printout of both the filtered and unfiltered signals is available. The printout shows model scale data at the measured distance without atmospheric or standard day corrections. Thus, the quick-look shows only as-measured data.

The filtered and unfiltered spectra are now merged using a time-share program which fits the amplitudes at 20 kHz. The sound pressure levels below 20 kHz are calculated using the unfiltered signal, while those above 20 kHz are calculated using the filtered signal. The jet noise spectra at a given angle is then obtained by computationally merging these two spectra.

For calculation of the acoustic power, atmospheric corrections to standard day scaling to other nozzle sizes, or extrapolation to different far-field distances, the data is sent to the Honeywell 6000 computer for data processing. This step is accomplished by transmitting the SPL's via direct time share link to the 6000 computer through a 1200 Band Modem. In the 6000 computer, the data are processed through the Full Scale Data Reduction (FSDR) Program where the appropriate calculations are performed. The SAE AIR 876A corrections for atmospheric absorption[13] were used in this program to correct the data to standard day conditions. The data printout is accomplished on a high speed terminal. In addition, the FSDR Program writes a magnetic tape which is used for Calcomp plotting of the data.

7.0 ANALYSIS OF STATIC AND SIMULATED FLIGHT DATA

7.1 REFERENCE NOZZLE DATA AND ACOUSTIC DATA NORMALIZATION

This section defines mean lines, derived from several sets of conical nozzle data to be used as reference lines calculating static and flight suppression levels. The section also explains the acoustic data normalization procedures.

The data normalization technique developed in Reference 14, modified to account for static ideal gross thrust, was adopted for presentation of acoustic results. Selection of mixed stream or mass averaged velocity as the basis for data comparisons seems physically appropriate because the noise is expressed in terms of a velocity calculated from the thermodynamic conditions of both streams. Mixed stream velocity also allows comparison of noise values at the same specific thrust, which is a meaningful propulsion performance parameter.

In general, acoustic data is presented as:

Noise Value - 10 $\log_{10} Fs(T_o/T_{sm})^{\omega-1}$ Vs V_{ma}, f or θ

where:

Noise Value = PNL, OASPL, OAPWL, or 1/3-OBSPL

Fs = Static Ideal Gross Thrust (Sum of Inner and Outer Streams)

T_o = Ambient Temperature, ° R

T_{sm} = Static temperature corresponding to mass averaged velocity, V_{ma}, and total temperature, T_{Tma}, ° R

ω = Jet density exponent (per SAE ARP 876) based on mass-averaged velocity (V_{ma})

$V_{ma} = \dfrac{W_iV_i + W_oV_o}{W_i+W_o}$, mass averaged Jet Velocity, ft/sec

$T_{Tma} = \dfrac{W_iT_{Ti}+W_oT_{To}}{W_i+W_o}$, mass averaged total temperature, ° R

where W and T_T are the exit plane values of mass flow and total temperature for the inner and outer (subscript i & o) streams, respectively, and f & θ are 1/3-octave band center frequency and angle relative to the inlet axis. In the case of turbojet test data, the flow parameters revert to the single stream notation.

When it contributes to ease of data handling and presentation, the normalization on the graphs is:

Noise Value - N, where,

$$N = 10 \log_{10} \frac{Fs}{10,000} (T_o/T_{sm})^{\omega-1}$$

All the acoustic results reported herein have been scaled up to 338 in.^{2} (total flow area) and extrapolated to a 2400 ft sideline. The introduction of a 10,000 pound reference thrust shifts noise levels by 40 dB and allows plotting of all positive values of the low level sideline noise data.

Several sets of conical nozzle static data are presented on Figure 7-1(a) from References 6, 9, and 10. A mean line fitted through the data was used as a reference line to establish static PNL suppression.

The data used to define the flight noise reference line were from free jet and Aerotrain test series (6, 9, 10). Two reference lines are established on Figure 7-1(b), the first uses data with free-stream velocities varied from 275 ft/sec to 300 ft/sec, and the second uses data with free-stream velocity of 400 ft/sec. These lines are used in conjunction with measured noise data for several suppressors to determine peak PNL suppression levels.

The unsuppressed AR = 2.0 coplanar-coannular nozzle evaluated in this test program represents the simplest baseline type nozzle for dual flow suppressor systems. Therefore the static and flight peak PNL suppression characteristics for this nozzle are summarized in this section. The static peak PNL noise characteristics are compared to the conical nozzle reference line of Figure 7-2(a). Modest peak noise suppression occurs ranging from 2 to 4 PNdB. The peak noise characteristics in flight are also summarized on Figure 7-2(b). The static and flight suppression levels are equivalent as shown on Figure 7-2(c) at mass average velocities above 2000 ft/sec, however, below this velocity flight suppression was 2-2.5 PNdB less than the static level. No other data is included in this report on this concept. The work currently underway under NAS3-19777 and 20619 (References 9 and 14) is pursuing a variation of this concept; e.g., Inverted Velocity Profile coannular plug nozzle.

The conical nozzle data are used in this report as the reference for comparison with the measured data for the five suppressor nozzles. The mean lines defined in this section will be used to define the peak noise suppression levels. However, directivity and spectra comparisons will be made using the conical nozzle data which most closely duplicates the mixed flow cycle conditions of the suppressor data being presented.

7.2 EVALUATION OF STATIC DATA

This section discusses the static noise characteristics of the five suppressor nozzles. The results are presented in terms of peak PNL and OASPL levels, directivity characteristics, and one-third octave spectra. Suppression levels for each of the configurations are established on the basis of OASPL and PNL using the conical nozzle reference lines established in Section 7.1.

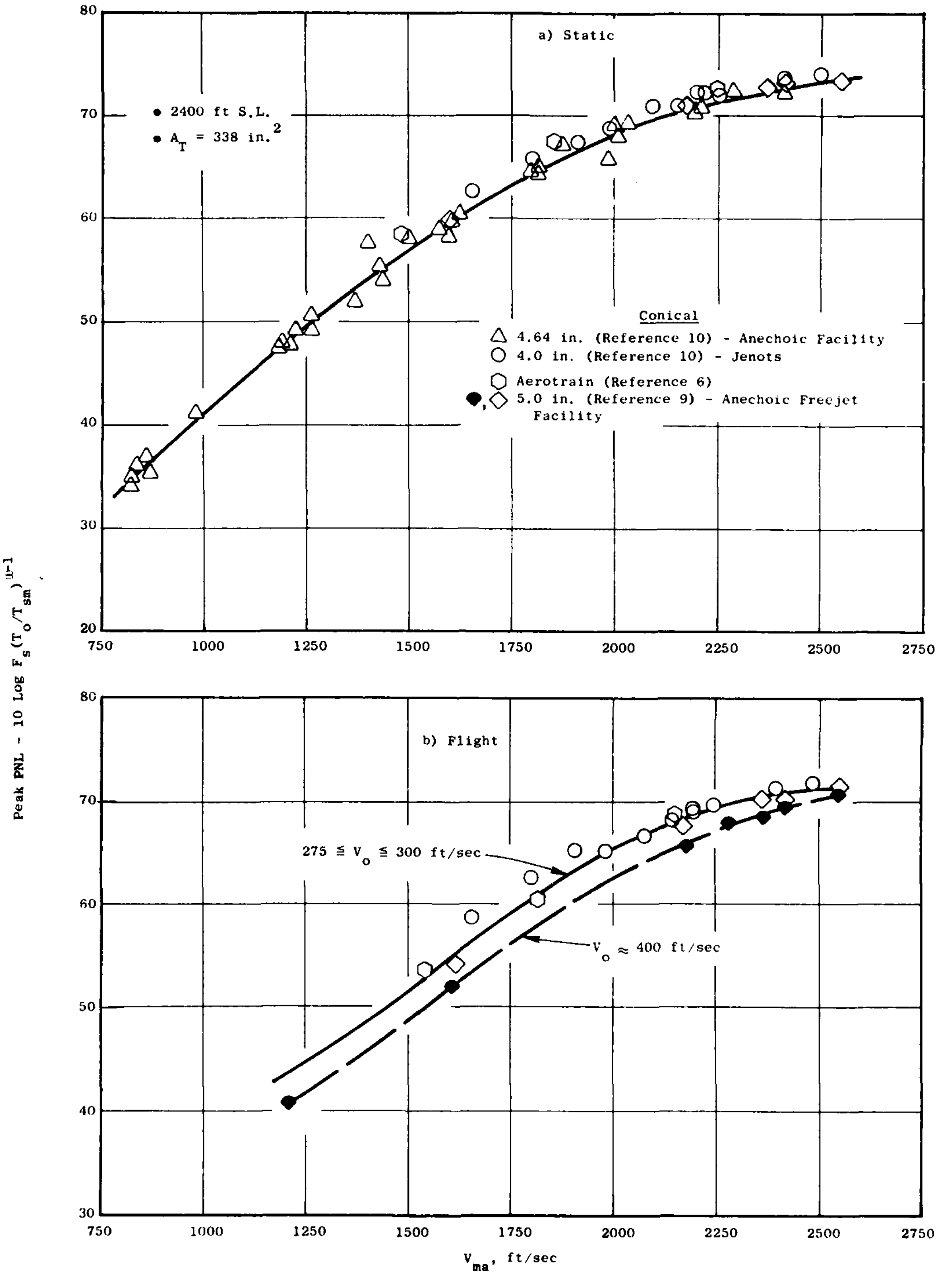

Figure 7-1. Conical Nozzle Static and Flight Peak PNL Noise Characteristics.

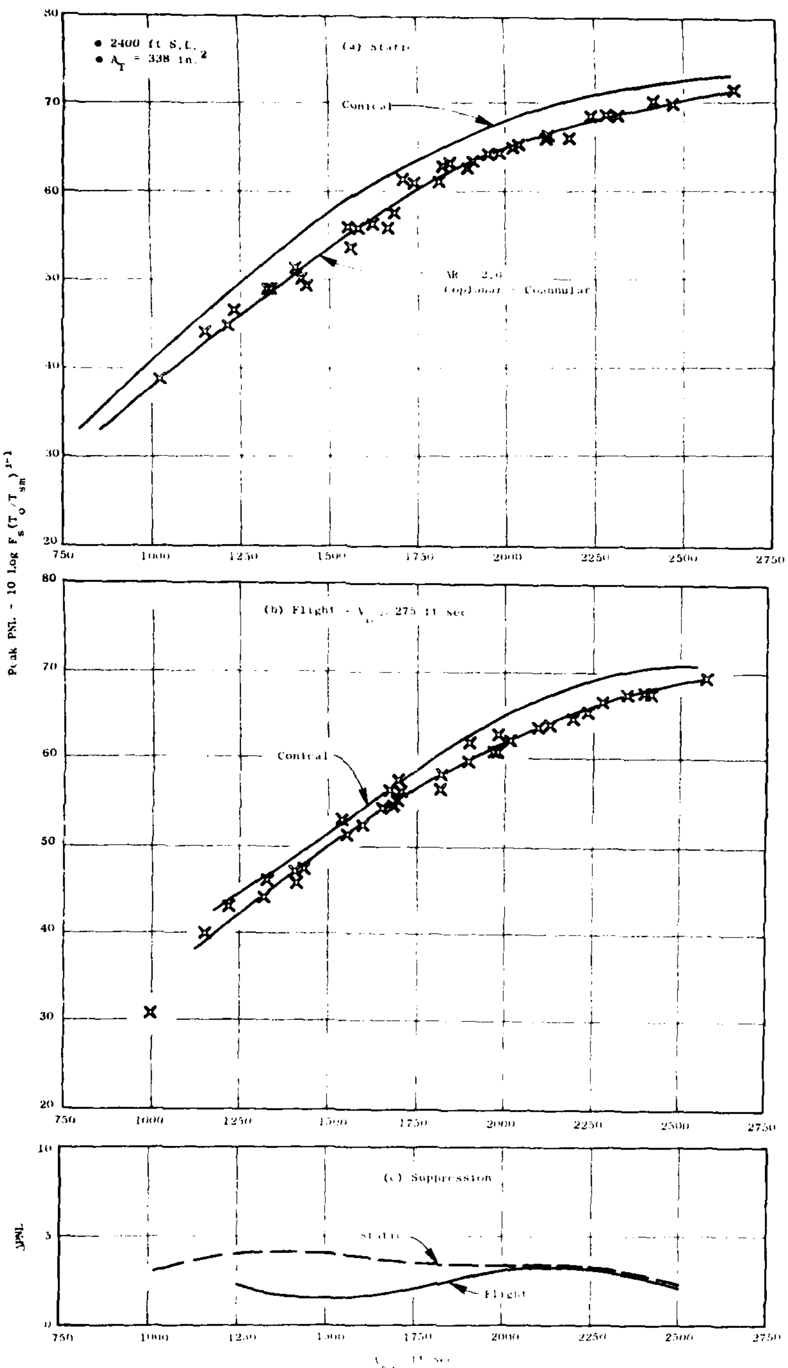

Figure 7-2. AR = 2.0 Coplanar Coannular Nozzle Peak PNL Noise Characteristics.

7.2.1 Peak Noise Trends

The peak PNL and OASPL levels as a function of jet velocity are presented in Figures 7-3 through 7-8 for the five suppressor nozzle configurations. Generally, the data presentation herein suggest that broad band shock cell noise has little or no effect at the angle of peak noise. Shock noise contamination is, however, apparent in the front quadrant ($\theta_I \geq 90°$) and is discussed in Sections 7.2.2 and 7.4.2. The 32-chute nozzle, Figure 7-3, demonstrated suppression levels from 4 to 13 PNdB, with the maximum suppression occuring in the 2100 to 2300 ft/sec mass average velocity range. OASPL suppression trends are different than the PNL characteristics, indicating that the maximum low frequency suppression occurs at a jet velocity of 1750 ft/sec.

The 40-shallow-chute nozzle static data are summarized on Figure 7-4. There is a wide variance of suppression level at a given mass average velocity. The variance is explained by examining the different combinations of outer and inner stream cycle conditions which may be used to produce the same mass average velocity. The noise and suppression characteristics of the 40-shallow-chute nozzle are, therefore, summarized for several cycle types on Figure 7-5 The suppressor is most effective when the inner flow is reduced to zero, Figure 7-5(a). Suppression levels in excess of 14 PNdB were measured. Mass average velocity was also varied holding velocity ratio constant, however, in all cases the inner pressure ratio was less than supercritical, which eliminated shock noise in the inner stream. The data appear to form a continuous line as a function of jet velocity for this series of data points. Suppression levels vary from 3 to 12 PNdB and peak in the mass average velocity range of 1750 ft/sec.

Cycles where the inner stream to outer stream weight flow ratio is held constant result in the poorest suppression characteristics. This is illustrated in Figure 7-5(c). Suppression for these types of cycle range from 7 to 10 PNdB, with maximum suppression occurring at a jet velocity of 1850 ft/sec. Comparison of the peak noise characteristics for the various cycle conditions is presented in Figure 7-4 showing a maximum variance of 5 PNdB at a given cycle condition.

The peak noise levels and corresponding suppression levels for the 36 C-D chute nozzle are summarized on Figure 7-6. This configuration has an outer to inner flow area ratio of 3.62. The results of the studies discussed in Reference 10 show that as outer to inner flow are ratio increases the variation of suppression due to changing inner flow condition is minimial. This observation is supported by comparing the scatter at a given mass average velocity between the 40-shallow-chute nozzle and this configuration. The 36-chute nozzle incorporates a (convergent-divergent) chute configuration which was designed to be shock free at a pressure ratio of 3.0. The PNL data points obtained at the design point are designated by a separate symbol. Comparison of these data with data obtained at off-design outer stream pressure ratio indicates that this design feature did not significantly improve the peak noise suppression levels. The suppression levels achieved using this design range from 2 to 13 PNdB, with a maximum occurring a mass average velocity of

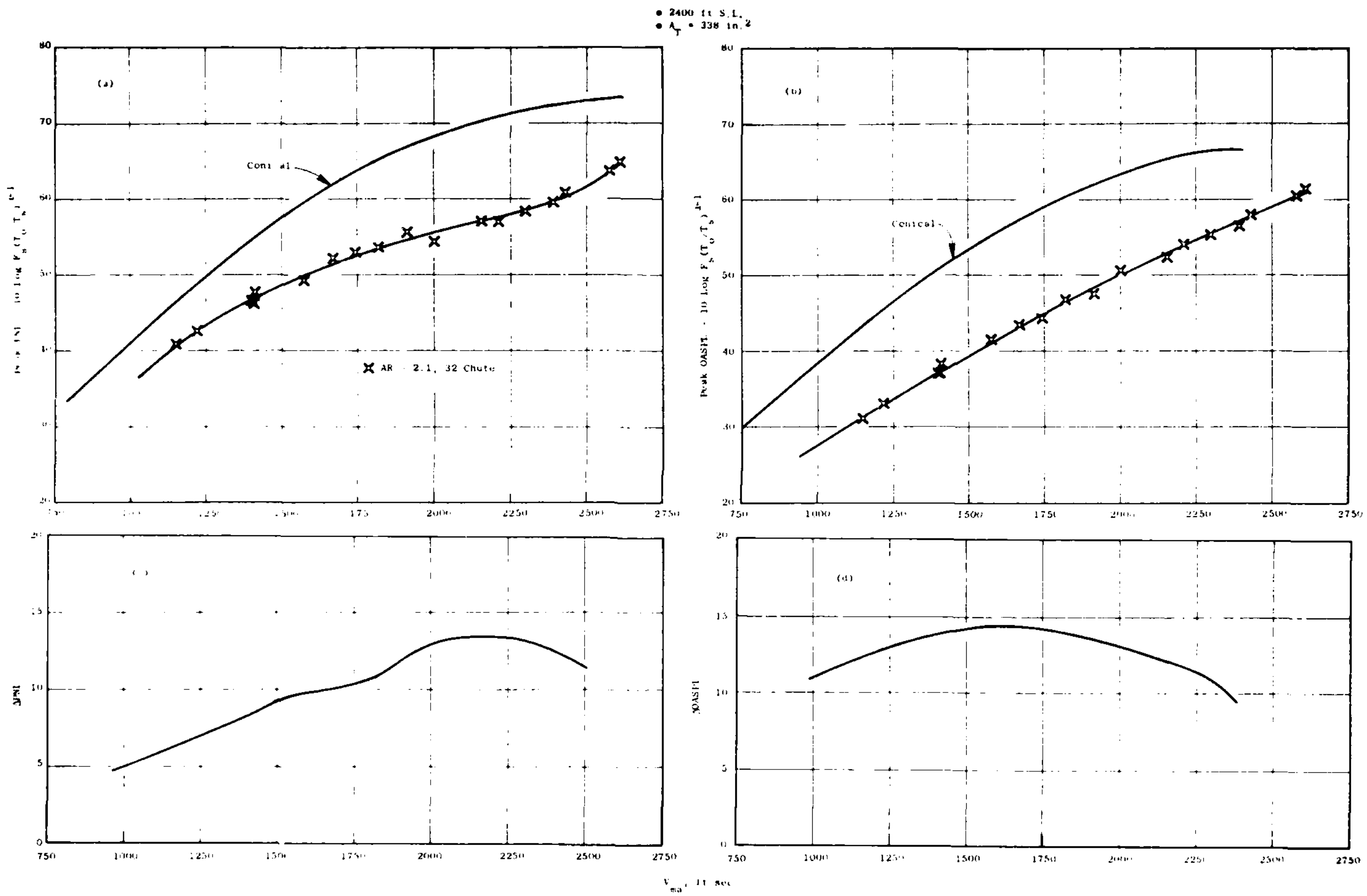

Figure 7-3. 32-Chute Static Peak Noise Characteristics.

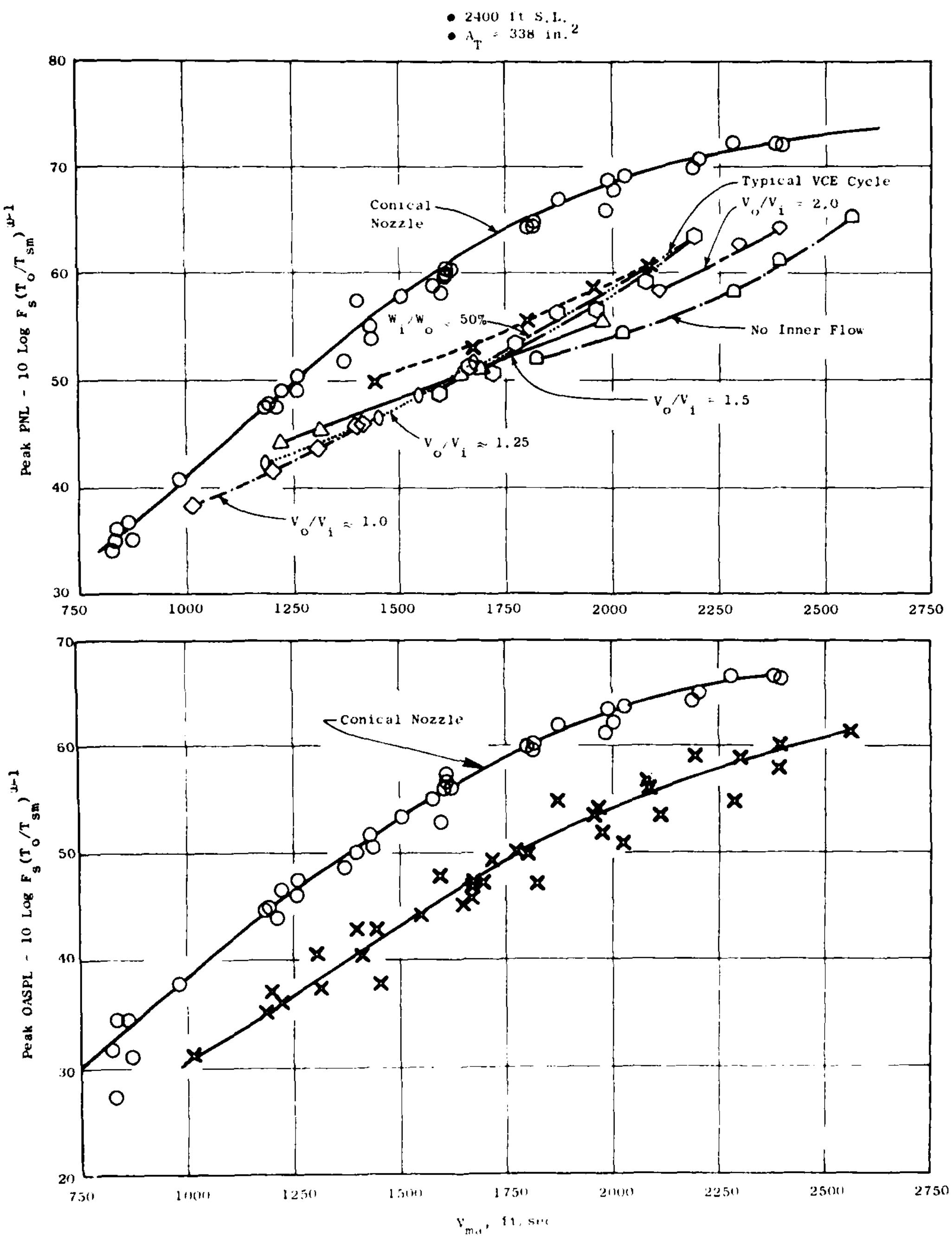

Figure 7-4. AR = 1.75 40 Shallow-Chute Peak Noise Characteristics.

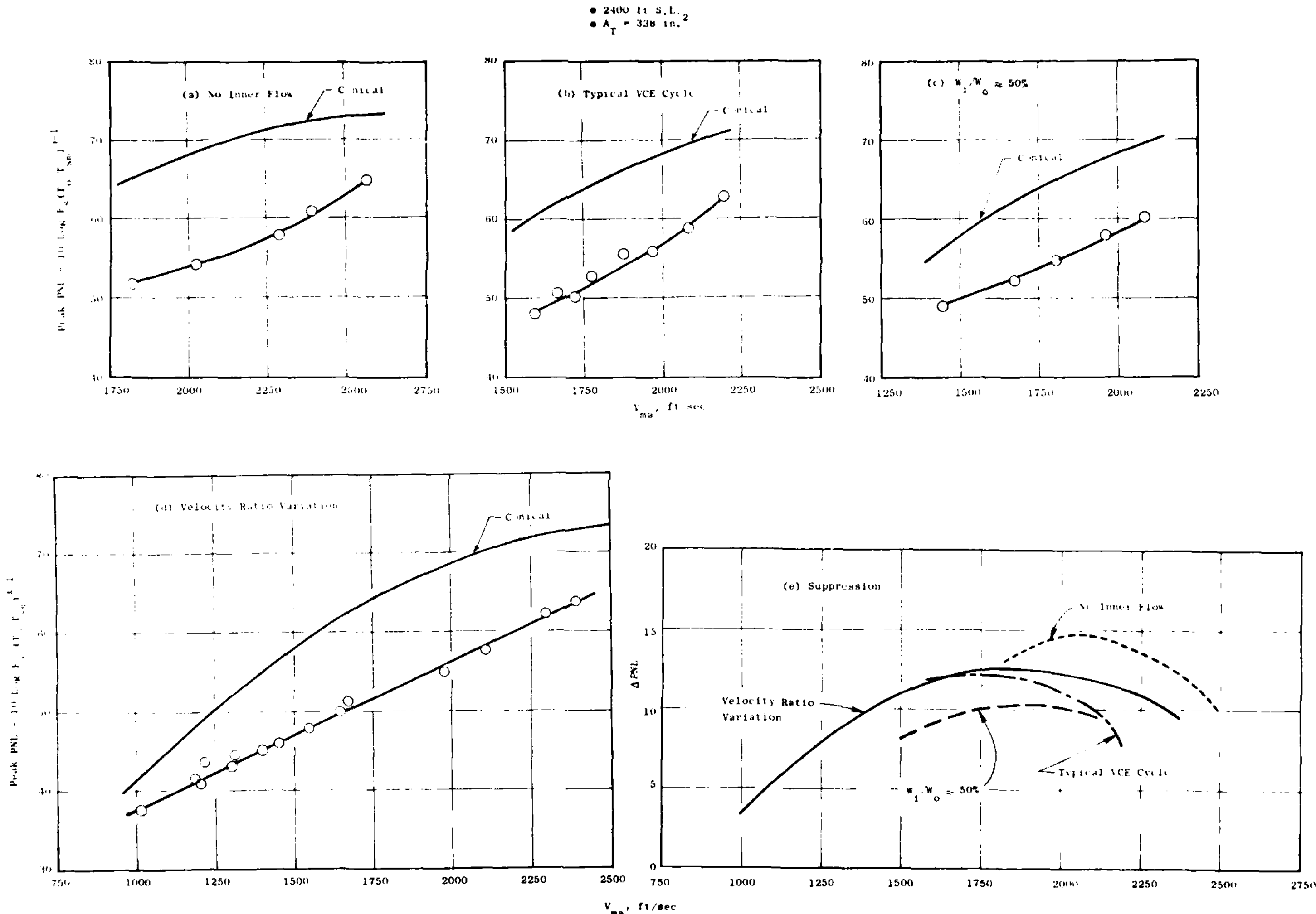

Figure 7-5. Impact of Cycle Variation on the 40 Shallow Chute Noise Characteristics.

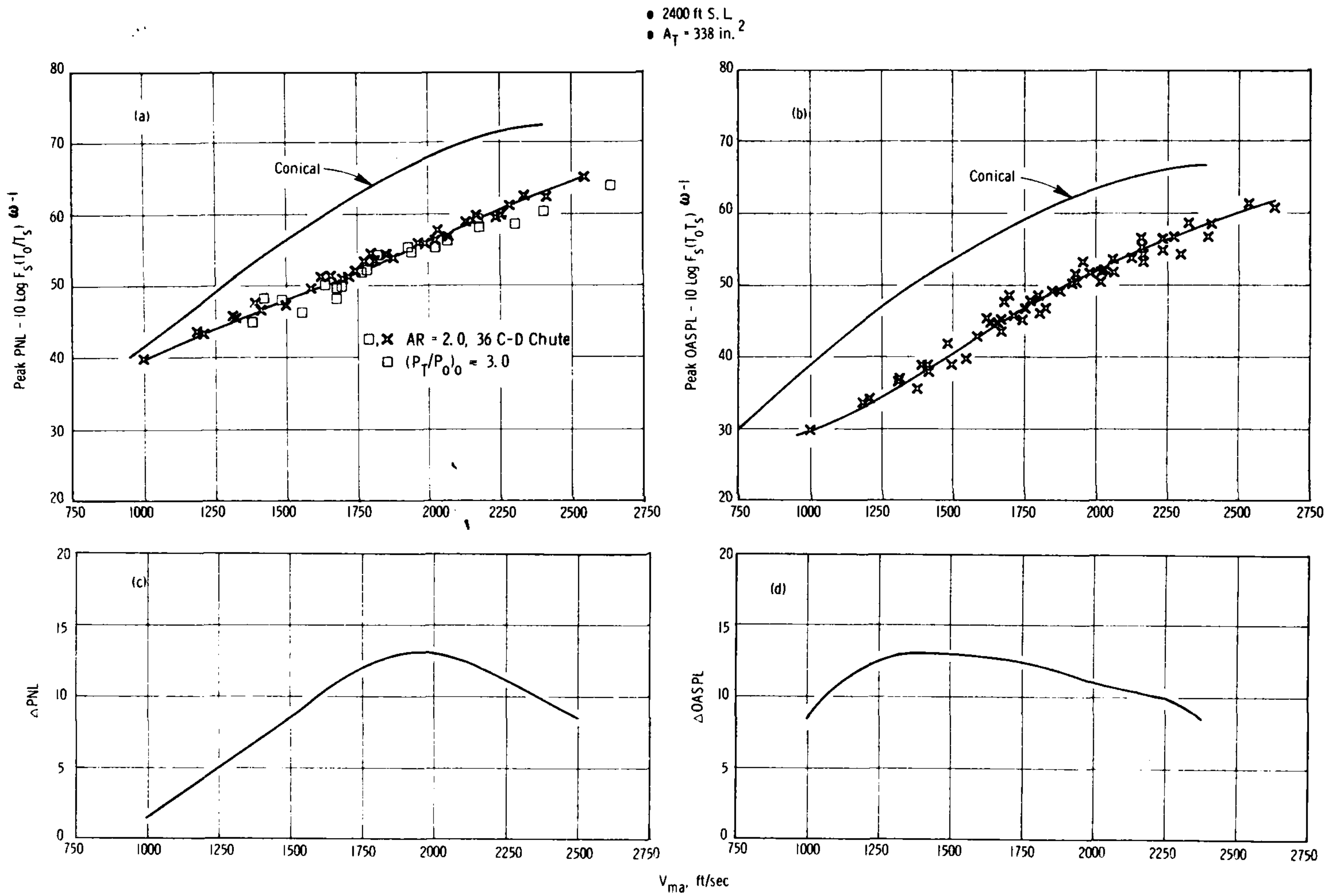

Figure 7-6. AR = 2.0 36 C-D Chute Nozzle Peak Noise Characteristics.

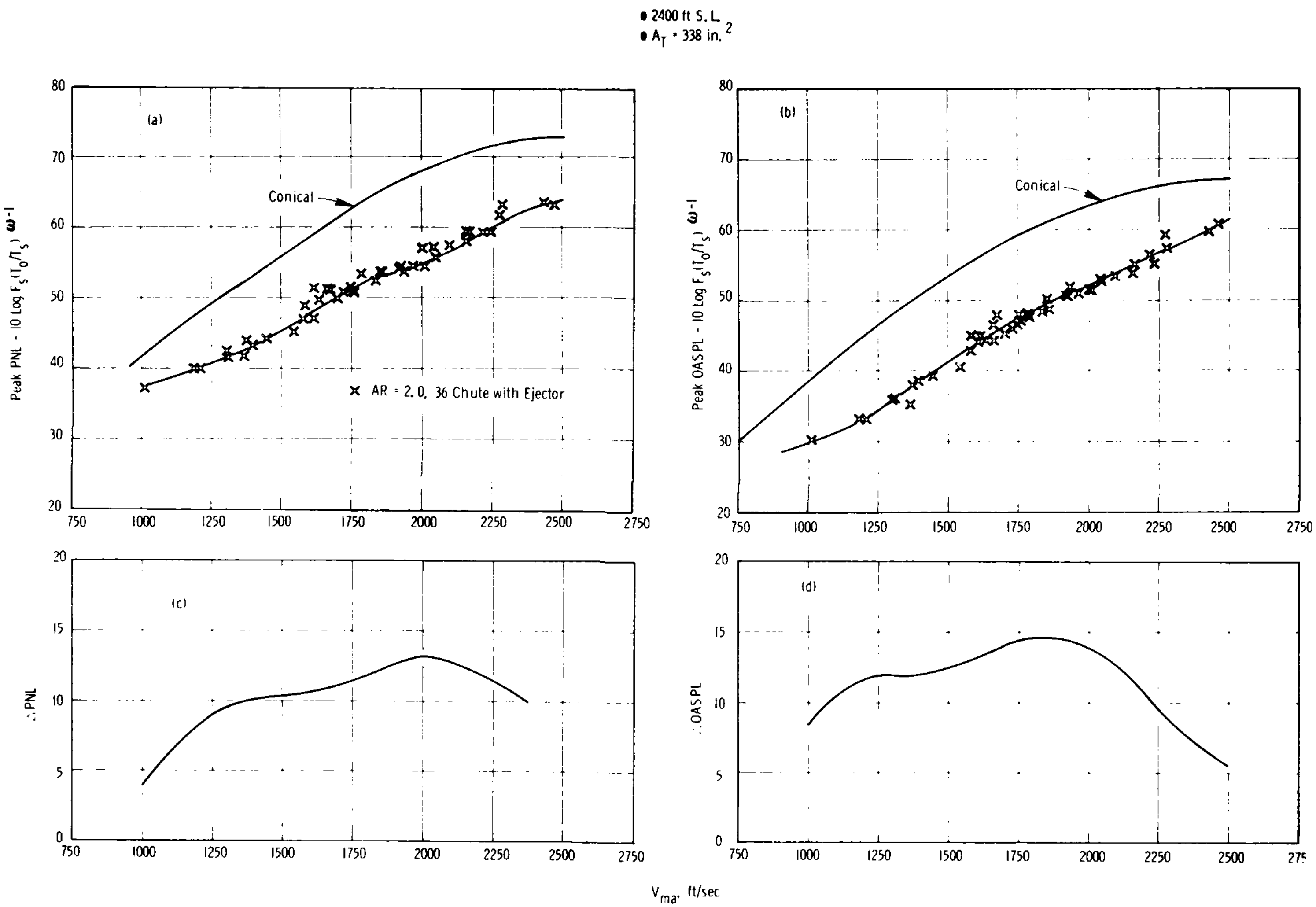

Figure 7-7. 36 C-D Chute with Treated Ejector Peak Noise Characteristics.

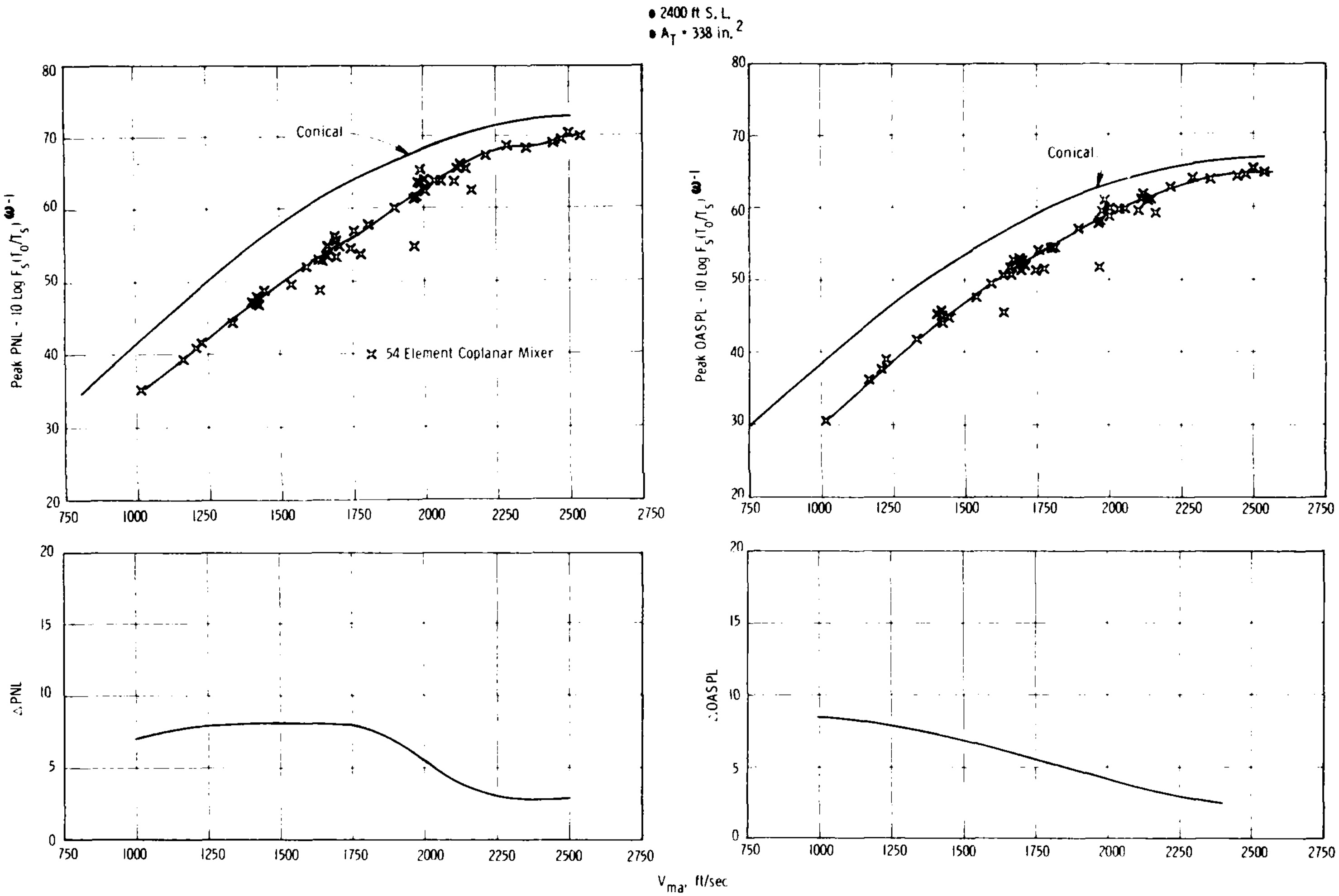

Figure 7-8. 54 Element Coplanar Mixer Peak Noise Characteristics.

2000 ft/sec. The maximum suppression occurs when the inner flow velocity is reduced to zero. The same trend is observed for the 40-shallow-chute nozzle. The data points with no inner flow may be eliminated because of the lack of practical application in a dual flow engine, and the peak noise suppression is then reduced to 12 PNdB.

The 36-chute nozzle was also tested using a treated ejector nozzle; these results in terms of peak noise and suppression levels are summarized on Figure 7-7. The suppression characteristics of this configuration also do not show a strong sensitivity to cycle variation. Suppression levels of 4.5 thru 13 PNdB were measured with the maximum suppression level occurring at 2000 ft/sec. Comparison of the suppression levels with and without the ejector indicate that the addition of the treated ejector results in little or no suppression improvement above a mass average velocity of about 1750 ft/sec. Some improvement in suppression due to incorporation of the ejector was found at the lower mass average velocities.

Peak PNL and OASPL noise levels are presented as a function of jet velocity on Figure 7-8 for the final configuration evaluated, the 54-element coplanar mixer nozzle. The suppression characteristics of this configuration were different than the previous configurations. The suppression levels are also summarized on Figure 7-8. The peak noise suppression levels based on a mean line fitted through the data range from 2 through 8 PNdB, with the maximum suppression level occurring at mass average velocities of 1250 to 1750 ft/sec. This configuration was not as effective as the previous nozzles in causing peak noise reduction and the largest suppression occurred at a much lower mass average velocity than for the other designs.

Laser velocimeter measurements were made in terms of mean velocity decay characteristics to determine the reasons for the poor suppression characteristics of this design at mass average velocities above 2000 ft/sec. The results are summarized on Figure 7-9 which shows three lines labeled A, B, and C. Line A represents the mean velocity decay characteristics of a conical nozzle as a function of normalized axial distance. Line B defines the peak mean velocity decay characteristics of the 40-shallow-chute nozzle, and is typical of most multielement suppressor nozzles. Line C is the measured peak velocity decay rate for the 54-element coplanar mixer nozzle. The 54-element coplanar mixer enhance the mean velocity decay rate to the same degree as the 40-shallow-chute nozzle. This is the reason why this design has poor suppression characteristics. Also, after the initial velocity decay between $0 < X/D \leq 2$, the plateau velocity level which occurs between $2 < X/D < 8$ correlates with the mass average velocity. Additional static acoustic data points were obtained on this configuration to determine if the suppression level could be improved through varying the inner and outer flow cycle conditions.

If the bypass stream (equivalent to inner in other dual flow nozzles) velocity is reduced to zero, the acoustic characteristics of the 54-element coplanar mixer nozzle should be identical to a 54-spoke nozzle having an area ratio of 1.5. The suppression characteristics of the spoke nozzle have been demonstrated to be good. Three series of measurements were made holding the

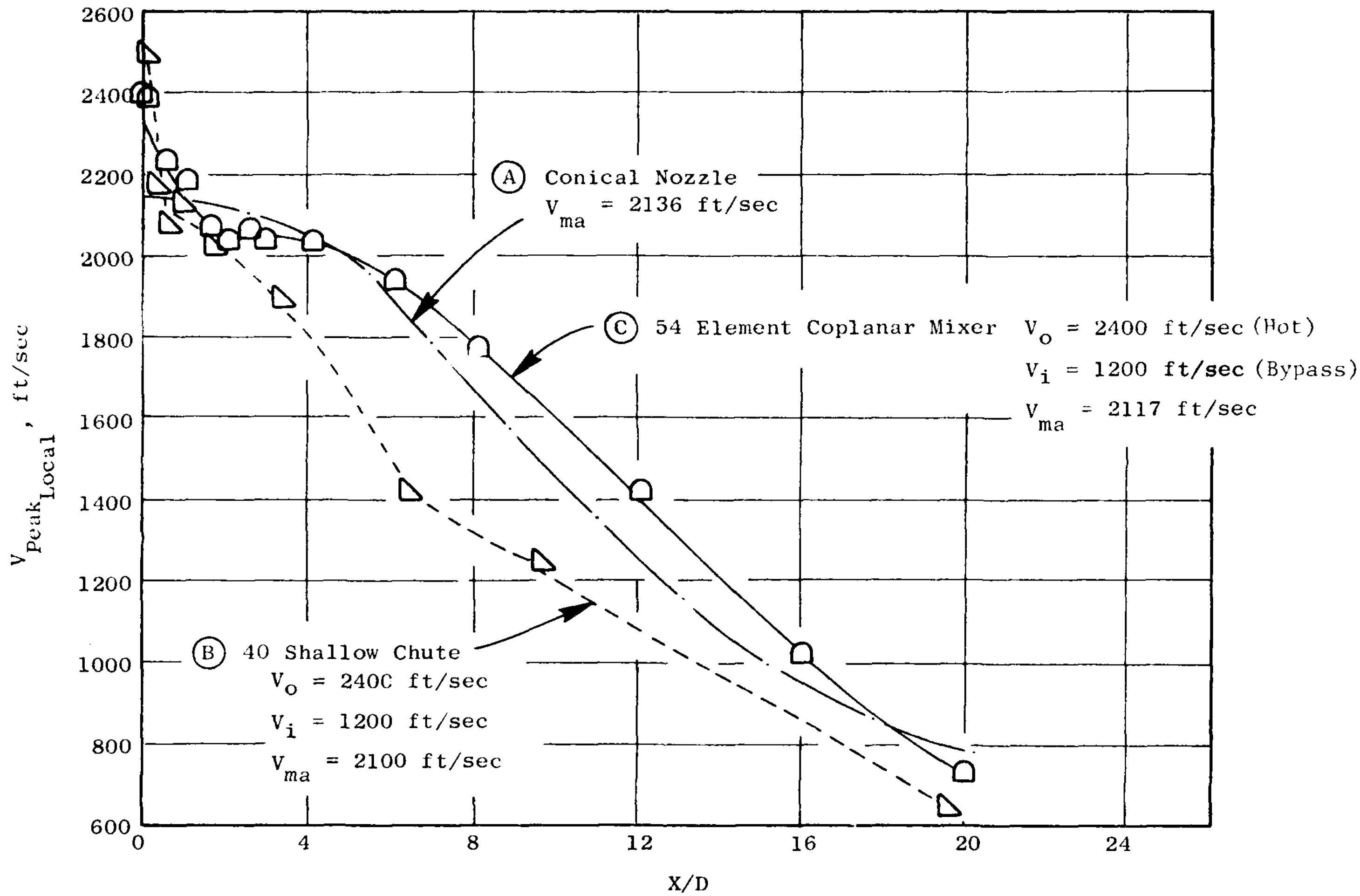

Figure 7-9. Comparison of Peak Mean Velocity Decay Characteristics.

hot (outer) stream conditions constant at nominal velocities of 1630 ft/sec, 1970 ft/sec, and 2400 ft/sec. The results of this study are summarized on Figure 7-10. Each cycle excursion, while holding the outer stream conditions constant, is designated by A, B, and C corresponding to the outer stream velocities of 2400 ft/sec, 1970 ft/sec, and 1630 ft/sec, respectively. Excursion "A" shows that, as the bypass (inner) stream velocity approaches zero, the suppression is improved from 4 to 8 PNdB relative to the mean line placed through the data. Similar comparisons for cycle excursions "B" and "C" show suppression improvements from 6 to 13 PNdB and from 7.5 to 11.5 PNdB. Cycle excursions "B" and "C" are significant in that zero core flow was achieved, whereas, for excursion "A", the lowest bypass (inner) stream velocity achieved was 432 ft/sec. The results of this study demonstrate that the static peak noise suppression characteristics of the 54-element coplanar mixer nozzle are improved significantly by controlling the velocity ratio between inner and outer streams.

The static peak noise suppression characteristics for all five suppressor configurations in terms of ΔPNL are summarized on Figure 7-11. Each configuration is unique in that the suppression characteristics as a function of velocity change for each nozzle. The maximum suppression level achieved was 14 PNdB utilizing the 40-shallow-chute nozzle with no inner flow. The 32-chute nozzle was second with 13 PNdB. Suppressing only the outer stream of dual flow nozzles was found to be slightly less effective than suppressing the entire stream on a single flow nozzle. The loss in suppression is between 1 and 2 PNdB.

7.2.2 PNL and OASPL Directivity Trends

In addition to the peak noise reduction of suppressor nozzles, the directivity characteristics are also important and are discussed in detail in Section 7.4 in conjunction with the flight data. Some general characteristics are also discussed in this section. The 50° and 90° acoustic angles can be used to illustrate the trends. The 90° peak PNL and OASPL levels for the five configurations are summarized on Figures 7-12 through 7-14. The delta suppression levels achieved using the 32-chute nozzle range from 0 to 7 PNdB, and increase as velocity is increased. 90° suppression levels of the 40-shallow-chute nozzle range from 2.5 to 8 PNdB and increase with increasing velocity. Similar to the trend at the peak noise angle, up to 5 PNdB variation in suppression occurs for given mass average velocity. Suppression levels for the 36-chute nozzle with and without a treated ejector range from 0 to 6 PNdB. In contrast to the 40-shallow-chute nozzle, the suppression level of the 36-chute configurations does not vary significantly at a given mass average velocity. The 90° suppression levels of the 54-element coplanar mixer nozzle range from 3 to 5 PNdB and do not exhibit the large variance with velocity that the peak noise suppression levels do. Overall, the suppression levels at 90° were significantly less than noise measured at the peak noise angle.

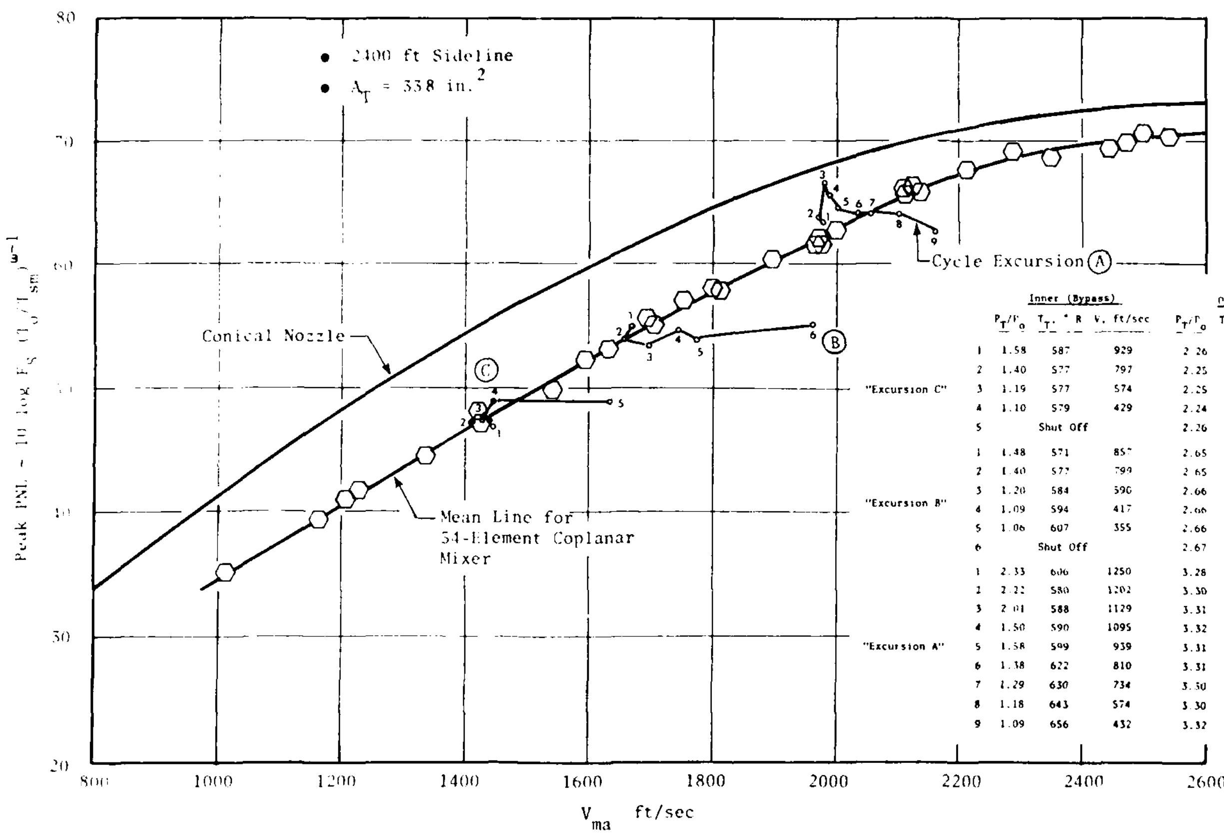

		Inner (Bypass)			Outer (Hot)			Mixed		
		P_T/P_o	T_T, °R	V, ft/sec	P_T/P_o	T_T, °R	V, ft/sec	P_T/P_o	T_T, °R	V, ft/sec
"Excursion C"	1	1.58	587	929	2.26	1070	1635	2.02	924	1421
	2	1.40	577	797	2.25	1067	1629	1.97	935	1415
	3	1.19	577	574	2.25	1074	1634	1.94	[illegible]	1427
	4	1.10	579	429	2.24	1072	1632	1.96	955	1444
	5	Shut Off			2.26	1069	1639	2.26	1069	1636
"Excursion B"	1	1.48	571	857	2.65	1333	1981	[illegible]	1122	1668
	2	1.40	577	799	2.65	[illegible]	1956	2.25	1116	1658
	3	1.20	584	590	2.66	1335	1962	2.25	1165	1695
	4	1.09	594	417	2.66	1328	1963	2.27	1208	1745
	5	1.06	607	355	2.66	1314	1968	2.31	1230	1775
	6	Shut Off			2.67	1306	1967	2.67	1306	1967
"Excursion A"	1	2.33	606	1250	3.28	1626	2387	2.84	1262	1941
	2	2.22	580	1202	3.30	1627	2391	2.82	1266	1977
	3	2.01	588	1129	3.31	1625	2392	2.77	1238	1952
	4	1.50	590	1095	3.32	1622	2392	2.73	1313	1989
	5	1.58	599	939	3.31	1626	2394	2.69	1351	2024
	6	1.38	622	810	3.31	1632	2397	2.67	1403	2037
	7	1.29	630	734	3.30	1633	2396	2.67	1427	2052
	8	1.18	643	574	3.30	1636	2399	2.71	1476	[illegible]
	9	1.09	656	432	3.32	1635	2402	2.79	1516	2163

Figure 7-10. 54-Element Coplanar Mixer Cycle Excursions.

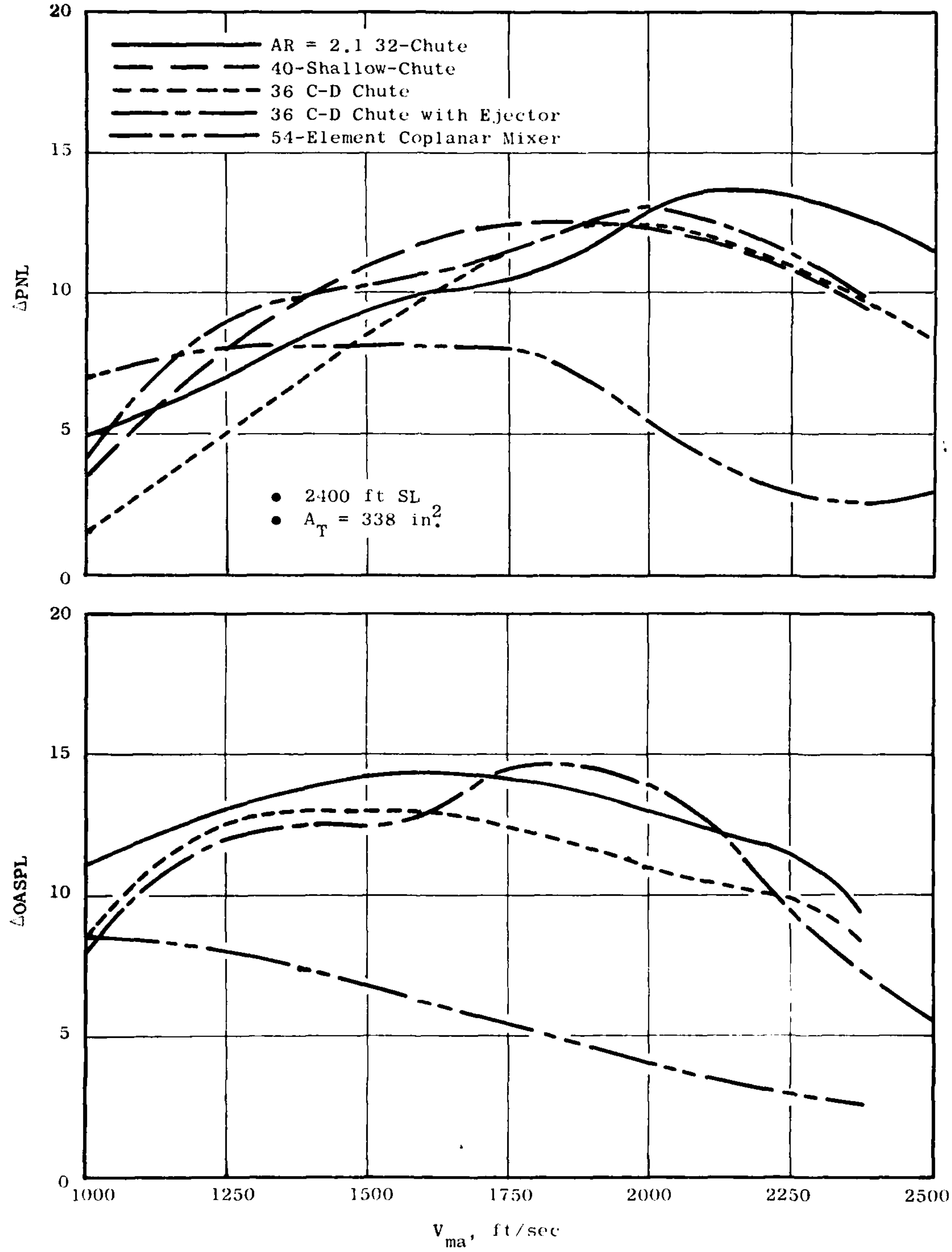

Figure 7-11. Summary of Static Peak Noise Suppression Characteristics.

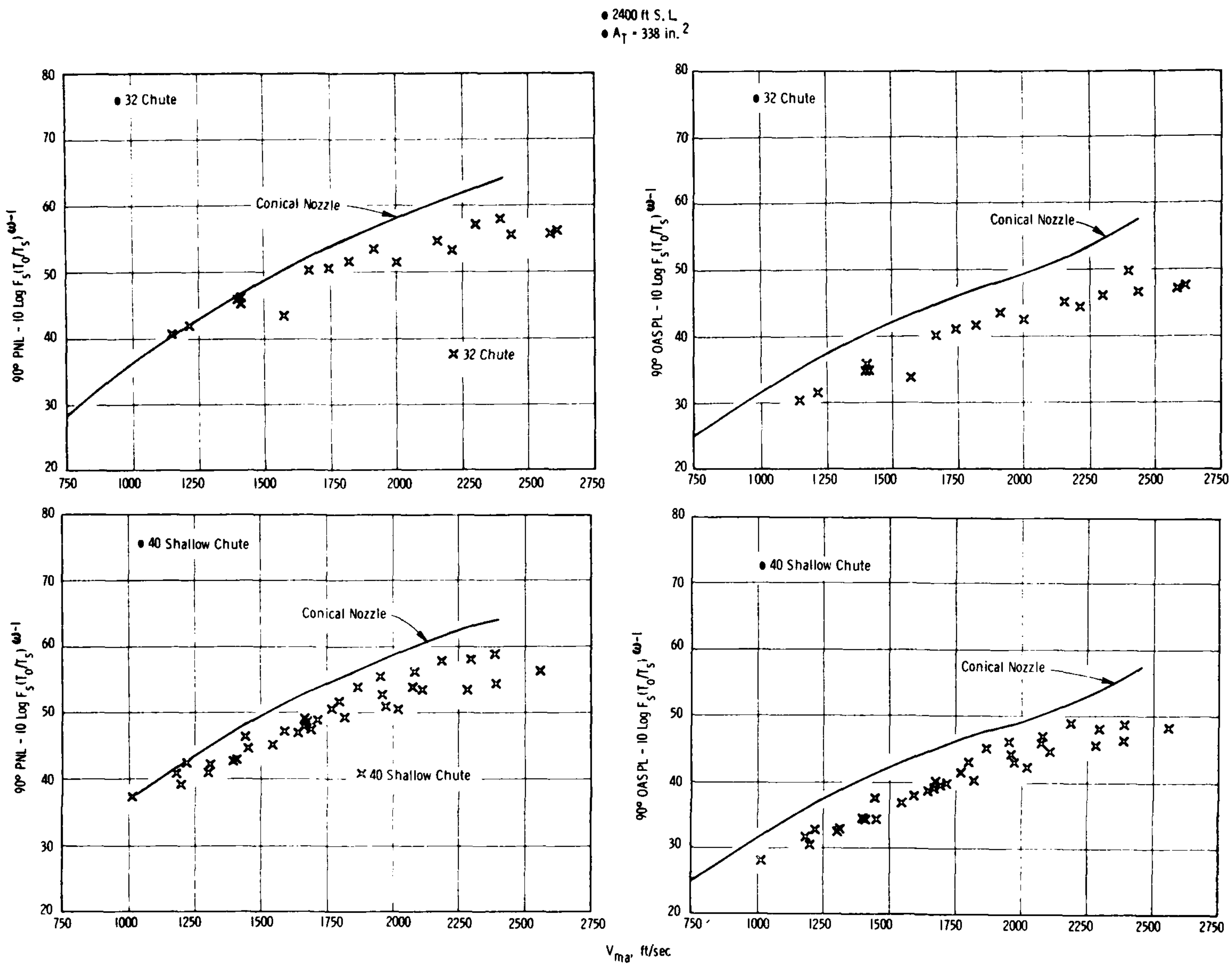

Figure 7-12. 32 Chute and 40 Shallow Chute Nozzle 90° OASPL and PNL Levels.

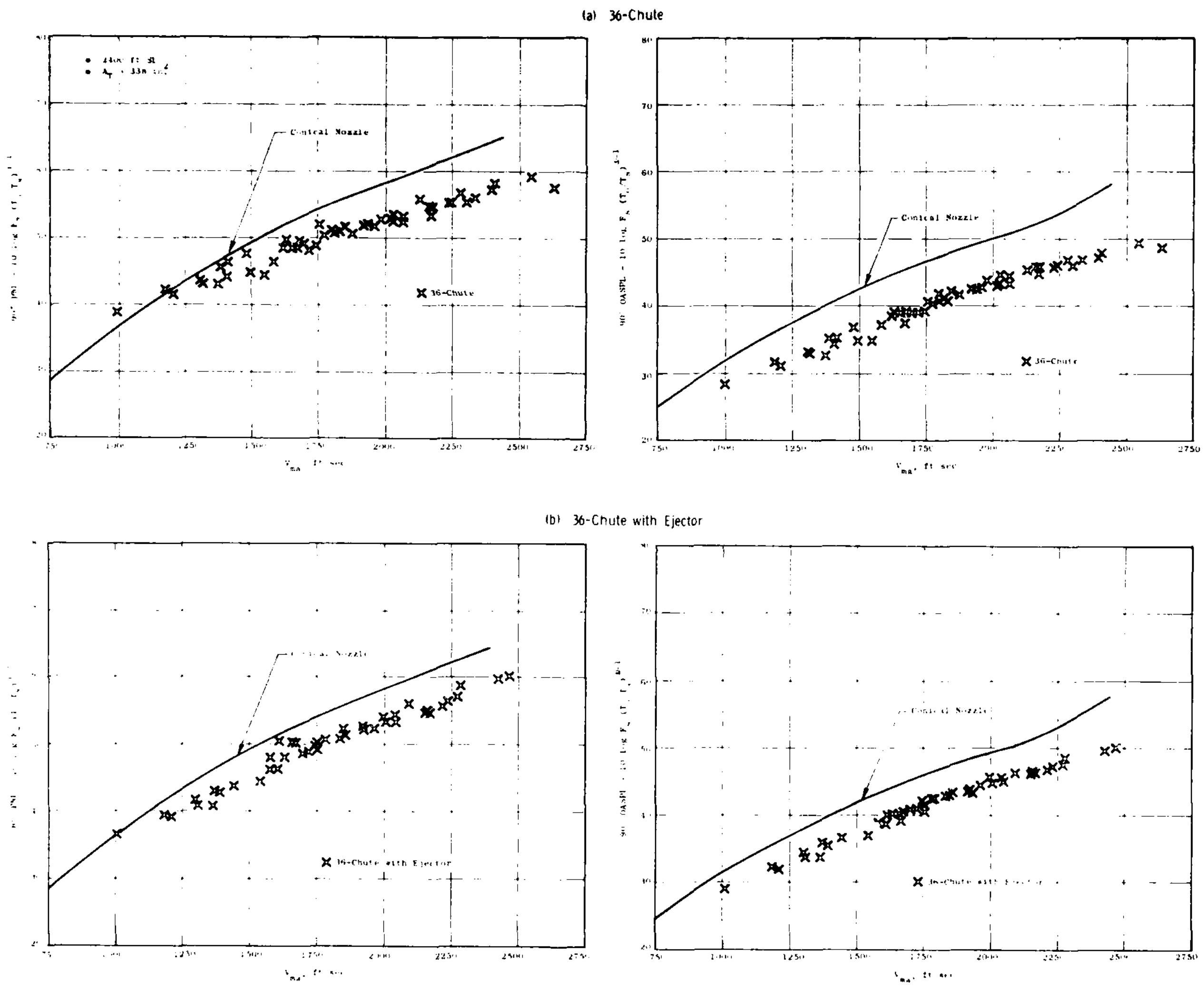

Figure 7-13. 36-Chute and 36-Chute with Treated Ejector Nozzle 90° OASPL and PNL Levels.

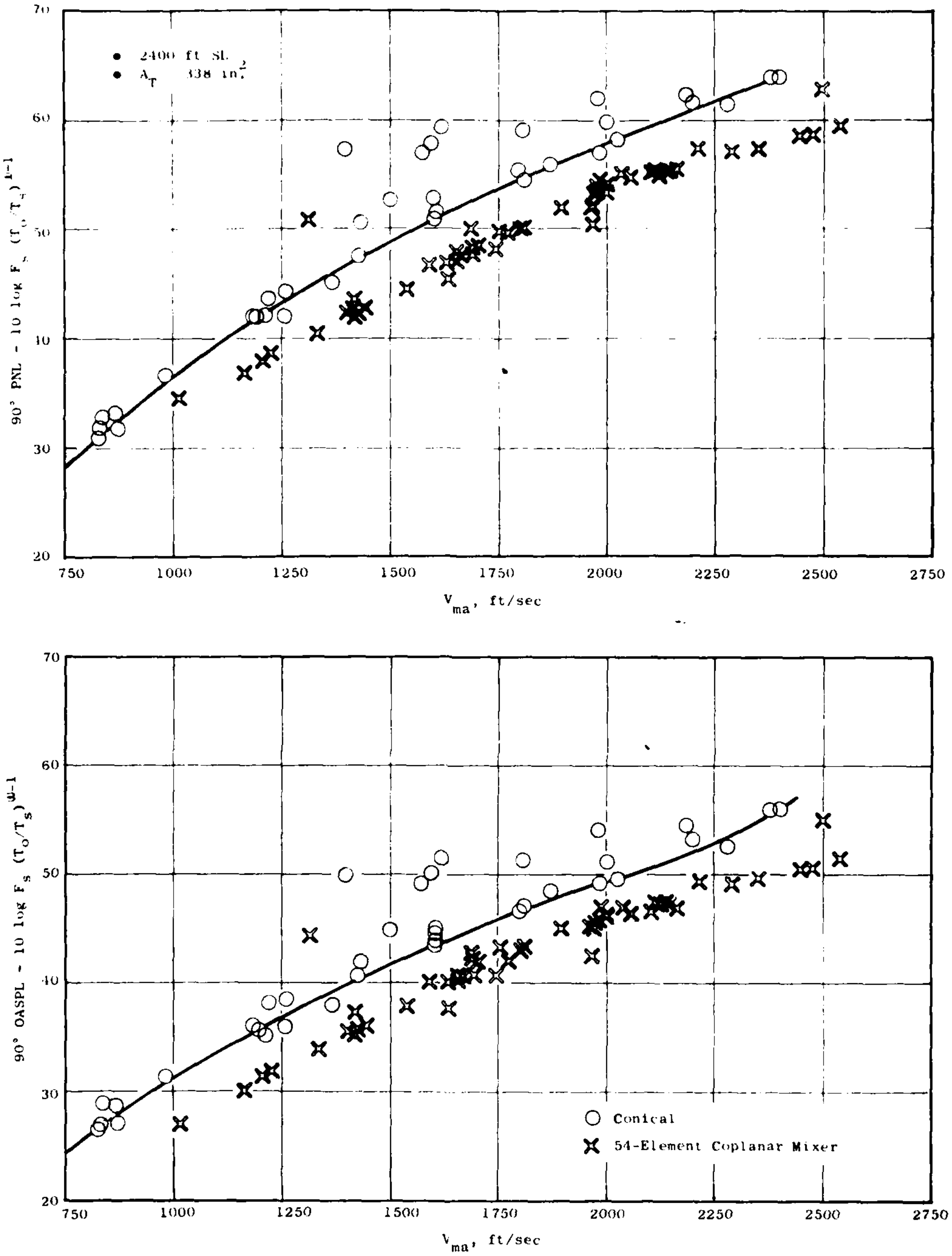

Figure 7-14. 54-Element Coplanar Mixer Nozzle 90° OASPL and PNL Levels.

The 50° acoustic angle is typical of the noise characteristics which occur in the forward quadrant. The conical nozzle, at supercritical pressure ratios, exhibit significant check noise at these angles. Figure 7-15 presents the conical nozzle noise characteristics as a function of mass average velocity and the noise levels are normalized by the conventional parameters used for jet noise. The normalization parameters do not collapse conical nozzle data into a unified line. This was also observed at the 90° inlet angle as shown in Figure 7-14. The data may be scrutinized for contamination by shock noise by plotting the OASPL levels as a function of the parameter β, where β is defined as $\sqrt{M^2-1}$, since conical nozzle shock cell broadband noise has been shown to be essentially nozzle pressure ratio dependent and independent of jet temperature. This result is presented on Figure 7-16.

Clearly the conical nozzle data collapses for this parameter, and also the suppressor nozzle data. This indicates that the OASPL levels based on this criteria, are dominated by shock noise. In addition, the PNL levels at this acoustic angle are also presented and found to correlate well about a line having a β^4 slope. A similar presentation for each of the four remaining suppressor configurations is presented on Figure 7-16 through 7-18. The dual flow data has been plotted as a function of β_{ma}, where β_{ma} is calculated based on the mass averaged flow parameters discussed in Section 7.1. These data also correlate about a line having a β^4 slope. Correlation of the suppressor data about a line having this slope suggests that shock noise is the dominant noise source at this particular acoustic angle. The comparison on absolute level basis between the conical and suppressor nozzles indicates that the suppressors are effective in reducing the shock noise. The suppression of shock noise is found to be constant with β but vary as a function of configuration.

A summary of the PNL and OASPL suppression characteristics at the 50° angle for the five configurations are presented on Table 7-1. The comparisons illustrate that suppression is a function of configuration and that multi-element suppressors are effective in reducing shock noise as well as jet mixing noise.

Figures 7-19 and 7-20 provide a comparison of the normalized PNL levels for the suppressor nozzle, with that of a conical nozzle at two typical velocity conditions. To illustrate how suppression varies with angle at these two conditions, the ΔPNL suppression varies with angle at these two conditions, the ΔPNL suppression is summarized on Figure 7-21 as a function of angle. The maximum suppression is observed to occur at inlet angles between 130° and 150°.

7.2.3 Spectra Trends

Typical static spectrum characteristics are summarized for the five configurations on Figures 7-22 through 7-25. Spectra at three angles, 50°, 90°, and 130° are presented. The spectral plots are shown at two jet velocities since it was recognized in the presentation of peak noise trends that the suppression, which is due to the relative relationship between the high and low frequencies, was a strong function of velocity.

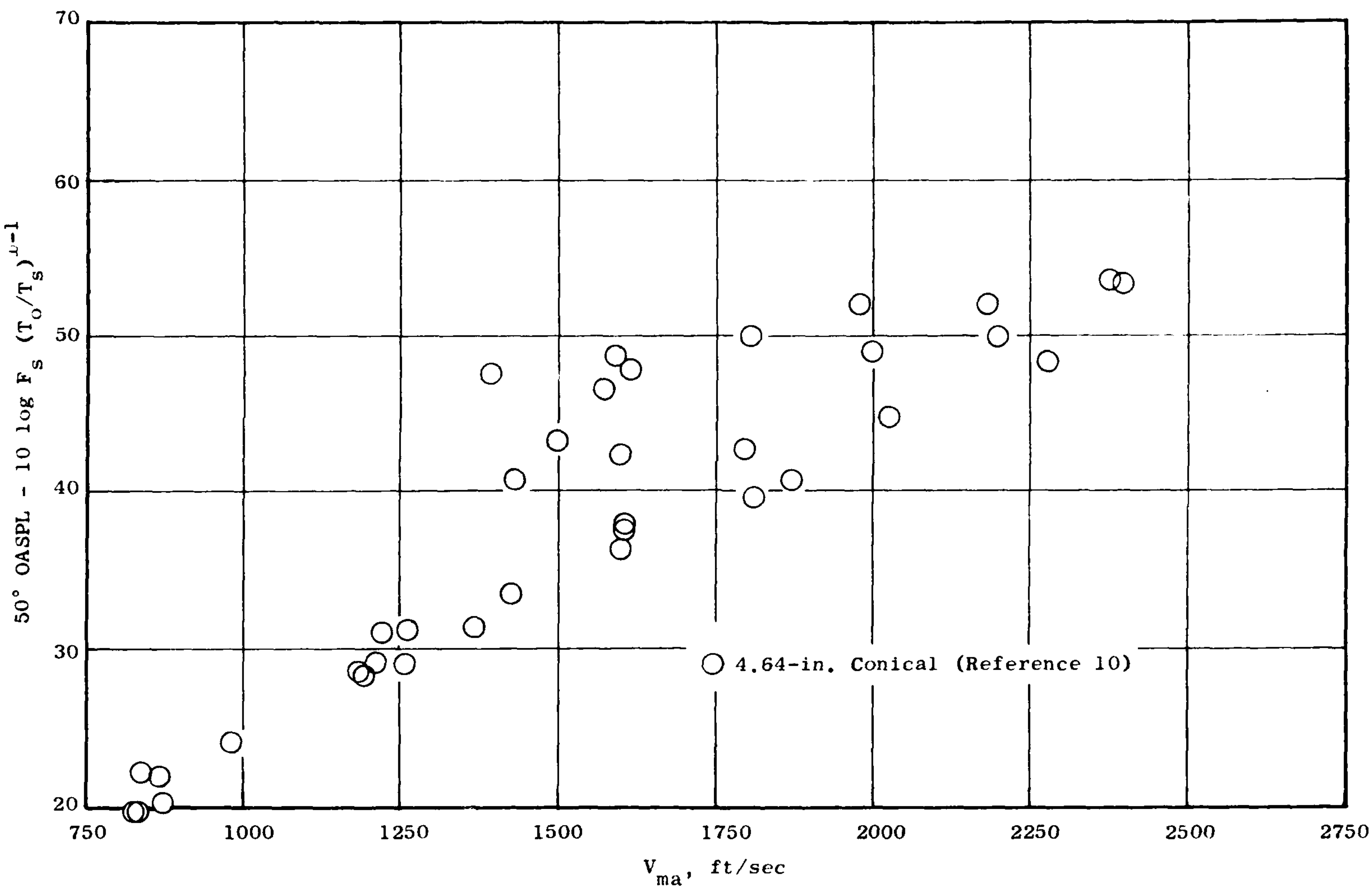

Figure 7-15. Summary of Conical Nozzle 50° Noise Characteristics.

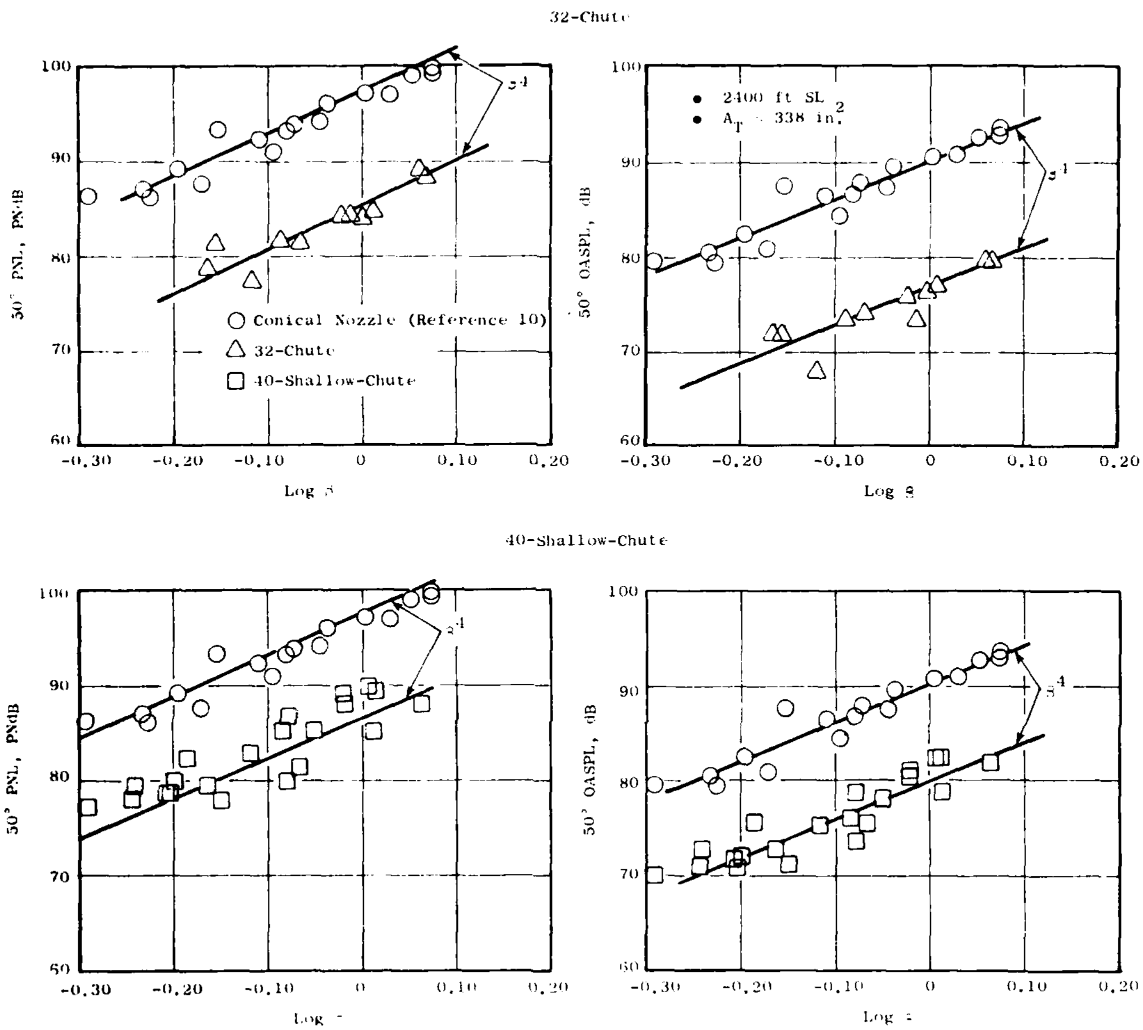

Figure 7-16. 32-Chute and 40-Shallow-Chute Nozzle 50° OASPL and PNL Levels.

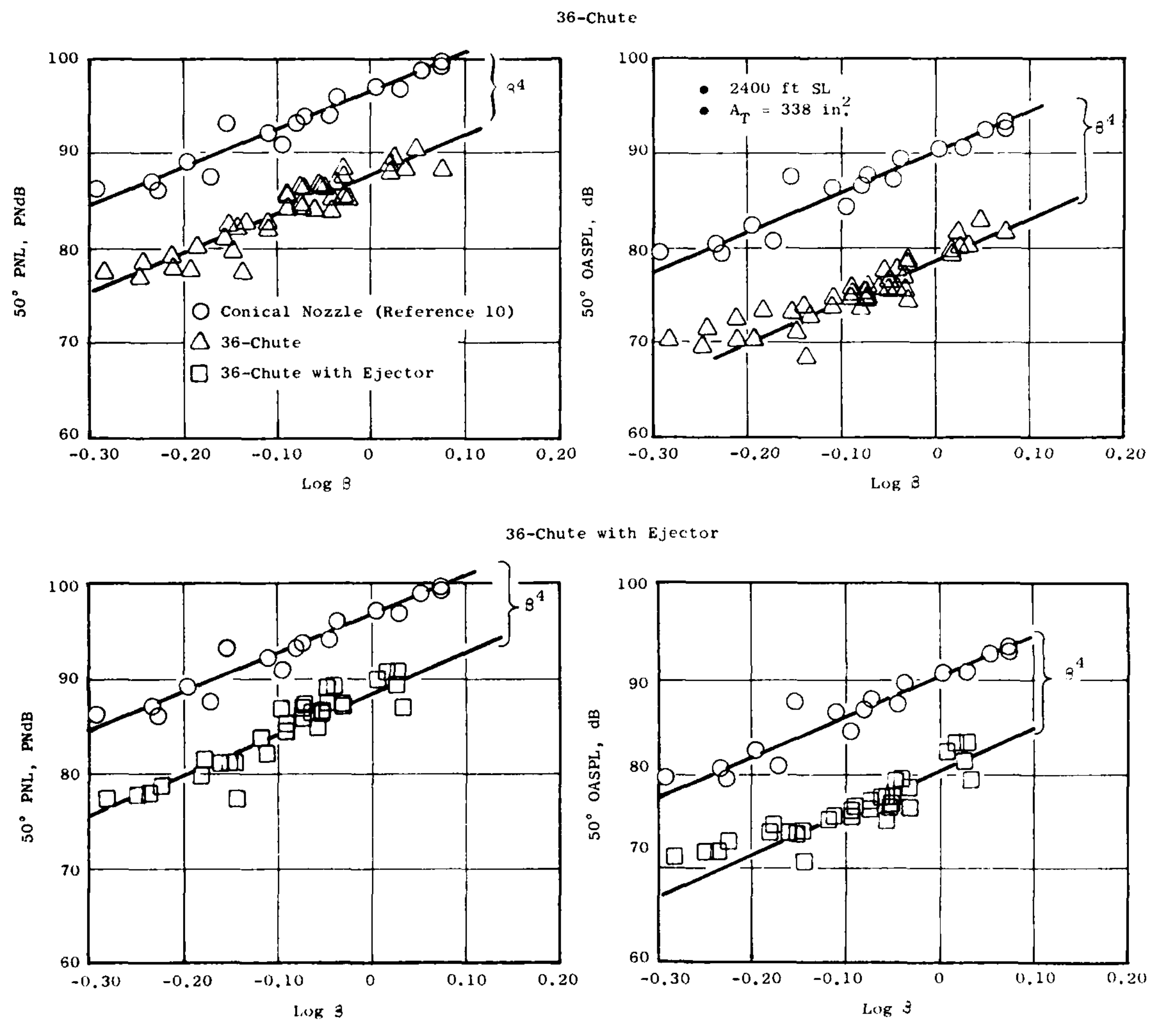

Figure 7-17. 36-Chute and 36-Chute with Ejector Nozzle 50° OASPL and PNL Levels.

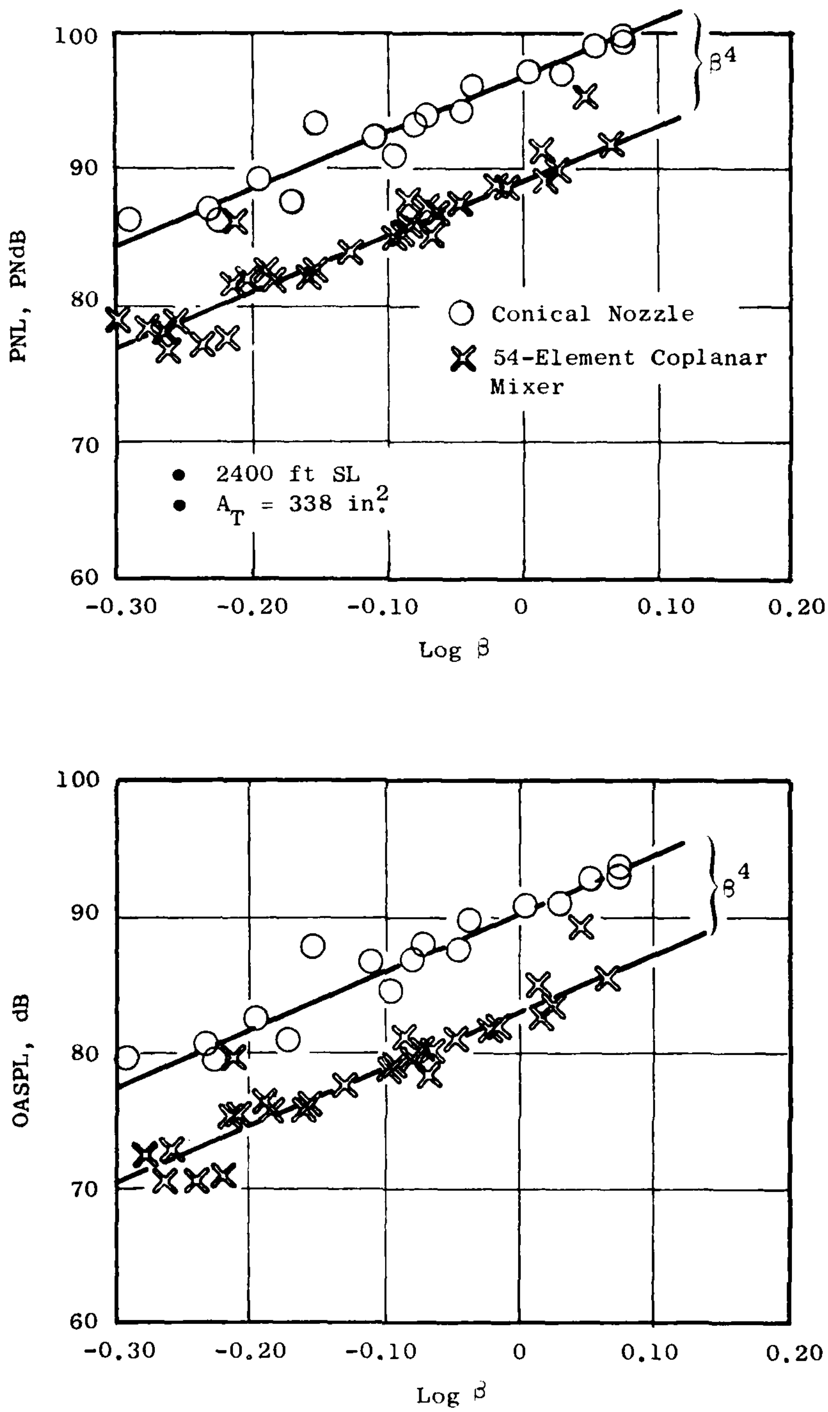

Figure 7-18. 54-Element Coplanar Mixer Nozzle 50° OASPL and PNL Levels.

Table 7-1. Summary of Shock Noise Suppression Characteristics at 50°.

Configuration	ΔPNL*	ΔOASPL*
32-Chute	11.0	12.5
40-Shallow Chute	10.5	10.5
36 C-D Chute	9.0	11.5
36 C-D Chute and Treated Ejector	8.5	10.0
54 Element Coplanar Mixer	7.5	7.0

*ΔPNL and ΔOASPL levels are relative to a mean line placed through the conical nozzle data.

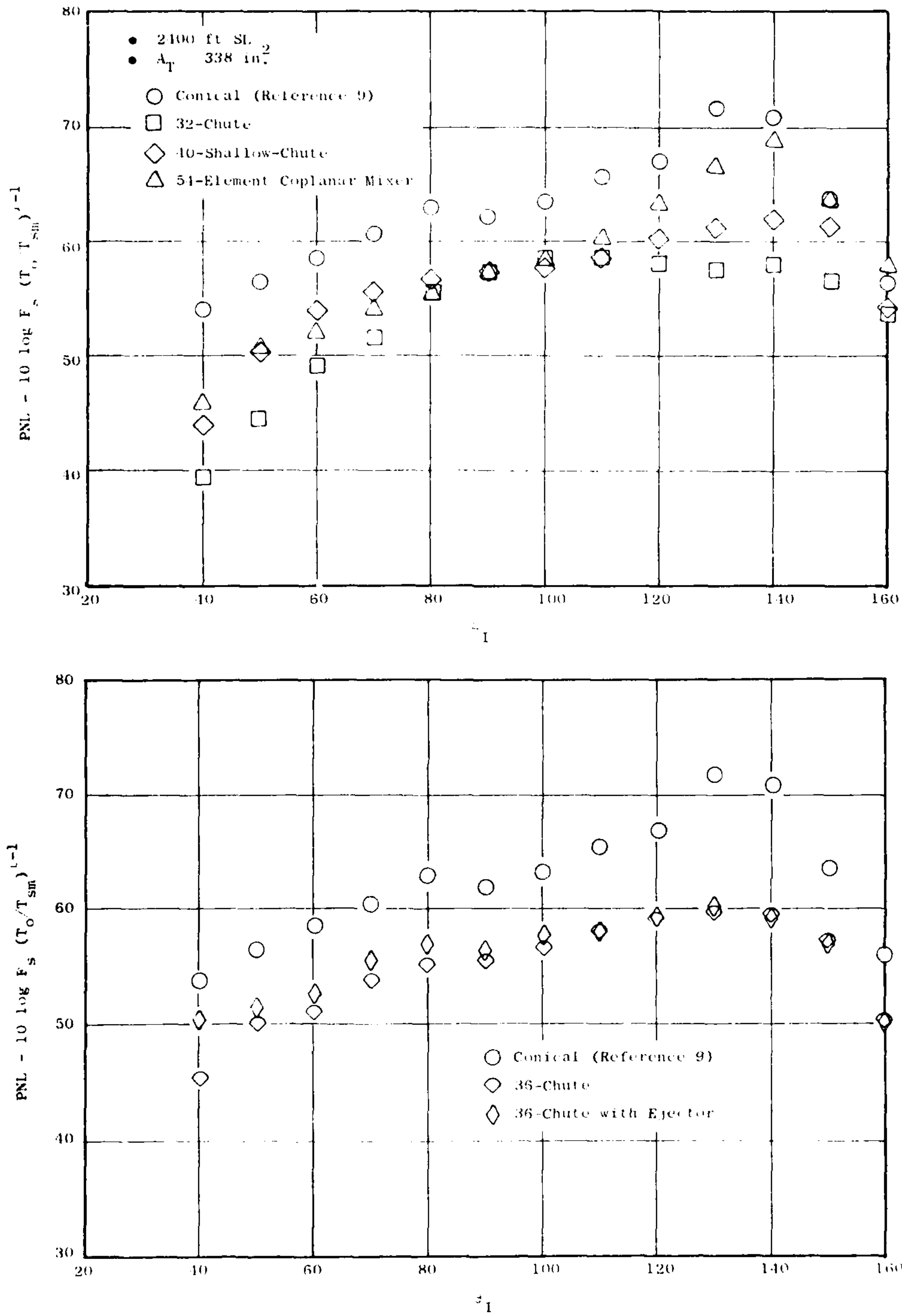

Figure 7-19. Summary of Static PNL Directivity Characteristics - $V_{ma} \approx 2280$ ft/sec.

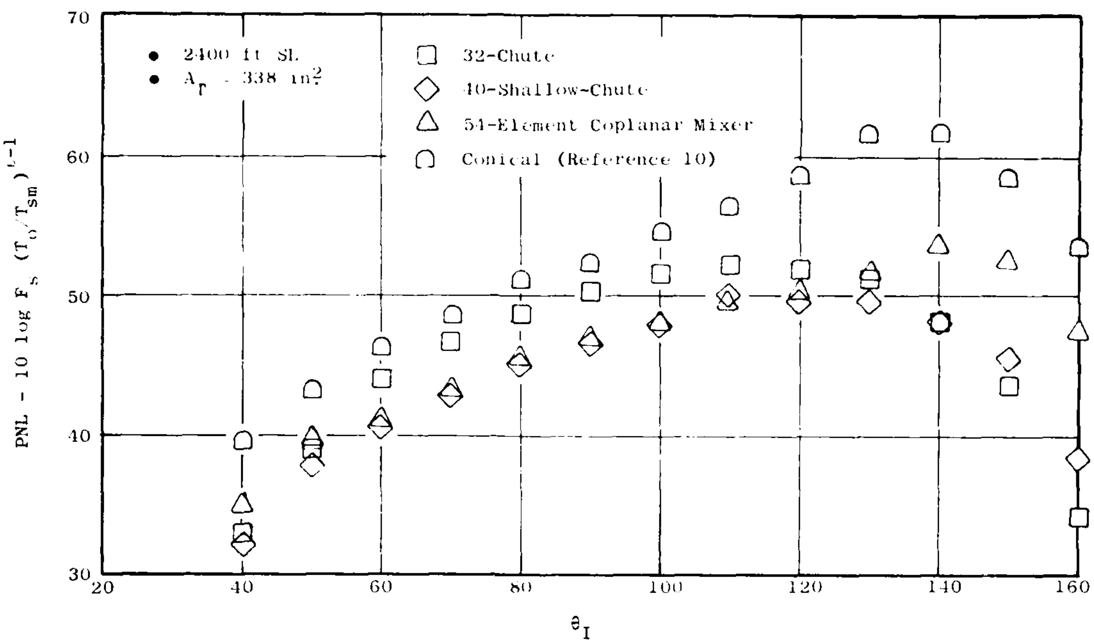

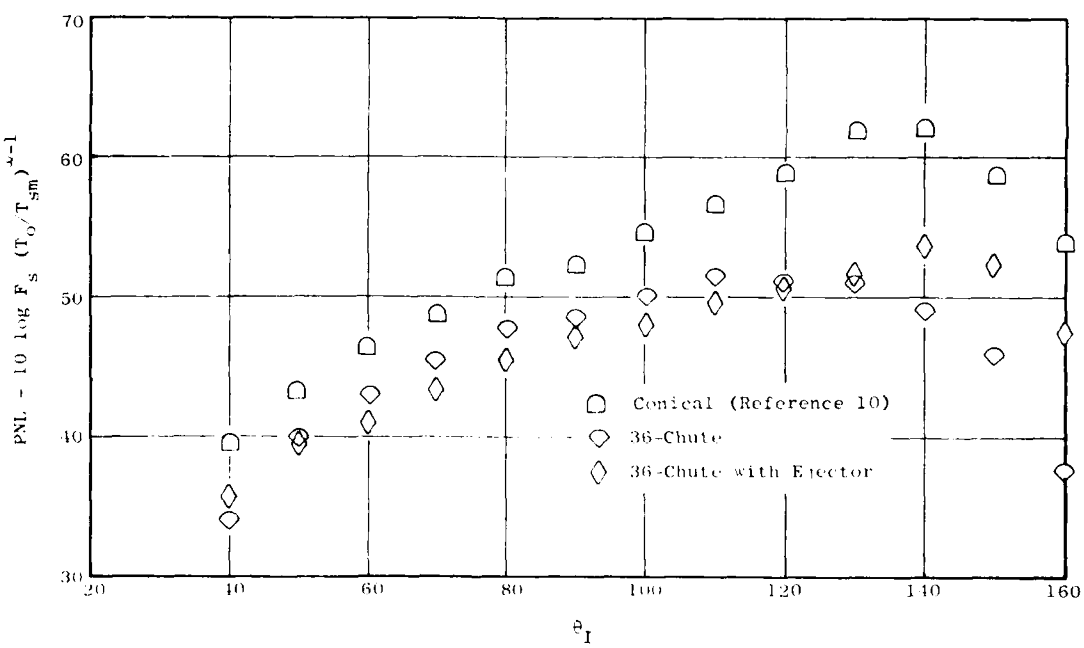

Figure 7-20. Summary of Static PNL Directivity Characteristics - $V_{ma} \approx 1640$ ft/sec.

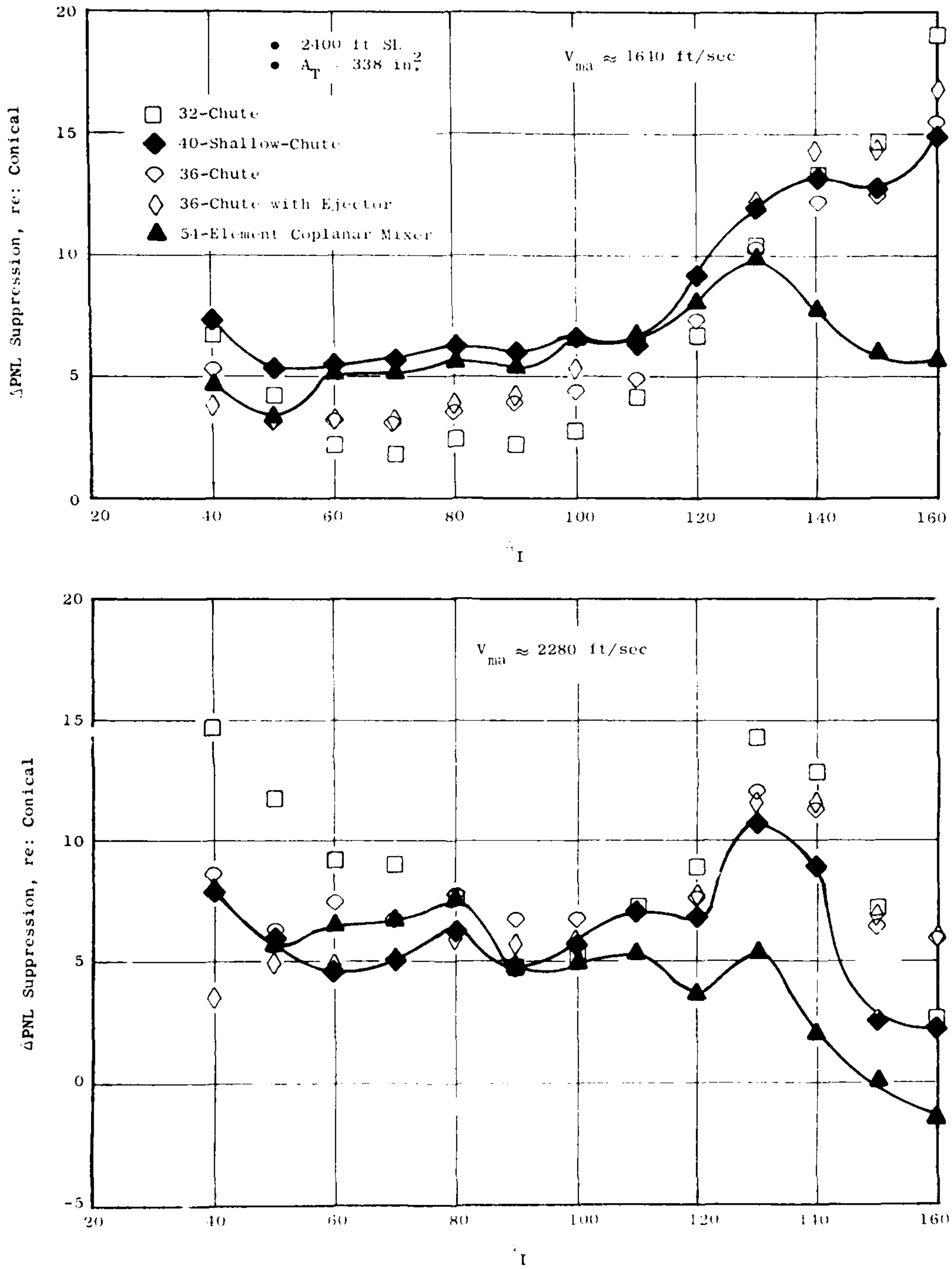

Figure 7-21. Summary PNL Directivity Suppression Levels.

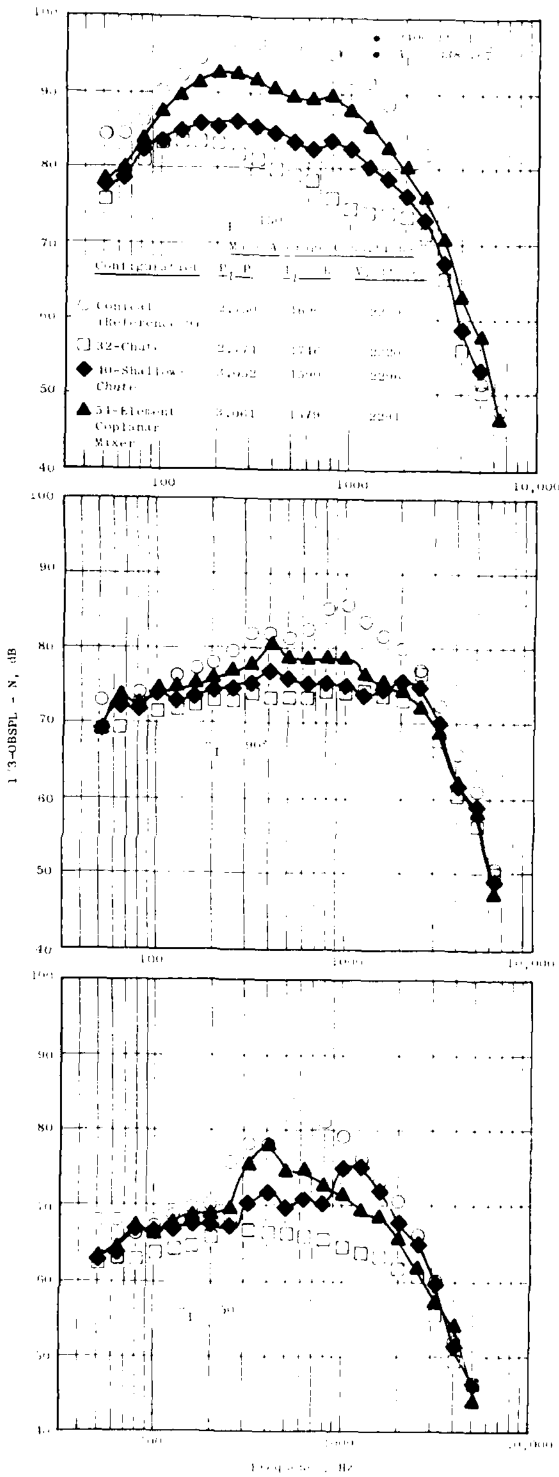

Figure 7-22. Comparison of Static Spectra Characteristics - $V_{ma} \approx 2280$ ft/sec.

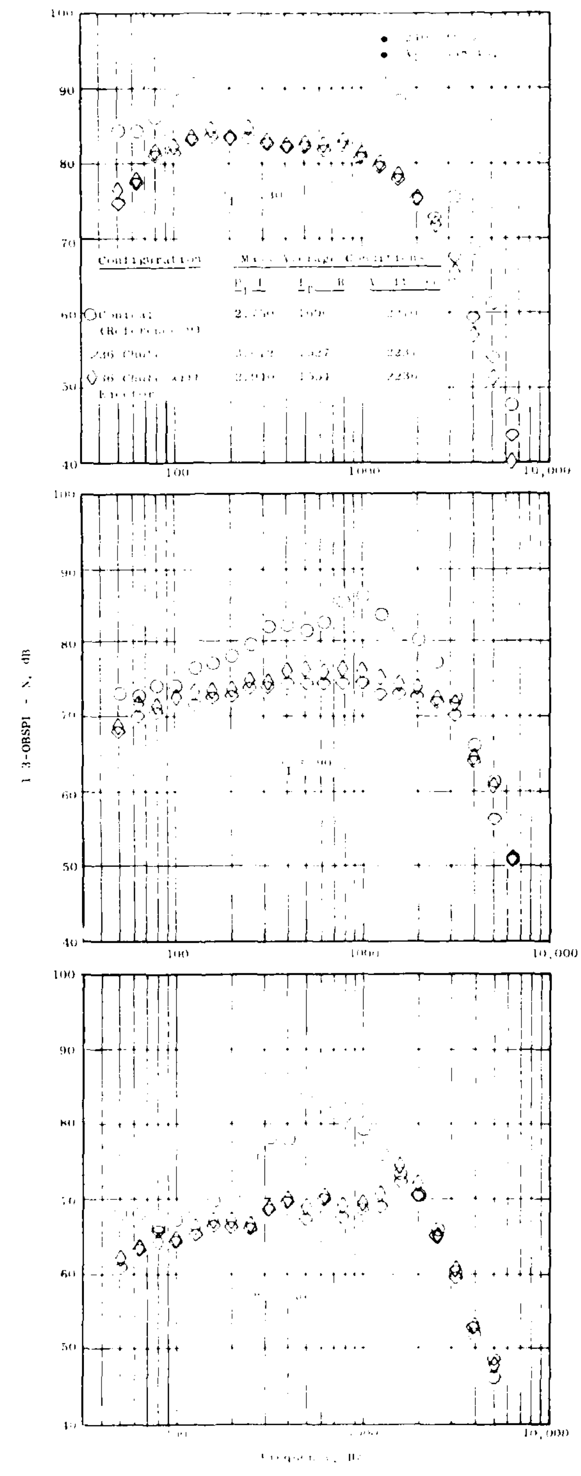

Figure 7-23. Comparison of Static Spectra Characteristics - $V_{ma} \approx 2280$ ft/sec.

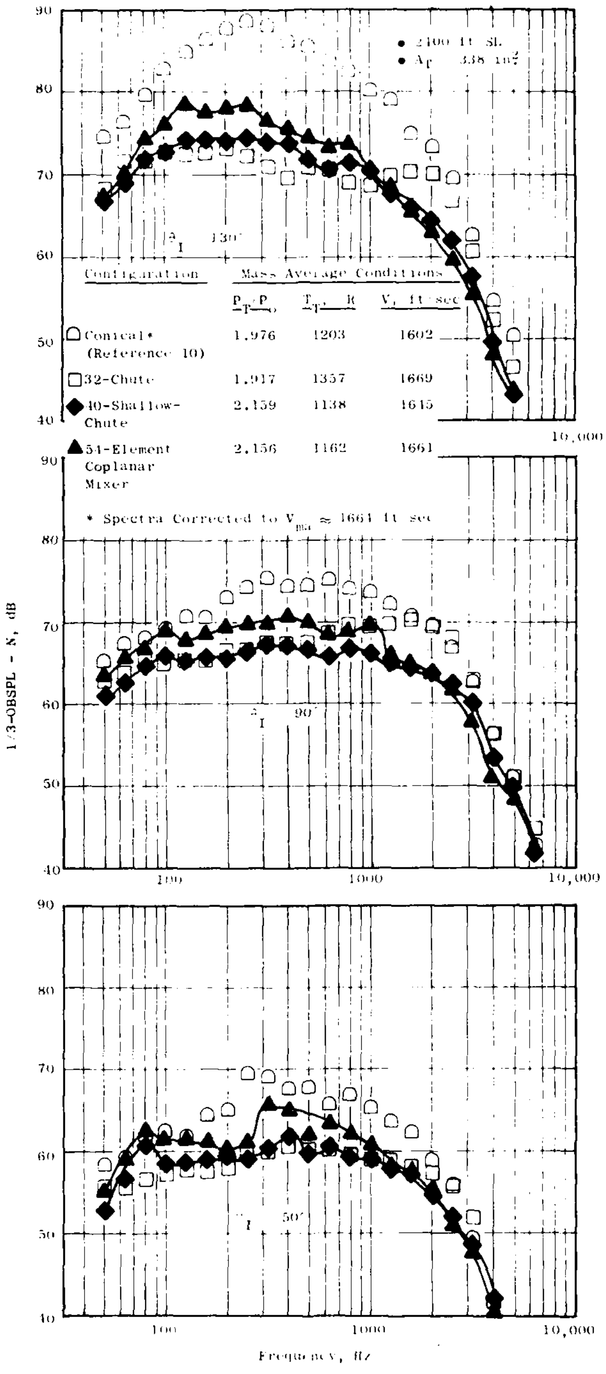

Figure 7-24. Comparison of Static Spectra Characteristics - $V_{ma} \approx 1640$ ft/sec.

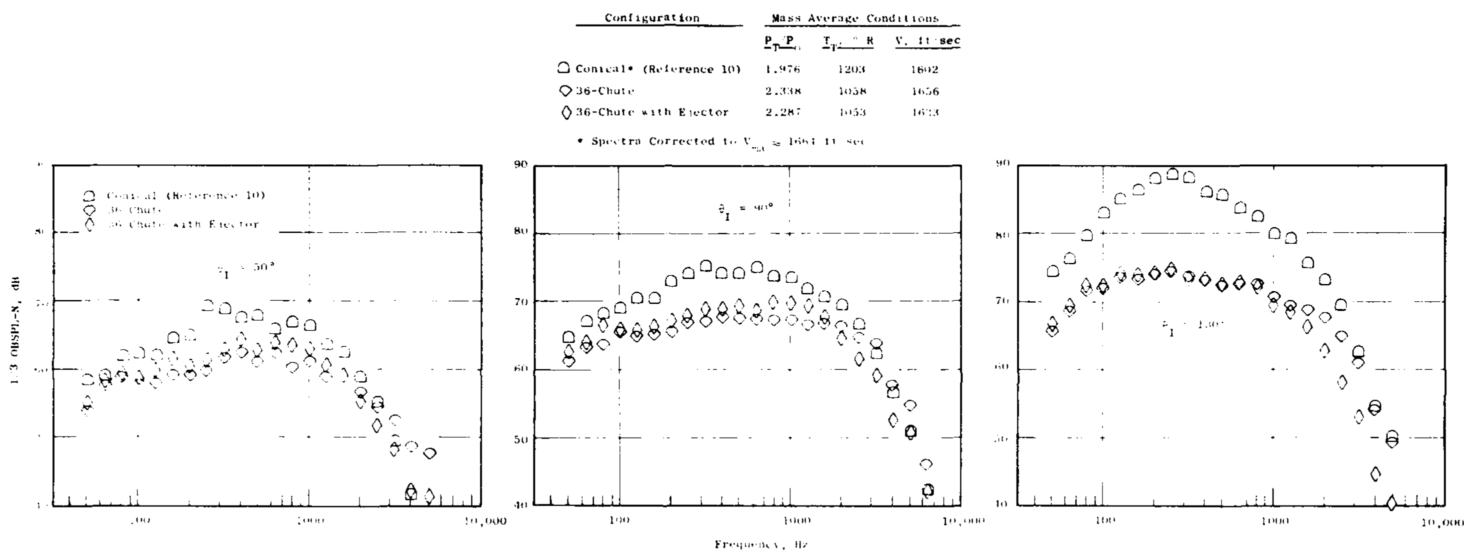

Figure 7-25. Comparison of Static Spectra Characteristics, $V_{ma} \approx 1640$ ft/sec.

The 32-chute, 40-shallow-chute, and 36-chute with and without a treated ejector all have spectrum shapes typical of multielement suppressors. When compared to the conical nozzle all these aforementioned suppressors exhibit the same characteristics, i.e. a significant amount of low and middle frequency reduction, no high frequency benefit.

Examination of Figure 7-22 clearly illustrates the uniqueness of the 54-element coplanar mixer nozzle's peak noise spectrum shape in that it is resembles more closely that of a conical nozzle.

7.3 GENERALIZED DESCRIPTION OF THE TRANSFORMATION PROCEDURE

This section briefly describes the recommended procedure for transformation of free jet noise data to represent flight noise. The background material for the development of this method is presented in detail in Reference 6. The transformation procedure, described in Reference 6, has been continued to be evaluated in the current program and some refinements have been made. These modifications have been based on the acquisition of additional free jet data for conical nozzles and the availability of data with the free jet operating at 400 ft/sec. The turbulence absorption corrections have been modified to be a maximum 3.0 dB rather than the previously used value of 6.0 dB. The cutoff of the turbulence absorption correction as a function of the frequency parameter has been eliminated. Also, if the error in fitting the 1/3-octave directivity bands is found to diverge as the singularity level is increased, the singularity level which had the minimum error is used to determine the dynamic effect. The computer program, a series of instructions for use, and a description of the logic is presented in Appendix B.

The objective of the free jet transformation process is to employ far-field SPL spectra at various angles to the jet axis (typically for $40 \leq \theta_I \leq 160°$ in increments of 10°) obtained in a free jet experiment, and to transform it to yield SPL spectra as would be measured in flight.

The concept employed is as follows: with area ratios (area of free jet/area of nozzle) of approximately 50:1, and with the primary nozzle exhaust plane displaced aft of the free jet plane sufficient enought to permit acquisition of acoustic data in the inlet arc (up to $\theta_I = 50°$), proper aerodynamic simulation of the effects of forward flight can be achieved. The free jet achieves acoustic simulation of the effects of uniform flow over the primary jet plume noise sources only to a limited extent. The free jet achieves the effect of the correct source mix radiating, however, into an environment that more nearly approaches a static environment than the environment of sources shrouded by either a finite or infinite extent of uniform nonturbulent flow. The acoustic sources in a free jet, of course, do not radiate into a completely static envrionment and hence some propagation effects of the free jet flow do have to be accounted for.

Based on the above picture, the broad outline of the procedure adopted is as follows. Defining the static directivity as the directivity pattern

(in various frequency bands) that the sources (of the primary jet exhaust plume altered by the effects of relative velocity due to imposition of the free jet) may be expected to produce if they radiated into a quiescent environment, the method first deduces this static directivity from the measured free jet experimental data by correcting the latter for propagation effects of the free jet. Since the free jet flow field includes intensely turbulent shear layers through which the sound field of the sources must pass before it reaches the far-field microphones (located in the quiescent ambient), some degree of empiricism (especially for the high frequency sound) is involved in attempting to account for these propagation effects.

Once such a static directivity is extracted, it still remains to deduce what the noise signature of the source distribution would be if the source distribution was not stationary relative to the ambient but moving relative to the ambient at the flight velocity. A multipole decomposition procedure suitable for the broad band jet noise problem which attempts to synthesize the static directivity by ascribing it to a mix of uncorrelated singularities was developed in order to enable the prediction of the flight noise. Once such a decomposition is completed, simply apply the dynamic exponent applicable to each singularity to derive the flight noise signature.

The method starts with narrow band directivities from the free jet experiment in various third-octave bands, corrects these directivities for free jet propagation effects in a frequency dependent manner to retrieve the static directivity, synthesizes the static directivity by a suitable mix of uncorrelated singularities and finally applies the dynamic effect appropriate to each singularity to predict the flight noise. It is an inherent feature of the method that it works separately with each third-octave band directivity pattern. The final flight predictions can then be summed to yield either OASPL of PNL directivities or simply displayed as flight SPL spectra at various angles to the jet axis. (Doppler shift effects on the frequency are fully accounted for). This procedure is described in Appendix B.

The major features of the transformation procedure are illustrated below in two sets of comparisons. The first comparison is of transformed free jet data obtained on a 4.0-inch conical nozzle, Reference 10, with actual aerotrain static and flight data. The comparison illustrates the ability of the procedure to reproduce flight results. The 4.0-inch conical nozzle was designed as a scale-model replica of the aerotrain conical nozzle.

Static and projected flight OASPL and PNL directivity comparisons are summarized in Figures 7-26 and 7-27. The transformed free jet data are found to match the static and flight directivity characteristics of those measured on the Aerotrain within $\pm$ 2 dB. Static and flight spectra comparisons are presented on Figure 7-28. Consistent differences are not observed in the flight spectra comparisons except to the extent that they were present for similar comparisons on a static basis. The flight comparisons could not be expected to agree any better than the static comparisons. Overall, excellent

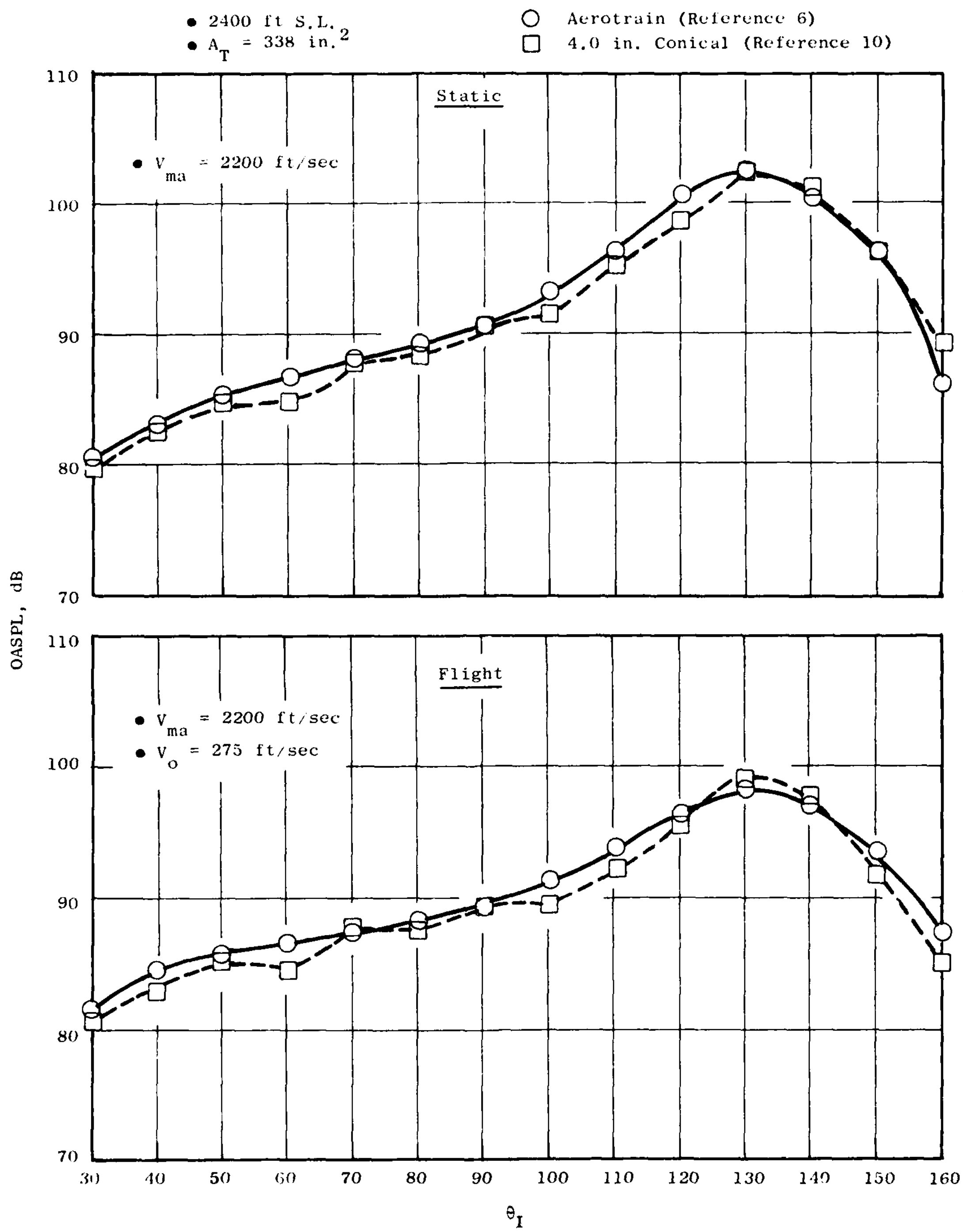

Figure 7-26. Comparison of Aerotrain and 4.0 in. Conical Nozzle OASPL Characteristics.

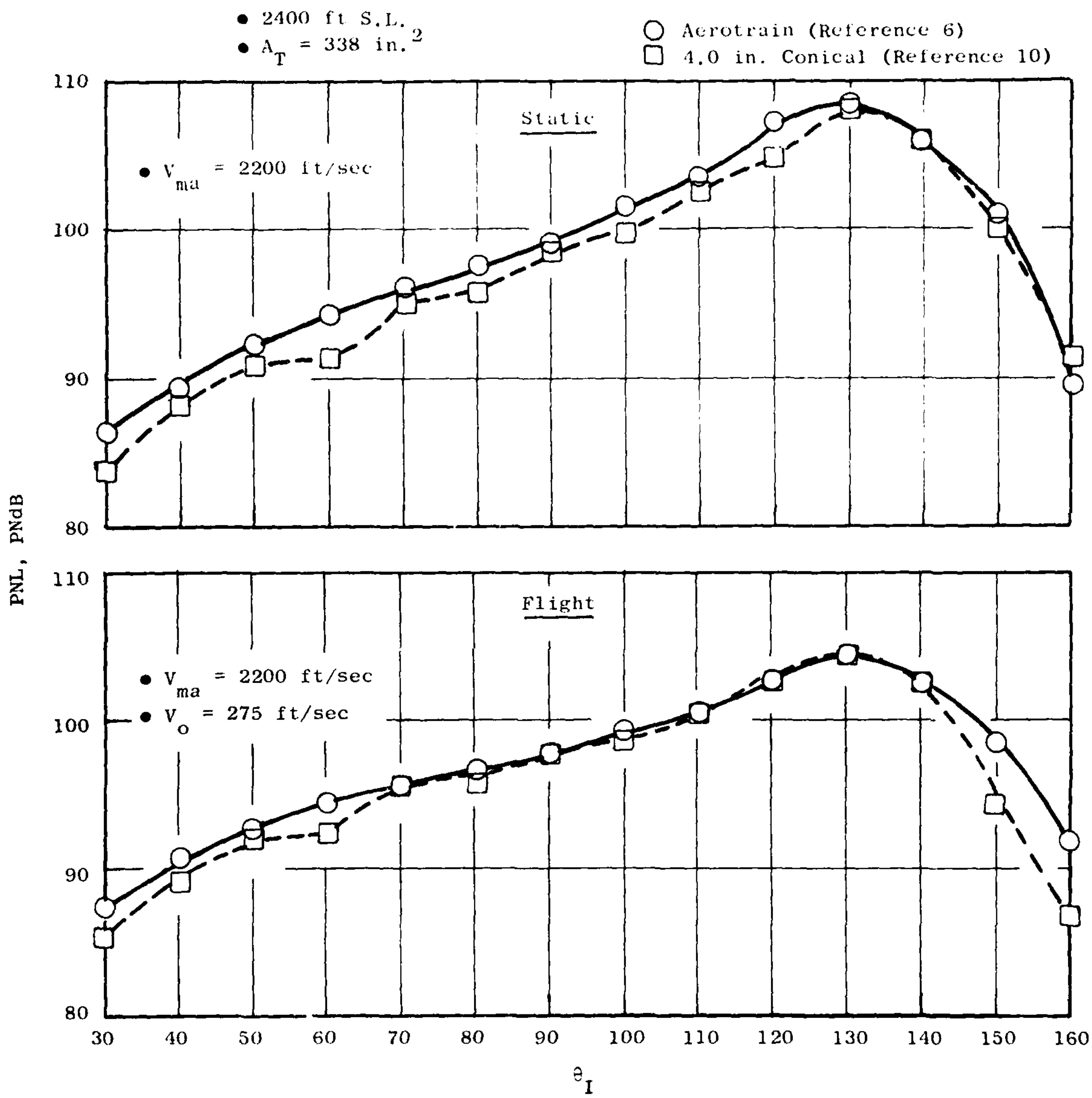

Figure 7-27. Comparison of Aerotrain and 4.0 in. Conical Nozzle PNL Characteristics.

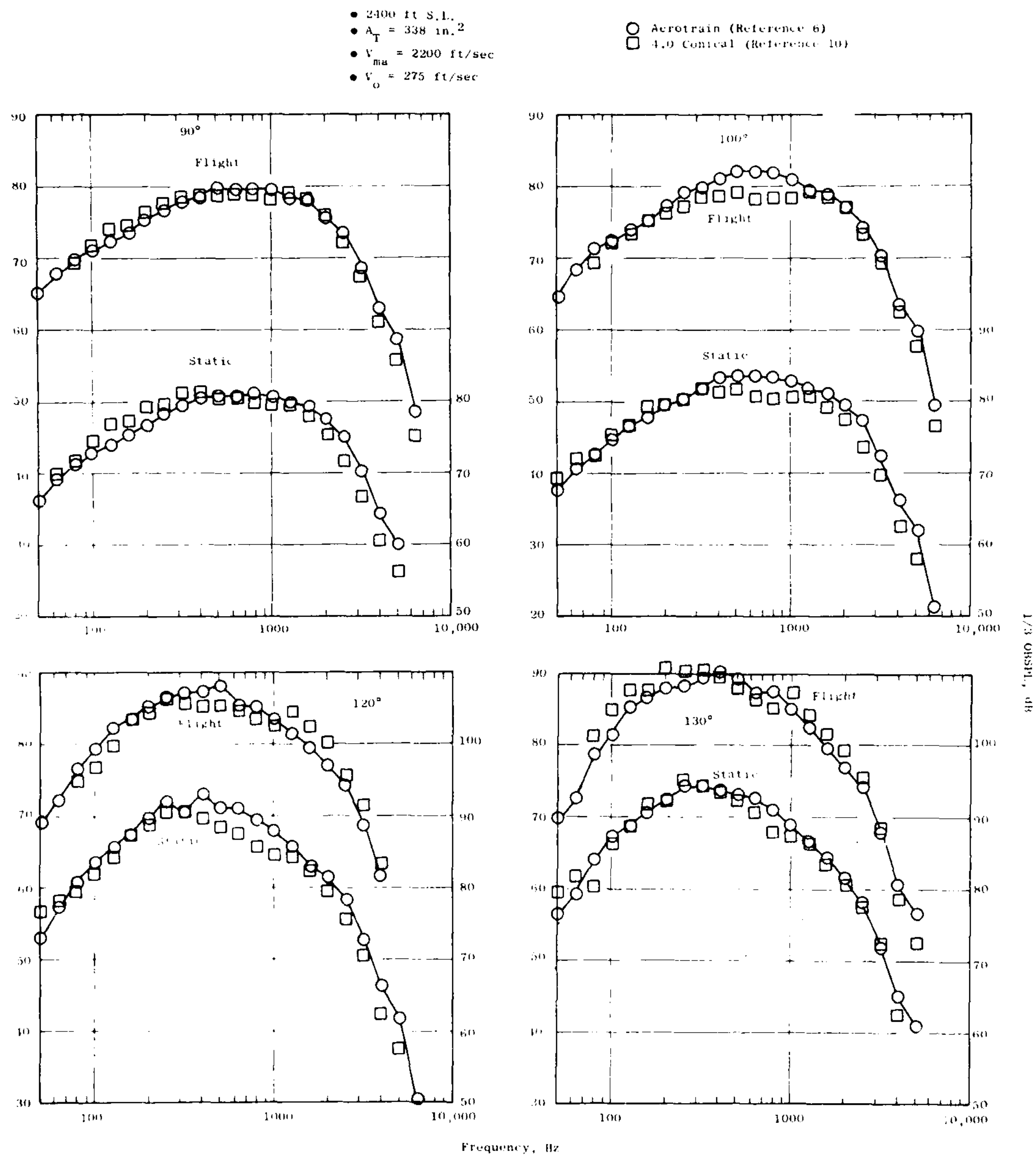

Figure 7-28. Conical Nozzle Spectra Comparisons with Aerotrain.

agreement is obtained between the transformed free jet data and the Aerotrain results. Additional comparison of Aerotrain and free jet results are presented in Reference 6.

Use of the free jet technique for understanding flight effects has the advantage of allowing source reduction and dynamic effects to be considered separately. The next series of comparisons illustrate the relative margitudes of the source and dynamic effects. A typical data point for the 32-chute nozzle is considered.

Free jet data are corrected for absorption and refraction to define the true source modification when compared to static data. That is, the difference between the projected flight spectra and the spectra corrected for refraction and absorption in the dynamic correction and the doppler frequency shift.

Comparisons at 50°, 90°, and 130° of measured static spectra, free jet data corrected for turbulence absorption and refraction, and projected flight spectra are presented in Figure 7-29. In the aft quadrant at 130°, essentially no low frequency (100 Hz < f < 1250 Hz) reduction occurs due to source modification. In the high frequency regime (f > 1250 Hz) an increase relative to the static data is observed. Application of dynamic effects and doppler shift result in a 2 to 6 dB reduction relative to static data in the frequency range from 50 Hz to 1000 Hz. At frequencies above 1000 Hz, the projected flight levels are equal to or slightly greater than static. The 90° spectra comparisons have no refraction or dynamic corrections and only a turbulence absorption correction is applied at high frequencies. At frequencies less than 2000 Hz a reduction of 1 to 3 dB is measured. The reduction is frequency dependent. At frequencies above 2000 Hz the free jet noise is either equal to or greater than the static. At the above 50° acoustic angle, there is a source reduction at frequencies below 500 Hz. However, at frequencies above 500 Hz the source noise is equal to or greater than the static noise. Application of dynamic corrections negates the low frequency source reduction and results in a 2 or 5 dB increase in the high frequency region of the spectrum.

The type of source singularities which are predicted to comprise each frequency regime may be deduced by examining the magnitude of the dynamic effect. The dynamic effect as a function of frequency is summarized in Figure 7-30. The correction, in terms of decibels, for each singularity type is also noted. In the aft quadrant the singularities are octupoles and quadrupoles, whereas in the forward quadrant they are primarily dipoles, with some monopole content in the high frequencies.

The free jet data presented in the remainder of this report will be transformed using the procedure described above.

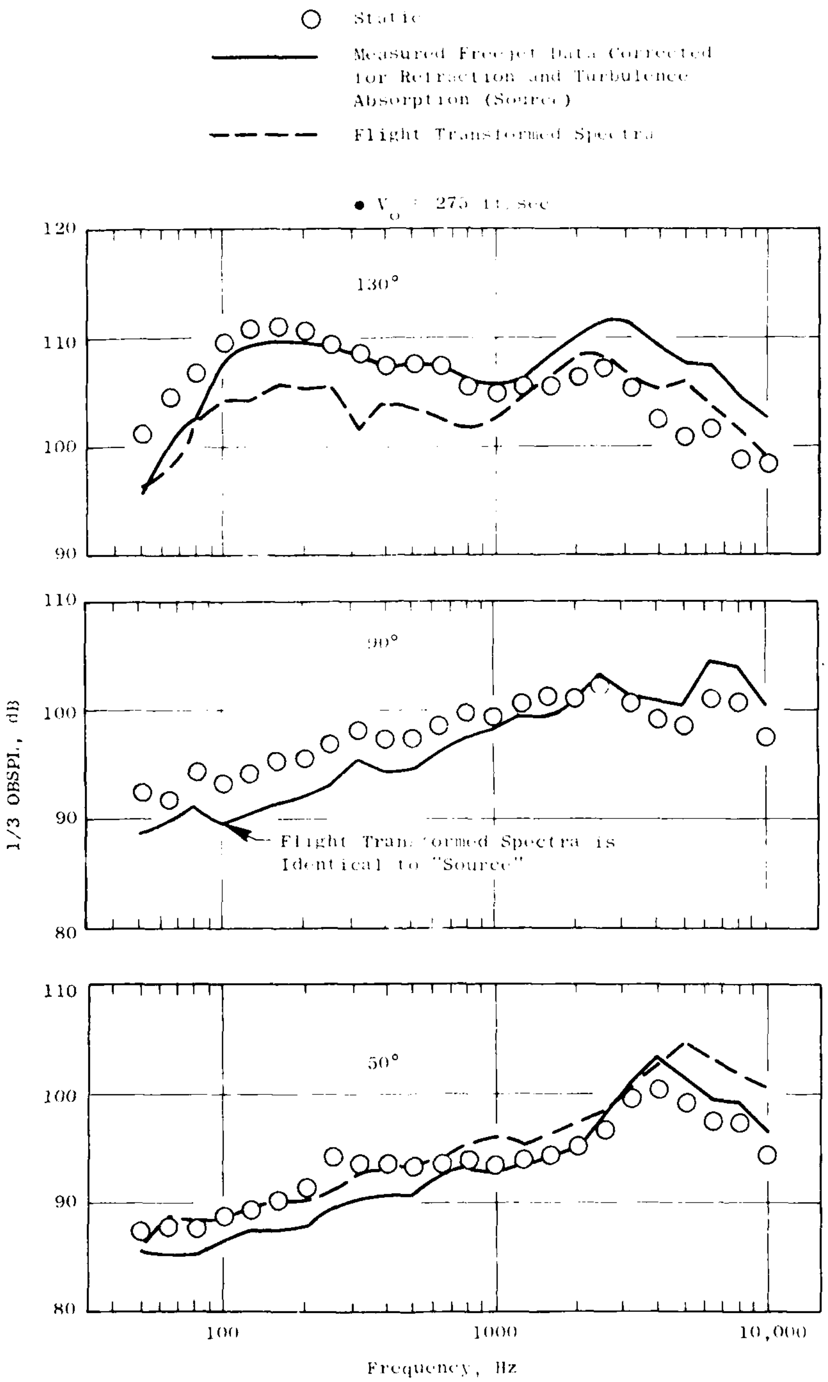

Figure 7-29. Typical Static, Source and Flight Spectra for a 32 Chute Nozzle.

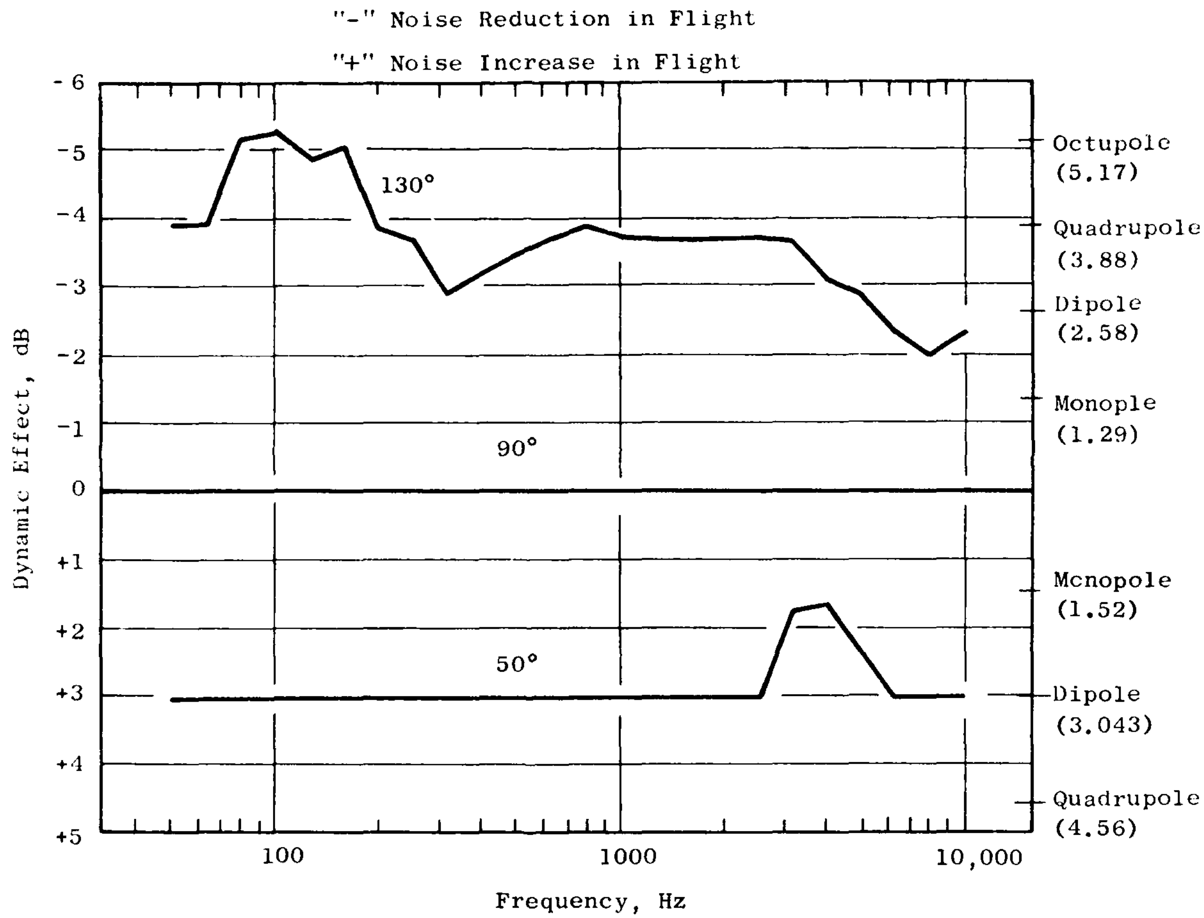

Figure 7-30. Typical Dynamic Effects for a 32 Chute Nozzle.

7.4 EVALUATION OF FLIGHT NOISE CHARACTERISTICS

This section discusses the flight noise characteristics for each of the five suppressor nozzle configurations based on transformed free jet data. Comparisons are presented on the basis of peak noise suppression level, directivity trends, and spectrum shape. The presentation of the results follows a format similar to that used in Section 7.2.

7.4.1 Peak Noise Trends

The PNL levels are summarized on Figure 7-3[illegible] for the 32-chute nozzle. Several lines representing nominal velocities of 275 and 360 ft/sec are presented. Conical data are also presented as a reference to establish the flight suppression levels. Flight suppression deltas are presented on Figure 7-31 for the various free jet velocities. Static suppression is also presented for comparison.

Flight suppression and static suppression levels are comparable at mass average velocities above 2300 ft/sec. At velocities below 2300 ft/sec the flight suppression levels are 0 to 7 dB less than the static suppression levels. The static-to-flight suppression loss increases as mass average velocity decreases and free stream velocity increases.

A similar set of comparisons for the 40 shallow-chute nozzle is presented on Figure 7-32. The peak noise suppression characteristics are evaluated for several types of cycle lines. Flight suppression levels in excess of 13 PNdB were measured with no inner flow. The suppression levels are reduced 2 PNdB with the addition of inner flow where the inner stream flow pressure ratio is subcritical. Suppression is degraded from 1 to 3 PNdB for cycle variations where the inner flow pressure ratio is supercritical. Flight peak noise suppression is comparable to the static noise suppression at mass average velocities above [illegible] ft/sec; below this velocity, flight suppression is 0 to 5 PNdB less than static. A [illegible] PNdB variation in suppression level due to cycle variations occurs at a mass average velocity of 2000 ft/sec.

The flight suppression characteristics of the 36 C-D chute nozzle are presented on Figures 7-33 and 7-34. The maximum flight suppression occurs for conditions with no inner flow, with a maximum suppression level of 13 PNdB occurring between [illegible] ft/sec and [illegible] ft/sec. The chute design for this configuration incorporated a convergent-divergent flowpath which was designed to be shock free at a pressure ratio [illegible]. Figure 7-33(b) was obtained with the outer flow operating at the design point. Only small improvements in suppression appear to be realized by this design feature on the basis of the peak noise comparisons. Overall, for the dual flow cycles evaluated, the flight suppression levels achieved were 13 PNdB for cases with no inner flow. Dual flow cycle suppression peaks at 10 to 11 PNdB. Increasing flight velocity from 275 ft/sec to 360 ft/sec causes an additional loss in suppression at velocities below 2200 ft/sec; at velocities above 2200

AD-A094 297 GENERAL ELECTRIC CO CINCINNATI OH AIRCRAFT ENGINE GROUP F/G 20/1
HIGH VELOCITY JET NOISE SOURCE LOCATION AND REDUCTION. TASK 5. --ETC(U)
JAN 79 N BAUMGARDT, J F BRAUSCH, W S CLAPPER DOT-OS-30034
UNCLASSIFIED R78AEG628 FAA-RD-76-79-5 NL

2 OF 3
AD
A094297

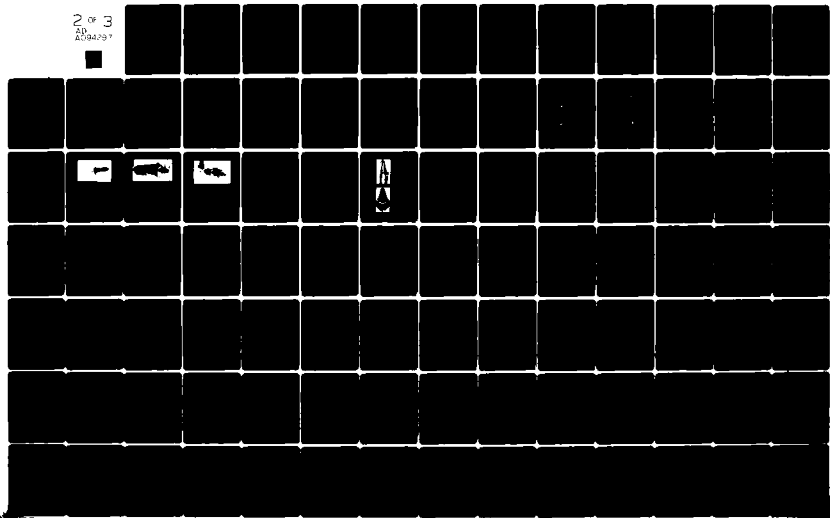

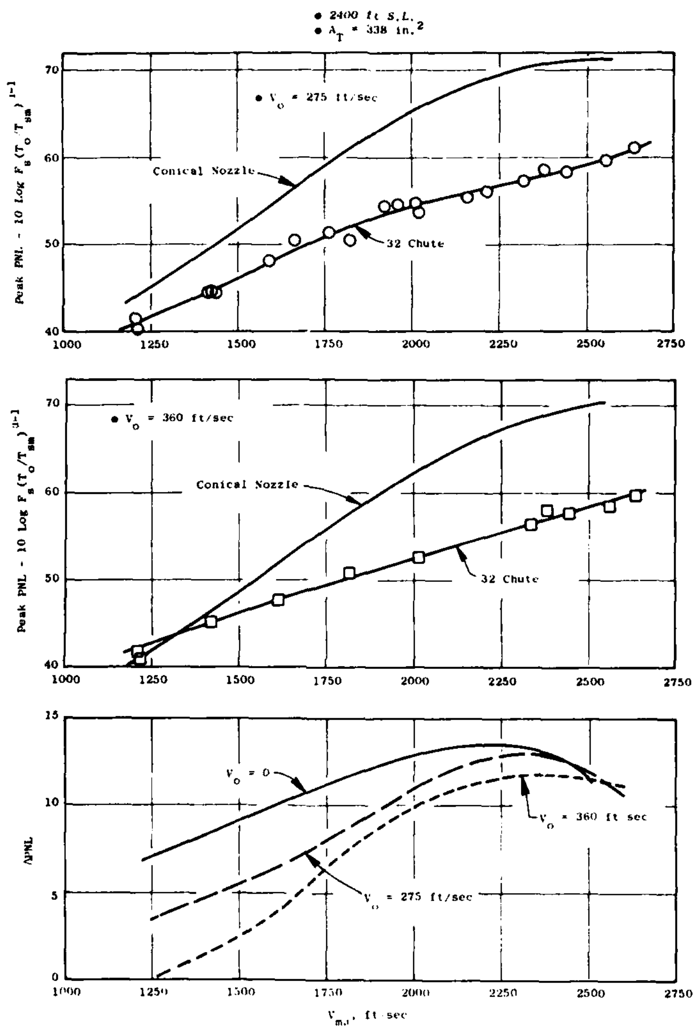

Figure 7-31. 32 Chute Nozzle Peak Flight Noise Suppression.

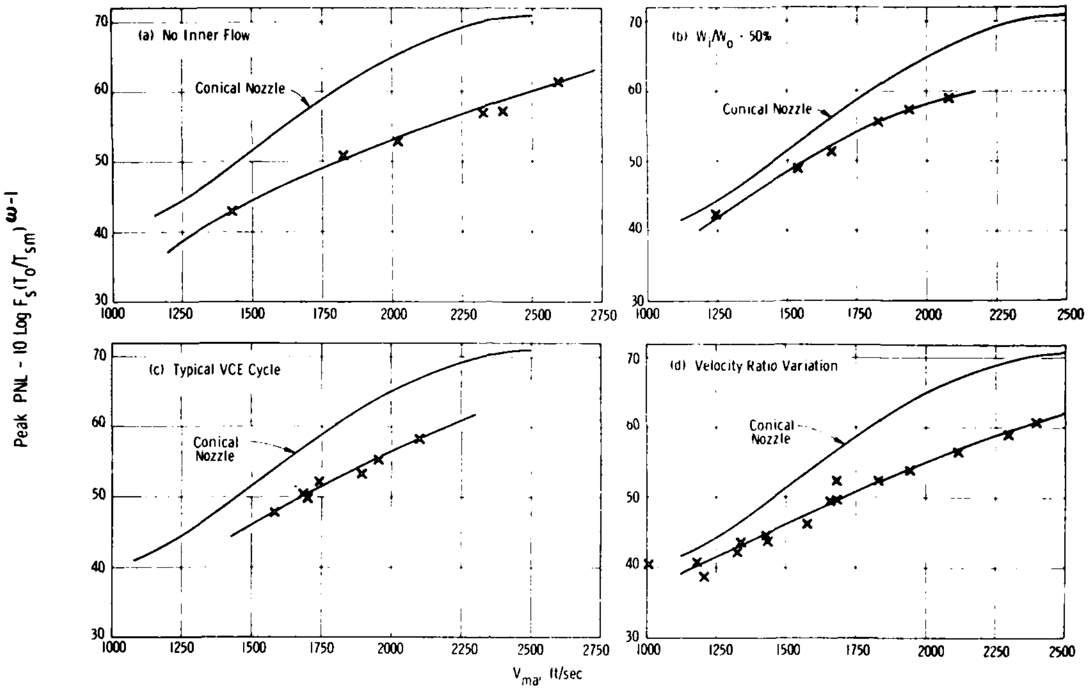

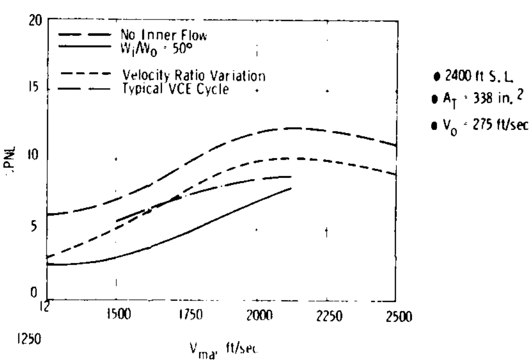

Figure 7-32. 40 Shallow Chute Peak Flight Noise Characteristics.

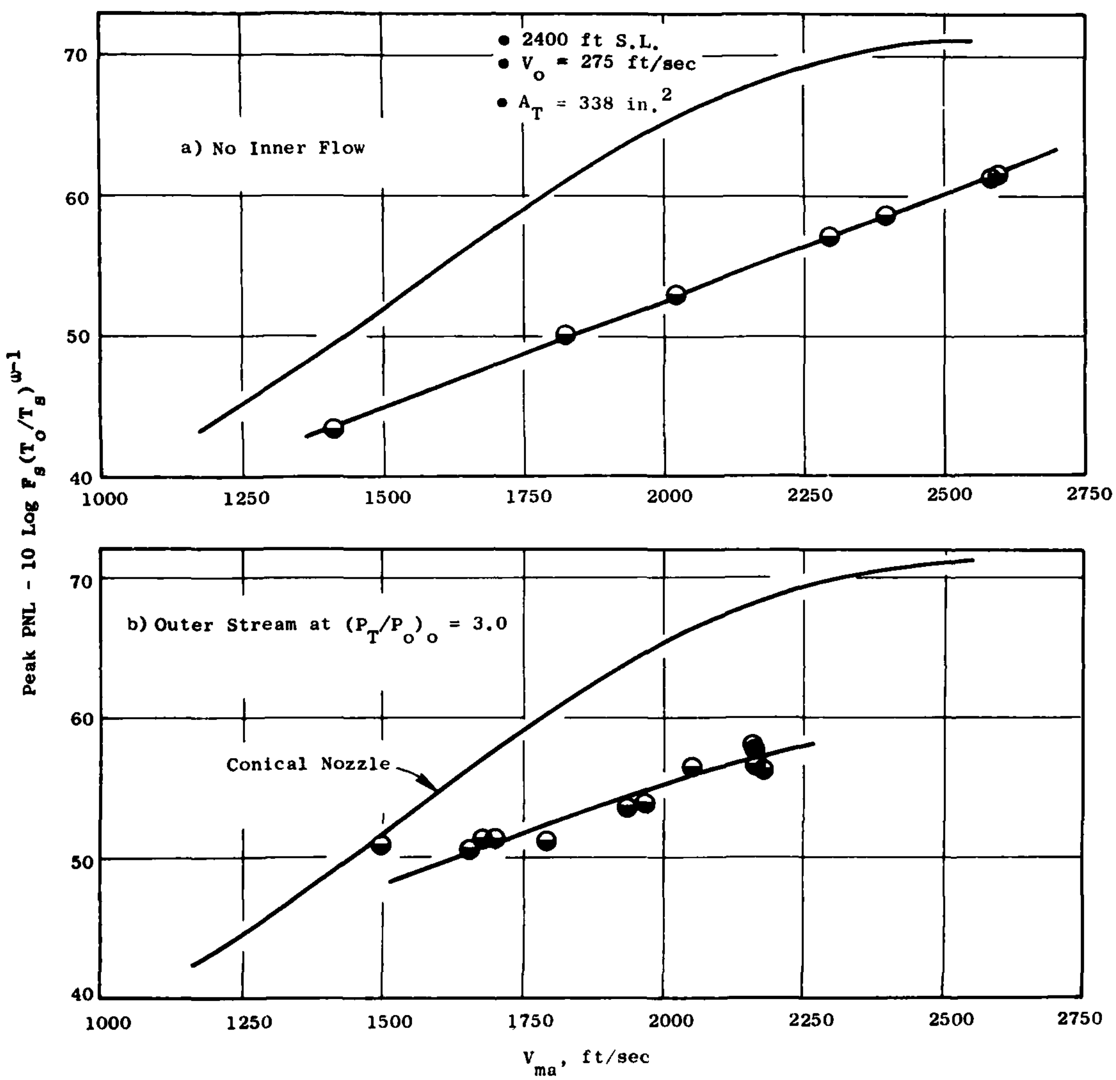

Figure 7-33. 36 Chute Nozzle Peak Flight Noise Characteristics.

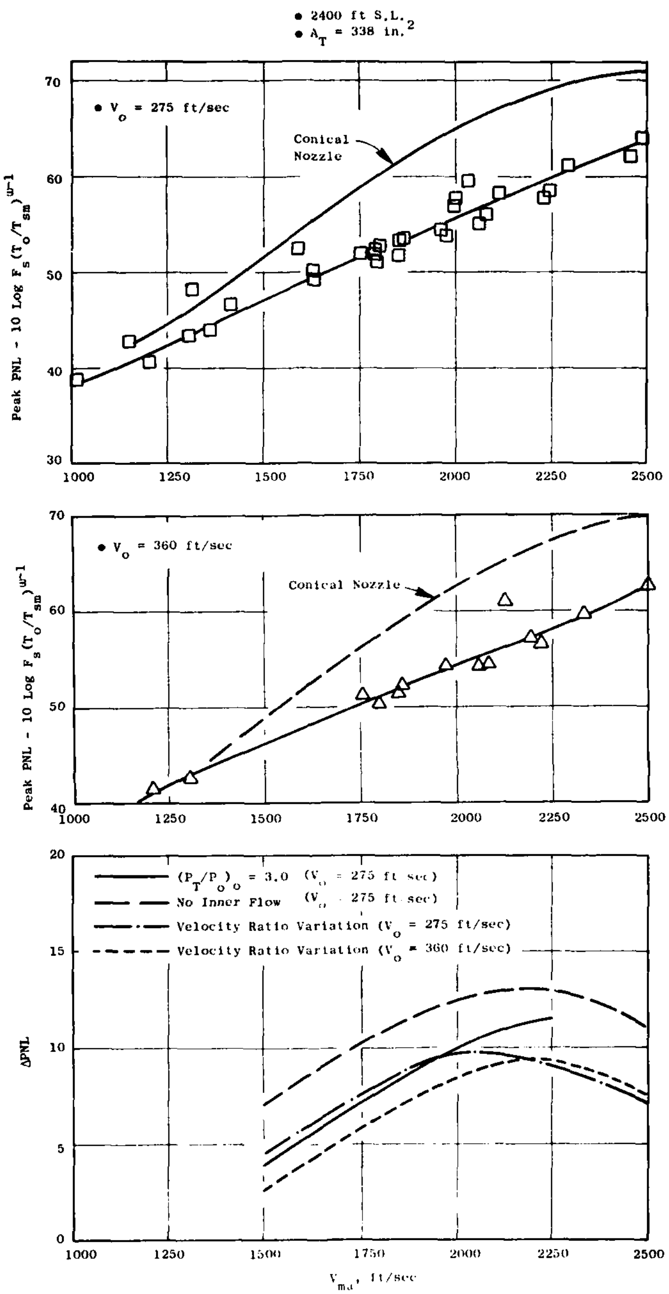

Figure 7-34. 36 Chute Nozzle Peak Flight Noise and Suppression Characteristics.

ft/sec suppression is slightly enhanced. Flight peak noise and suppression characteristics of the 36-chute nozzle with a treated ejector are summarized on Figures 7-35 and 7-36. Improved suppression of 1 to 3 PNdB is observed at 360 ft/sec flight velocity for the ejector configuration indicating that the ejector effectively reduces the high frequency noise caused by the premerged region of the jet. The only cycle variation where the ejector did not result in improved flight suppression was for the case with no inner flow. The ejector also caused the variation in suppression at a given mass average velocity to be less.

Flight noise peak PNL characteristics for the 54-element coplanar mixer nozzle are summarized on Figure 7-37. Static and flight suppression levels are also presented. The suppression characteristics of this configuration are different than the previous four nozzles, and the results in flight exhibit different trends. The velocity range over which the peak suppression occurs is much lower, and the ranges from 1000 to 1800 ft/sec. The other four suppressors peak at much higher velocity (2000 to 2500 ft/sec). The other four designs experience a flight suppression decrease as the mass average velocity decreases; whereas this configurations flight suppression is within 0.5 PNdB of the static suppression for the mass average velocity range evaluated. This indicates that changes in noise from static to flight for this nozzle are similar to a conical nozzle.

A summary of the peak noise suppression and the corresponding velocity range for each configuration is presented in the following table.

Configuration	Peak Flight PNL Suppression	Velocity Range
32-Chute	12-13 PNdB	2100 ft/sec→2500 ft/sec
40-Shallow-Chute	10-11 PNdB	1900 ft/sec→2500 ft/sec
36-C-D-Chute	11-12 PNdB	2050 ft/sec→2250 ft/sec
36-C-D-Chute and Treated Ejector	11.5-12.5 PNdB	2025 ft/sec→2250 ft/sec
54-Element Coplanar Mixer	7-7.5 PNdB	1000 ft/sec→1800 ft/sec

The above levels were established by using all the cycle lines except those with no inner flow. Overall, with the exception of the 54-element coplanar mixer nozzle, the peak suppression levels occur over similar velocity ranges. The 13 PNdB flight suppression level of the 32-chute nozzle represents the largest suppression. However, the suppression level of the 36-chute and 36-chute with treated ejector were within 1 and 0.5 PNdB, respectively, of the 32-chute nozzle. Although some loss in suppression occurs in flight for select configurations, in general these suppressor designs are effective in causing peak flight noise reduction in excess of 11 PNdB in the high velocity regime.

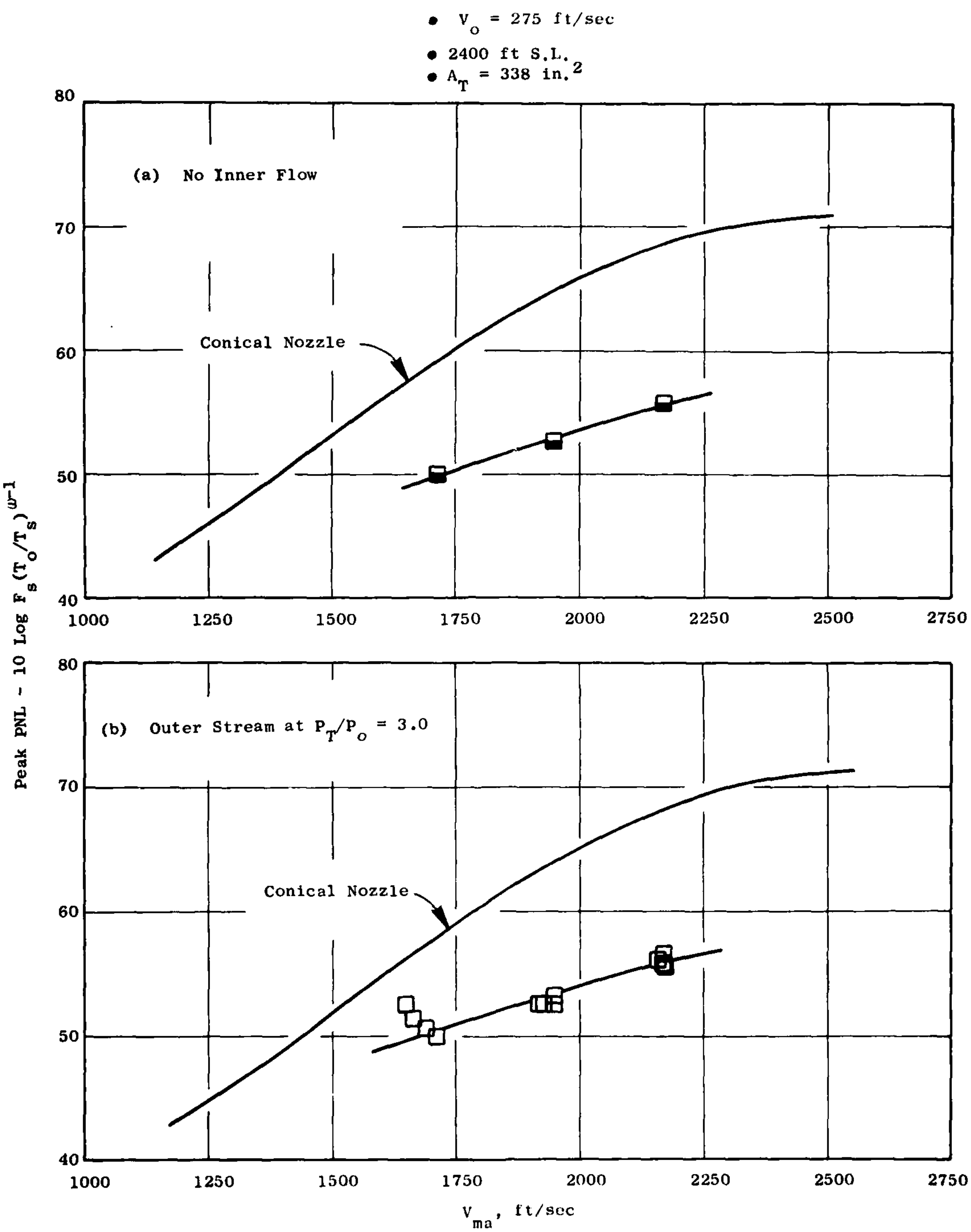

Figure 7-35. 36 Chute with Treated Ejector Flight Noise Characteristics.

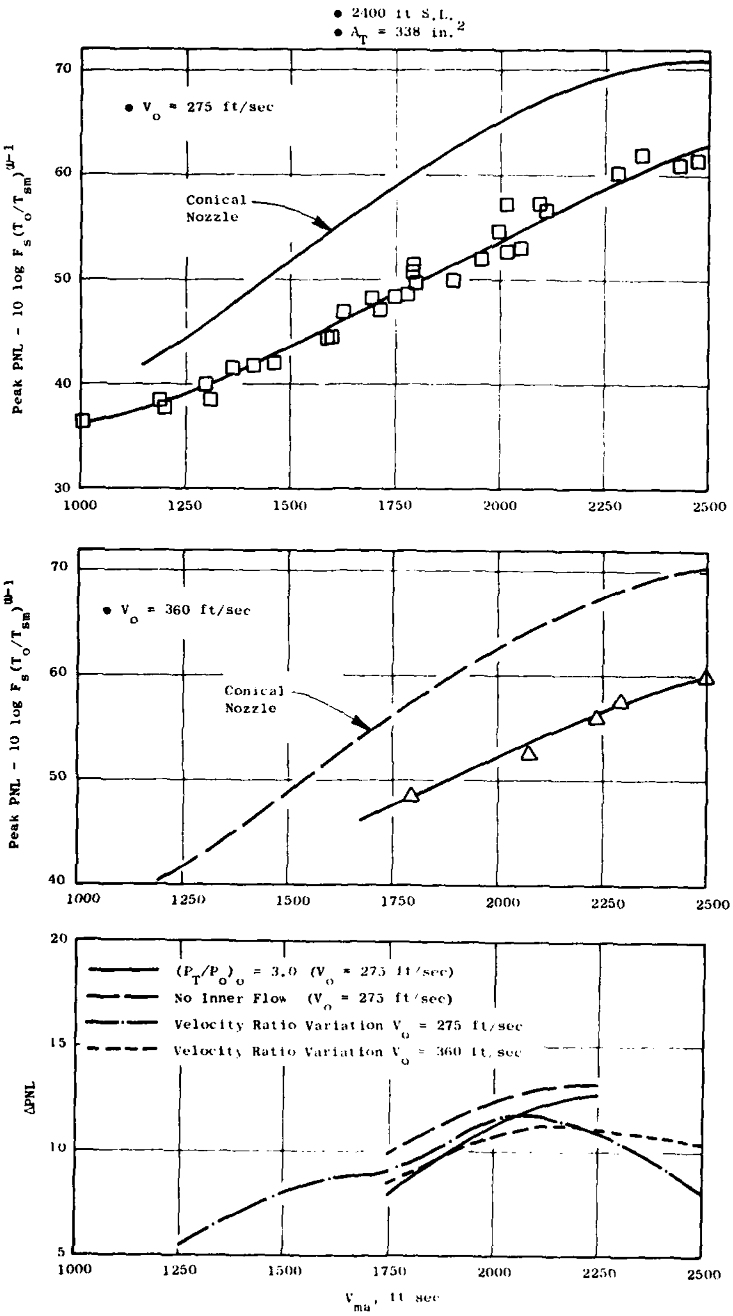

Figure 7-36. 36 Chute with Treated Ejector Flight Noise and Suppression Characteristics.

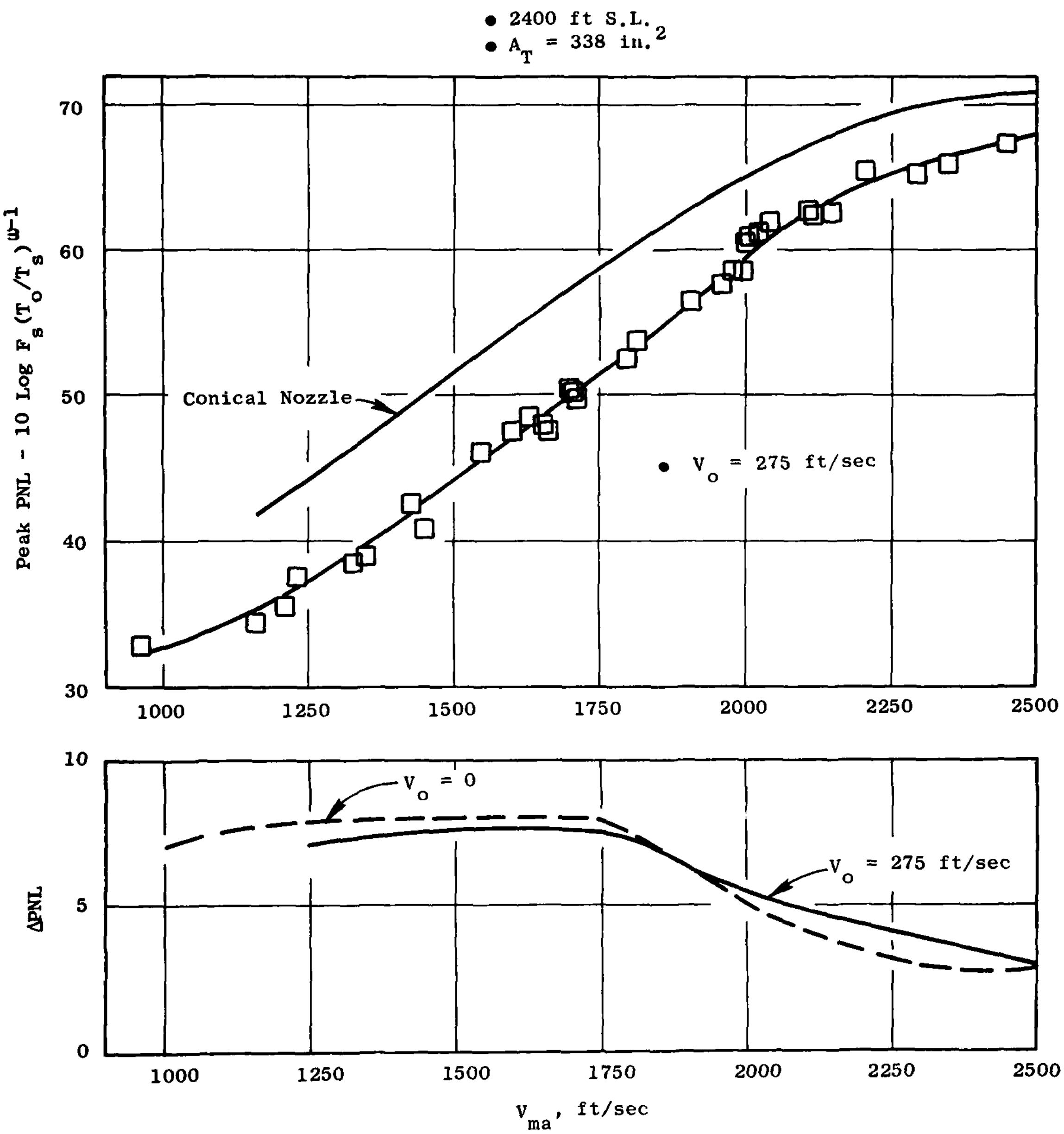

Figure 7-37. 54 Element Coplanar Mixer Nozzle Peak Flight Noise and Suppression Characteristics.

7.4.2 Suppressor Flight Directivity and Spectra

Static and flight directivity and spectra characteristics are discussed in this section. The data are presented at mass average velocities ranging from 2250 to 2350 ft/sec. Conical nozzle data are also presented from Reference 9 to establish the changes in directivity and spectrum characteristics caused by the suppressor nozzles. Static data are also presented for comparison with flight data to illustrate the differences. All flight data presented has been transformed using the procedure discussed in Section 7.3.

The PNL and OASPL directivity characteristics of the 32-chute nozzle are summarized on Figure 7-38. This mass average velocity is typical of those being considered for advanced variable cycle engines. The directivity characteristics of this suppressor are much different than those of the conical nozzle which has a distinct aft quadrant peak at 130° in both the static and flight case. The peak noise angle for the 32-chute suppressor nozzle is less distinct and shifts in location slightly as flight velocity is varied. At the extreme angles in the aft quadrant ($140° < \theta_I < 160°$), the changes from static to flight are generally equivalent for both the conical and 32-chute nozzle. At 90° very little change is observed from static to flight for the conical nozzle, but a 3 PNdB reduction occurs for the 32-chute suppressor. However, the reduction is not a function of flight velocity. In the forward quadrant, using 50° as a typical case, the conical nozzle PNL levels are increased by 5 PNdB, whereas for the 32-chute, only a 2 PNdB increased is observed. The spectra comparisons presented on Figure 7-39 at 50° illustrate that a conical nozzle spectra is typical of one which is dominated by shock noise. The 32-chute spectra does not have this classic shape. For frequencies below 630 Hz, no noise increase occurs from static to flight; an increase does occur in the higher frequencies. At the peak frequency shock noise is reduced by 25 dB. The 90° spectra comparisons for the 32-chute nozzle show significant low frequency reduction from static to flight, whereas there is no change or a slight increment at the high frequencies. The 32-chute suppressor is most effective in the mid-frequency range. All 110° and 130° (typical of the maximum noise angle), trends similar to those at 90° are observed. The most significant trend is that the conical nozzle shows high frequency noise reduction from static to flight, whereas the 32-chute suppressor does not.

Comparisons similar to those above are presented for the 40-shallow-chute nozzle on Figure 7-40 and 7-41. The magnitude of suppression in the forward quadrant is not as large due to the fact that the outer flow stream (to which the suppressor is applied) is operating at a much higher pressure ratio than the 32-chute nozzle. This can be seen by comparing the levels in the premerged noise region between the 32-chute nozzle and the 40-shallow-chute nozzle (the 1250 Hz 50° forward quadrant level is 62 dB for the 32-chute and 74 dB for the 40-shallow-chute).

Directivity and spectra comparisons for the 36-chute nozzle with and without a treated ejector are summarized on Figures 7-42 through 7-45.

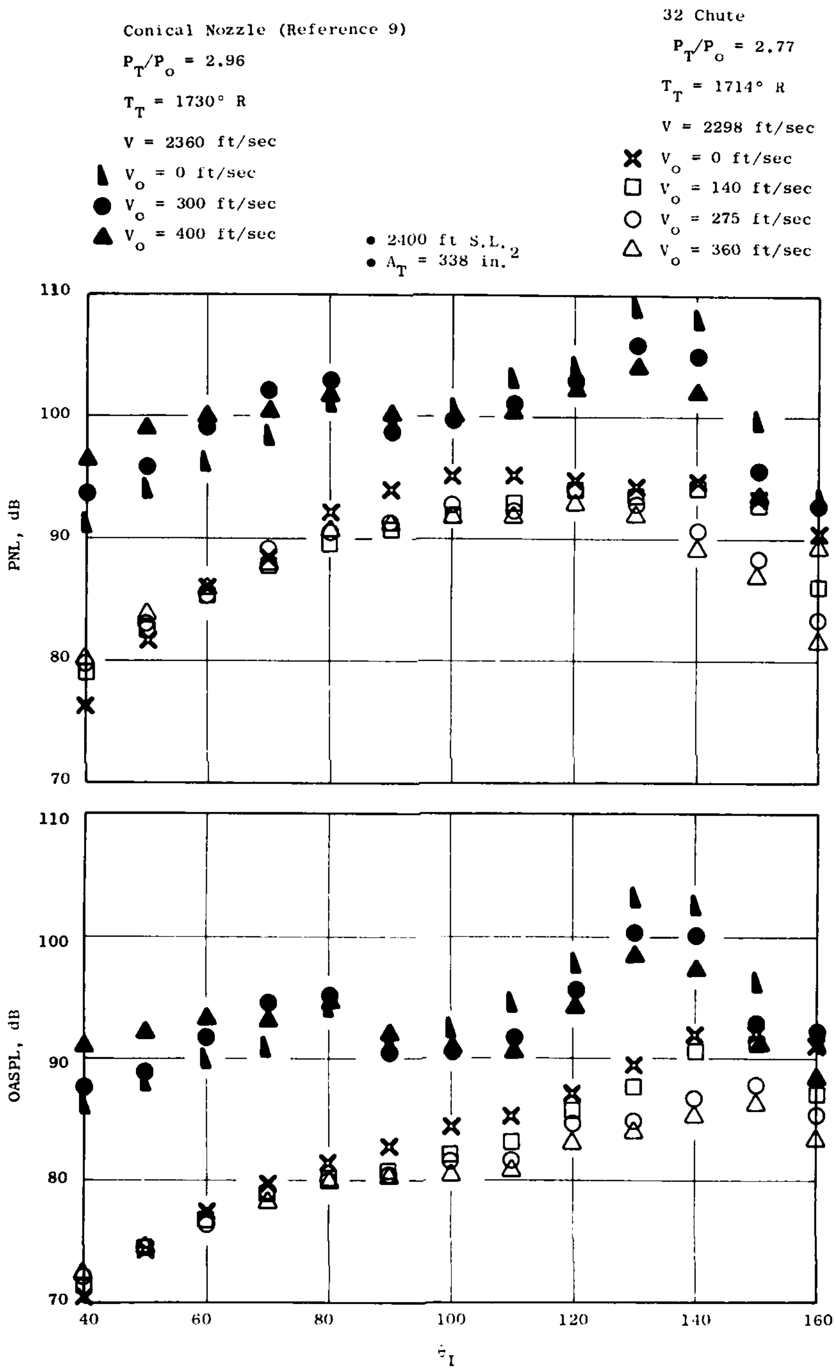

Figure 7-38. 32 Chute Nozzle - PNL and OASPL Directivity.

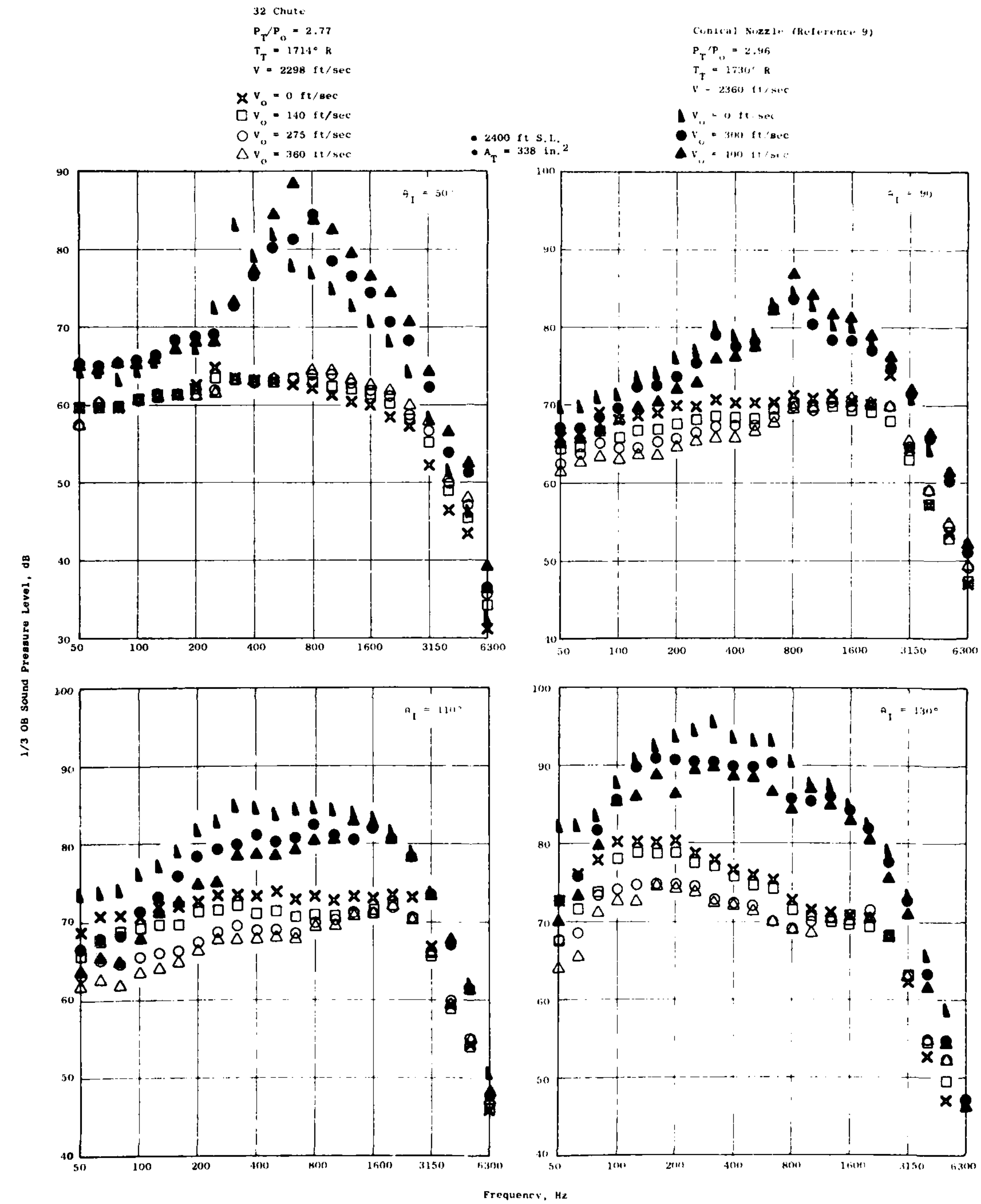

Figure 7-39. 32 Chute Nozzle - Static and Flight Spectra.

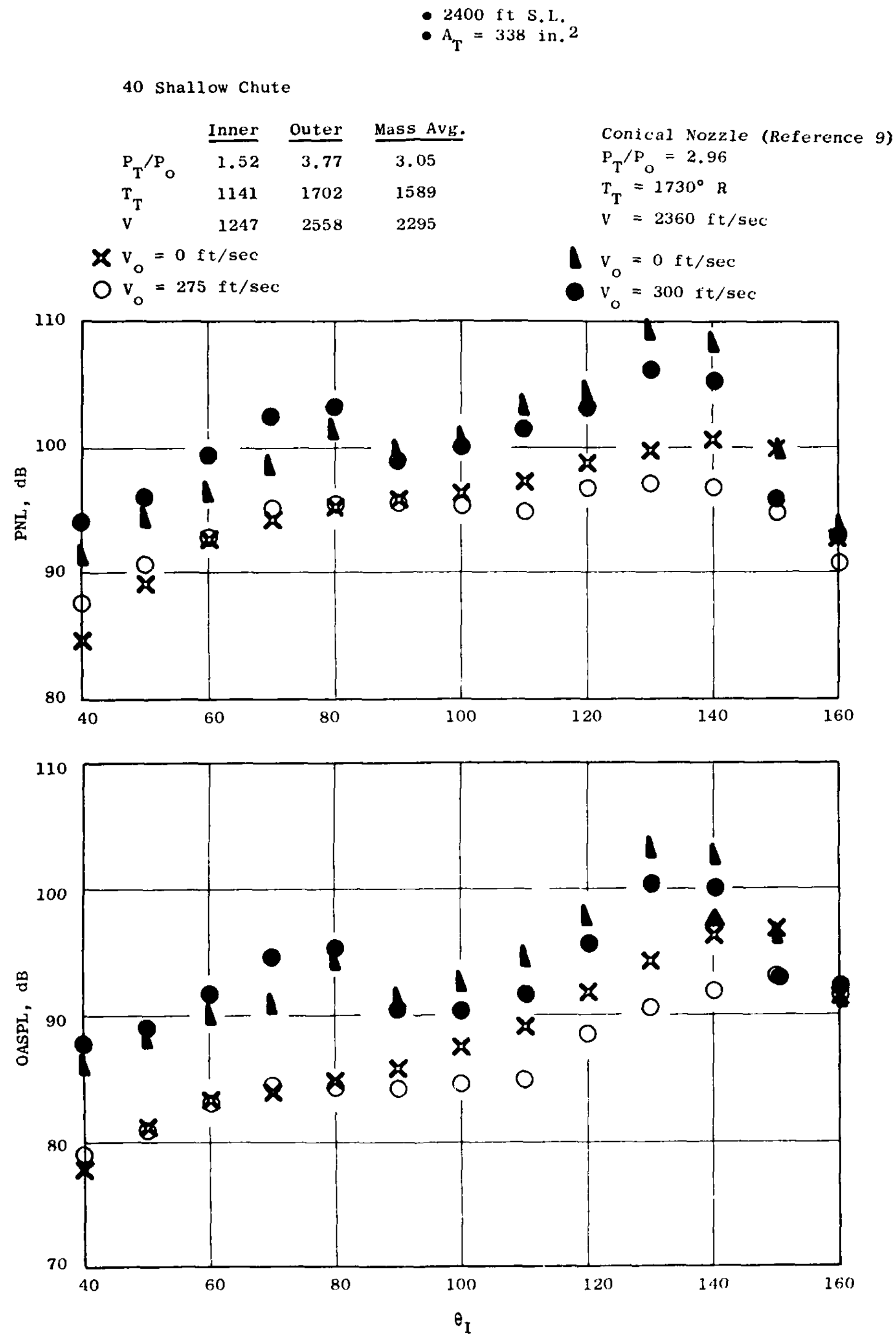

Figure 7-40. 40 Shallow Chute - PNL and OASPL Directivity.

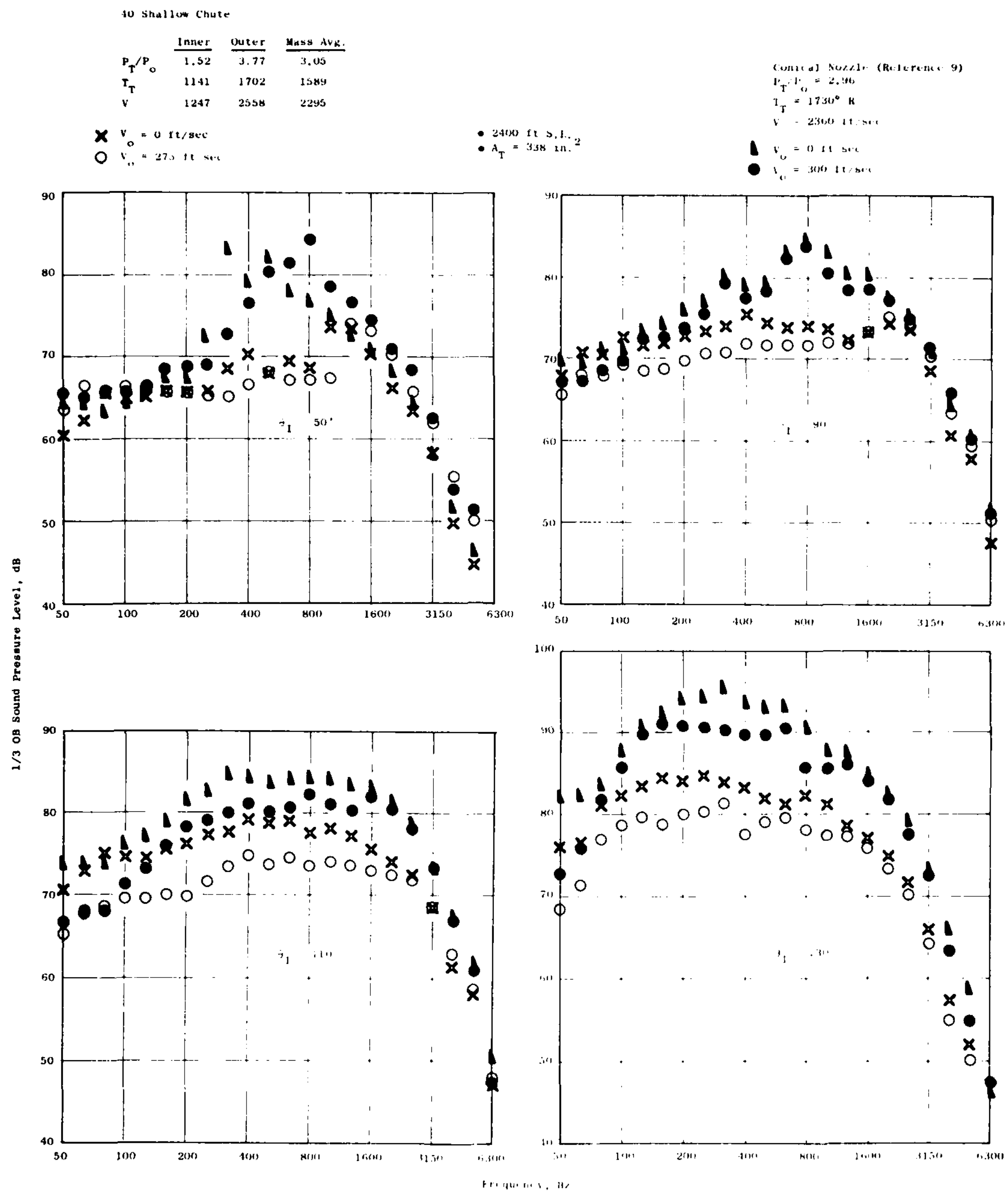

Figure 7-41. 40 Shallow Chute Nozzle - Static and Flight Spectra.

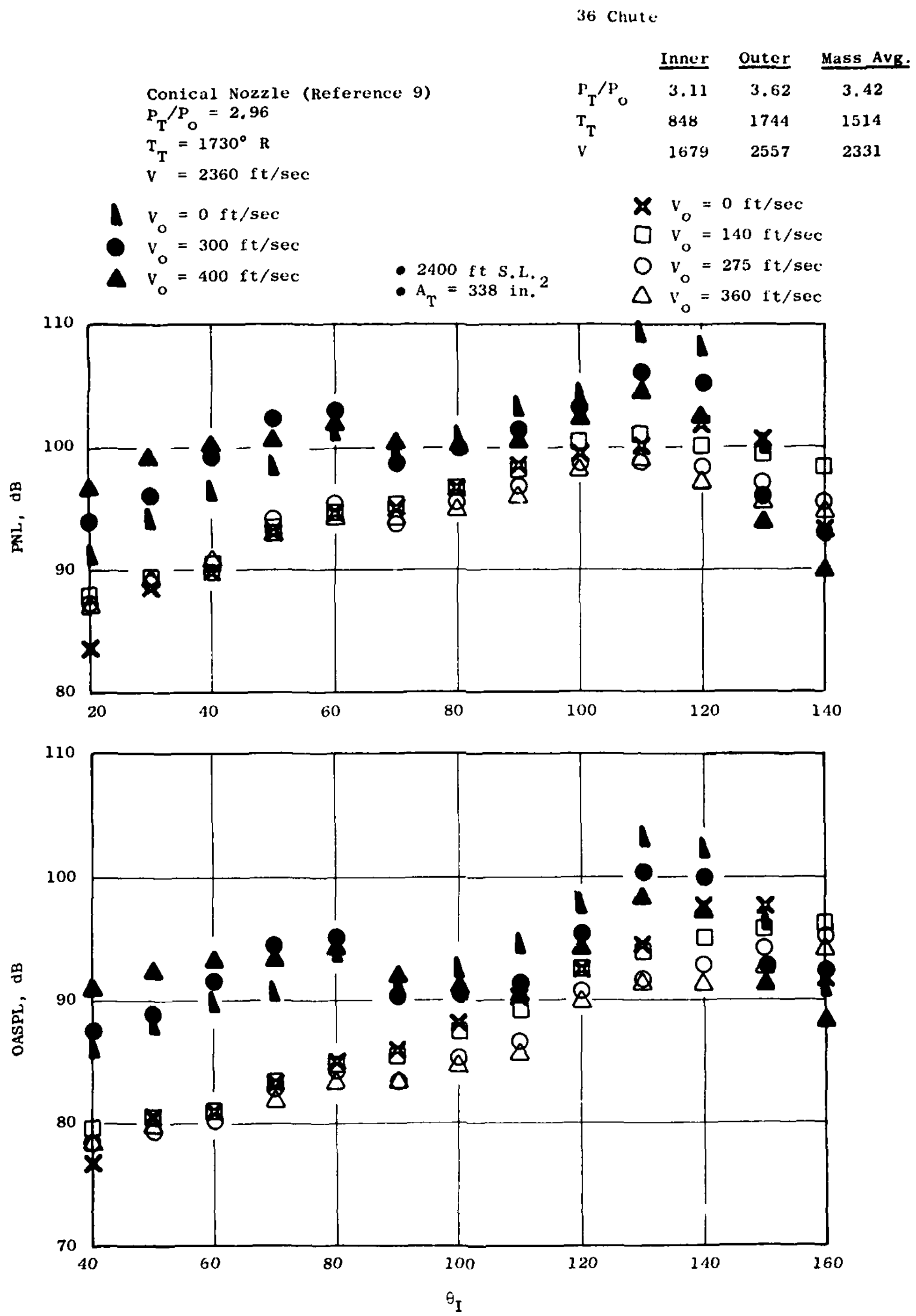

Figure 7-42. 36 Chute Nozzle - PNL and OASPL Directivity.

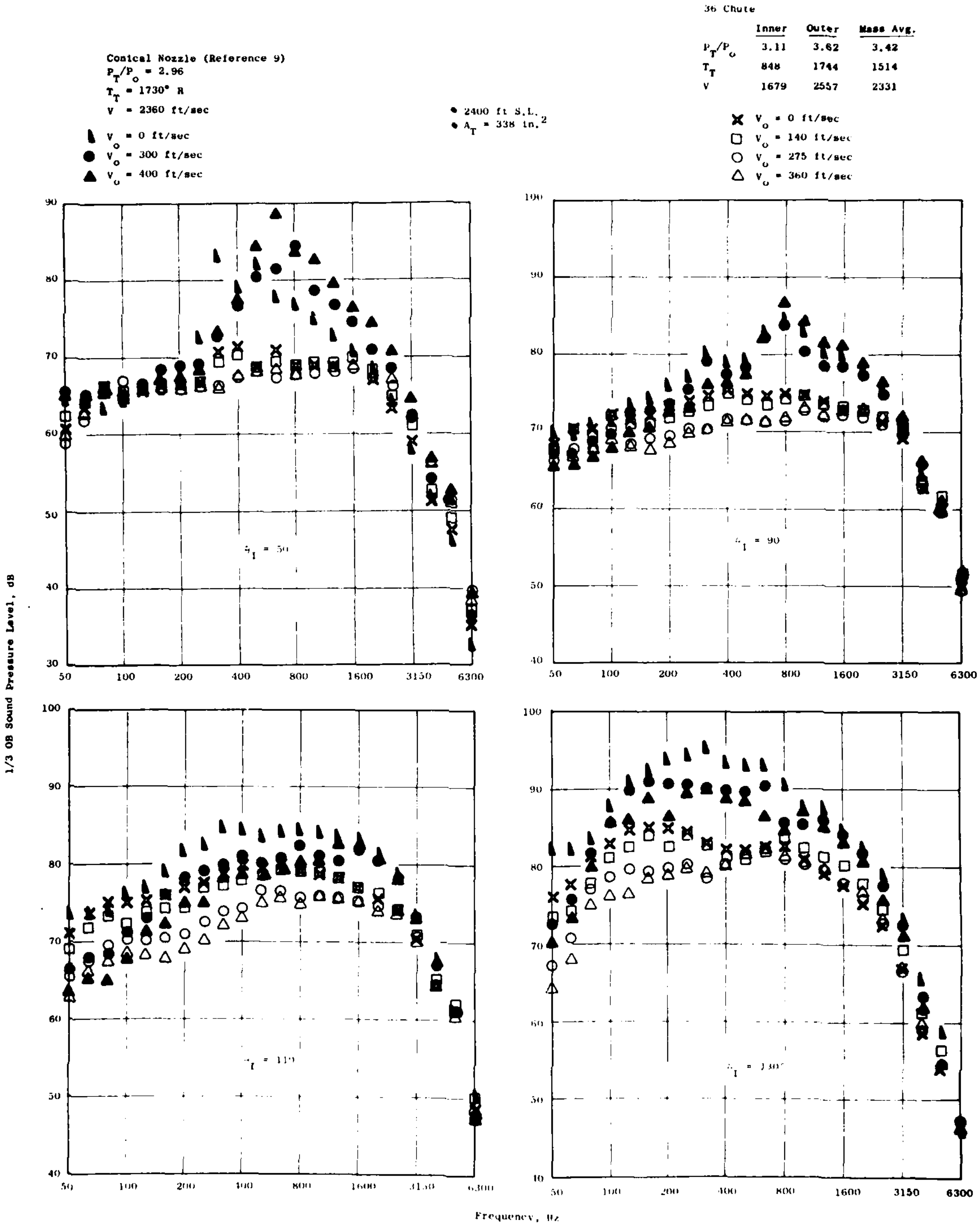

Figure 7-43. 36 Chute Nozzle Static and Flight Spectra.

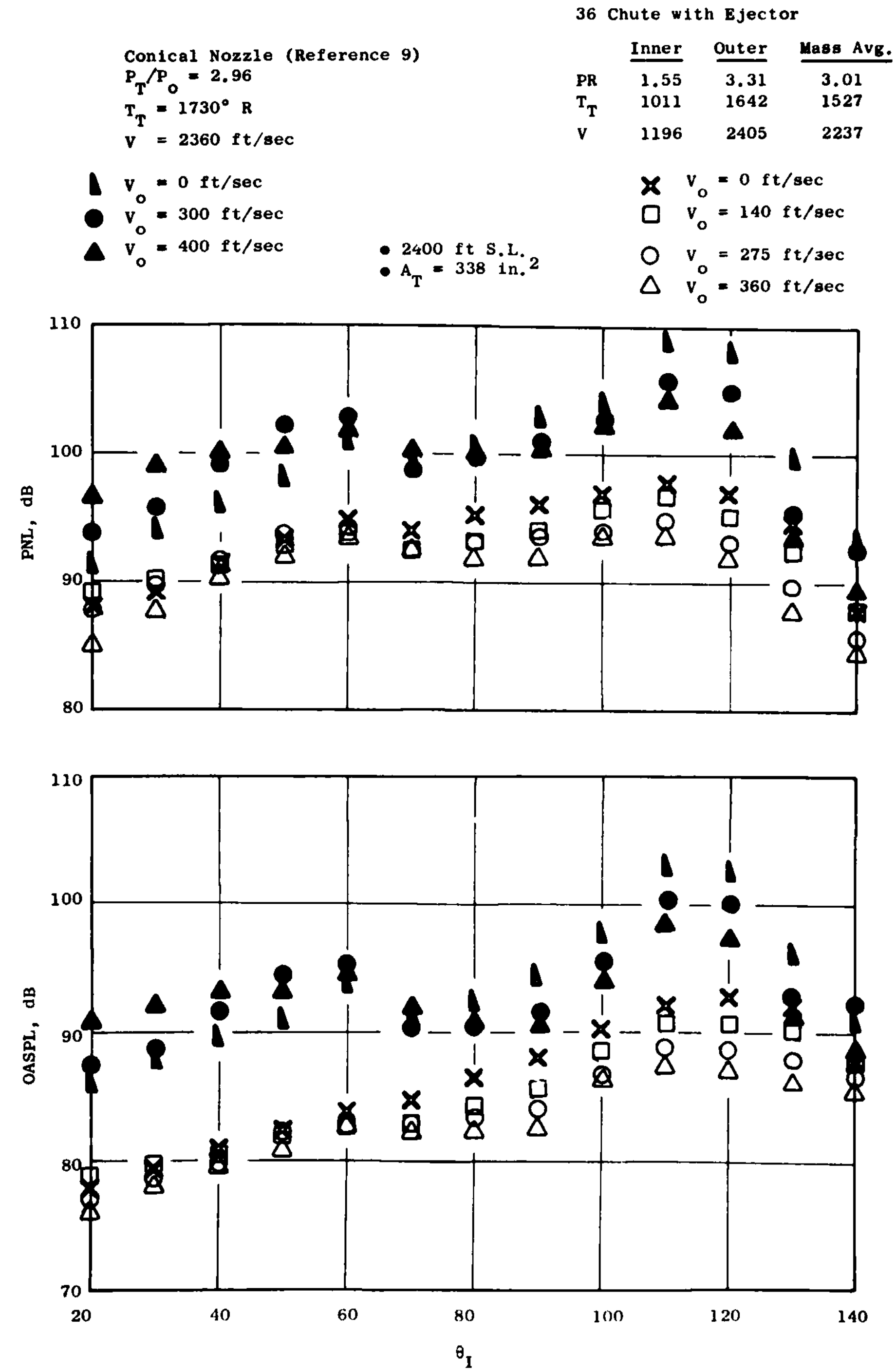

Figure 7-44. 36 Chute with Treated Ejector - PNL and OASPL Directivity.

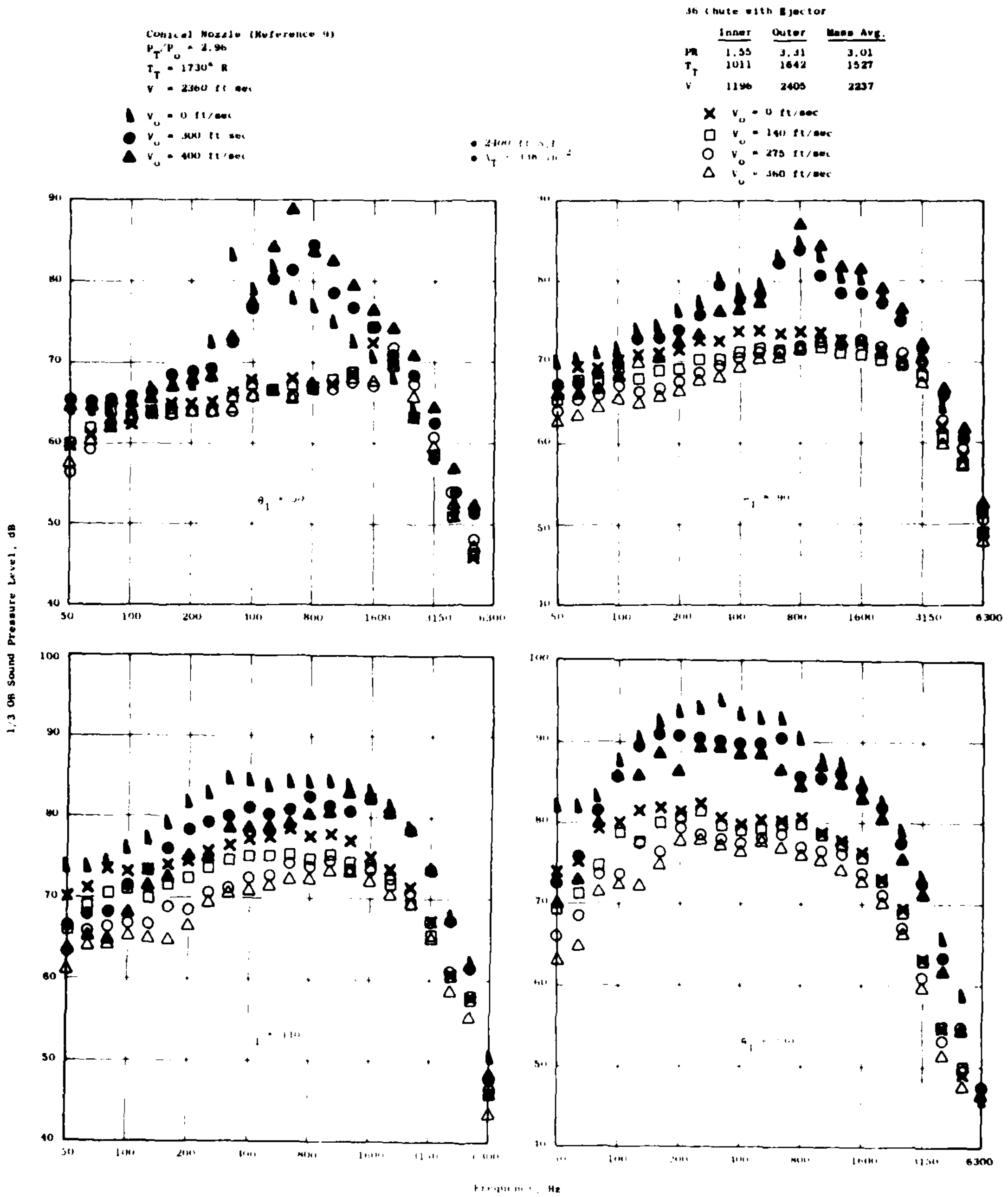

Figure 7-45. 36 Chute Nozzle with Treated Ejector - Static and Flight Spectra.

Directivity and spectrum trends for these configurations are similar to the 40-shallow-chute nozzle.

Directivity and spectrum comparisons for the 54-element coplanar mixer nozzle are summarized on Figures 7-46 and 7-47. Significant shock noise reduction occurs in the forward quadrant, and there is minimal change in the forward quadrant noise level. At 90°, in contrast to the other four suppressor designs, a decrease in high frequency noise occurs from static to flight. The flight effects at 110° and 130° are larger than observed for the conical nozzle. Also, the location of peak noise for this configuration is at 140°, whereas most other suppressor configurations peak at 110 to 120°.

These directivity and spectra comparisons illustrate that the flight effects for suppressor nozzles vary as a function of configuration, flight velocity, acoustic angle, and frequency. Flight generally enhances suppression in the forward quadrant at supercritical pressure ratios because conical nozzle shock noise amplification is not apparently present in the suppressors. At 90°, and in the aft quadrant, there is significant low frequency reduction from static to flight, however, there is little or no high frequency reduction.

In Section 7.2, the static 50° OASPL and PNL levels for each of the suppressors are plotted as function of β to determine if the 50° OASPL data in particular will collapse about a line having a β^4 slope. Similar plots for the flight noise characteristics are presented on Figures 7-48 through 7-50. The conical nozzle data from Reference 10 is also presented for comparison on these figures. The conical nozzle illustrates a noise increase in flight, which correlates well with 40 log of the doppler factor. Mean lines based on the static and flight suppressor data do not show a similar trend indicating that, although the static suppressor data do, in general, collapse about a line having a β^4 slope, the amplification in flight is predicted to be less than a conical nozzle.

Suppressors such as the 32-chute nozzle lose their effectiveness as mass average velocity decreases, whereas a design such as the 54-element coplanar mixer nozzle maintains its suppression level relative to a conical nozzle. Several spectra for the 32-chute nozzle at 130° acoustic angle are presented on Figure 7-51. These spectra are presented for mass average velocities ranging from 2610 to 1742 ft/sec. At jet velocities such as 2610 ft/sec, the static spectra are dominated by low frequency noise which enjoys a large flight effect. Conversely, at 1742 ft/sec the high frequency and low frequency noise levels are within 4 dB and although the low frequency levels are reduced in flight on a PNL basis, the high frequency dominates, which results in poorer suppression when compared to a conical nozzle. A similar set of comparisons (Figure 7-52) are presented for the 54-element coplanar mixer nozzle. The spectrum shape is different than that of the 32-chute nozzle. This nozzle enjoys a flight effect in the high frequencies in contrast to the 32-chute nozzle. The spectrum shapes for this configuration differ from the typical double-humped spectra characteristic of multielement suppressor nozzles.

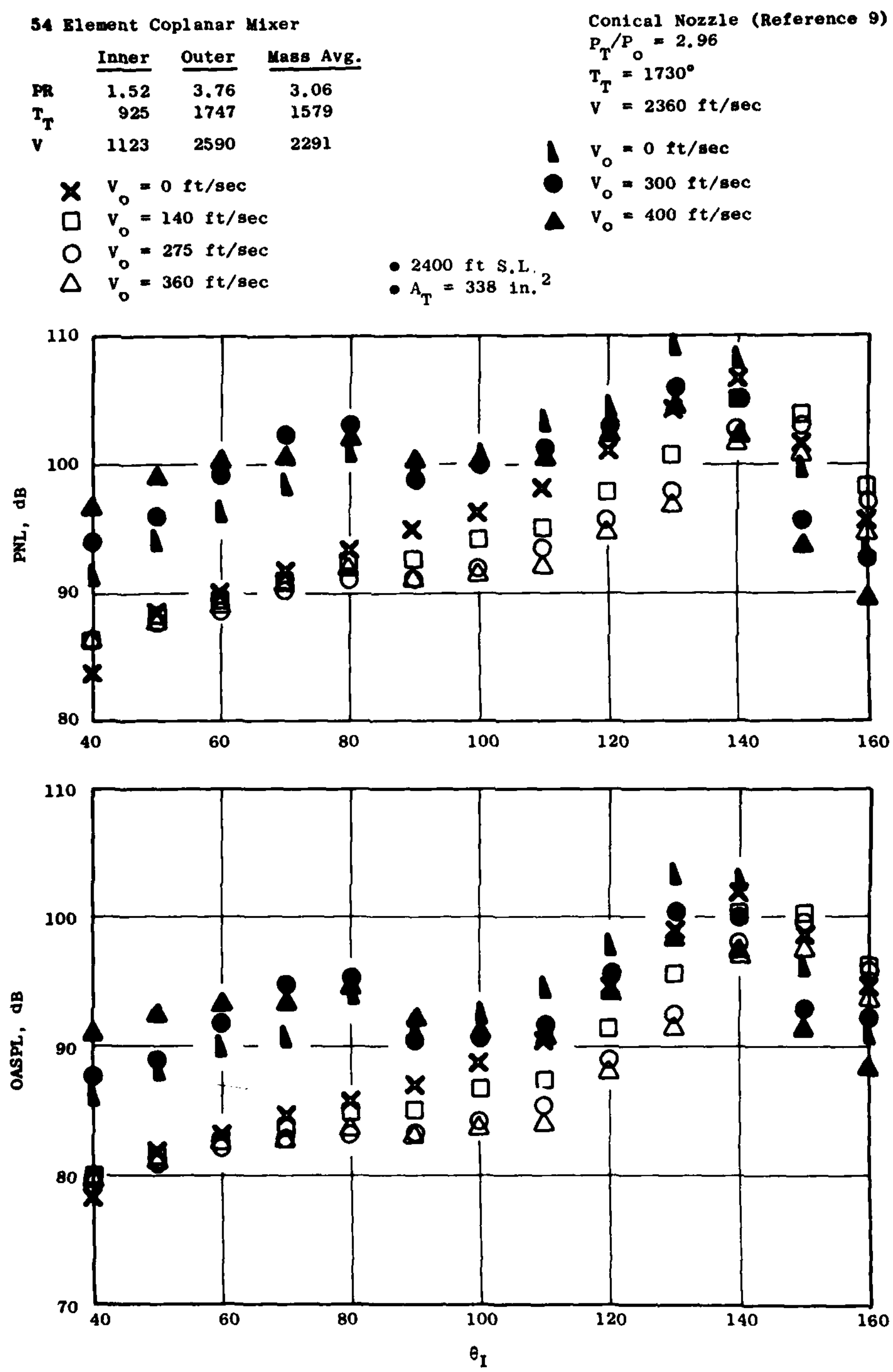

Figure 7-46. 54 Element Coplanar Mixer Nozzle - PNL and OASPL Directivity.

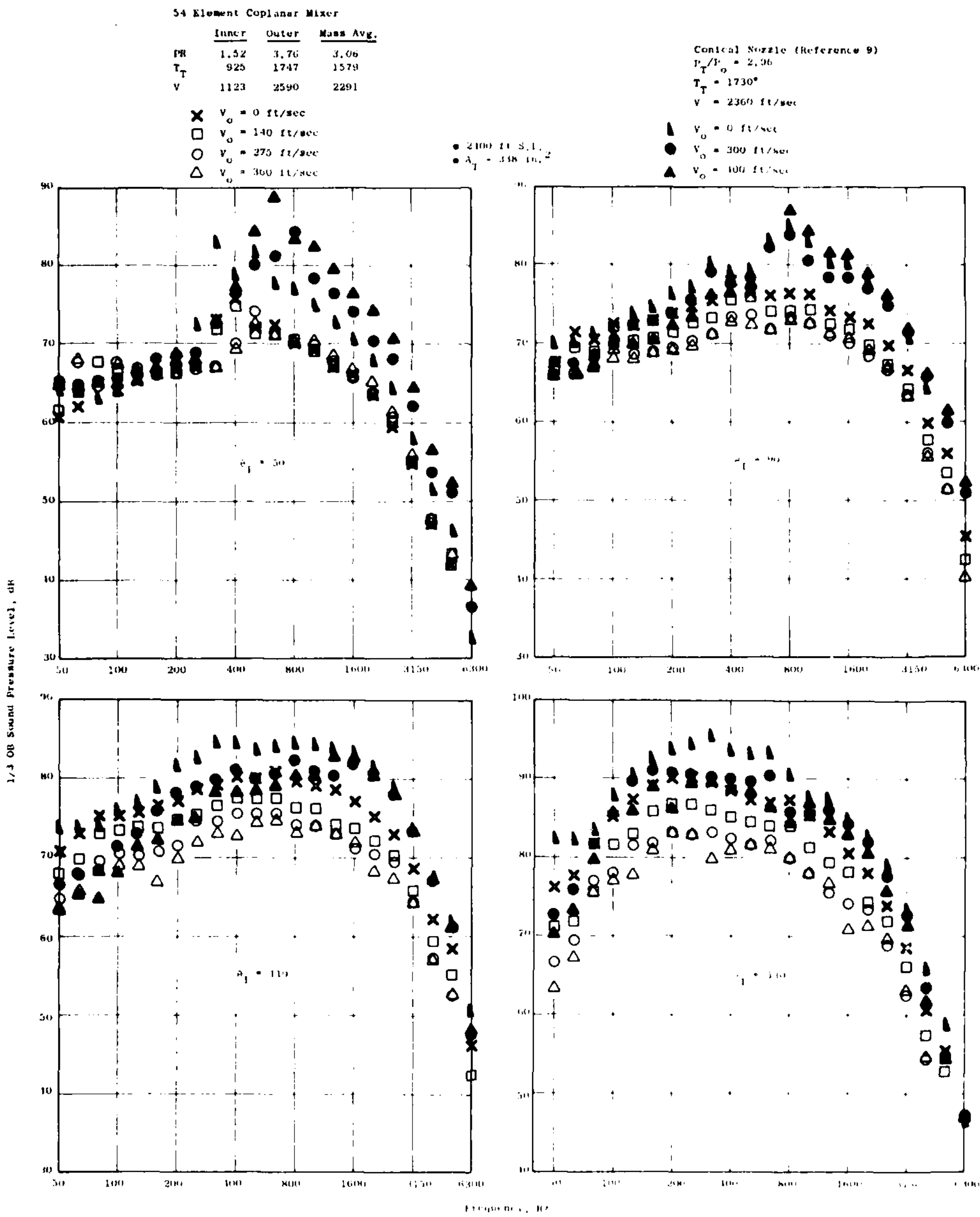

Figure 7-47. 54 Element Coplanar Mixer Nozzle Static and Flight Spectra.

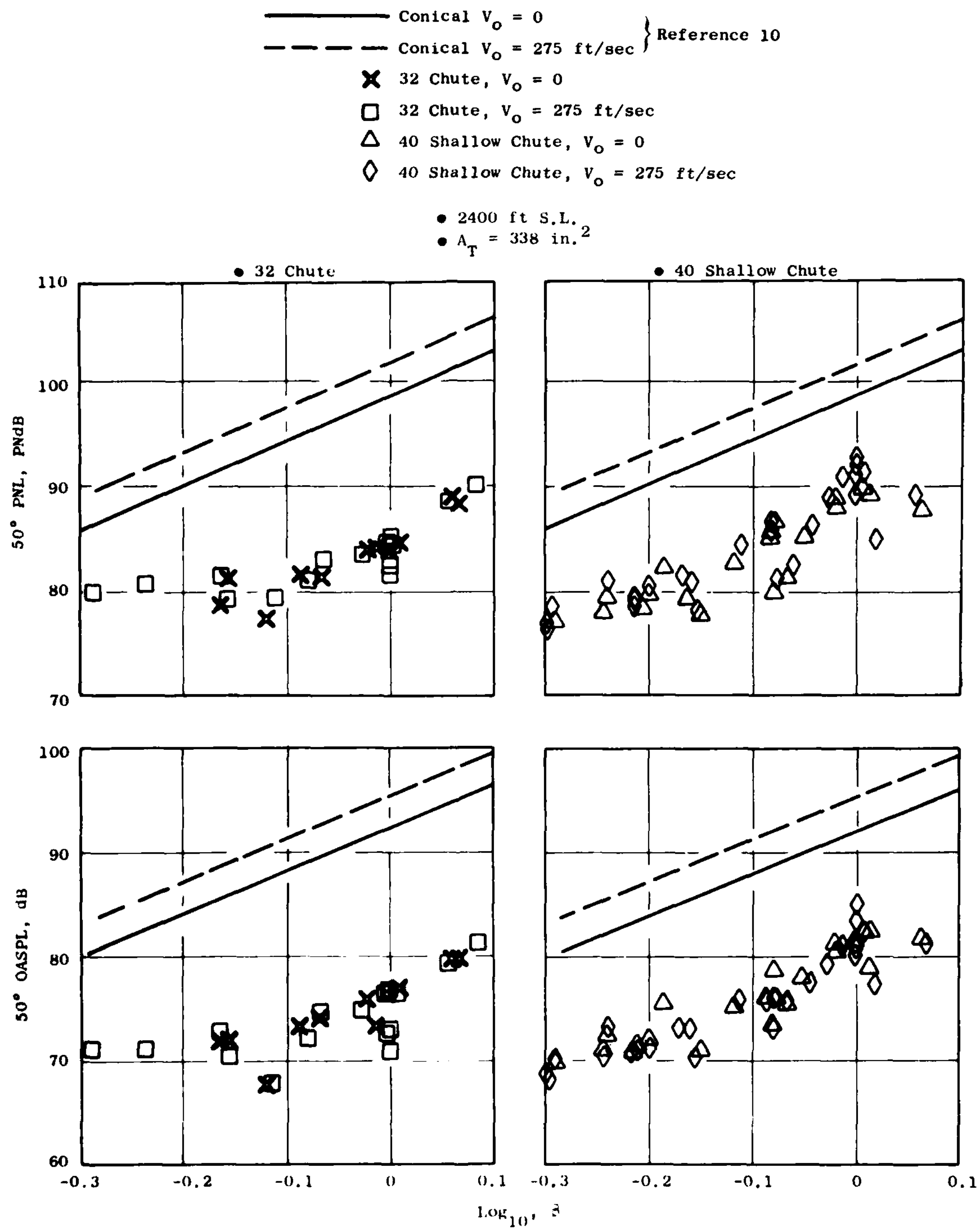

Figure 7-48. 32 Chute and 40 Shallow Chute 50° Noise Characteristics.

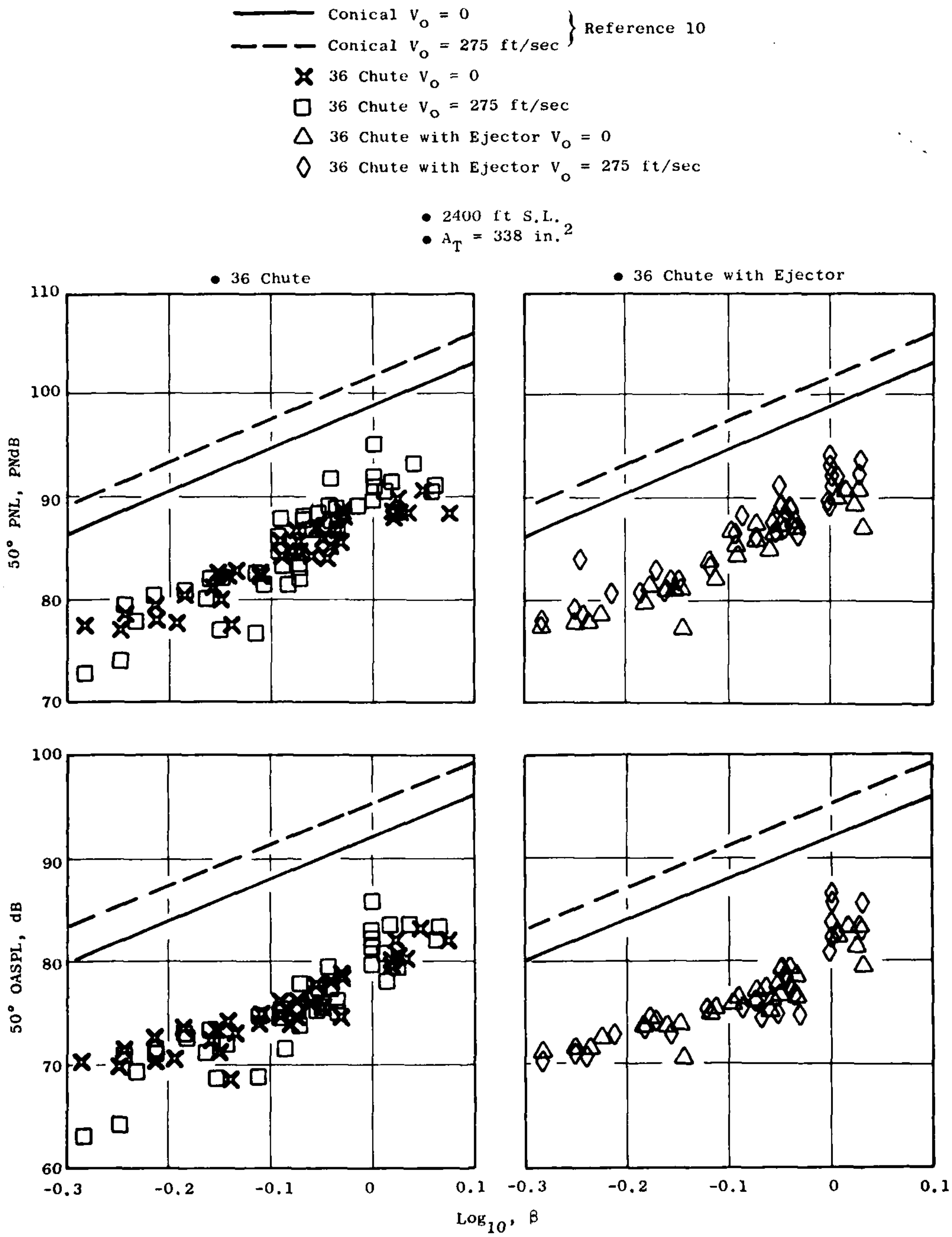

Figure 7-49. 36 Chute Nozzle with and Without a Treated Ejector 50° Noise Characteristics.

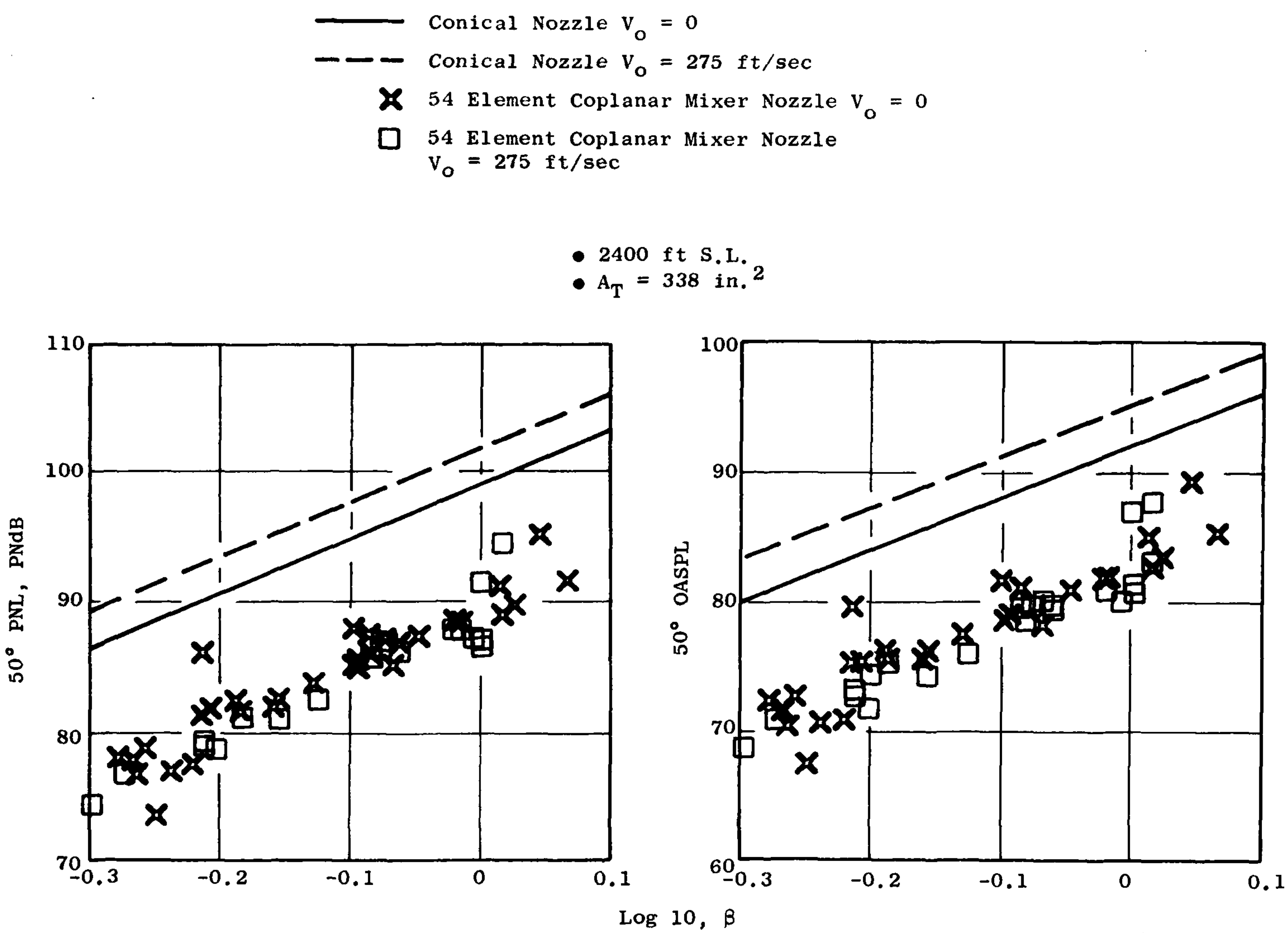

Figure 7-50. 54 Element Coplanar Mixer Nozzle 50° Noise Characteristics.

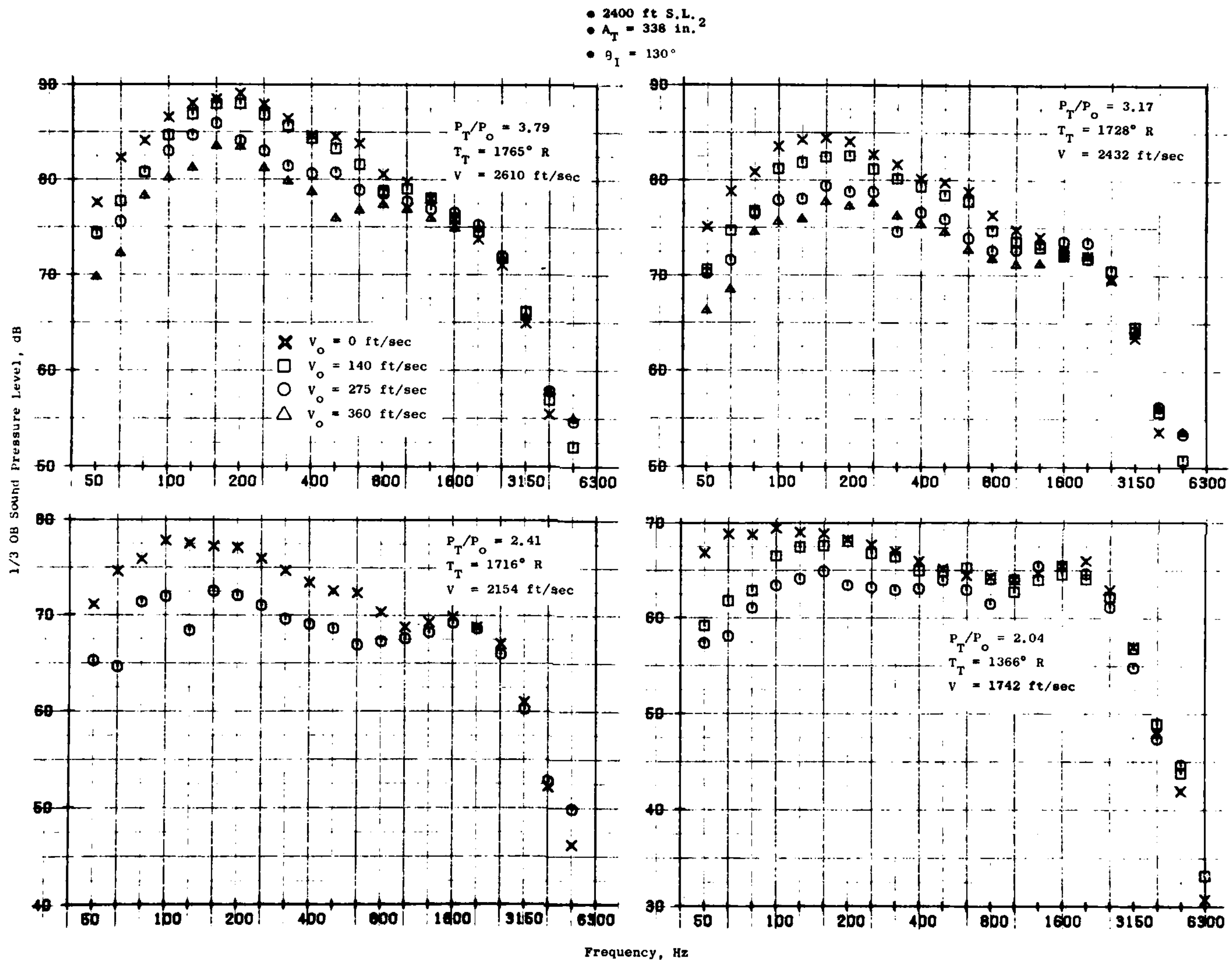

Figure 7-51. 32 Chute Nozzle Spectra Variation with Mass Average Velocity.

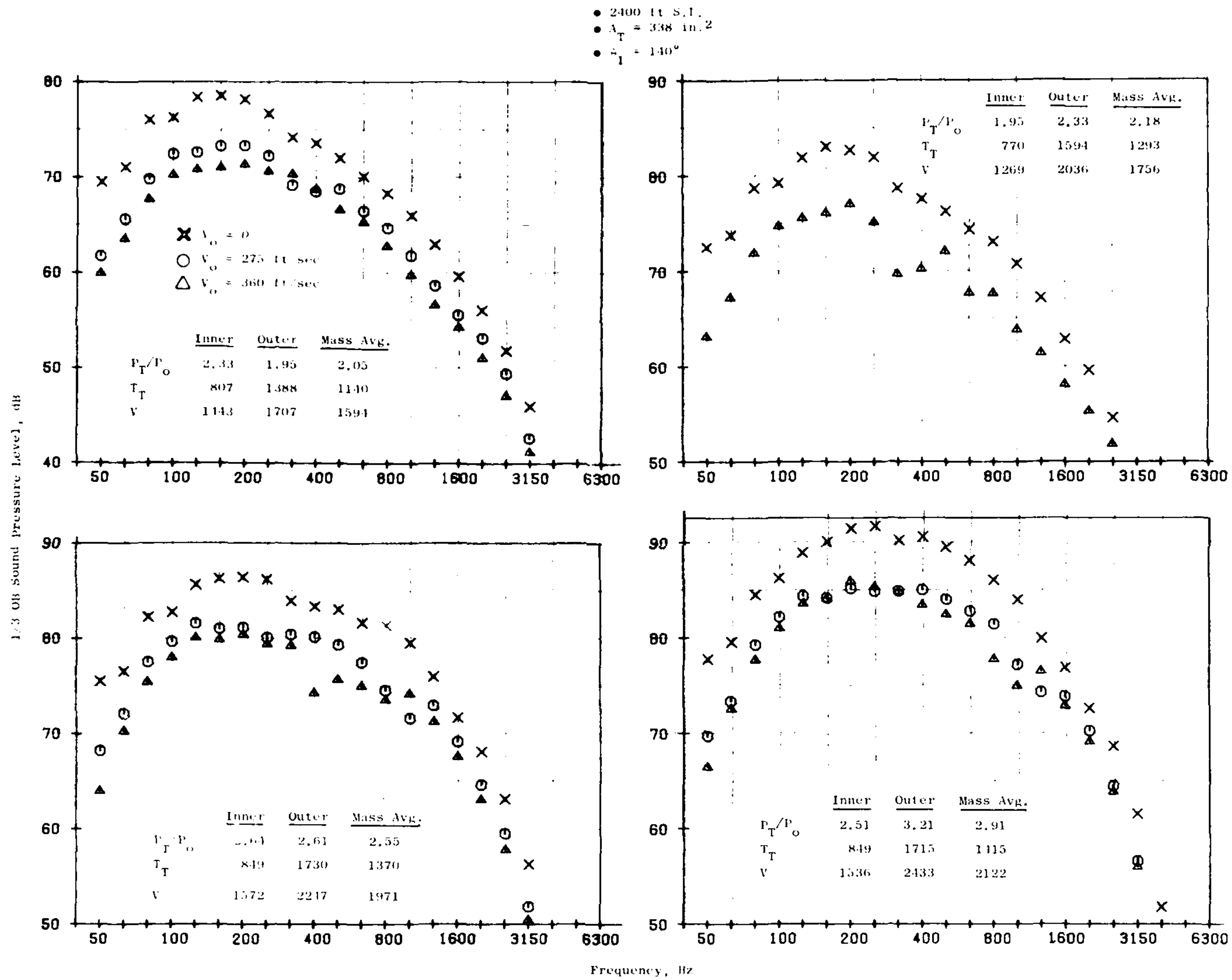

Figure 7-52. 54 Element Coplanar Mixer Nozzle Spectra Variation with Mass Average Velocity.

This section has presented the flight noise characteristics of the five suppressor nozzles. At high velocities, the suppression levels measured statically and in flight are comparable. As mass average velocity is decreased, the flight suppression levels are less than those measured statically, from 0 to 5 PNdB. The reason for the loss of suppression is that the premerged noise produced by a multielement suppressor nozzle realizes only minimal alteration in flight, and as mass average velocity decreases the level of the p-emerged noise and postmerged noise approach each other. Therefore, on a PNL bases, very little flight effect is realized. In all cases, the suppressor noise levels in flight were lower than their static counterparts and also lower than the conical nozzle in flight. In the forward quadrant, multielement suppressors are effective in reducing shock noise; also, the forward quadrant noise for a suppressor is not amplified to the same degree as a conical nozzle.

8.0 IMPLICATIONS OF AERODYNAMIC PERFORMANCE, WEIGHT AND SUPPRESSION

The results presented in prior sections have focused on establishing the flight noise suppression characteristics of the five suppressor nozzles. Based on the results of the studies presented in Reference 3, the addition of a suppressor allows the use of a smaller engine to meet a specified noise goal. However, two penalties are incurred due to the addition of a suppressor. The first is a thrust loss relative to the unsuppressed engine and the second is an increase in engine weight due to the addition of a mechanical suppressor. This section provides aerodynamic performance and weight estimates for the five suppressor designs considered in this study. The performance characteristics will be summarized in terms of thrust coefficient, C_{f_g}, as a function of inner and outer stream pressure ratio. The weight estimates presented are for the turbojet (single flow) and variable cycle (dual flow) engines discussed in Reference 3. In addition, delta suppression to delta performance ratios ($\Delta PNL/\Delta C_{f_g}$) are established for the five suppressor designs. Finally, suppression levels in terms of EPNdB at representative AST takeoff power settings, are presented to illustrate how suppression levels are affected with changes in engine size (scaling effects).

8.1 AERODYNAMIC PERFORMANCE CHARACTERISTICS

The AR = 2.1 32-chute nozzle design was evolved as the final configuration in the FAS/DOT SST Phase II study (1). An aerodynamic performance model was tested in the FluiDyne Engineering Corporation's 66 by 66-inch Transonic Wind Tunnel, both statically and at Mach 0.36. A photograph of the Model and the results of this test are shown in Figure 8-1. In the pressure ratio range currently being considered for advanced turbojet engines (2.7 to 3.5) this configuration has a thrust coefficient which ranges from 0.92 to 0.93.

The $(AR)_o$ = 1.75 40-shallow-chute nozzle was tested for aerodynamic performance in the NASA-Lewis Research Center 8 by 6-foot Supersonic Wind Tunnel under Task 3[10] A photograph of the model installed in the wind tunnel and the results of the test are shown in Figure 8-2 for both static and Mach 0.36 conditions. Performance characteristics are presented as a function of outer stream pressure ratio while holding the inner stream pressure ratio constant at levels currently being considered for VCE-cycles. Thrust coefficients for this configuration over the pressure range of interest vary from 0.895 to 0.905.

The $(AR)_o$ = 2.0 C-D 36-chute nozzle was not tested to obtain aerodynamic performance. However, its performance characteristics were estimated utilizing the available chute suppressor data base[10] and correlation techniques being developed for the Task 6 Design Guide[17] under this contract. With the exception of the chute depth and cross sectional shape, this nozzle is similar to the 36-chute $(AR)_o$ = 2 nozzle tested as part of Task 3[10], Figure 8-3. The task 3 nozzle was, therefore,

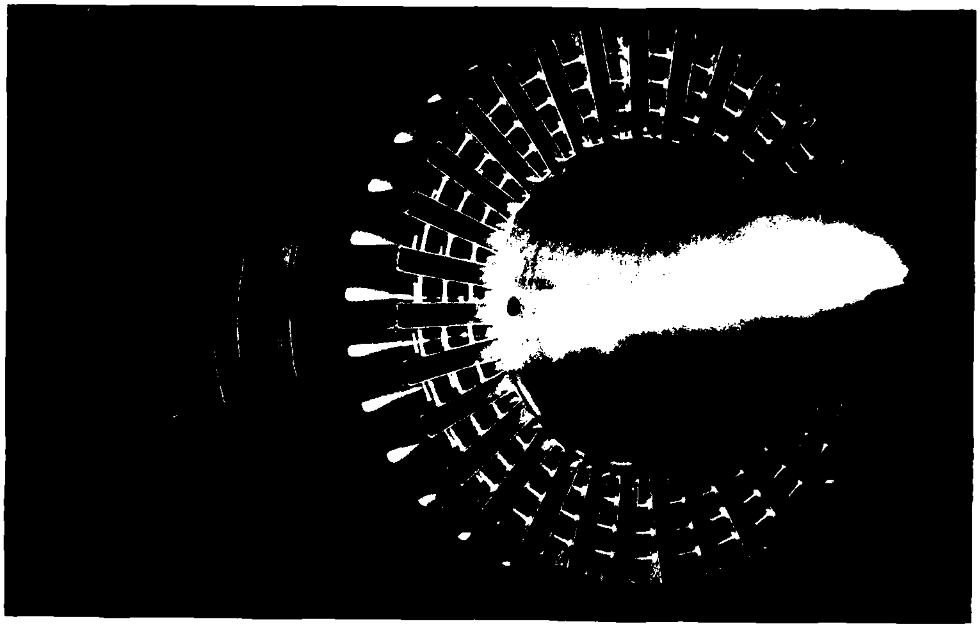

• AR = 2.1 32 Chute Nozzle

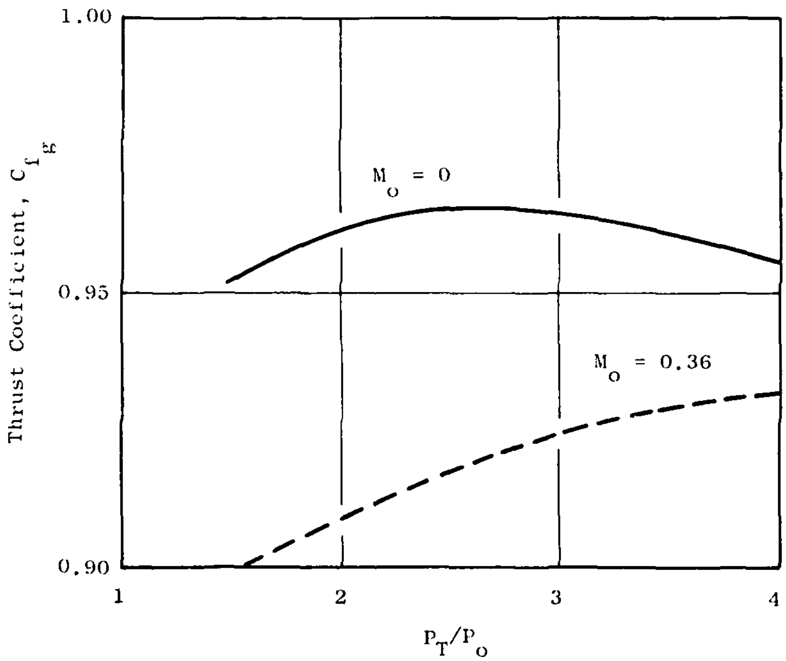

Figure 8-1. AR = 2.1 32 Chute Nozzle Performance Characteristics.

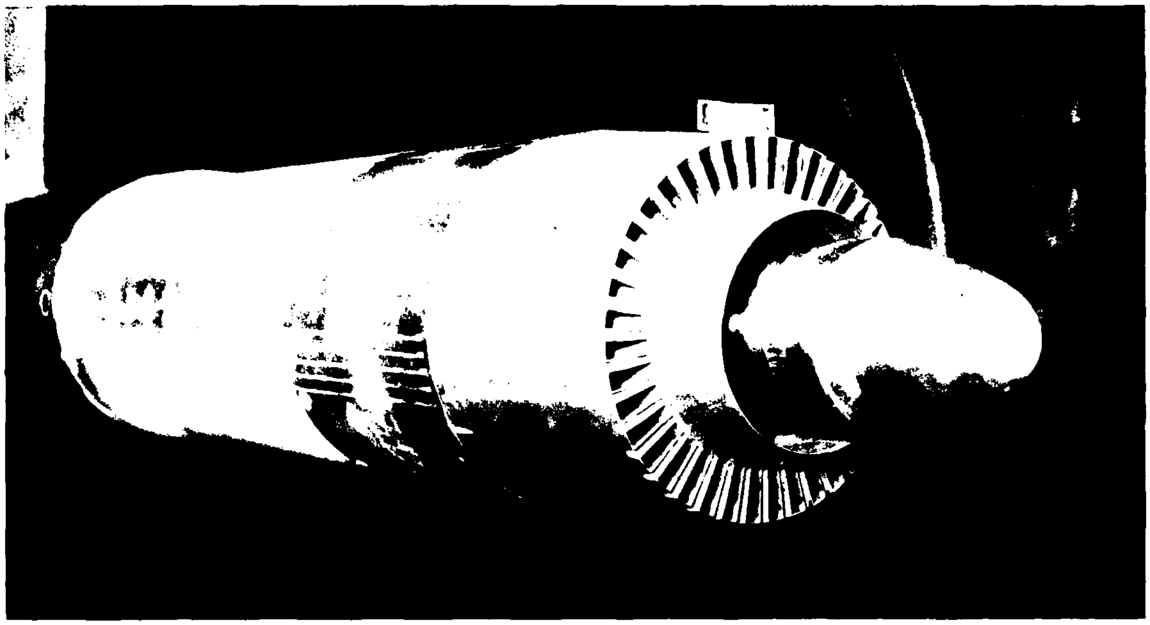

• $(AR)_o$ = 1.75 40 Shallow Chute Nozzle

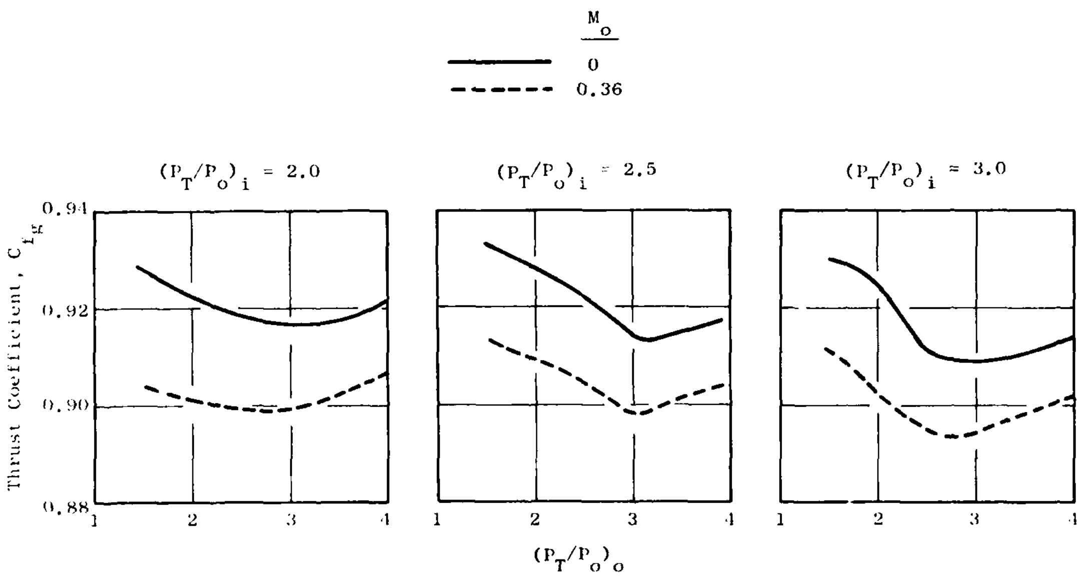

Figure 8-2. 40 Shallow Chute.

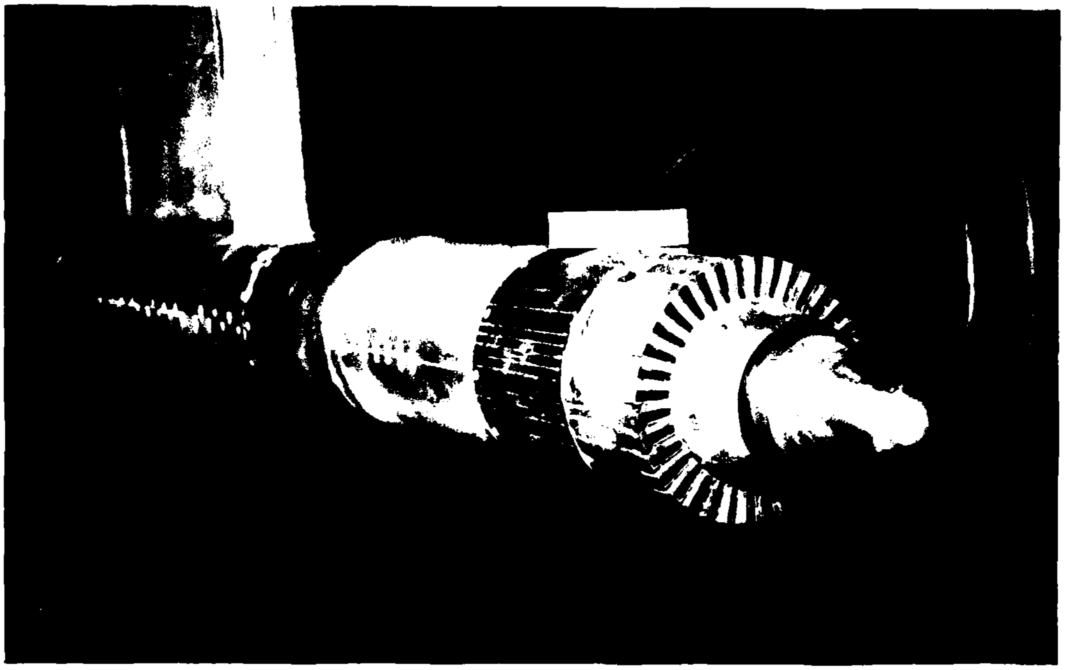

• $(AR)_o$ = 2.0 36 Chute Reference Nozzle from Reference (10)

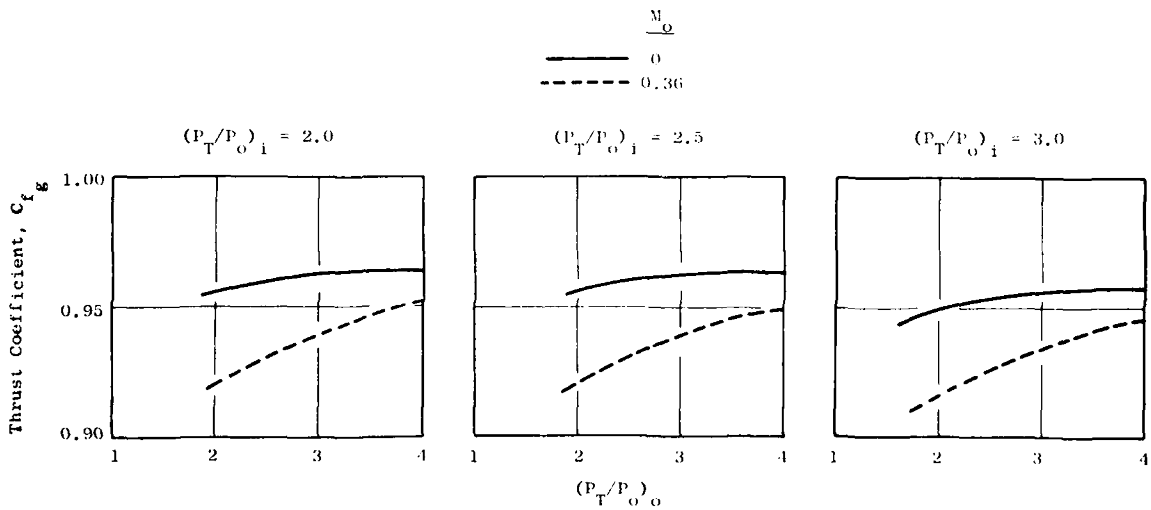

Figure 8-3. 36 C-D Chute Nozzle Performance Characteristics (Estimated).

used as a baseline for the performance estimate. This baseline nozzle performance was adjusted to account for differences in chute geometry. The Task 3 model was instrumented with suppressor element base pressure taps which were used to calculate a loss in thrust coefficient due to lower than ambient base pressures. The generalized chute suppressor base pressure correlation equation, derived from the Task 6 Design Guide(17) was then used to estimate the base pressures for the new suppressor Typically, the new design reduced base drag losses by 50% due to the increased chute depth. In addition, the convergent-divergent chute design reduces the projected base area. The results of the performance estimation are shown in Figure 8-3. This configuration has improved performance over the 40-shallow-chute design. Thrust coefficient range from 0.935 to 0.945 over the pressure ratio range of interest.

The aerodynamic performance of the 36-chute nozzle with a treated ejector was estimated by applying increments in thrust coefficients derived from previous annular chute suppressor ejector wind tunnel tests. During the FAA/DOT SST Phase II study(1) a 36-chute, AR = 2.3 and a 32-chute, AR = 2.1 suppressor were tested with and without ejectors statically and at Mach 0.36. Results from these tests indicated that at a typical takeoff nozzle pressure ratio of 3.0, the ejector improved static performance of both suppressors by 2.8%. At Mach 0.36, the ejector improved the performance of both suppressors by 0.6%. These results, as a function of nozzle pressure ratio, were applied to the "bare" 36-chute suppressor to yield the estimates shown in Figure 8-4. The ejector configuration exhibits a much steeper performance gradient with pressure ratio than the previous configurations. However, at outer stream pressure ratios above 3.0, a C_{f_g} of 0.95 may be attainable.

Performance estimates for the 54-element coplanar suppressor exhaust nozzle were derived empirically. In general, the coplanar nozzle, Figure 8-5, is geometrically similar to an unsuppressed single flow annular nozzle with the exception of the amount of wetted perimeter at the nozzle throat. An unsuppressed annular nozzle also shown in Figure 8-5 was, therefore, used as a baseline for the performance prediction. In order to account for the viscous losses (internal) associated with the mixing chutes, Boeing data(18) was utilized. A schematic of a 70-lobe suppressor(18) is shown in Figure 8-6. Boeing(18) generalized performance data from several models of this type as a function of nozzle perimeter are shown in Figure 8-7. These curves were entered at perimeters corresponding to both the coplanar nozzle and the baseline nozzle. The resulting difference in velocity coefficient was then applied to the baseline nozzle test data to arrive at an overall installed thrust coefficient. At a nozzle pressure ratio of 3.0, the installed thrust coefficient is estimated to be 0.95 as compared to an unsuppressed value of 0.980. Estimate performance as a function of nozzle pressure ratio is shown in Figure 8-8. Note that the estimate is for both Mach 0, 0.36. Due to the lack of large base areas typical of other suppressor designs, the performance of this nozzle should not be sensitive to external flow effects. This curve may be used to establish the thrust performance for various combinations of inner and outer stream pressure ratios by simply using the curve to determine the thrust coefficient at the appropriate pressure ratio for both the inner and outer streams and applying it to the ideal thrust for each of the streams.

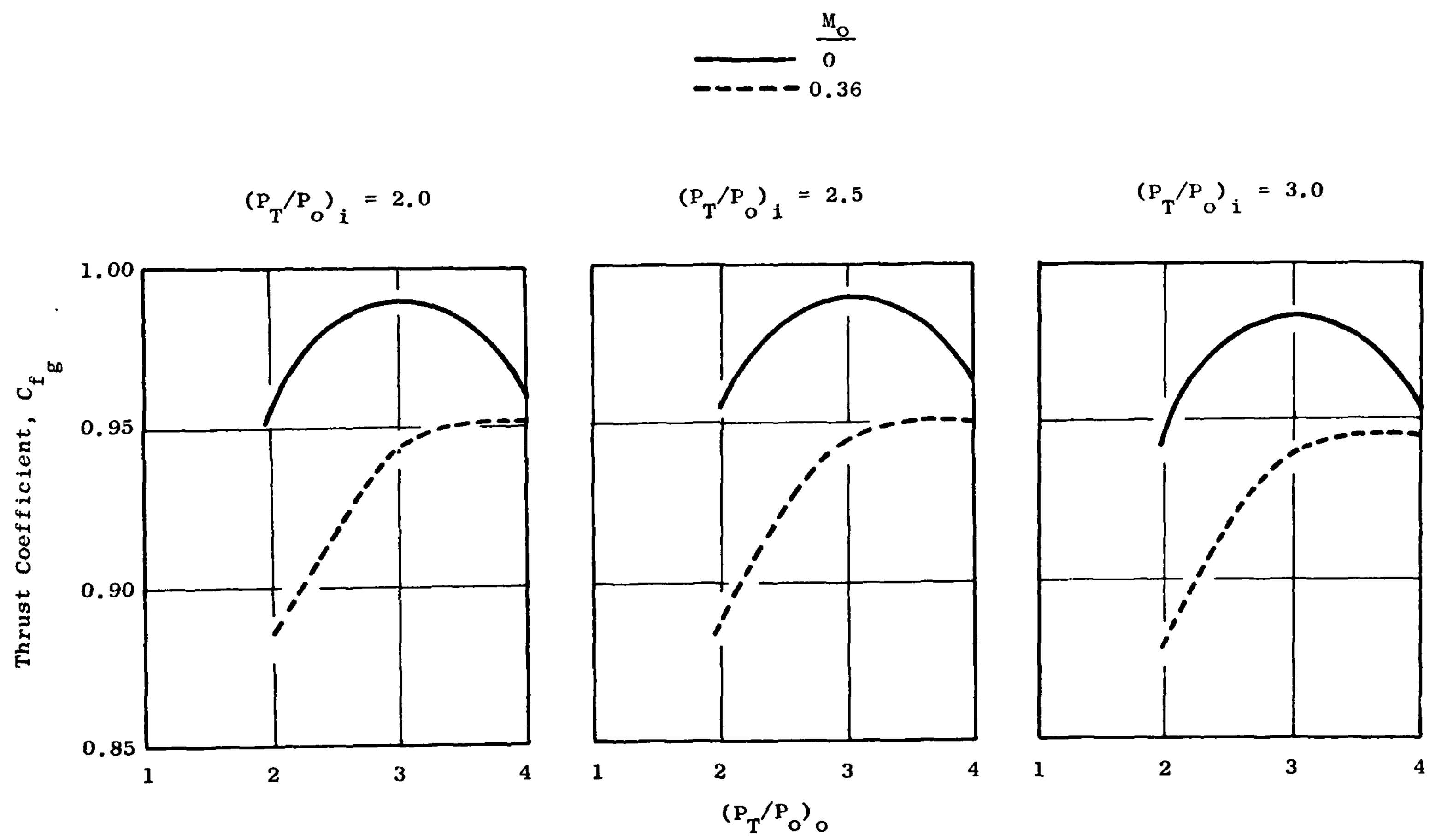

Figure 8-4. 36 C-D Chute Nozzle with Ejector Performance Characteristics (Estimated).

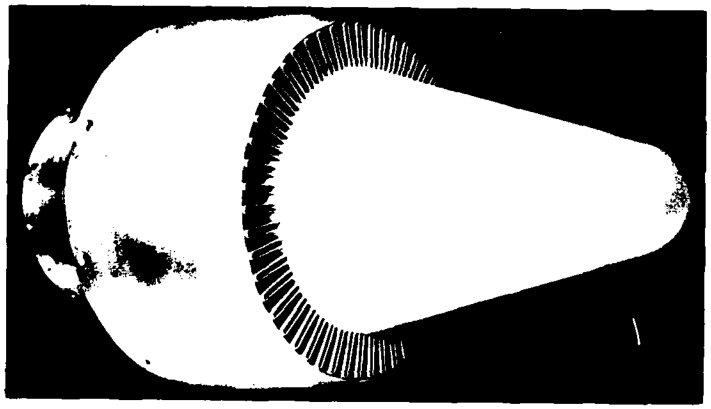

• 54 Coplanar Mixer

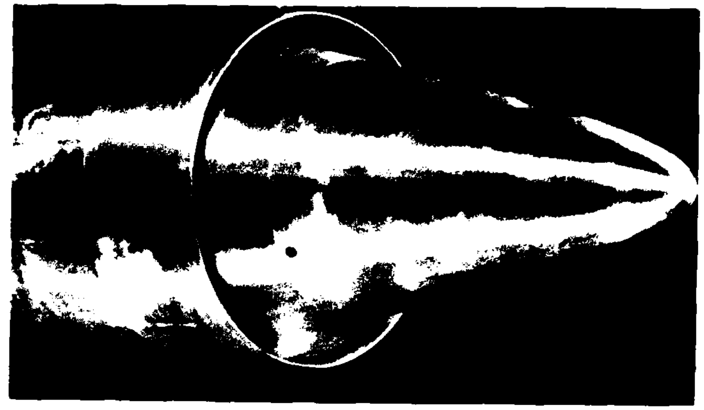

• Unsuppressed Annular

Figure 8-5. Unsuppressed Annular Plug and 54 Element Coplanar Mixer Nozzles.

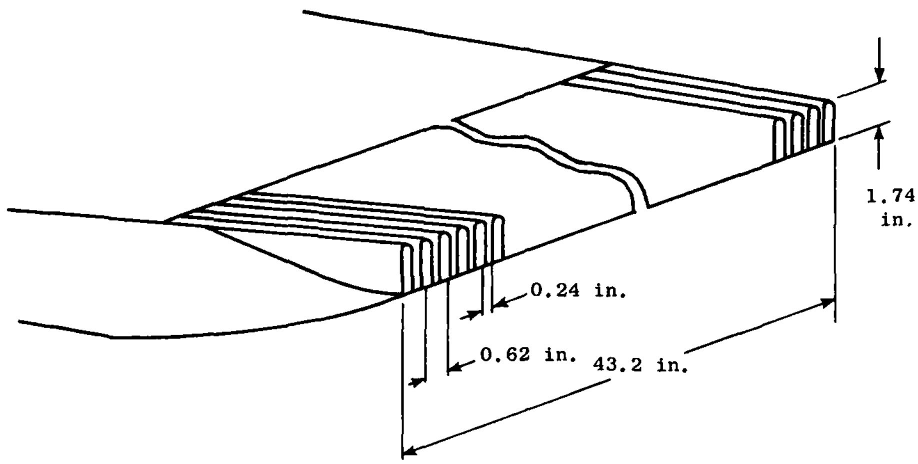

- 70-Lobe Nozzle
- Spacing Ratio = 4.0
- Nozzle Area = 18.7 sq in.

Note: Reference 18, Figure 6-35

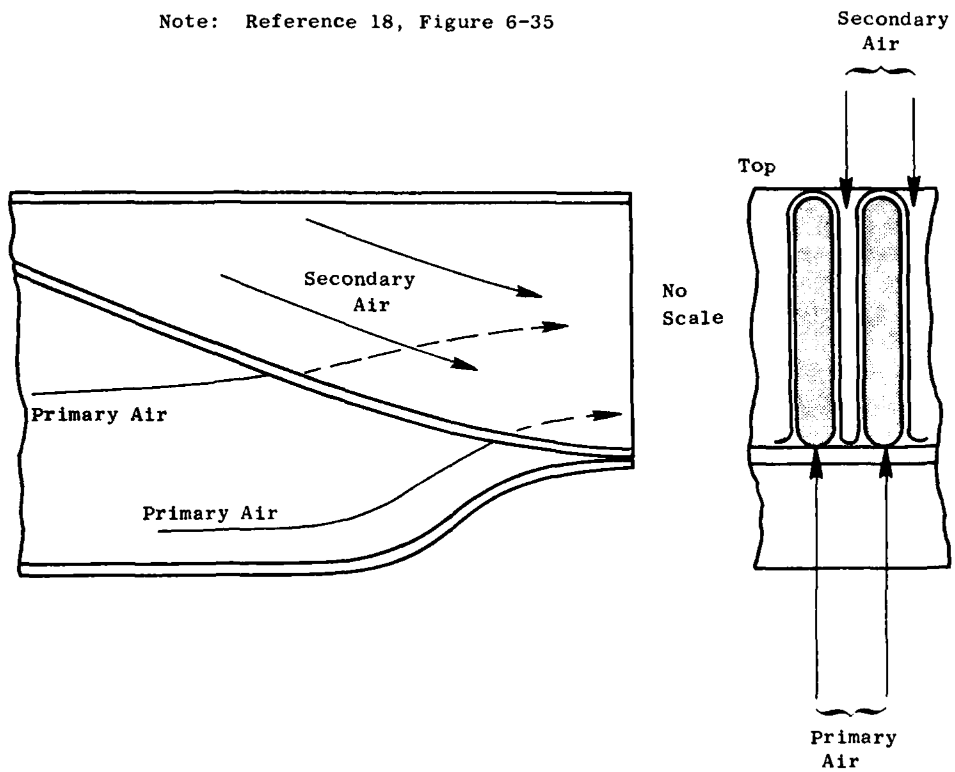

Figure 8-6. Test Configurations - Lobe Nozzles (Reference 18).

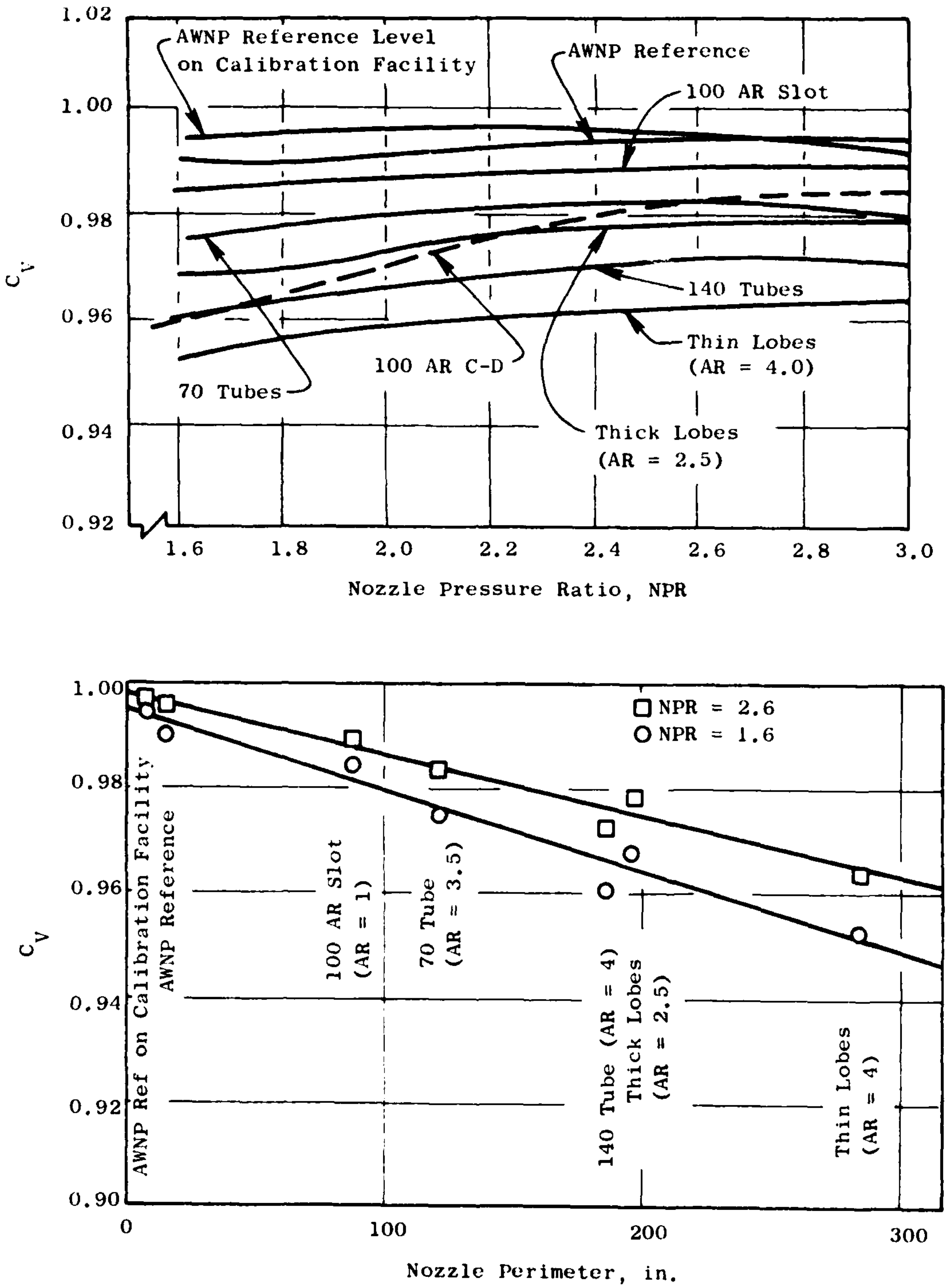

Figure 8-7. Primary Nozzle Performance (Reference 18).

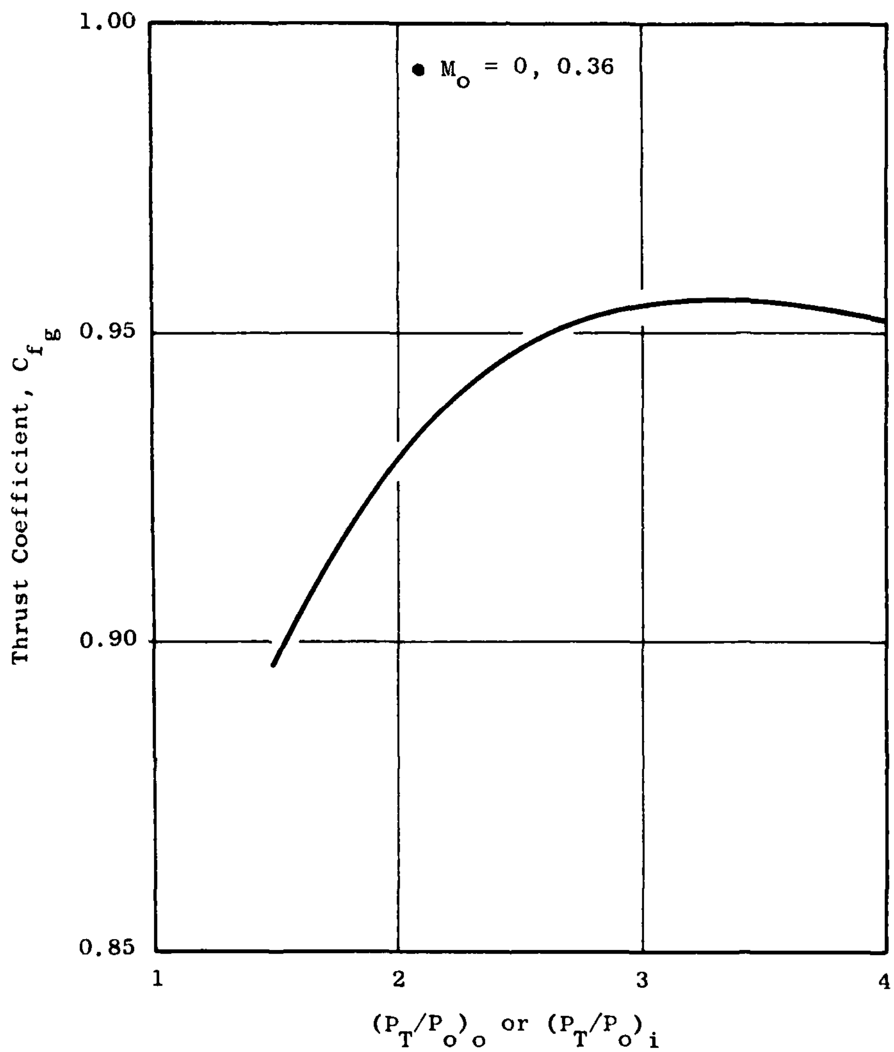

Figure 8-8. 54 Element Coplanar Mixer Nozzle Performance Characteristics (Estimated).

8.2 IMPACT OF MECHANICAL SUPPRESSORS ON ENGINE WEIGHT

The addition of a mechanical suppressor causes a weight increase relative to a reference nozzle(3). In general, this weight increase may be significant relative to the total engine weight. This section will, therefore, provide examples of how each of the suppressor designs evaluated in the current study might effect total exhaust system weight as well as providing some estimates on the impact of these exhaust system weights on the total engine. The turbojet and variable cycle engines from the Task 3 Aircraft Integration Study(3) will be used for this example. The reference nozzle for the turbojet study is a plug nozzle, estimated to weigh 2950 lb on a 770 lbm/sec* engine while its variable cycle counterpart is a coannular plug nozzle weighing about 2800 lb on a 840 lb/sec* engine. A summary of the weight in terms of an increment relative to the reference nozzle and the percent increase in engine weight is summarized on Table 8-1. The 54-element coplanar mixer and the 40-shallow-chute nozzle are the lightest due to minimal mechanical complexity. Recall that these weight estimates are for the engines considered in Reference(3) and represent only an example and not a generalized result.

Table 8-1. Summary of Optimum Nozzle Weight Characteristics.

Configuration	Weight Increase re: Reference Nozzle	% Increase Reference Nozzle Weight	% Increase Engine Weight	Reference Airflow Size lbm/sec
32-chute, AR = 2.1	1150	39	7	770
$(AR)_o$ = 1.74 40 Shallow Chute	550	19.6	4.1	840
$(AR)_o$ = 2.0 36-chute	1300	46.4	9.6	840
$(AR)_o$ = 2.0 36-chute With Ejector	3500	125	25.9	840
54-Element Coplanar Mixer	440	15.7	3.2	840

8.3 PERFORMANCE VERSUS SUPPRESSION TRADES AND SCALING IMPLICATIONS

One common method of presenting the aerodynamic performance and acoustic results is in terms of suppression effectiveness ratio, $\Delta PNL/\Delta C_{f_8}$. Reference 3 shows the importance of establishing this ratio in terms of flight suppression

*Sea level corrected engine airflow

level and flight performance level. The reference level used herein is that of the Supersonic Tunnel Association (STA) nozzle and the reference to establish suppression in a conical nozzle. The characteristics of the five optimum nozzles are summarized on Figure 8-9. The optimum nozzles evaluated in this study show a marked improvement in suppressor effectiveness ratio ($\Delta PNL/\Delta C_{f_g}$) over designs previously evaluated.

The results of this study have considered, weight, performance, and suppression for the designs evaluated. Two typical VCE engine cycles were selected to illustrate the jet noise levels in terms of EPNL which could be achieved using these designs at the sideline and community monitoring locations for a typical AST flight trajectory. The cycles chosen represent 700 lbm/sec variable cycle engines which were high flowed at takeoff at values of 10% and 20%. The pertinent cycle parameters for each of the engines are summarized on Table 8-2. The sideline and community EPNL levels which would occur for each of the suppressors implemented on these engines were predicted and are summarized on Tables 8-3 and 8-4. Maximum sideline noise was assumed to occur when the aircraft was at a 800 ft altitude and the altitude over the 0.35 nautical mile community point was 1040 ft. Noise estimates were made by scaling the measured free jet data for each of the nozzles to the appropriate size and distance. Corrections were applied for the number of engines (+6.0 EPNdB), ground effects (+1.5 EPNdB) and shielding (-4.0 EPNdB). The shielding correction was based on the data presented in Reference 20 and applied to the sideline monitoring point only.

The performance based on the data presented in the previous section is also presented. Note that the comparisons are made for a constant engine weight flow and do not reflect a comparison at constant thrust. However, corrections for upsizing the engine to constant thrust would affect the noise levels a maximum of 0.5 EPNL. Typical engine weight increases caused by the addition of the suppressor, based on the studies presented in Reference 3, and not including engine weight increases due to upsizing to constant net thrust, are also presented. Table 8-3 shows that traded EPNL levels of approximately 105 may be achived with a suppressor such as the 32-chute nozzle implemented on 10% high flowed variable cycle engine. The 40-shallow-chute, and AR = 2.0 36-chute with and without ejector nozzles were found to achieve traded levels of between 106-109 EPNL. The 54-element coplanar mixer nozzle had a level of approximately 110 EPNL. This nozzle has a higher traded noise level because of its poor suppression characteristics at high jet velocities. A similar comparison for a 20% high flowed VCE engine is presented on Table 8-4. In general, this results in a 1.5 to 2.5 EPNL improvement over the previous cycle considered. The mojor reason for improvement is due to a reduction of mixed flow velocity from 2375 ft/sec to 2184 ft/sec. The major advantage of using this cycle is that all the configurations have traded EPNL of 1.1 to 4.0 EPNL less than the FAR36(1969)108 level. Conical reference levels are also presented based on the prediction procedure described in Reference 17 to illustrate the levels of suppression achieved.

The preceding discussion has dealt with representative examples of the noise levels, performance levels and weight increments which may be incurred when the nozzles evaluated in this study were implemented on an advanced

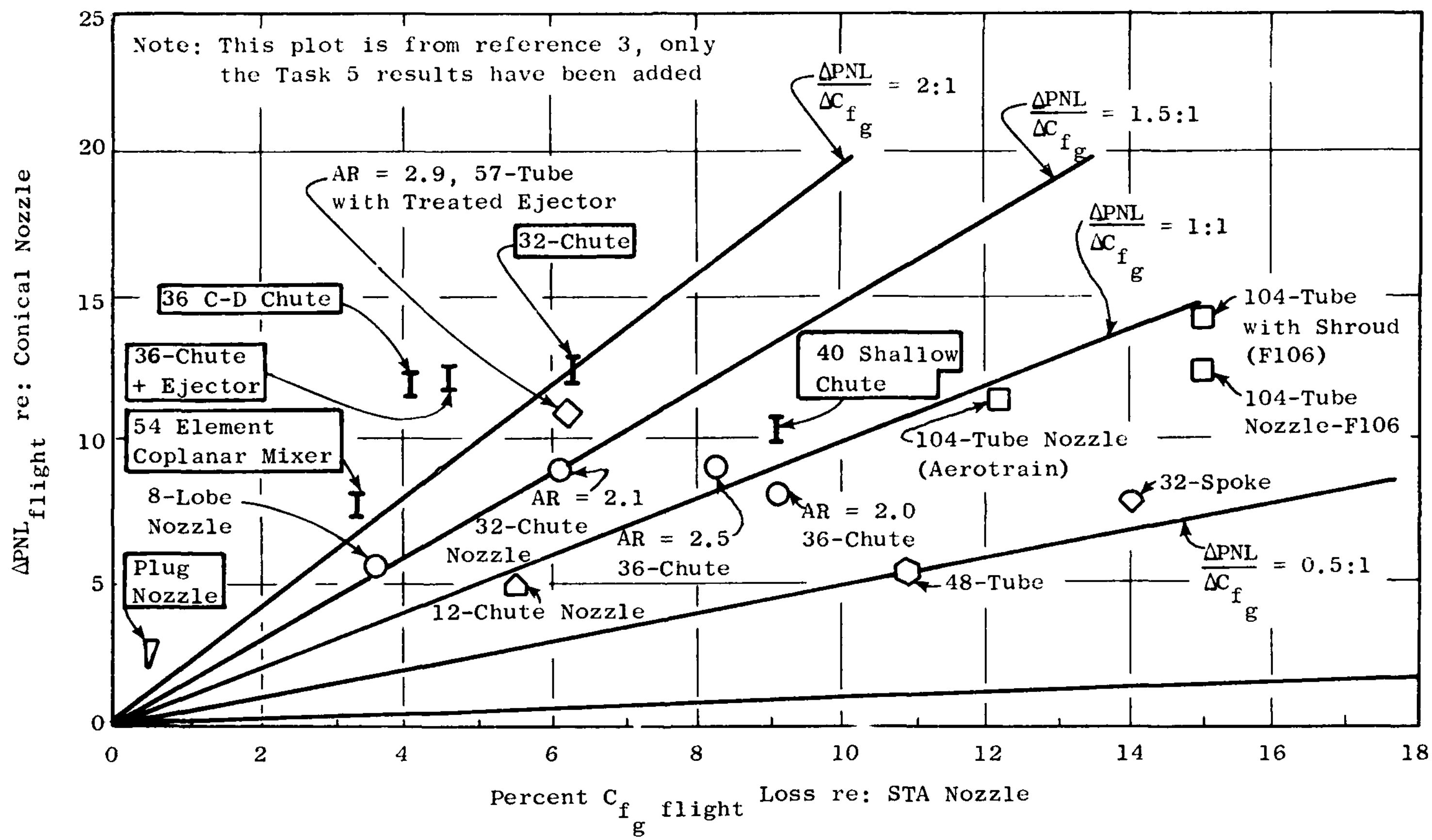

Figure 8-9. Summary of Projected Flight Performance and Suppression Characteristics.

Table 8-2. Summary of Aircraft and Engine Parameters Used for Jet Noise Estimates.

	10% VCE Engine		20% VCE Engine	
	Takeoff	Cut Back	Takeoff	Cut Back
Nominal Net Thrust/Nominal Gross Thrust	44,462/55971	23845/32,353	44,462/57023	23845/33169
Altitude, ft	900	1040	900	1040
Aircraft Speed (ft/sec)	397	397	397	397
Total weight Flow (lbm/sec)	758	588	840	652
Mixed Jet Velocity (ft/sec)	2375	1762	2184	1637
Mixed Pressure Ratio	3.23	2.16	2.82	2.05

Table 8-3. Summary of Noise, Performance and Weight Characteristics for a 10% Variable Cycle Engine.

Configuration	Performance, C_{fg}		Suppressor Weight Increment	EPNL SL	EPNL Comm.	Traded
	T/O	C/B				
AR = 2.1 32-Chute	0.927	0.912	1130	106.0	104.0	105
$(AR)_o$ = 1.75 40-Shallow-Chute	0.897	0.908	490	108.6	109.8	109.2
$(AR)_o$ = 2.0 36-Chute	0.939	0.924	1150	108.9	104.4	106.9
$(AR)_o$ = 2.0 36-Chute + Ejector	0.942	0.898	3100	107.2	107.1	107.2
54-element Coplanar	0.955	0.937	390	112.0	105.3	110.0
Fully Mixed Conical(1) Nozzle	0.986	0.986	0	115.1	113.1	114.1

(1) Predicted based on reference 17.

Table 8-4. Summary of Noise, Performance and Weight Characteristics for a 20% Variable Cycle Engine.

Configuration	Performance, C_{fg} T/O	Performance, C_{fg} C/B	Suppressor Weight Increments, lbs	EPNL SL	EPNL Comm.	Traded EPNL
AR = 2.1 32-Chute	0.922	0.91	1280	104	103.2	103.6
$(AR)_o$ = 1.75 40-Shallow-Chute	0.898	0.918	550	106.8	109.1	107.9
$(AR)_o$ = 2.0 36-Chute	0.934	0.922	1300	106.3	104.5	105.[illegible]
$(AR)_o$ = 2.0 36-Chute + Ejector	0.936	0.89	3500	105.5	104.3	104.9
54-Element Coplanar Mixer	0.952	0.932	440	108.5	105.2	106.8
Fully Mixed Conical(1) Nozzle	0.986	0.986	---	113.4	111.4	112.4

(1) Predicted based on reference 17.

technology variable cycle engine. However, the levels which may be achieved utilizing these designs are strong function of the mission and thrust requirements for a given aircraft and do not represent a lower limit with regard to noise suppression capability. In fact, these designs were evolved in Reference 3 (based primarily on static noise data) and using the results of the current program, both the aerodynamic performance levels and the suppression levels could be improved by further design studies.

9.0 CONCLUSIONS

This report describes the experimental investigation of the effect of flight on five suppressor nozzle designs. The suppression characteristics were established for the five suppressor nozzle designs in terms of peak noise characteristics, directivity and spectra as a function of flight Mach number.

The effect of flight on the peak noise characteristics of suppressors was found to vary as a function of mass average velocity. At high velocities for example, suppressors actually realize more peak noise reduction than a conical nozzle. However, at mass average velocities below 2000 ft/sec, suppressors generally lost 0 to 5 PNdB suppression in flight. On a directivity basis, flight reduces the noise in the aft quadrant, causes modest change at 90°, and causes only slight changes relative to static in the forward quadrant. Spectrum changes are dependent on frequency, angle, and flight velocity. Overall, no reduction of high frequency noise occured, even in the aft quadrant, except for the 54-element coplanar mixer nozzle. The flight effect on this configuration resembles more closely that of a conical nozzle. All the "optimum" suppressors tested exhibited lower noise levels in flight than statically and were lower in noise than the conical nozzle in flight.

The acoustic results of incorporating convergent-divergent chutes in the 36-chute suppressor design were inconclusive from the point of view of affecting the shock noise contribution to the total measured noise, especially on a peak PNL basis. A suppressor on a single flow cycle was found to be more effective in shock noise reduction than only suppressing the outer stream of a dual flow nozzle. This is attributed to two effects: 1) the partial span forward quadrant data is correlated as a function of mixed flow Mach number, which may not be the proper correlating parameter, 2) if the inner stream is at supercritical pressure ratio, the shock noise would not be influenced by the suppressor and would resemble that of an unsuppressed plug nozzle.

The addition of a treated ejector generally improved peak flight noise suppression 1 to 3 PNdB. The suppression characteristics of a 54-element coplanar mixer nozzle for conventional cycle conditions in the high velocity regime was substantially less than most suppressor designs. It was found that the suppression could be improved by reducing the inner flow velocity to zero. This 54-element coplanar mixer nozzle was the only design which had equivalent static and flight suppression levels for the mass average velocity range evaluated.

Overall, flight effects for suppressors were demonstrated to be a function of the specific suppressor design. Suppressing only the outer stream of dual flow nozzles was found to be slightly less effective than suppressing the entire stream on a single flow nozzle. The loss in suppression effectiveness is between 1 and 2 PNdB. In general, noise change due to cycle

variation at a given mass average velocity, was found to be more dominant for configurations having smaller outer to inner flow area ratios. For example, variance up to 5 PNdB for a given mass average velocity was found for a 40-shallow-chute nozzle.

The addition of a mechanical suppressor increases weight, reduces performance and may have less favorable peak noise flight effect. Nevertheless, for a given gross takeoff weight, payload, and specified noise goal, a suppressor allows the use of a smaller engine, which should result in a range advantage over an unsuppressed system, because adding a suppressor is less costly than reducing noise by enlarging the engine to reduce jet velocity. Overall, suppression characteristics measured statically are different than in flight and are a function of the specific compressor design.

APPENDIX A

SUMMARY OF THERMODYNAMIC AND ACOUSTIC DATA

This appendix contains a summary of the test data obtained during the subject program. Thermodynamic and acoustic properties are documented for each of the data points. Thermodynamic conditions are presented for the individual stream in terms of pressure ratio (P_T/P_O), stagnation temperature (T_T) and jet velocity (V). Subscripts "O" and "i" are used to denote inner and outer stream conditions for dual flow nozzles. Also, for the dual flow nozzle configurations, a similar set of mass averaged (mixed) flow parameters are presented. The external flow velocity of the tertiary stream is also presented in terms of V_{FS}. The acoustic results are presented in terms of PNL and OASPL levels at the 50, 90, and maximum noise angles.

Table A-1. 32-Chute Nozzle Test Matrix.

Model No. 1 AR = 2.1
Config. 32 Chute
A_{FS} = 338 in.^{2} A_i = 26.15 in.^{2}

	Inner						2400 ft Sideline 50°		2400 ft Sideline 90°		2400 ft Sideline Peak			
Point	$(P_T/P_O)_i$	T_{T_i} °R	V_i ft/sec	V_{FS} ft/sec	Log β	10 $Log_{10}[F_s(T_O/T_{sm})^{\omega-1}]$	OASPL	PNL	OASPL	PNL	OASPL	θ	PPNL	POASPL
1	2.706	1333	2000	0	-0.087	37.8	73.5	81.8	80.3	89.5	84.2	120	92.3	88.5
2	3.052	1475	2210	0	-0.022	38.2	76.0	84.2	82.7	91.7	92.3	140	95.3	92.4
3	2.466	1206	1819	0	-0.157	37.6	72.2	81.4	79.2	89.3	80.9	110	91.4	84.5
4	3.220	1640	2393	0	0.010	38.2	77.2	84.8	88.0	96.3	94.7	140	97.8	94.8
5	3.681	1745	2581	0	0.060	38.8	79.9	89.2	86.1	94.7	99.3	140	102.6	99.3
6	1.971	938	1410	0	-0.574	37.9	66.3	75.4	72.7	83.2	73.9	100	84.3	75.0
7	3.788	1765	2610	0	-0.066	38.9	79.8	88.5	86.6	95.3	100.5	140	103.9	100.5
8	1.997	613	1150	0	-0.512	38.7	60.8	69.9	69.0	79.5	69.5	110	79.7	69.8
9	2.608	681	1400	0	-0.120	40.5	67.9	77.6	75.4	86.5	76.4	110	87.1	77.6
10	3.144	737	1573	0	-0.014	41.6	73.5	84.3	75.4	85.2	81.7	100	91.0	83.2
11	3.168	1728	2432	0	-0.002	37.7	76.5	84.0	84.4	93.4	95.6	140	98.7	95.6
12	2.774	1714	2298	0	-0.057	36.8	74.2	81.5	82.9	94.1	84.4	100	95.2	92.1
13	2.409	1716	2154	0	-0.165	35.7	72.0	78.9	80.9	90.5	84.9	120	92.9	88.1
14	2.048	1627	1913	0	-0.384	34.7	69.3	76.5	78.3	88.3	80.4	110	90.5	82.3
15	2.179	1660	2007	0	-0.274	35.1	---	---	78.6	87.9	---	---	---	---
16	1.759	829	1219	0	---	37.7	60.6	69.4	69.3	79.7	70.3	110	80.4	70.8
17	2.262	1520	1959	0	-0.232	35.8	---	---	79.2	89.3	---	---	---	---
18	1.917	1357	1669	0	-0.681	35.5	66.7	74.5	75.7	85.8	77.6	110	87.8	79.0
19	1.650	1235	1410	0	---	35.8	64.4	73.5	71.7	82.1	73.4	110	83.6	74.1
20	2.035	1366	1742	0	-0.417	35.7	67.7	75.0	76.8	86.4	78.7	110	88.8	80.1
1	2.757	1343	2021	141	-0.078	37.9	72.6	81.7	78.7	88.4	83.0	120	91.6	87.2
3	2.480	1207	1824	140	-0.015	37.6	71.1	81.3	77.0	87.5	80.4	120	89.9	81.2
4	3.223	1634	2376	138	0.004	38.1	77.2	85.5	81.9	91.1	87.0	100	96.7	93.0
5	3.681	1732	2561	142	0.055	38.8	79.5	89.4	84.4	93.5	98.0	140	101.3	98.7
6	1.972	956	1423	140	-0.577	37.8	64.9	75.4	70.8	82.0	71.7	100	82.6	72.8
7	4.023	1743	2640	144	0.085	39.3	81.7	91.3	85.8	94.7	100.3	140	103.7	100.3
8	2.086	639	1206	140	-0.386	39.0	63.4	74.0	68.2	79.6	68.9	100	80.3	68.8
10	3.201	731	1576	142	-0.006	41.7	72.9	84.9	76.3	87.8	79.3	110	89.0	80.0
11	3.174	1749	2447	143	-0.002	31.7	76.9	85.6	82.7	92.0	94.6	140	97.8	95.0
12	2.772	1751	2321	143	-0.068	36.7	74.4	82.5	80.9	90.7	85.7	120	94.1	91.3
16	1.751	820	1207	140	---	37.7	60.9	70.9	66.5	77.3	67.4	100	78.1	68.2
17	2.264	1531	1966	139	-0.232	35.8	71.1	79.9	77.7	88.5	81.1	120	90.7	81.5
18	1.929	1345	1668	141	-0.640	35.6	67.1	76.1	73.6	84.1	77.1	120	86.7	77.1
19	1.660	1230	1414	140	---	35.8	63.0	73.0	69.3	80.0	72.8	120	82.3	72.8
20	2.017	1383	1743	140	-0.440	35.6	68.0	76.6	74.6	84.9	78.1	120	87.5	78.1

Table A-1. 32-Chute Nozzle Test Matrix (Concluded).

Model No. 1 AR = 2.1
Config. 32 Chute
A_{FS} = 338 in.^{2} A_i = 26.15 in.^{2}

	Inner						2400 ft Sideline								
							50°		90°		Peak				
Point	$(P_T/P_o)_i$	T_{T_i} °R	V_i ft/sec	V_{FS} ft/sec	Log β	10 Log_{10} $[F_s(T_o/T_{sm})^{\omega-1}]$	OASPL	PNL	OASPL	PNL	OASPL	θ	PPNL	POASPL
1	2.741	1344	2018	279	-0.080	37.8	72.2	81.2	77.4	88.1	82.1	120	91.6	82.8
2	3.019	1488	2211	280	-0.027	38.1	74.8	83.5	80.1	90.5	84.7	120	94.1	87.9
3	2.466	1209	1822	280	-0.157	37.6	70.3	79.3	75.6	86.6	78.2	120	88.0	78.6
4	3.215	1635	2375	274	0.003	38.1	76.4	84.7	81.2	91.7	85.7	100	96.7	91.4
5	3.659	1728	2555	278	0.054	38.7	79.0	88.2	83.7	94.1	89.8	120	98.4	95.8
6	1.968	950	1417	279	-0.585	37.8	64.8	74.9	70.3	82.2	70.7	80	82.5	71.9
7	4.014	1734	2632	282	0.084	39.4	80.9	90.1	84.9	94.9	97.3	140	100.4	97.3
8	2.086	642	1209	281	-0.386	39.0	62.9	73.7	68.2	80.3	68.3	80	80.5	68.3
9	2.638	705	1432	284	-0.112	40.5	67.7	79.5	72.1	83.9	72.7	100	84.7	73.9
10	3.221	737	1587	279	-0.003	41.7	78.6	84.8	74.1	85.9	78.5	100	89.9	78.3
11	3.178	1745	2446	278	-0.001	37.7	76.8	86.2	62.3	92.8	86.7	120	95.9	92.2
12	2.774	1746	2320	276	-0.067	36.7	74.6	83.0	80.4	91.4	84.6	120	94.0	87.8
13	2.410	1712	2152	277	-0.165	35.7	72.6	81.2	78.3	89.3	81.4	120	91.1	82.9
14	2.064	1626	1922	277	-0.367	34.7	70.0	73.7	75.8	86.8	79.7	120	89.2	79.7
15	2.157	1680	2007	277	-0.288	35.0	71.1	80.0	76.9	88.0	80.2	120	89.9	80.2
16	1.757	819	1211	281	0	37.7	60.8	71.4	66.4	77.9	66.4	90	77.9	66.9
17	2.252	1516	1951	277	-0.238	35.8	71.0	80.4	76.8	88.3	80.4	120	90.4	80.4
18	1.924	1343	1664	280	-0.658	35.6	67.2	76.5	73.2	84.6	76.5	120	86.1	76.5
19	1.650	1238	1412	279	0	35.8	63.0	72.5	68.7	79.9	71.9	120	87.2	71.9
20	2.040	1374	1751	281	-0.408	35.7	68.6	77.8	74.3	85.5	77.7	120	87.2	77.7
1	2.746	1335	2013	367	-0.079	37.9	72.8	82.4	77.4	88.6	80.7	120	90.5	80.7
3	2.473	1205	1821	367	-0.155	37.6	70.9	80.4	75.6	86.7	78.8	120	88.5	78.8
4	3.208	1640	2378	366	-0.003	38.1	76.5	85.2	80.6	91.4	85.0	100	96.1	86.9
5	3.677	1728	2558	366	-0.55	38.8	79.4	88.9	83.3	94.1	88.1	120	99.1	94.0
6	1.967	947	1414	367	-0.590	37.8	65.8	76.2	70.9	82.9	70.9	90	82.9	71.1
7	4.014	1733	2632	366	0.084	39.4	81.0	90.8	84.3	94.6	95.5	140	99.1	96.3
8	2.087	648	1216	371	-0.382	39.0	64.0	75.1	68.5	80.5	68.6	80	80.8	68.6
10	3.301	738	1602	369	0.008	41.9	73.6	85.9	74.9	87.0	78.6	100	89.8	78.6
11	3.176	1748	2448	366	-0.001	37.7	76.9	85.6	81.4	91.9	85.1	120	95.3	90.1
12	2.761	1763	2327	365	-0.069	35.6	74.9	83.7	80.1	91.2	83.1	120	92.9	85.2
16	1.758	829	1219	368	0	37.7	62.7	73.4	67.2	78.6	67.2	90	78.6	67.4

Table A-2. 40-Shallow-Chute Nozzle Test Matrix.

Model No. 2, (AR) = 1.75
Config. 40 Shall Chute
A_{FS} = 338 in.^{2}, A_i = 12.39 in.^{2}, A_o = 23.758 in.^{2}

	Inner			Outer			Mass Averaged								2400 ft Sideline							
															50°		90°		Peak			
Point	$(P_T/P_0)_i$	T_{T_i} °R	V_i ft/sec	$(P_T/P_0)_o$	T_{T_o} °R	V_o ft/sec	P_T/P_0	T_T °R	V ft/sec	V_o/V_i	W_o/W_i	V_{FS} ft/sec	log λ	$10\log_{10}[F_S(T_0/T_{SM})^{-1}]$	OASPL	PNL	OASPL	PNL	OASPL	θ	PPNL	POASPL
1				1.964	999	1452	1.964	999	1452			0	-0.507	37.6	65.2	73.0	72.0	82.3	74.7	110	84.1	75.6
2				2.484	1198	1820	2.484	1198	1820			0	-0.151	37.7	71.2	77.9	77.9	87.0	83.2	120	89.8	84.9
3				2.742	1344	2019	2.742	1344	2019			0	-0.080	37.9	73.6	80.0	80.2	88.4	87.9	130	92.4	89.0
4				2.779	1689	2282	2.779	1689	2282			0	-0.067	36.9	75.6	81.4	82.4	90.4	91.9	140	95.2	91.9
5				3.296	1625	2389	3.286	1625	2389			0	-0.013	36.3	78.9	85.1	84.5	92.8	96.3	140	99.7	96.4
6				3.757	1706	2559	3.757	1706	2559			0	-0.063	39.0	81.9	88.0	87.2	95.4	100.6	140	104.4	100.6
7	1.613	539	909	1.964	918	1392	1.828	784	1221	1.531	1.826	0	0	38.1	69.0	71.8	70.2	79.8	73.6	120	81.8	73.6
8	1.750	543	982	2.484	1021	1676	2.198	861	1494	1.707	1.990	0	-0.291	38.9	69.3	76.7	75.7	84.7	80.8	120	88.1	81.2
9	1.835	558	1034	2.746	1339	2016	2.364	1064	1670	1.950	1.839	0	-0.200	38.4	71.4	79.3	78.0	86.8	83.6	120	90.8	84.7
10	1.649	560	964	2.717	1671	2248	2.260	1290	1799	2.332	1.861	0	-0.241	37.0	72.1	78.8	79.3	88.0	85.0	120	71.9	86.3
11	2.089	[illegible]	1148	3.325	1632	2405	2.759	1216	1934	2.094	1.785	0	-0.029	38.6	78.1	86.1	84.0	93.4	90.0	120	96.7	91.6
12	2.317	574	1213	3.727	1716	2571	3.085	1306	2083	2.120	1.784	0	-0.020	39.3	79.9	87.5	85.4	94.8	94.9	140	99.5	94.9
13	1.484	1356	1370	1.963	941	1408	1.792	1060	1399	1.028	3.340	0	0	37.0	64.2	70.7	70.8	79.0	74.7	110	82.2	79.4
14	1.488	1351	1372	2.393	1193	1783	2.092	1249	1693	1.300	3.579	0	-0.361	36.4	68.4	74.4	75.3	83.3	79.3	110	86.9	83.0
15	1.490	1460	1378	2.881	1427	2125	2.433	1434	1974	1.542	3.930	0	-0.162	36.6	72.1	78.8	79.0	86.9	86.6	130	91.6	88.0
16	1.494	[illegible]	1380	4.020	1678	2589	3.248	1642	2388	1.876	5.001	0	-0.007	38.1	80.8	89.2	86.2	96.3	97.6	140	101.7	92.7
17	1.521	1221	1290	1.852	887	1312	1.736	974	1306	1.017	2.860		0	37.2	62.9	69.1	69.0	77.6	72.6	110	80.3	77.1
18	1.522	1218	1290	2.229	1076	1629	1.993	1111	1547	1.263	3.109	0	-0.506	37.0	66.6	72.9	73.1	81.5	77.1	110	84.9	80.7
20	1.522	1141	1247	3.767	1702	2558	3.052	1590	2296	2.051	4.000	0	-0.027	37.6	[illegible]	88.4	[illegible]	95.2	95.6	140	99.9	96.1
21	1.549	1002	1190	1.747	817	1204	1.680	870	1200	1.012	2.470	0	0	37.4	60.8	67.1	67.2	75.9	70.3	110	78.4	73.9
22	1.542	947	1154	2.078	984	1494	1.900	987	1420	1.262	2.679	0	-1.041	[illegible]	[illegible]	71.3	[illegible]	79.8	74.7	110	83.8	77.4
23	1.550	998	1189	2.462	1186	1803	2.159	1138	1644	1.516	2.876	0	-0.311	37.2	[illegible]	[illegible]	[illegible]	83.5	79.1	110	87.2	81.9
24	[illegible]	1003	1195	3.300	1620	2387	2.718	1476	2108	1.998	3.270	0	-0.082	[illegible]	[illegible]	84.6	81.4	90.2	[illegible]	130	95.0	90.4
25	[illegible]	528	998	1.512	753	1027	1.619	667	1015	1.029	1.380	0	[illegible]	[illegible]	[illegible]	[illegible]	[illegible]	[illegible]	[illegible]	[illegible]	[illegible]	[illegible]
26	1.779	[illegible]	[illegible]	1.798	916	1303	[illegible]	[illegible]	1187	1.295	1.509	0	0	[illegible]	[illegible]	[illegible]	[illegible]	[illegible]	[illegible]	[illegible]	[illegible]	[illegible]
27	[illegible]	[illegible]	[illegible]	[illegible]	[illegible]	1500	[illegible]	828	[illegible]	1.500	1.662	[illegible]	[illegible]	[illegible]	[illegible]	[illegible]	[illegible]	[illegible]	[illegible]	[illegible]	[illegible]	[illegible]
28	1.781	[illegible]	[illegible]	2.742	1328	2007	[illegible]	1065	[illegible]	[illegible]	1.913	0	-0.206	[illegible]	[illegible]	[illegible]	[illegible]	85.5	[illegible]	[illegible]	[illegible]	[illegible]
29	1.994	849	[illegible]	2.044	[illegible]	1902	1.994	1296	[illegible]	1.407	[illegible]	0	[illegible]	[illegible]	[illegible]	[illegible]	[illegible]	[illegible]	[illegible]	[illegible]	[illegible]	[illegible]
30	[illegible]	[illegible]	[illegible]	2.408	1671	2124	[illegible]	1315	1868	1.384	[illegible]	0	-0.186	[illegible]	[illegible]	[illegible]	[illegible]	[illegible]	[illegible]	[illegible]	[illegible]	[illegible]
31	2.502	[illegible]	[illegible]	3.191	[illegible]	2386	2.888	1363	2076	1.550	[illegible]	0	-0.051	[illegible]	[illegible]	[illegible]	[illegible]	[illegible]	[illegible]	[illegible]	[illegible]	[illegible]
32	[illegible]	[illegible]	[illegible]	3.617	1722	2540	3.318	1366	2189	1.536	[illegible]	[illegible]	[illegible]	[illegible]	[illegible]	[illegible]	[illegible]	[illegible]	[illegible]	[illegible]	[illegible]	[illegible]
33	[illegible]	[illegible]	[illegible]	2.310	1582	[illegible]	2.332	1210	1771	1.374	1.193	0	-0.209	[illegible]	[illegible]	[illegible]	[illegible]	[illegible]	[illegible]	[illegible]	[illegible]	[illegible]
34	[illegible]	[illegible]	1369	2.662	1722	2262	2.589	1338	1962	1.442	1.308	0	-0.118	[illegible]	[illegible]	[illegible]	[illegible]	[illegible]	[illegible]	[illegible]	[illegible]	[illegible]
35	[illegible]	[illegible]	[illegible]	2.221	1513	1934	2.262	[illegible]	1716	1.330	1.204	0	[illegible]	[illegible]	[illegible]	[illegible]	[illegible]	[illegible]	[illegible]	[illegible]	[illegible]	[illegible]
36	[illegible]	[illegible]	1484	[illegible]	1376	1690	2.100	1104	1593	1.139	1.126	0	-0.363	[illegible]	[illegible]	[illegible]	[illegible]	[illegible]	[illegible]	[illegible]	[illegible]	[illegible]

Table A-2. 40-Shallow-Chute Nozzle Test Matrix (Continued).

Model No. 2, (AR) = 1.75
Config. 40 Shallow Chute
A_{FS} = 338 in.^{2} A_i = 12.39 in.^{2}, A_o = 23.758 in.^{2}

Point	Inner			Outer			Mass Averaged								2400 ft Sideline							
															50°		90°		Peak			
	$(P_T/P_o)_i$	T_{T_i} °R	V_i ft/sec	$(P_T/P_o)_o$	T_{T_o} °R	V_o ft/sec	P_T/P_o	T_T °R	V ft/sec	V_o/V_i	W_o/W_i	V_{FS} ft/sec	Log ε	$10 \log_{10} (F_S (T_o/T_{sm})^{ε-1})$	OASPL	PNL	OASPL	PNL	OASPL	θ	PPNL	POASPL
1				1.968	952	1419	1.968	952	1419			143	-0.583	37.8	62.5	71.5	68.0	79.1	71.4	120	81.1	71.4
6				3.840	1739	2601	3.840	1739	2601			140	0.070	39.1	82.9	89.5	86.3	94.9	100.7	140	104.4	100.9
7	1.617	544	916	1.977	951	1423	1.836	806	1242	1.554	1.807	143	0	38.1	63.0	71.5	68.0	78.6	70.9	120	79.6	71.1
12	2.231	569	1184	3.662	1714	2545	2.991	1304	2057	2.150	1.789	140	-0.034	39.0	78.9	87.3	83.2	93.2	92.1	130	98.3	93.2
16	1.495	1442	1375	4.039	1710	2618	3.260	1665	2409	1.904	4.950	141	0.009	38.0	82.5	90.1	85.3	95.6	96.8	140	101.6	97.9
21	1.577	987	1204	1.756	831	1219	1.695	877	1215	1.012	2.384	138	0	37.5	60.9	68.8	65.3	74.9	69.1	120	77.2	72.1
23	1.570	1010	1213	2.489	1208	1829	2.182	1157	1669	1.508	2.844	141	0.891	37.2	69.0	76.2	74.3	83.3	80.7	130	86.2	81.6
24	1.558	1004	1199	3.320	1631	2415	2.773	1486	2134	2.014	3.326	139	-0.072	37.5	76.7	86.7	80.7	89.9	90.3	140	93.3	91.0
27	1.803	557	1619	2.156	991	1500	1.961	828	1319	1.472	1.659	141	-0.609	38.4	65.0	73.4	69.8	79.9	73.5	120	82.1	74.4
32	2.889	842	1627	3.559	1684	2498	3.233	1366	2169	1.535	1.647	142	0.002	39.2	80.5	88.2	85.2	94.8	96.3	140	100.6	97.3
33	2.016	765	1292	2.347	1588	2043	2.184	1263	1746	1.581	1.530	141	-0.287	36.8	70.1	76.9	76.3	[illegible]	81.1	120	88.6	83.2
35	2.530	764	1462	2.183	1506	1911	2.252	1163	1704	1.307	1.166	140	-0.250	37.5	70.8	79.1	78.5	84.2	80.5	120	88.0	85.8
1				1.978	954	1425	1.973	954	1425			279	-0.558	37.8	62.4	71.5	67.4	79.2	70.5	120	80.7	71.8
2				2.478	1206	1824	2.478	1206	1824			277	-0.153	37.2	70.4	78.2	75.0	86.2	79.6	120	88.6	79.6
3				2.761	1338	2020	2.761	1338	2020			277	-0.026	38.0	73.1	81.1	77.7	88.6	82.3	120	90.9	83.8
4				2.793	1742	2325	2.793	1742	2325			276	-0.063	36.8	75.6	82.5	80.3	90.7	85.7	120	93.7	87.3
5				3.335	1618	2394	3.335	1618	2394			277	0.018	38.4	77.5	85.1	81.9	[illegible]	91.6	140	95.5	92.6
6				3.819	1737	2595	3.819	1737	2595			276	0.068	39.0	81.3	89.1	85.1	95.1	96.9	140	100.4	97.3
7	1.607	543	910	1.975	950	1420	1.830	805	1239	1.561	1.815	280	[illegible]	38.1	62.7	71.6	66.7	76.3	70.0	120	79.9	71.4
8	1.734	562	991	2.492	1205	1828	2.188	982	1538	1.845	1.884	276	-0.298	38.3	67.3	75.8	72.4	83.0	77.7	120	86.5	77.7
9	1.832	559	1033	2.749	1333	2012	2.366	1062	1669	1.948	1.851	276	0.200	38.4	70.8	79.6	75.3	86.1	80.5	120	89.1	80.8
10	1.644	573	955	2.741	1743	2306	2.263	1330	1829	2.415	1.833	276	-0.238	36.8	[illegible]	80.3	77.5	88.2	83.4	120	91.8	83.6
11	2.041	565	1119	3.329	1618	2392	2.748	1245	1941	2.138	1.824	276	-0.081	38.6	75.3	85.1	80.7	90.9	86.7	120	95.3	87.1
12	2.275	571	1198	3.744	1740	2582	3.046	1320	2085	2.155	1.783	277	-0.025	39.1	78.7	88.1	83.2	94.3	90.8	130	97.4	91.0
13	1.503	1492	1408	1.981	962	1432	1.809	1085	1426	1.017	3.311	277	[illegible]	36.9	64.2	72.2	68.2	79.0	72.3	120	81.0	75.4
14	1.498	1457	1385	2.413	1160	1764	2.105	1225	1682	1.274	3.639	277	-0.351	36.6	68.2	75.8	72.7	83.2	77.1	120	85.7	79.6
15	1.497	1356	1336	2.900	1396	2107	2.449	1388	1947	1.577	1.824	277	-0.159	36.9	72.5	80.2	77.1	88.8	82.6	120	90.1	84.4
16	1.497	1457	1385	4.036	1690	2602	3.261	1651	2399	1.879	4.995	279	0.009	38.1	81.8	90.7	84.9	[illegible]	[illegible]	130	98.3	95.4
17	1.536	1256	1322	1.872	888	1323	1.753	983	1323	1.001	2.894	274	0	37.2	61.5	70.5	65.7	76.3	69.6	120	78.7	72.6
18	1.537	1212	1300	2.249	1116	1667	2.010	1140	1576	1.282	3.028	279	-0.472	36.9	66.3	74.4	70.9	81.8	72.0	110	82.6	76.6
19	1.529	1233	1304	2.695	1323	1988	2.315	1302	1832	1.523	3.375	280	-0.214	36.7	70.4	78.2	75.3	85.5	80.3	120	88.6	81.8
20	1.539	1235	1315	3.817	1657	2532	3.097	1576	2298	1.925	4.207	280	-0.014	37.9	80.2	89.9	83.5	[illegible]	89.9	130	96.3	92.3
21	1.564	1015	1210	1.767	827	1223	1.698	881	1219	1.011	2.472	277	0	37.4	59.2	68.5	63.8	74.9	64.6	100	75.5	68.2
22	1.565	1016	1212	2.087	1005	1515	1.913	1008	1432	1.250	2.649	276	-0.834	37.4	63.4	72.5	68.8	74.8	71.5	120	80.6	72.9
23	1.563	1003	1202	2.482	1211	1829	2.175	1157	1666	1.522	2.843	277	-0.298	37.2	68.1	76.2	73.1	83.7	77.3	120	86.0	78.4

Table A-2. 40-Shallow-Chute Nozzle Test Matrix (Concluded).

Model No. 2, (AR)$_S$ = 1.75
Config. 40 Shallow Chute
A_{FS} = 338 in.^{2} A_i = 12.39 in.^{2}, A_o = 23.758 in.^{2}

Point	Inner $(P_T/P_o)_i$	Inner T_{T_i} °R	Inner V_i ft/sec	Outer $(P_T/P_o)_o$	Outer T_{T_o} °R	Outer V_o ft/sec	Mass Averaged P_T/P_o	Mass Averaged T_T °R	Mass Averaged V ft/sec	V_o/V_i	W_o/W_i	V_{FS} ft/sec	Log r	$10 \log_{10} [F_S(T_o/T_{sm})^{\omega-1}]$
[illegible]	[illegible]	1010	1205	3.32	1630	2400	2.734	1485	2120	1.992	[illegible]	278	-0.080	32.3
[illegible]	[illegible]	[illegible]	1019	1.559	712	1010	[illegible]	647	1014	0.991	1.420	281	0	37.3
[illegible]	[illegible]	[illegible]	1029	1.841	856	1283	1.814	748	1186	1.247	1.616	[illegible]	0	38.1
[illegible]	[illegible]	[illegible]	1018	2.085	1013	1520	1.960	845	1332	1.493	1.665	[illegible]	-0.611	38.4
[illegible]	[illegible]	[illegible]	1025	2.719	1373	2033	2.333	1089	1679	1.983	1.844	[illegible]	-0.213	38.1
[illegible]	[illegible]	862	1322	2.070	1602	1910	2.020	1296	1688	1.392	1.422	276	-0.442	36.2
[illegible]	[illegible]	863	1549	2.461	1680	2154	2.422	1329	1894	1.391	1.329	276	-0.170	37.2
[illegible]	[illegible]	863	1552	3.238	1679	2415	2.923	1381	2100	1.556	1.742	280	-0.045	38.4
[illegible]	[illegible]	[illegible]	1242	2.337	1579	2033	2.179	1257	[illegible]	1.574	1.529	276	-0.291	36.8
[illegible]	[illegible]	[illegible]	[illegible]	[illegible]	1671	2234	2.609	1318	1954	[illegible]	[illegible]	279	-0.113	37.8
[illegible]	[illegible]	[illegible]	[illegible]	[illegible]	[illegible]	1897	2.269	1149	1700	1.285	1.133	276	-0.242	37.6
36	[illegible]	[illegible]	[illegible]	1.934	[illegible]	[illegible]	2.101	1086	1581	1.166	1.108	[illegible]	-0.363	37.5

Point	2400 ft Sideline 50° OASPL	50° PNL	90° OASPL	90° PNL	Peak OASPL	Peak θ	Peak PPNL	POASPL
[illegible]	75.5	86.0	79.9	90.5	[illegible]	120	93.3	87.2
[illegible]	60.6	70.4	63.8	76.0	70.5	80	[illegible]	70.5
[illegible]	60.4	70.2	64.9	76.6	67.6	120	78.0	67.6
[illegible]	63.4	72.9	68.2	79.5	71.7	120	81.4	71.7
[illegible]	70.2	78.9	75.3	86.0	[illegible]	120	89.8	81.0
[illegible]	68.7	76.8	[illegible]	84.4	77.1	120	85.9	78.6
[illegible]	72.4	80.8	77.0	87.6	81.3	120	89.9	85.8
[illegible]	76.9	85.4	81.7	92.4	88.0	120	96.0	91.1
[illegible]	69.5	77.9	75.3	86.4	79.3	120	88.3	80.3
[illegible]	75.0	83.8	79.7	90.4	84.7	120	92.4	[illegible]
[illegible]	69.8	78.9	74.4	86.0	77.9	120	86.8	81.5
36	[illegible]	77.4	72.3	84.3	[illegible]	120	[illegible]	79.3

Table A-3. 36-C-D Chute Nozzle Test Matrix.

Model [illegible] (AF)e = 2.00
[illegible]
[illegible] A_i = 6.562 in.², A_o = 23.756 in.²

Test Point	Inner $(P_T/P_0)_i$	Inner T_{T_i}, °R	Inner V_i ft/sec	Outer $(P_T/P_0)_o$	Outer T_{T_o}, °R	Outer V_o ft/sec	Mass Averaged P_T/P_0	Mass Averaged T_T, °R	Mass Averaged V ft/sec	V_o/V_i	W_o/W_i	V_{FS} ft/sec	log ε	10 Log10 $[F_s(T_0/T_{sm})^{\omega-1}]$	2400 ft Sideline 50° OASPL	50° PNL	90° OASPL	90° PNL	Peak OASPL	Peak θ	Peak PPNL	POASPL
[illegible]				1.920	952	1419	1.970	952	1419			0	-0.583	37.8	65.9	74.3	73.0	84.1	75.3	110	86.1	75.7
2				2.495	1204	1827	2.495	1204	1827			0	-0.149	37.7	71.3	80.0	78.4	88.7	81.6	110	91.6	84.2
[illegible]				2.778	1332	2019	2.778	1332	2019			0	-0.073	38.0	74.7	84.7	80.9	90.8	87.4	130	93.4	88.2
[illegible]				2.812	1700	2300	2.812	1700	2300			0	-0.061	37.0	76.0	84.4	82.9	92.3	90.1	130	95.7	91.1
[illegible]				3.337	1623	2397	3.337	1623	2397			0	0.018	38.4	80.2	88.8	85.4	95.6	93.5	130	98.9	94.9
[illegible]				3.898	1762	2630	3.898	1762	2630			0	0.075	39.1	82.1	88.6	87.7	96.5	99.6	140	103.3	99.6
[illegible]	[illegible]	[illegible]	[illegible]	1.968	945	1413	1.901	858	1324	[illegible]	[illegible]	0	1.083	38.1	64.9	72.8	71.2	81.7	73.6	110	83.9	74.4
[illegible]	[illegible]	[illegible]	1086	2.508	1197	1826	2.338	1058	1656	1.682	[illegible]	0	-0.212	38.2	70.4	78.1	77.1	86.7	80.1	110	89.6	82.9
[illegible]	[illegible]	[illegible]	[illegible]	2.779	1337	2021	2.546	1164	1813	1.822	[illegible]	0	-0.134	38.2	73.2	82.9	79.3	88.8	84.5	120	92.2	86.2
[illegible]	[illegible]	[illegible]	[illegible]	2.800	1722	2311	2.499	1574	2028	2.184	[illegible]	0	[illegible]	36.9	74.3	82.3	81.3	90.4	87.2	120	94.6	88.7
[illegible]	[illegible]	[illegible]	[illegible]	[illegible]	[illegible]	[illegible]	3.010	1387	2129	1.821	3.176	0	[illegible]	38.6	78.9	88.8	83.8	94.2	91.5	130	97.7	92.1
[illegible]	[illegible]	[illegible]	[illegible]	[illegible]	[illegible]	[illegible]	3.361	1465	2279	[illegible]	3.133	0	[illegible]	39.2	79.7	88.2	85.9	95.9	94.1	130	100.2	95.7
[illegible]	[illegible]	[illegible]	[illegible]	[illegible]	914	[illegible]	1.879	1007	1413	1.012	6.262	0	[illegible]	37.4	65.2	73.3	71.5	81.5	74.7	120	84.0	76.0
[illegible]	[illegible]	[illegible]	[illegible]	[illegible]	[illegible]	1765	2.254	1184	1721	[illegible]	[illegible]	0	[illegible]	37.2	69.8	77.2	76.2	85.4	79.4	110	88.6	82.6
[illegible]	[illegible]	[illegible]	[illegible]	[illegible]	[illegible]	2109	2.612	1410	2023	1.511	7.310	0	0.112	37.2	74.1	82.8	80.6	89.6	87.8	130	93.6	88.6
[illegible]	[illegible]	[illegible]	[illegible]	[illegible]	[illegible]	[illegible]	3.594	1732	2542	1.902	9.149	[illegible]	[illegible]	[illegible]	83.3	90.8	87.8	97.8	99.6	140	103.8	99.6
[illegible]	[illegible]	[illegible]	[illegible]	[illegible]	[illegible]	1318	1.778	953	1318	1.002	5.247	0	[illegible]	37.3	64.3	[illegible]	70.4	80.6	73.4	120	82.9	74.2
[illegible]	[illegible]	[illegible]	[illegible]	[illegible]	[illegible]	[illegible]	2.112	1087	1587	1.238	5.938	0	[illegible]	[illegible]	68.1	75.5	74.4	83.8	78.3	120	87.0	80.0
[illegible]	[illegible]	[illegible]	[illegible]	[illegible]	[illegible]	[illegible]	2.462	1284	1876	1.508	6.353	0	[illegible]	37.2	72.5	81.3	78.5	87.8	83.8	120	91.3	86.1
[illegible]	[illegible]	[illegible]	[illegible]	[illegible]	[illegible]	[illegible]	3.391	1624	2459	1.934	7.905	[illegible]	[illegible]	[illegible]	82.0	90.0	86.2	96.5	96.7	140	101.0	96.8
[illegible]	[illegible]	[illegible]	[illegible]	[illegible]	[illegible]	[illegible]	1.692	873	1210	1.001	4.517	0	---	[illegible]	62.8	70.7	68.5	79.1	70.6	110	80.9	71.4
[illegible]	[illegible]	[illegible]	[illegible]	[illegible]	[illegible]	[illegible]	2.070	995	1498	1.024	[illegible]	[illegible]	[illegible]	[illegible]	66.4	74.1	72.2	82.8	76.2	120	85.3	76.7
[illegible]	[illegible]	[illegible]	[illegible]	[illegible]	[illegible]	[illegible]	[illegible]	1155	1745	1.236	4.102	0	[illegible]	[illegible]	70.6	78.0	77.0	86.5	80.4	110	89.8	82.8
[illegible]	[illegible]	[illegible]	[illegible]	[illegible]	[illegible]	[illegible]	3.312	1527	2237	1.650	4.669	0	[illegible]	[illegible]	78.5	88.2	83.7	93.4	91.8	130	97.8	92.8
[illegible]	[illegible]	[illegible]	[illegible]	[illegible]		[illegible]	1.592	673	[illegible]	1.012	2.634		--	[illegible]	60.2	68.5	65.5	76.0	66.8	100	77.0	66.8
[illegible]	[illegible]	[illegible]	[illegible]	[illegible]	[illegible]	[illegible]	1.790	767	1199	1.282	2.913	0	[illegible]	[illegible]	[illegible]	71.2	69.6	[illegible]	72.2	110	81.7	71.6
[illegible]	[illegible]	[illegible]	[illegible]	[illegible]	[illegible]	[illegible]	1.992	903	1392	[illegible]	3.110	0	-0.526	38.2	66.9	74.5	73.3	83.8	[illegible]	110	85.9	76.9
[illegible]	[illegible]	[illegible]	[illegible]	[illegible]	[illegible]	[illegible]	[illegible]	1126	1800	2.007	3.577	0	-0.153	38.0	73.5	[illegible]	79.8	89.2	86.4	130	92.5	86.4
[illegible]	[illegible]	[illegible]	[illegible]	[illegible]	[illegible]	[illegible]	[illegible]	[illegible]	1809	1.183	1.866	0	-0.284	36.3	70.4	77.6	[illegible]	87.2	80.3	110	[illegible]	82.3
[illegible]	[illegible]	[illegible]	[illegible]	[illegible]	[illegible]	[illegible]	2.373	1381	1982	1.403	2.371	0	-0.185	36.5	73.7	80.5	80.2	89.4	85.4	120	[illegible]	88.1
[illegible]	[illegible]	[illegible]	[illegible]	[illegible]	[illegible]	[illegible]	[illegible]	[illegible]	2242	1.584	3.194	0	-0.033	38.0	78.6	87.8	[illegible]	[illegible]	93.7	140	98.1	94.2
[illegible]	[illegible]	[illegible]	[illegible]	[illegible]	[illegible]	[illegible]	3.417	[illegible]	2331	1.523	2.889	0	0.026	39.1	80.5	[illegible]	85.9	[illegible]	97.6	140	[illegible]	97.6
[illegible]	[illegible]	[illegible]	[illegible]	[illegible]	[illegible]	[illegible]	[illegible]	1329	1871	1.373	2.265	0	-0.214	36.8	72.8	79.6	78.9	[illegible]	81.8	120	91.3	85.8
[illegible]	[illegible]	[illegible]	[illegible]	[illegible]	[illegible]	[illegible]	2.613	1468	2066	1.447	2.479	0	-0.109	37.2	75.1	82.4	81.6	[illegible]	88.8	130	94.3	90.6
[illegible]	[illegible]	[illegible]	[illegible]	[illegible]	[illegible]	[illegible]	2.254	1358	2226	1.302	2.259	0	-0.243	36.9	71.7	78.8	[illegible]	[illegible]	[illegible]	[illegible]	90.4	84.5

Table A-3. 36-C-D Chute Nozzle Test Matrix (Continued).

Model No. 3, $(AR)_o$ = 2.6
Config. 36-Chute
A_{FS} = 138 in.², A_i = 6.582 in.², A_o = 23.758 in.²

Point	Inner $(P_T/P_0)_i$	Inner T_{T_i}, °R	Inner V_i ft/sec	Outer $(P_T/P_0)_o$	Outer T_{T_o}, °R	Outer V_o ft/sec	Mass Averaged P_T/P_0	Mass Averaged T_T, °R	Mass Averaged V ft/sec	V_o/V_i	W_o/W_i	V_{FS} ft/sec	Log [illegible]	10 Log $(F_s C_i T_{sm})$	2400 ft Sideline 50° OASPL	50° PNL	90° OASPL	90° PNL	Peak OASPL	Peak θ	EPNL	POASPL
36	2.524	794	1459	1.950	1354	1686	[illegible]	117[illegible]	[illegible]	1.13[illegible]	[illegible]	[illegible]	-0.406	36.9	69.5	76.8	[illegible]	85.5	78.3	110	88.2	82.2
37	[illegible]	868	1612	3.024	1200	2365	[illegible]	1477	[illegible]	[illegible]	[illegible]	[illegible]	-0.025	38.[illegible]	76.2	84.2	82.8	91.5	90.4	130	96.4	91.2
38	[illegible]	851	1620	3.028	1494	2217	[illegible]	1329	[illegible]	1.369	[illegible]	[illegible]	-0.062	[illegible]	76.0	85.4	81.8	90.9	89.3	130	95.1	90.1
39	1.971	852	1343	3.026	1307	2069	2.768	1223	1930	[illegible]	[illegible]	[illegible]	-0.073	38.5	76.3	86.1	80.9	90.5	87.8	130	93.7	88.8
40	1.975	846	1340	3.017	1069	1864	2.793	1031	[illegible]	1.391	4.69	[illegible]	-0.176	39.3	75.9	86.7	79.6	89.8	84.1	120	91.5	86.8
41	1.901	850	1336	3.020	921	1731	2.803	910	167[illegible]	[illegible]	[illegible]	[illegible]	-0.074	40.0	75.1	85.8	78.[illegible]	88.6	82.4	120	89.8	85.2
42	1.989	839	1341	2.987	704	1507	2.776	724	1483	1.124	[illegible]	[illegible]	-0.179	40.8	74.0	84.6	77.[illegible]	88.4	77.3	80	88.9	82.5
43	1.483	873	1057	3.024	1711	2376	2.682	1581	2171	[illegible]	[illegible]		-0.090	37.0	76.2	84.4	82.8	91.7	90.4	130	96.4	91.1
44	[illegible]	861	1050	3.023	1297	2060	2.702	1237	1921	1.962	[illegible]		[illegible]	38.1	75.4	85.5	80.6	90.0	86.2	120	93.5	88.2
45	[illegible]	835	1046	3.025	902	1714	2.719	894	1614	[illegible]	[illegible]		-0.092	39.8	74.9	85.9	78.9	89.6	82.5	120	90.0	84.5
46	[illegible]	[illegible]	1560	3.026	1696	2364	[illegible]	[illegible]	2163	[illegible]	[illegible]		[illegible]	37.6	77.8	87.1	83.4	92.7	91.1	130	97.0	93.0
47	2.555	[illegible]	1542	3.030	1275	2014	2.907	1179	[illegible]	[illegible]	[illegible]		[illegible]	38.9	76.7	86.9	81.4	91.2	88.3	130	93.9	90.3
48	2.516	862	1529	3.038	901	1716	[illegible]	894	[illegible]	[illegible]	[illegible]	[illegible]	[illegible]	40.3	75.9	86.1	79.5	89.8	86.8	140	90.5	87.9
49				2.039	858	1378	[illegible]	858	[illegible]				[illegible]	38.4	64.3	72.5	71.0	81.6	72.9	110	83.4	73.8
50				2.345	[illegible]	1522	[illegible]	[illegible]	[illegible]				-0.138	39.[illegible]	68.6	77.7	74.4	84.2	77.0	110	86.1	79.3
51				[illegible]	[illegible]	1672	[illegible]	[illegible]	[illegible]				[illegible]	40.8	74.7	85.8	78.3	89.5	83.3	130	89.2	84.3
52				[illegible]	[illegible]	[illegible]	[illegible]	[illegible]	[illegible]				[illegible]	41.8	80.4	88.6	82.5	93.9	82.9	80	93.9	88.3
53	[illegible]	860	[illegible]	[illegible]	1690	2360	[illegible]	[illegible]	[illegible]	1.417	2.568		[illegible]	38.[illegible]	78.1	87.2	83.8	93.0	93.8	140	98.2	94.6
54	[illegible]	[illegible]	1661	[illegible]	[illegible]	2060	[illegible]	1183	[illegible]	[illegible]	[illegible]	[illegible]	-0.013	39.2	77.0	86.3	81.9	91.2	91.4	140	95.3	92.3
55	[illegible]	[illegible]	1655	[illegible]	898	[illegible]	3.019	882	[illegible]	[illegible]	[illegible]		[illegible]	[illegible]	75.8	85.9	79.7	89.9	87.9	140	91.7	84.1
[illegible]	1.[illegible]	987	1127	3.308	1626	2392	[illegible]	1557	2222	[illegible]	6.750	147	-0.04[illegible]	[illegible]	79.0	89.5	82.7	93.1	90.8	130	97.4	90.8
[illegible]	1.568	976	1290	3.233	1637	2391	2.826	1540	2257	2.901	5.831	146	[illegible]	37.6	79.4	89.6	83.2	93.5	91.1	140	96.8	91.1
[illegible]	[illegible]	[illegible]	[illegible]	2.066	992	[illegible]	1.995	889	1383	1.109	3.220	143	[illegible]	38.2	65.9	74.6	71.0	82.0	72.7	110	83.7	73.9
[illegible]	3.122	[illegible]	2677	3.791	[illegible]	2565	[illegible]	1517	2326	1.548	2.862	146	[illegible]	39.0	80.5	89.4	85.4	95.3	93.8	130	100.9	96.3
[illegible]	2.[illegible]	723	1476	2.332	1584	2033	2.332	1347	1863	1.377	2.278	143	-0.206	36.8	72.7	80.5	78.[illegible]	89.0	80.2	110	90.4	84.2
[illegible]1				1.975	935	1409	1.975	935	1409			279	[illegible]	37.9	62.1	72.4	68.9	80.9	70.9	120	81.3	70.9
[illegible]				2.493	1200	1823	2.493	1200	1823			280	-0.130	37.[illegible]	68.4	77.4	74.2	85.5	78.6	120	87.8	79.1
[illegible]3				2.739	1340	2013	2.739	1340	2013			280	-0.082	37.9	71.6	81.4	77.2	88.4	81.9	120	90.8	82.9
[illegible]				2.756	1711	2288	2.756	1711	2288			280	[illegible]	36.8	73.7	8[illegible].1	79.1	89.8	86.5	130	93.8	86.5
[illegible]				3.321	1615	2387	3.321	1615	2387			280	-0.016	38.4	78.0	89.3	82.6	94.1	90.1	[illegible]	97.1	90.1
[illegible]				3.752	1751	2591	3.752	1751	2591			282	0.062	35.9	82.1	90.5	86.3	96.5	93.8	[illegible]	100.4	95.4
68				3.771	1739	2586	3.771	1739	2586			279	0.064	35.9	83.1	91.2	86.7	97.0	93.5	130	100.2	95.4

Table A-3. 36-C-D Chute Nozzle Test Matrix (Continued).

Model No. 3, $(AR)_c$ = 2.00
Config. In-Chute
A_{FS} = 335 in.^{2} A_i = [illegible] in.^{2}, A_o = 23.758 in.^{2}

Point	Inner $(P_T/P_o)_i$	Inner T_{T_i} °R	Inner V ft/sec	Outer $(P_T/P_o)_o$	Outer T_{T_o} °R	Outer V ft/sec	Mass Averaged P_T/P_o	Mass Averaged T_T °R	Mass Averaged V ft/sec	V_o/V_i	W_o/W_i	V_{FS} ft/sec	Log ϵ	10 Log_{10} $[F_s(T_o/T_{sm})^{\omega-1}]$	2400 ft Sideline 50° OASPL	50° PNL	90° OASPL	90° PNL	Peak OASPL	Peak θ	Peak PPNL	POASPL
7	1.681	561	964	1.966	938	1407	1.891	850	1304	1.460	3.298	279	0	38.1	62.7	72.7	68.5	80.5	71.1	120	81.5	71.1
8	1.842	547	1026	2.473	1201	1817	2.295	1047	1631	1.771	3.252	279	-0.233	38.2	68.8	78.0	74.5	86.0	78.7	120	88.3	79.2
9	1.908	[illegible]	1161	2.760	1342	2018	2.512	1167	1804	1.862	3.381	280	-0.144	38.1	71.9	82.0	77.4	88.7	82.0	120	91.0	82.7
10	1.728	586	1069	2.756	1311	2296	2.451	1454	1995	2.270	3.336	280	-0.157	36.9	73.3	82.0	79.1	89.8	86.0	130	93.7	86.0
11	2.150	604	1194	3.303	1634	2397	2.949	1396	2119	2.008	3.324	281	-0.040	38.4	79.5	91.5	81.9	93.7	89.3	130	96.7	89.3
12	2.371	596	1231	3.777	1757	2601	3.319	1486	2287	2.079	3.297	281	0.014	39.1	80.7	90.4	85.4	96.9	93.0	130	100.3	93.0
13	1.483	1452	1366	1.959	935	1401	1.850	1006	1396	1.026	6.293	279	0	37.3	---	---	---	---	---	---	---	---
14	1.483	1448	1364	2.382	1194	1778	2.192	1227	1724	1.303	6.725	280	-0.283	36.8	62.9	72.6	68.6	80.4	71.5	120	81.9	71.5
15	1.487	1459	1374	2.884	1410	2111	2.601	1416	2024	1.536	7.457	280	-0.113	37.2	68.6	76.8	74.1	85.1	78.0	120	87.5	78.2
16	1.481	1496	1385	3.992	1705	2604	3.517	1685	2488	1.880	9.515	279	0.039	38.5	83.4	93.2	88.4	99.0	94.9	130	102.5	94.9
17	1.507	1271	1276	1.864	886	1317	1.784	938	1311	1.032	5.491	281	0	37.5	66.2	75.2	71.9	83.1	75.5	120	85.2	75.9
18	[illegible]	1215	1276	2.234	1081	1634	2.081	1100	1582	1.281	5.910	271	-0.382	37.2	71.0	80.3	76.2	87.1	82.1	130	89.4	82.1
19	1.512	1215	1277	2.683	1265	1937	2.442	1258	1849	1.517	6.527	271	-0.165	37.3	83.3	92.5	85.9	97.4	92.5	130	99.7	92.9
20	1.515	1268	1308	3.784	1755	2601	3.339	1700	2456	1.988	7.899	271	0.019	38.1	83.4	91.5	85.7	96.7	92.9	130	100.3	94.1
21	1.537	985	1170	1.745	814	1199	1.699	844	1194	1.025	4.651	279	0	37.5	62.1	72.1	67.6	79.3	68.4	110	80.4	69.9
22	1.539	1004	1183	2.072	978	1488	1.962	982	1438	1.258	5.110	279	-0.600	37.6	60.7	70.8	66.3	78.2	66.3	90	78.2	67.2
23	1.539	1004	1183	2.450	1156	1797	2.258	1158	1702	1.519	5.450	279	-0.248	37.3	64.0	73.7	69.7	81.4	73.0	120	83.3	73.0
24	1.541	995	1179	3.311	1635	2502	2.938	1548	2232	2.033	6.177	283	-0.040	37.7	77.5	89.1	81.5	93.0	88.4	130	95.7	88.4
24R	1.566	976	1188	3.234	1634	2379	2.877	1538	2205	2.002	5.851	279	-0.051	37.6	77.4	88.4	81.3	92.3	88.3	130	95.3	88.5
25	1.782	531	985	1.553	733	1097	1.599	677	1010	1.036	2.603	279	0	37.2	59.6	69.6	64.5	75.8	64.8	80	75.9	64.8
26	1.752	540	980	1.788	886	1276	1.769	797	1200	1.302	2.881	278	0	37.9	60.9	70.8	66.7	78.6	66.7	90	78.6	66.9
27	1.754	548	988	2.088	956	1476	1.998	860	1362	1.494	3.266	279	-0.516	38.4	63.5	72.9	68.8	80.4	72.1	120	82.3	72.1
28	1.719	585	1004	2.720	1313	1986	2.460	1161	1782	1.978	3.804	278	-0.161	37.9	70.9	80.1	76.4	87.3	80.8	[illegible]	89.5	81.7
29	1.986	841	1341	2.048	1612	1903	2.001	1401	1749	1.419	2.653	284	-0.453	35.6	68.6	77.5	74.0	85.0	77.9	[illegible]	87.4	77.9
29R	2.009	815	1330	2.047	1602	1896	2.009	1383	1738	1.426	2.589	277	-0.452	35.7	68.3	77.0	74.1	85.1	77.7	[illegible]	86.9	77.7
[illegible]	[illegible]	857	1541	2.398	1726	2154	2.372	1470	1974	1.398	2.399	280	-0.185	36.5	72.9	81.0	77.8	88.6	82.0	120	90.6	83.7
[illegible]	2.524	856	[illegible]	2.404	1701	2141	2.392	1449	1963	1.393	2.389	278	-0.182	36.6	72.6	80.6	77.6	88.3	82.1	120	90.9	83.1
[illegible]	[illegible]	858	1543	3.204	1751	2457	2.988	1537	2238	1.592	3.179	282	-0.032	38.0	77.9	89.3	82.0	92.9	89.1	130	96.5	91.7
[illegible]	[illegible]	830	1661	3.164	1751	2565	3.419	1513	2331	1.544	2.861	281	0.026	39.1	79.4	89.0	83.4	93.6	91.6	130	88.7	95.2
[illegible]	[illegible]	761	1465	2.313	1594	2035	2.313	1336	1855	1.386	2.232	284	-0.214	36.8	71.6	80.3	76.4	87.5	81.1	120	90.2	[illegible]
[illegible]	[illegible]	[illegible]	1467	2.319	1582	2025	2.314	1337	1856	1.380	2.300	276	-0.214	36.7	70.9	79.4	75.9	86.6	80.8	130	88.6	80.9
[illegible]	[illegible]	[illegible]	1551	2.674	1960	2291	2.603	1486	2076	1.477	2.434	282	-0.112	37.2	74.8	83.0	79.9	90.3	85.7	130	93.0	86.1
[illegible]	2.677	840	1573	2.674	1727	2269	2.613	1472	2069	1.442	2.477	276	-0.109	37.2	73.9	81.7	78.9	89.0	85.2	130	[illegible]	[illegible]
[illegible]	[illegible]	766	1459	2.233	1503	1933	2.254	1277	1788	1.325	2.266	282	-0.245	36.8	69.9	78.5	74.9	85.8	78.8	120	87.9	79.8
[illegible]	[illegible]	762	1467	2.232	1515	1940	2.259	1281	1792	1.324	2.216	279	-0.242	36.8	70.6	79.6	75.8	87.2	79.9	120	89.3	[illegible]

Table A-3. 36-C-D Chute Nozzle Test Matrix (Concluded).

Model No. [illegible] (AR) [illegible]
Config. [illegible] chute
[illegible] in.², A_i = [illegible] in.², A_o = [illegible] in.²

Point	Inner $(P_T/P_0)_i$	Inner T_{Ti} °R	Inner V_i ft/sec	Outer $(P_T/P_0)_o$	Outer T_{To} °R	Outer V_o ft/sec	Mass Averaged P_T/P_0	Mass Averaged T_T °R	Mass Averaged V ft/sec	V_o/V_i	W_o/W_i	V_{FS} ft/sec	Log r	$10 \log_{10}[F_S(T_0/T_{sm})^{-1}]$	2400 ft Sideline 50° OASPL	50° PNL	90° OASPL	90° PNL	Peak OASPL	Peak θ	PPNL	POASPL
36	[illegible]	804	[illegible]	[illegible]	[illegible]	[illegible]	[illegible]	1153	1625	1.121	2.090	279	-0.408	36.8	67.8	77.4	73.6	85.5	76.2	120	86.1	77.2
37	[illegible]	859	1363	[illegible]	[illegible]	[illegible]	2.721	1529	[illegible]	1.742	[illegible]	283	-0.072	37.4	75.7	84.7	81.3	91.9	86.7	120	94.8	87.5
37R	[illegible]	[illegible]	[illegible]	3.038	[illegible]	[illegible]	[illegible]	[illegible]	[illegible]	[illegible]	3.814	280	[illegible]	37.5	75.0	83.1	80.0	90.0	87.2	130	94.4	87.2
38	[illegible]	[illegible]	1360	[illegible]	[illegible]	2212	[illegible]	1362	[illegible]	1.626	[illegible]	280	-0.071	38.0	75.2	85.6	79.9	90.8	86.9	130	94.4	86.9
39	[illegible]	[illegible]	1361	[illegible]	[illegible]	[illegible]	[illegible]	[illegible]	[illegible]	[illegible]	[illegible]	279	-0.068	38.6	75.6	87.8	79.0	90.7	83.5	120	92.0	84.8
40	[illegible]	[illegible]	1352	[illegible]	[illegible]	[illegible]	[illegible]	[illegible]	[illegible]	[illegible]	[illegible]	280	-0.070	39.3	75.7	88.3	78.3	91.1	81.5	120	90.4	83.0
41	[illegible]	[illegible]	[illegible]	3.028	[illegible]	[illegible]	[illegible]	[illegible]	[illegible]	[illegible]	[illegible]	279	-0.071	40.1	77.7	88.5	81.8	93.0	89.2	130	96.5	89.4
42	[illegible]	[illegible]	[illegible]	3.038	[illegible]	[illegible]	[illegible]	[illegible]	[illegible]	[illegible]	[illegible]	280	-0.071	40.9	74.7	87.1	76.2	89.6	78.3	80	91.8	78.3
43	[illegible]	[illegible]	[illegible]	[illegible]	[illegible]	2377	2.691	[illegible]	[illegible]	[illegible]	[illegible]	283	-0.088	[illegible]	74.6	83.8	79.5	89.6	86.7	130	94.2	86.8
43R	[illegible]	[illegible]	[illegible]	[illegible]	[illegible]	[illegible]	[illegible]	[illegible]	[illegible]	[illegible]	[illegible]	279	-0.090	37.0	75.2	84.8	80.5	91.2	87.4	130	95.0	87.4
[illegible]	[illegible]	[illegible]	[illegible]	[illegible]	[illegible]	[illegible]	[illegible]	[illegible]	1928	[illegible]	[illegible]	279	[illegible]	[illegible]	74.3	86.3	78.3	90.3	83.5	120	92.0	84.5
[illegible]	[illegible]	[illegible]	[illegible]	[illegible]	[illegible]	[illegible]	[illegible]	[illegible]	[illegible]	[illegible]	[illegible]	283	[illegible]	39.8	75.1	87.9	76.6	90.1	78.0	80	91.6	[illegible]
[illegible]	[illegible]	[illegible]	[illegible]	[illegible]	[illegible]	[illegible]	[illegible]	[illegible]	[illegible]	[illegible]	[illegible]	[illegible]	[illegible]	37.8	76.6	86.8	81.1	91.6	86.9	120	95.1	[illegible]
[illegible]	[illegible]	[illegible]	[illegible]	[illegible]	[illegible]	[illegible]	[illegible]	1491	[illegible]	1.523	[illegible]	[illegible]	-0.353	37.9	76.3	86.4	80.3	90.4	87.2	130	[illegible]	87.2
47	[illegible]	[illegible]	[illegible]	[illegible]	[illegible]	[illegible]	[illegible]	1202	[illegible]	1.336	[illegible]	[illegible]	[illegible]	38.8	75.9	87.9	79.6	91.6	80.0	80	92.4	85.8
[illegible]	[illegible]	[illegible]	[illegible]	[illegible]	[illegible]	[illegible]	[illegible]	[illegible]	[illegible]	[illegible]	[illegible]	[illegible]	[illegible]	[illegible]	75.3	87.4	77.5	90.3	78.6	80	91.7	82.1
[illegible]	[illegible]	[illegible]	[illegible]	[illegible]	[illegible]	[illegible]	[illegible]	[illegible]	2161	[illegible]	[illegible]	282	[illegible]	38.2	77.3	87.7	82.2	93.2	87.1	120	95.7	90.4
[illegible]	[illegible]	[illegible]	[illegible]	[illegible]	[illegible]	2364	2.066	[illegible]	[illegible]	1.413	[illegible]	[illegible]	[illegible]	38.2	76.5	86.5	80.7	91.2	87.4	130	94.4	89.4
[illegible]	[illegible]	[illegible]	[illegible]	[illegible]	[illegible]	[illegible]	[illegible]	[illegible]	1968	[illegible]	[illegible]	[illegible]	[illegible]	39.1	76.0	87.2	79.6	91.1	84.3	120	91.0	86.3
[illegible]	[illegible]	[illegible]	[illegible]	[illegible]	[illegible]	[illegible]	[illegible]	[illegible]	1702	[illegible]	[illegible]	279	[illegible]	[illegible]	74.9	[illegible]	77.8	90.3	78.8	80	91.9	84.6
[illegible]	[illegible]	[illegible]	[illegible]	[illegible]	[illegible]	[illegible]	[illegible]	[illegible]	[illegible]	[illegible]	[illegible]	[illegible]	---	[illegible]	63.7	74.0	68.6	80.4	70.4	120	81.0	70.4
[illegible]	[illegible]	[illegible]	[illegible]	[illegible]	[illegible]	[illegible]	[illegible]	[illegible]	[illegible]	[illegible]	[illegible]	[illegible]	[illegible]	38.4	81.7	91.6	85.2	96.7	91.5	130	99.4	91.5
[illegible]	[illegible]	[illegible]	[illegible]	[illegible]	[illegible]	[illegible]	[illegible]	[illegible]	[illegible]	[illegible]	[illegible]	[illegible]	-0.039	38.5	86.5	94.6	87.4	98.4	94.0	130	101.5	[illegible]
[illegible]	[illegible]	[illegible]	[illegible]	[illegible]	[illegible]	1216	1.719	[illegible]	1208	[illegible]	[illegible]	369	---	[illegible]	62.3	72.3	66.5	78.6	68.5	120	78.9	68.5
[illegible]	[illegible]	[illegible]	[illegible]	[illegible]	[illegible]	[illegible]	[illegible]	1341	[illegible]	[illegible]	6.18	371	[illegible]	[illegible]	78.2	89.7	81.1	92.8	87.3	130	94.6	87.3
[illegible]	[illegible]	[illegible]	[illegible]	[illegible]	[illegible]	[illegible]	[illegible]	[illegible]	2203	[illegible]	[illegible]	362	[illegible]	[illegible]	78.6	89.7	81.3	92.8	87.6	130	[illegible]	87.6
[illegible]	[illegible]	[illegible]	[illegible]	[illegible]	[illegible]	1941	[illegible]	[illegible]	[illegible]	1.430	[illegible]	370	[illegible]	[illegible]	69.3	[illegible]	74.1	[illegible]	77.3	120	86.8	[illegible]
[illegible]	[illegible]	[illegible]	[illegible]	[illegible]	[illegible]	[illegible]	[illegible]	[illegible]	[illegible]	1.413	[illegible]	366	[illegible]	35.6	69.2	[illegible]	74.1	85.2	77.4	120	86.9	[illegible]
[illegible]	[illegible]	[illegible]	[illegible]	[illegible]	[illegible]	2160	2.368	1477	1977	1.403	[illegible]	369	-0.157	36.5	72.4	81.2	77.0	88.0	81.6	120	[illegible]	83.3
[illegible]	[illegible]	[illegible]	[illegible]	[illegible]	[illegible]	[illegible]	3.413	1519	2335	[illegible]	[illegible]	369	[illegible]	39.1	[illegible]	89.4	83.4	94.1	91.2	130	[illegible]	[illegible]
[illegible]	[illegible]	[illegible]	[illegible]	[illegible]	[illegible]	[illegible]	2.426	1342	[illegible]	1.381	2.264	371	-0.208	36.8	71.6	80.7	76.1	87.3	80.0	120	89.1	[illegible]
[illegible]	[illegible]	[illegible]	[illegible]	[illegible]	[illegible]	[illegible]	2.312	1327	1848	1.390	2.263	368	-0.215	36.8	71.5	80.5	75.7	86.7	79.4	120	88.5	79.8
[illegible]	[illegible]	[illegible]	[illegible]	2.675	[illegible]	[illegible]	[illegible]	1489	2079	[illegible]	2.552	369	-0.110	37.2	[illegible]	83.2	79.1	89.8	83.5	120	91.9	[illegible]
[illegible]	[illegible]	[illegible]	[illegible]	[illegible]	[illegible]	[illegible]	[illegible]	[illegible]	2059	[illegible]	2.488	366	-0.108	37.3	74.1	82.6	[illegible]	88.9	84.1	130	91.6	84.1
[illegible]	[illegible]	[illegible]	[illegible]	[illegible]	[illegible]	1936	[illegible]	1283	1792	1.326	[illegible]	371	[illegible]	36.8	70.9	80.4	75.6	87.3	[illegible]	130	[illegible]	[illegible]
[illegible]	[illegible]	[illegible]	[illegible]	[illegible]	[illegible]	1453	[illegible]	1286	1796	1.323	[illegible]	[illegible]	-0.242	36.8	70.5	79.7	[illegible]	86.1	[illegible]	[illegible]	[illegible]	[illegible]

Table A-4. 36-C-D Chute with Treated Ejector Test Matrix.

Model No. 4, $(AR)_o = 2.00$
Config. 36 Chute with Treated Ejector
A_{FS} = 338 in.^{2}, A_i = 6.582 in.^{2}, A_o = 23.758 in.^{2}

Point	Inner $(P_T/P_o)_i$	Inner T_{Ti} °R	Inner V_i ft/sec	Outer $(P_T/P_o)_o$	Outer T_{To} °R	Outer V_o ft/sec	Mass Averaged P_T/P_o	Mass Averaged T_T °R	Mass Averaged V ft/sec	V_o/V_i	W_o/W_i	V_{FS} ft/sec	Log r	10 Log_{10} $[F_s(T_o/T_{sm})^{\omega-1}]$	2400 ft Sideline 50° OASPL	50° PNL	90° OASPL	90° PNL	Peak OASPL	Peak θ	Peak PPNL	POASPL
7	1.670	541	946	1.940	960	1415	1.874	860	1303	1.50	3.18	0	---	38.0	66.3	72.2	72.4	79.9	73.5	100	80.5	74.0
8	1.830	552	1030	2.440	1207	1818	2.287	1053	1633	1.77	3.25	0	-0.236	38.1	71.7	78.0	78.3	86.2	80.4	110	87.9	82.5
9	1.911	552	1057	2.743	1323	2003	2.507	1145	1784	1.90	3.32	0	-0.146	38.2	74.1	81.3	80.7	88.9	84.9	120	91.7	86.3
10	1.607	592	954	2.698	1549	2294	2.392	1496	2000	2.40	3.56	0	-0.177	36.5	74.6	81.6	82.0	90.5	85.4	110	93.6	88.0
11	1.953	592	1114	3.291	1594	2364	2.914	1379	2095	2.12	3.65	0	-0.047	38.4	79.3	89.2	84.6	94.3	91.7	140	96.0	91.7
12	2.142	623	1166	3.728	1730	2571	3.256	1501	2282	2.21	3.87	0	0.007	38.8	82.5	90.1	87.2	97.6	96.0	130	102.2	96.0
13	1.482	1450	1364	1.968	923	1397	1.858	995	1393	1.02	6.37	0	---	37.4	66.7	72.7	72.9	80.3	74.0	110	80.7	76.0
14	1.488	1449	1370	2.384	1156	1751	2.197	1194	1702	1.28	6.82	0	-0.282	37.0	71.3	77.5	77.9	85.6	79.9	110	86.9	82.2
15	1.492	1449	1376	2.862	1395	2094	2.587	1401	2008	1.52	7.38	0	-0.117	37.2	75.1	84.0	82.0	90.4	83.5	140	91.9	88.5
16	1.498	[illegible]	1384	3.881	1711	2588	2.430	1685	2467	1.87	8.96	0	0.088	38.3	83.5	91.0	88.3	98.4	98.9	150	101.7	98.9
17	1.510	1242	1290	1.864	878	1312	1.786	934	1309	1.02	5.36	0	---	37.5	65.6	71.7	71.3	78.4	73.3	120	79.1	73.7
18	1.514	1228	1287	2.237	1071	1629	2.087	1094	1580	1.27	5.96	0	-0.376	37.3	70.0	75.8	76.1	83.5	77.7	110	84.4	80.1
19	1.514	1225	1285	2.695	1269	1945	2.455	1263	1858	1.51	6.56	0	-0.160	37.3	73.9	81.2	80.6	88.7	84.6	120	91.0	86.0
20	1.519	1211	1283	3.761	1726	2575	3.323	1667	2427	2.01	7.71	0	-0.017	38.2	83.3	91.0	87.7	98.0	97.8	140	101.9	97.8
21	[illegible]	994	1185	1.752	828	1215	1.709	858	1210	1.03	4.62	0	---	37.5	64.2	70.3	69.5	76.7	70.6	100	77.5	70.6
22	1.546	1004	1189	2.078	983	1494	1.967	987	1444	1.26	5.08	0	-0.583	37.6	67.9	73.7	74.2	81.4	76.1	120	81.9	16.8
23	1.548	1004	1191	1.469	1207	1822	2.279	1175	1124	1.53	5.41	0	-0.236	37.3	71.9	78.2	78.3	86.1	81.9	120	88.1	83.3
24	1.549	1011	1196	3.308	1642	2405	2.940	1554	2236	2.01	6.17	0	-0.039	37.7	79.4	89.3	83.8	94.1	92.8	140	97.1	92.8
25	1.793	535	994	1.560	721	1017	1.608	670	1011	1.02	2.63	0	---	37.2	61.9	68.2	66.3	73.7	67.4	100	24.4	67.4
26	1.777	531	983	1.800	846	1234	1.785	765	1185	1.28	2.90	0	---	38.0	65.0	71.2	70.3	77.4	71.1	100	77.9	71.1
27	1.724	552	978	2.065	994	1496	1.974	890	1374	1.53	3.24	0	-0.571	38.2	68.1	74.1	74.1	81.2	76.1	120	82.1	76.1
28	1.746	558	994	2.754	1314	1999	2.489	1153	1785	2.01	3.70	0	-0.152	38.1	73.8	81.2	80.4	88.8	84.9	120	91.6	85.7
29	1.969	347	1139	2.031	1620	1899	1.994	1409	1746	1.48	2.66	0	-0.475	35.5	70.8	76.8	77.6	85.2	80.0	110	87.1	82.1
30	2.551	846	1545	2.396	1707	2142	2.382	1450	1964	1.39	2.35	0	-0.182	36.6	74.0	80.0	81.0	88.9	83.8	110	91.2	87.5
31	2.497	862	1544	3.193	1710	2425	2.986	1510	2217	1.57	3.23	0	-0.032	38.1	78.7	87.8	84.8	93.7	94.0	140	97.5	94.5
32	3.109	802	1636	3.621	1663	2496	3.422	1441	2274	1.53	2.88	0	0.026	39.3	81.4	87.5	86.8	96.3	98.5	150	101.2	98.5
33	2.520	756	1452	2.291	1573	2007	2.293	1321	1836	1.38	2.25	0	-0.224	36.8	72.8	78.8	79.6	87.5	82.2	110	98.3	85.2
34	2.661	826	1557	2.660	1696	2245	2.605	1446	2047	1.44	2.48	0	-0.112	37.3	75.5	82.2	82.3	90.5	85.4	110	93.1	89.9
35	2.528	766	1464	2.210	1441	1882	2.247	1235	1755	1.29	2.28	0	-0.250	37.0	71.8	77.9	78.5	86.1	80.9	110	88.0	84.2
36	2.532	776	1475	1.929	1357	1676	2.040	1167	1610	1.14	2.06	0	-0.425	36.9	69.2	75.4	75.6	83.2	77.4	110	84.1	81.0
37	1.995	844	1349	3.028	1695	2367	2.766	1518	2155	1.76	3.81	0	-0.073	37.5	77.3	86.0	83.6	92.1	91.2	130	97.1	91.4
39	1.990	[illegible]	1355	3.025	1277	2046	2.799	1200	1920	1.51	4.46	0	-0.072	38.6	77.3	87.6	82.0	91.2	84.9	110	92.8	89.2
41	1.988	845	1346	3.012	909	1719	2.803	899	1660	1.28	5.28	0	-0.074	40.0	76.4	87.0	80.2	90.2	80.4	80	91.3	86.5
43	1.488	871	1048	3.023	1693	2364	2.684	1561	2158	2.26	5.38	0	-0.090	37.0	76.6	84.6	83.5	92.1	90.8	140	95.2	90.8
44	1.501	850	1053	3.022	1309	2071	2.706	1242	1926	1.97	6.03	0	-0.091	38.1	76.5	85.4	81.8	90.4	88.7	140	92.7	88.7
45	1.492	772	1001	3.009	892	1701	2.704	877	1615	1.70	7.10	0	-0.096	39.9	76.0	87.0	79.9	90.3	80.2	80	91.3	89.8
46	2.499	863	1546	3.024	1700	2369	2.857	1494	2167	1.53	3.07	0	-0.055	37.8	77.6	86.6	85.0	72.6	91.7	130	97.4	92.9
47	2.550	849	1548	3.021	1276	2044	2.907	1180	1933	3.32	3.46	0	-0.051	38.9	76.9	86.6	82.2	91.1	90.0	140	93.0	90.7
48	2.501	859	1543	3.008	896	1705	2.902	889	1674	1.11	4.25	0	-0.054	40.3	76.4	86.8	80.7	90.4	80.7	80	91.5	88.7

Table A-4. 36-C-D Chute with Treated Ejecotr Test Matrix (Continued).

Model ... (A8 ... = 2.0...)
Config. 36-Chute with Treated Ejector
A_{PE} = 338 in.^{2} A_i = 6.582 in.^{2}, A_o = 23.758 in.^{2}

Point	Inner $(P_T/P_o)_i$	Inner T_{T_i} °R	Inner V_i ft/sec	Outer $(P_T/P_o)_o$	Outer T_{T_o} °R	Outer V_o ft/sec	Mass Averaged P_T/P_o	Mass Averaged T_T °R	Mass Averaged V ft/sec	V_o/V_i	W_o/W_i	V_{FS} ft/sec	Log ω	10 Log_{10} $[F_s(T_o/T_{sm})^{\omega-1}]$	2400 ft Sideline 50° OASPL	50° PNL	90° OASPL	90° PNL	Peak OASPL	Peak θ	Peak PPNL	POASPL
49	---	---	---	2.019	853	1366	2.019	853	1366	---	---	0	-0.473	38.4	66.9	73.0	72.2	79.2	73.5	100	80.1	73.6
50	---	---	---	2.524	852	1543	2.524	852	1543	---	---	0	-0..44	39.6	70.8	77.5	76.5	84.0	78.4	120	84.3	80.1
51	---	---	---	3.027	851	1666	3.027	851	1666	---	---	0	-0.032	40.8	76.5	87.3	80.0	90.7	80.1	80	91.9	85.1
52	---	---	---	3.518	848	1754	3.518	848	1754	---	---	0	0.033	41.8	79.5	87.2	82.4	92.0	89.4	140	93.0	89.7
53	2.990	561	1346	3.008	1729	2385	2.826	1345	2043	1.77	2.04	0	-0.064	38.5	77.6	86.5	84.0	92.8	91.5	140	85.7	91.5
54	2.995	550	1334	3.048	1298	2069	2.938	1076	1851	1.55	2.37	0	-0.048	39.6	77.5	87.4	82.5	91.8	89.4	140	93.2	89.7
55	2.980	533	1311	2.903	895	1681	2.882	798	1581	1.28	2.71	0	-0.058	40.8	75.2	85.1	79.6	88.8	79.7	80	87.8	85.8
7	1.653	536	928	1.959	940	1405	1.877	846	1293	1.514	3.273	140	0	38.1	65.8	72.0	70.1	77.8	70.0	100	78.5	71.0
12	1.949	622	1139	3.694	1732	2564	3.217	1512	2281	2.251	4.037	141	0.002	38.7	83.1	91.1	85.7	96.7	93.9	130	100.2	94.8
16	1.509	1437	1367	3.927	1716	2600	3.464	1688	2478	1.874	8.897	142	0.033	38.4	84.6	92.0	87.4	97.7	98.5	140	103.0	98.8
21	1.553	1019	1204	1.734	824	1200	1.694	859	1201	0.997	4.604	140	0	37.5	62.7	69.4	66.6	74.4	67.5	110	75.2	67.5
23	1.554	1034	1213	2.448	1188	1798	2.259	1164	1707	1.482	5.453	140	-0.246	37.3	71.1	77.7	76.2	84.1	79.4	120	85.9	80.6
24	1.555	984	1184	3.280	1618	2379	2.915	1528	2209	2.009	6.049	143	-0.044	37.7	79.7	90.1	82.9	92.7	90.8	130	96.9	90.8
27	1.722	567	990	2.061	1008	1504	1.970	904	1383	1.519	3.253	141	-0.581	38.1	67.4	73.7	71.8	79.4	72.5	100	80.1	73.4
32	2.925	821	1614	3.603	1722	2536	3.365	1498	2307	1.571	3.024	143	0.020	39.0	81.0	89.4	85.2	95.1	96.1	140	100.2	97.2
33	2.495	757	1446	2.328	1588	2033	2.313	1335	1855	1.406	2.295	142	-0.214	36.8	---	---	---	---	---	---	---	---
7	1.638	537	921	1.963	943	1409	1.877	849	1295	1.529	3.313	277	0	38.1	65.4	72.8	69.7	78.0	70.0	100	78.2	70.2
8	1.950	542	981	2.460	1215	1823	2.265	1061	1631	1.858	3.381	276	-0.248	38.0	70.9	79.0	75.4	84.2	77.8	120	85.0	77.8
9	1.810	552	1017	2.736	1328	2009	2.495	1156	1789	1.976	3.517	277	-0.150	38.1	73.4	82.0	78.2	87.8	81.4	120	88.1	52.2
10	1.639	605	978	2.709	1733	2286	2.406	1484	1997	2.338	3.525	276	-0.172	36.6	74.4	88.9	79.3	88.7	84.1	120	91.4	84.5
11	1.908	575	1079	3.288	1597	2365	2.896	1379	2090	2.192	3.683	277	-0.050	38.4	79.1	90.8	82.5	93.8	88.9	130	94.5	88.9
12	1.948	614	1131	3.701	1734	2567	3.219	1511	2281	2.270	4.019	277	0.002	38.7	82.4	92.1	85.8	97.3	92.2	130	99.0	92.2
13	1.503	1447	1386	1.997	932	1417	1.884	1003	1413	1.022	6.289	279	0	37.4	66.2	73.6	69.9	78.8	71.0	100	79.4	71.9
14	1.498	1454	1384	2.387	1151	1747	2.198	1190	1700	1.262	6.779	278	-0.281	37.0	70.1	77.9	75.3	84.2	76.5	80	85.4	77.6
15	1.503	1439	1382	2.851	1424	2112	2.577	1426	2023	1.528	7.168	278	-0.119	37.1	74.6	83.4	79.3	89.3	82.9	120	90.0	84.3
16	1.510	1454	1396	3.912	1712	2594	3.452	1686	2473	1.858	8.928	279	0.032	38.4	85.3	93.4	86.8	97.9	93.1	130	99.7	95.3
17	1.536	1228	1307	1.842	888	1307	1.773	942	1307	1.000	5.294	279	0	36.4	63.5	70.9	68.1	76.4	68.1	100	76.1	68.1
18	1.538	1228	1309	2.236	1064	1637	2.088	1105	1589	1.251	5.790	279	-0.375	37.2	68.8	76.2	72.8	81.2	73.3	100	81.6	74.4
19	1.535	1218	1301	2.698	1301	1970	2.458	1290	1879	1.514	6.337	279	-0.158	37.2	72.6	80.8	77.1	86.2	80.3	120	87.4	81.5
20	1.505	1203	1264	3.686	1758	2582	3.253	1693	2428	2.043	7.553	277	0.008	38.0	82.5	92.3	85.5	97.0	92.1	130	99.0	92.3
21	1.551	1015	1200	1.746	814	1200	1.703	849	1200	1.000	4.669	278	0	37.5	62.2	69.8	66.6	75.0	6615	80	75.1	66.8
22	1.553	1011	1199	2.064	1018	1513	1.955	1017	1460	1.262	4.929	279	-0.614	37.4	66.9	74.3	70.8	78.9	91.4	100	79.4	72.0
23	1.558	994	1193	2.465	1206	1818	2.273	1172	1719	1.524	5.316	279	-0.239	37.3	70.5	78.2	75.3	83.0	77.4	120	84.5	77.3
24	1.554	978	1180	3.292	1614	2379	2.924	1524	2209	2.016	6.061	278	-0.43	37.7	78.6	89.7	82.9	93.6	88.8	130	95.0	88.8
25	1.766	530	977	1.552	725	1014	1.595	671	1004	1.038	2.640	278	0	37.1	60.3	69.1	64.0	73.0	64.3	80	73.7	64.4
26	1.730	539	978	1.819	841	1260	1.795	766	1190	1.288	3.014	278	0	38.0	63.4	71.0	67.9	76.5	67.9	90	76.5	67.8
27	1.717	534	976	2.069	985	1490	1.975	884	1370	1.528	3.279	279	-0.569	38.2	66.3	73.7	70.8	79.0	71.7	100	79.9	71.7
28	1.774	559	1007	2.743	1336	2011	2.479	1167	1792	1.997	3.589	276	-0.155	38.0	73.3	82.1	78.1	87.7	81.6	120	89.2	82.3
29	1.970	865	1353	2.013	1644	1901	1.978	1430	1750	1.405	2.638	278	-0.500	35.4	69.6	77.3	74.9	83.8	76.9	120	83.8	76.9
30	2.538	847	1542	2.393	1704	2138	2.376	1449	1961	1.387	2.364	280	-0.184	36.6	73.4	81.0	78.2	86.9	81.6	120	88.5	82.9
31	2.536	849	1543	3.148	1737	2411	2.949	1519	2214	1.575	3.085	279	-0.038	38.0	118.0	88.8	82.5	92.9	88.8	130	99.9	88.8

Table A-4. 36-C-D Chute with Treated Ejector Test Matrix (Concluded).

Model No. 4. $(AR)_o$ = 2.00
Config. 36-Chute with Treated Ejector
A_{FS} = 338 in.^{2} A_i = 6.582 in.^{2}, A_o = 23.758 in.^{2}

Point	Inner			Outer			Mass Averaged								2400 ft Sideline							
															50°		90°		Peak			
	$(P_T/P_o)_i$	T_{T_i} °R	V_i ft/sec	$(P_T/P_o)_o$	T_{T_o} °R	V_o ft/sec	P_T/P_o	T_T °R	V ft/sec	V_o/V_i	W_o/W_i	V_{FS} ft/sec	Log β	10 $\log_{10}$ $[F_s(T_o/T_{sm})^{\omega-1}]$	OASPL	PNL	OASPL	PNL	OASPL	θ	PPNL	POASPL
32	3.117	838	1671	3.659	1754	2573	3.443	1518	2341	1.539	2.884	279	-0.029	39.1	82.8	92.2	85.1	96.3	91.8	130	98.6	92.2
33	2.504	764	1455	2.322	1577	2023	2.313	1330	1851	1.390	2.300	278	-0.214	36.8	72.6	80.5	76.8	85.6	77.6	110	86.4	79.7
34	2.669	825	1557	2.628	1734	2256	2.573	1468	2051	1.449	2.414	277	-0.119	37.1	75.2	83.0	79.8	89.1	83.4	120	90.0	85.3
35	2.491	754	1442	2.228	1501	1929	2.244	1272	1780	1.338	2.261	278	-0.250	36.8	76.1	79.0	75.8	84.8	78.7	120	85.5	79.8
36	2.527	770	1467	1.941	1347	1676	2.047	1160	1608	1.142	2.078	278	-0.418	36.9	68.2	76.3	72.7	81.7	72.7	90	81.7	75.9
37	1.997	851	1345	3.032	1701	2371	2.763	1526	2160	1.763	3.857	278	-0.073	37.4	76.6	86.1	81.9	92.1	87.5	130	93.4	87.5
39	1.988	831	1334	3.030	1297	2062	2.793	1210	1926	1.546	4.369	278	-0.073	38.5	75.5	86.5	79.6	90.4	83.5	120	91.1	84.8
41	2.003	853	1358	3.040	908	1723	2.824	899	1665	1.269	5.311	279	-0.069	40.1	74.7	87.1	77.9	90.3	78.8	80	91.5	80.9
43	1.486	856	1049	3.033	1706	2375	2.688	1573	2168	2.264	5.400	278	-0.089	37.0	76.5	81.1	81.4	91.2	87.2	130	93.1	87.2
44	1.477	844	1034	3.028	1299	2063	2.704	1236	1921	1.995	6.231	278	-0.092	38.1	75.4	86.7	80.0	90.4	84.4	130	90.5	84.4
45	1.491	853	1051	3.064	911	1731	2.750	904	1651	1.647	7.524	279	-0.085	39.8	88.8	88.1	78.1	90.6	79.4	80	92.2	79.6
46	2.542	859	1554	3.078	1686	2374	2.905	1483	2173	1.528	3.074	279	-0.047	38.0	79.3	87.2	81.8	91.8	87.5	130	93.5	88.5
47	2.531	845	1538	3.020	1304	2065	2.893	1201	1946	1.343	3.459	278	-0.053	38.8	66.4	77.4	70.1	88.8	70.4	80	92.1	95.5
48	2.490	856	1536	3.031	909	1722	2.916	899	1687	1.121	4.264	279	-0.052	40.3	74.7	86.6	77.9	90.0	98.4	70	90.9	81.7
53	2.988	850	1656	3.035	1698	2370	2.953	1460	2169	1.431	2.556	278	-0.038	38.2	77.4	87.0	82.3	92.7	87.9	130	94.0	89.8
54	2.988	853	1659	3.023	1281	2047	2.994	1172	1949	1.234	2.957	279	-0.036	39.2	76.5	87.5	80.2	91.1	80.3	80	91.8	87.6
55	3.036	857	1673	3.031	910	1723	3.032	898	1712	1.030	3.498	279	-0.032	40.6	74.6	86.0	78.0	88.6	78.5	80	90.6	84.3
16	1.512	1447	1395	4.094	1691	2612	3.605	1667	2495	1.872	9.355	372	0.048	38.7	85.5	93.4	86.3	97.1	91.7	130	98.6	93.9
24	1.570	994	1202	3.347	1630	2405	2.971	1540	2236	2.000	6.101	372	-0.034	37.8	77.9	87.7	82.2	92.4	87.3	130	93.7	87.3
32	3.180	908	1653	3.725	1709	2553	3.502	1476	2320	1.544	2.864	372	0.035	39.4	81.0	90.8	84.3	95.2	90.3	130	96.8	92.1
34	2.691	837	1574	2.669	1754	2285	2.608	1487	2078	1.452	2.434	372	-0.110	37.2	75.5	83.6	79.3	88.6	80.7	120	89.7	84.1
35	2.307	761	1453	2.212	1535	1943	2.233	1294	1791	1.337	2.215	372	-0.256	36.7	71.6	79.5	75.8	85.0	76.0	80	85.1	78.6

Table A-5. 54-Element Coplanar Mixer Nozzle Test Matrix.

Model No. 5
Config. 54-Element Coplanar Mixer
A_{FS} = 338 in.^{2} A_i = 11.30 in.^{2}, A_o = 23.498 in.^{2}

Point	Inner $(P_T/P_o)_i$	Inner T_{T_i} °R	Inner V_i ft/sec	Outer $(P_T/P_o)_o$	Outer T_{T_o} °R	Outer V_o ft/sec	Mass Averaged P_T/P_o	Mass Averaged T_T °R	Mass Averaged V ft/sec	V_o/V_i	W_o/W_i	V_{FS} ft/sec	Log [illegible]	$10\ Log_{10}$ $[I_s(T_o/T_{sm})^{-1}]$	2400 ft Sideline 50° OASPL	2400 ft Sideline 50° PNL	2400 ft Sideline 90° OASPL	2400 ft Sideline 90° PNL	2400 ft Sideline Peak OASPL	2400 ft Sideline Peak θ	2400 ft Sideline Peak PPNL	2400 ft Sideline POASPL
1	1.774	549	999	1.568	726	1026	1.632	658	1016	1.027	1.591	0	---	37.3	59.5	64.8	64.3	71.8	65.7	110	72.5	67.8
1R	---	---	---	---	---	---	---	---	---	---	---	---	---	---	59.5	65.0	64.1	71.6	86.8	110	72.5	68.0
2	1.777	552	1002	1.801	853	1260	1.783	743	1166	1.258	1.734	0	---	38.0	62.8	68.2	68.1	74.8	73.0	130	77.3	74.2
3	1.277	566	678	1.967	941	1411	1.753	848	1228	2.081	3.010	0	---	37.6	63.9	69.3	69.5	76.2	75.1	130	79.3	76.6
4	1.775	561	1009	2.092	996	1510	1.968	845	1336	1.497	1.884	0	-0.087	38.2	66.6	72.1	72.3	78.8	78.5	130	82.9	80.1
5	1.549	994	1186	2.090	995	1308	1.921	995	1427	1.272	2.457	0	-0.276	37.5	67.5	73.1	73.2	79.8	81.7	140	84.4	81.7
6	1.557	997	1195	1.585	995	1215	1.577	996	1209	1.017	2.174	0	---	36.8	62.3	67.3	68.2	74.7	72.8	120	77.8	74.4
7	1.626	1069	1292	2.222	1073	1624	2.036	1072	1540	1.257	2.948	0	-0.439	37.3	69.1	74.6	75.2	81.7	84.5	140	87.1	84.6
8	1.675	1163	1386	2.374	1161	1751	2.156	1162	1661	1.263	3.046	0	-0.312	37.1	71.1	76.8	77.4	84.1	87.8	140	90.7	87.8
9	1.525	1221	1294	1.557	1223	1325	1.548	1222	1315	1.024	2.283	0	---	35.8	73.9	79.2	80.1	86.7	86.7	130	90.6	87.4
10	1.556	1000	1196	2.441	1198	1804	2.164	1150	1657	1.508	3.121	0	-0.306	[illegible]	71.2	77.0	77.7	84.3	87.7	140	90.6	88.1
11	1.508	922	1108	2.437	1201	1805	2.146	1133	1636	1.629	3.121	0	-0.321	37.2	[illegible]	76.7	77.4	84.1	87.4	140	90.2	87.8
12	2.329	807	1443	1.949	1388	1707	2.047	1140	1594	1.283	1.342	0	-0.219	37.1	70.3	[illegible]	77.2	83.8	86.5	140	89.2	86.5
13	1.726	583	1006	2.698	1343	2003	2.331	1104	1690	1.991	2.181	0	[illegible]	38.0	79.7	[illegible]	80.7	83.0	90.6	120	94.3	91.0
14	[illegible]	931	1113	2.710	1351	2014	2.334	1253	1804	1.810	3.232	0	-0.207	37.0	75.5	81.9	80.0	87.1	91.5	140	94.9	91.5
15	1.530	1236	1310	2.657	1284	1945	2.314	1274	1811	1.484	3.733	0	-0.215	36.8	75.3	81.4	80.2	87.0	91.2	140	94.6	91.2
16	1.514	1463	1405	1.538	1458	1429	1.531	1460	1421	1.017	2.177	0	---	34.6	63.1	69.9	71.9	78.1	79.3	130	82.6	80.2
17	1.511	1445	1393	2.866	1405	2104	2.459	1413	1969	1.510	4.258	0	-0.155	36.7	76.3	82.7	81.7	83.9	94.8	140	98.7	94.8
17R	1.502	1458	1391	2.854	1401	2097	2.448	1412	1964	1.508	4.296	0	-0.159	36.7	75.7	82.1	81.9	88.9	94.5	140	98.3	94.5
18	2.474	782	1464	2.138	1510	1891	2.203	1194	1706	1.292	1.306	0	-0.278	37.2	[illegible]	78.2	79.2	85.8	89.0	140	92.1	89.2
19	1.953	[illegible]	1269	2.323	1594	2036	2.159	1293	1756	1.604	1.734	0	-0.303	36.5	73.1	78.3	77.8	86.3	90.6	140	93.6	90.6
20	1.996	835	1358	2.050	1618	1909	2.002	1320	1694	1.406	1.563	0	-0.368	36.0	71.5	77.2	78.0	84.4	88.8	140	91.6	88.6
21	1.545	1022	1200	3.319	1618	2390	2.771	1491	2137	1.992	3.702	0	-0.072	37.4	80.4	87.2	85.0	92.8	98.6	140	103.2	98.6
21R	1.548	1026	1205	3.332	1625	2398	2.779	1498	2144	1.990	3.703	0	-0.071	37.4	80.3	87.0	84.9	92.8	98.8	140	103.2	98.5
[illegible]	[illegible]	[illegible]	[illegible]	3.316	1619	2390	[illegible]	[illegible]	[illegible]	[illegible]	[illegible]	0	[illegible]	37.4	80.3	86.9	84.9	92.8	98.7	140	103.3	98.7
22R	[illegible]	912	1067	3.306	1631	2396	2.731	1479	2115	2.246	3.730	0	-0.081	37.4	79.6	86.3	84.7	92.7	98.6	140	103.1	98.6
23	[illegible]	859	1545	2.414	1705	2145	2.382	1356	1897	1.388	1.423	0	-0.185	36.9	75.7	81.7	81.9	88.9	93.6	140	97.2	94.0
24	[illegible]	849	1572	2.607	1730	2247	[illegible]	1370	1971	1.429	1.448	0	-0.129	37.4	77.6	83.9	83.1	[illegible]	95.1	140	99.0	95.6
25	[illegible]	[illegible]	1649	3.628	1707	2531	3.121	1395	2213	1.534	1.776	0	+0.014	39.3	85.0	91.3	88.6	[illegible]	102.2	140	106.9	102.2
26	[illegible]	849	1536	3.206	1715	2433	2.909	1415	2122	1.584	1.862	0	-0.047	38.2	81.0	87.5	[illegible]	[illegible]	100.1	140	104.5	100.1
27	[illegible]	940	1169	2.781	1711	2298	2.361	1519	2002	2.072	3.020	0	-0.188	36.2	76.4	82.5	82.6	[illegible]	94.9	[illegible]	98.3	[illegible]
[illegible]	[illegible]	925	1123	3.754	1747	2590	3.061	1579	2291	2.306	3.900	0	-0.020	37.9	81.9	88.7	[illegible]	[illegible]	[illegible]	140	106.8	[illegible]
[illegible]	[illegible]	1236	1303	3.743	1745	2585	3.086	1653	2352	1.984	4.500	0	-0.015	37.7	81.9	88.6	87.3	[illegible]	101.6	[illegible]	106.2	[illegible]
[illegible]	[illegible]	[illegible]	1413	4.042	1734	2638	3.323	1695	2448	1.867	5.439	0	0.017	38.0	82.6	89.0	88.4	[illegible]	101.8	[illegible]	107.3	[illegible]
[illegible]	[illegible]	[illegible]	1677	4.055	1761	2661	3.399	1703	2475	1.587	4.282	0	0.026	38.2	[illegible]	89.9	88.7	[illegible]	[illegible]	[illegible]	107.9	102.9
[illegible]	[illegible]	[illegible]	1994	4.088	1743	2653	3.583	1680	2500	1.331	3.204	0	0.046	38.7	[illegible]	95.2	93.6	[illegible]	104.2	140	[illegible]	[illegible]
[illegible]	[illegible]	[illegible]	[illegible]	4.081	1727	2679	3.820	1667	2540	1.210	2.346	0	0.067	39.2	[illegible]	91.7	[illegible]	[illegible]	[illegible]	130	[illegible]	[illegible]

Table A-5. 54-Element Coplanar Mixer Nozzle Test Matrix (Continued).

Model No. 5
Config. 54-Element Coplanar Mixer
A_{FS} = 338 in.^{2} A_i = 11.30 in.^{2}, A_o = 23.49 in.^{2}

Point	Inner			Outer			Mass Averaged			V_o/V_i	W_o/W_i	V_{FS} ft/sec	Log F	10 Log_{10} $[F_s(T_o/T_{sm})^{\omega-1}]$	2400 ft Sideline							
															50°		90°		Peak			
	$(P_T/P_o)_i$	T_{Ti} °R	V_i ft/sec	$(P_T/P_o)_o$	T_{To} °R	V_o ft/sec	P_T/P_o	T_T °R	V ft/sec						OASPL	PNL	OASPL	PNL	OASPL	θ	PPNL	POASPL
3	1.191	572	578	1.978	945	1418	1.747	865	1237	2.453	3.649	143	-0.559	37.3	---	---	---	---	---	---	---	---
4	1.779	565	1015	2.089	1006	1515	1.965	852	1341	1.493	1.870	140	-0.594	38.3	64.7	70.1	68.9	76.0	77.3	140	80.1	78.9
6	1.570	1003	1208	1.608	1007	1240	1.596	1006	1230	1.027	2.185	140	0	36.8	61.5	66.8	65.0	72.4	68.9	120	74.2	72.7
10	1.562	1002	1201	2.463	1203	1815	2.180	1154	1666	1.511	3.130	143	-0.295	37.1	70.2	75.8	75.1	82.1	87.2	150	89.1	87.2
21	1.556	1001	1195	3.340	1678	2394	2.782	1485	2136	2.003	3.651	141	-0.070	37.5	80.2	86.6	83.1	91.2	98.4	150	102.0	98.4
25	3.102	841	1671	3.625	1709	2531	3.345	1389	2214	1.515	1.714	140	0.016	39.3	87.0	93.3	88.9	96.3	102.1	140	106.7	102.6
28	1.497	915	1094	3.747	1738	2580	3.046	1572	2281	2.358	3.975	140	-0.022	37.9	81.5	88.3	85.1	92.3	100.4	140	105.1	100.4
30	1.512	1457	1400	4.051	1740	2643	3.323	1696	2448	1.888	5.383	138	0.017	38.0	83.5	90.1	86.6	94.5	102.5	140	107.4	102.5
1	1.783	550	1003	1.452	736	945	1.556	659	969	0.942	1.409	285	0	36.9	61.3	66.4	60.0	69.8	60.0	90	69.8	60.9
2	1.781	551	1003	1.810	857	1267	1.789	745	1170	1.263	1.732	281	0	38.0	61.0	66.9	62.3	71.5	65.3	120	72.5	68.7
3	1.192	563	575	1.972	944	1414	1.742	861	1233	2.459	3.600	282	-0.577	37.3	61.3	67.0	63.6	72.6	67.5	120	74.8	71.2
4	1.772	563	1010	2.103	1003	1519	1.973	851	1343	1.504	1.890	283	-0.574	38.4	63.8	69.7	66.7	75.2	72.4	130	77.3	75.6
5	1.574	1006	1213	2.114	996	1518	1.943	999	1441	1.251	2.942	282	-0.661	37.5	64.9	70.9	68.0	76.1	73.7	130	78.5	77.1
6	1.566	1003	1205	1.600	995	1226	1.589	998	1219	1.017	2.190	284	0	36.8	61.1	66.8	63.0	71.7	66.4	120	72.4	69.9
7	1.637	1080	1307	2.239	1080	1635	2.049	1080	1552	1.251	2.948	282	-0.421	37.3	66.7	72.6	70.2	78.0	78.5	140	81.3	80.2
8	1.698	1163	1403	2.391	1167	1761	2.173	1166	1672	1.255	2.007	282	-0.299	37.1	68.5	74.5	72.1	79.7	79.5	130	84.6	83.0
9	1.539	1218	1304	1.560	1237	1334	1.553	1231	1325	1.023	2.146	282	-0.342	35.8	62.2	67.1	64.5	72.6	68.6	120	74.2	72.1
10	1.563	999	1200	2.456	1213	1820	2.175	1161	1669	1.517	3.100	283	-0.298	37.1	68.7	74.7	72.4	79.8	81.7	140	84.9	83.7
11	1.443	906	1041	2.453	1213	1819	2.138	1142	1638	1.747	3.305	277	-0.327	37.1	70.3	75.7	72.3	80.1	82.3	140	85.4	83.8
12	2.334	808	1445	1.970	1385	1717	2.061	1140	1602	1.188	1.355	278	-0.401	37.1	70.8	76.3	72.3	79.7	79.9	130	84.4	82.5
13	1.768	597	1036	2.723	1357	2021	2.359	1116	1710	1.947	2.156	283	-0.201	38.0	71.4	78.4	75.0	83.5	84.2	140	87.5	86.2
14	1.451	910	1050	2.718	1350	2014	2.321	1251	1797	1.918	3.443	277	-0.213	36.9	73.2	79.1	75.5	83.5	86.1	140	89.4	88.1
15	1.526	1223	1295	2.677	1284	1950	2.323	1271	1813	1.506	3.763	278	-0.212	36.8	72.7	79.4	76.0	83.9	88.6	150	90.6	88.6
16	1.507	1459	1396	1.544	1458	1434	1.532	1458	1422	1.027	2.197	277	0	34.6	66.9	71.5	66.9	74.5	71.7	120	77.0	75.9
17	1.517	1446	1400	2.873	1414	2111	2.461	1420	1975	1.508	4.221	278	-0.155	36.7	74.1	80.7	77.8	85.7	91.8	150	93.8	91.8
18	2.476	785	1467	2.150	1507	1894	2.210	1195	1710	1.291	1.315	277	-0.273	37.1	70.9	76.7	74.3	81.7	84.2	140	87.3	85.7
19*	1.961	787	1287	2.336	1598	2043	2.170	1303	1768	1.588	1.751	277	-0.295	36.5	---	---	---	---	---	---	---	---
20	1.988	855	1353	2.059	1615	1923	2.002	1331	1701	1.421	1.568	278	-0.468	35.9	70.1	75.1	73.4	80.6	83.7	140	86.4	85.1
21	1.544	1003	1187	3.323	1621	2397	2.782	1489	2139	2.019	3.690	276	-0.070	37.4	79.9	86.8	81.5	89.9	97.2	150	100.0	97.2
22	1.427	933	1041	3.324	1627	2397	2.740	1487	2124	2.303	3.968	276	-0.079	37.3	78.5	85.5	81.3	89.8	96.7	150	99.7	96.7
23	2.490	846	1527	2.424	1750	2181	2.378	1376	1910	1.428	1.415	278	-0.185	36.8	75.1	80.6	77.7	85.1	91.2	150	93.2	91.2
24	2.653	839	1566	2.630	1754	2270	2.558	1378	1981	1.450	1.433	276	-0.126	37.4	75.6	82.4	79.2	87.3	93.1	150	95.9	93.1
25	3.102	839	1669	3.632	1707	2531	3.349	1388	2214	1.517	1.717	277	0.017	39.4	87.5	94.3	88.5	96.2	100.5	140	104.8	101.3

Table A-5. 54-Element Coplanar Mixer Nozzle Test Matrix (Continued).

[illegible]
[illegible] 54-Element Coplanar Mixer
[illegible] A_j = 23.49 in.²

Point	Outer P/P	Outer T °R	Outer V_j ft/sec	Inner P/P	Inner T °R	Inner V_j ft/sec	Mass Averaged P/P	Mass Averaged T	Mass Averaged V ft/sec	[illegible]	[illegible]	V_{FS} ft/sec	ω	$10 \log_{10} [F_S(T_0/T_{sm})^{\omega-1}]$	2400 ft Sideline 50° OASPL	50° PNL	90° OASPL	90° PNL	Peak OASPL	Peak θ	Peak PPNL	POASPL
[illegible]	[illegible]	[illegible]	[illegible]	[illegible]	[illegible]	[illegible]	[illegible]	[illegible]	[illegible]	[illegible]	[illegible]		[illegible]	38.7	80.1	86.8	84.5	92.4	98.3	140	102.4	98.3
[illegible]	[illegible]	[illegible]	[illegible]	[illegible]	[illegible]	[illegible]	[illegible]	[illegible]	[illegible]	[illegible]	[illegible]		[illegible]	38.6	80.0	86.5	84.1	92.0	98.2	140	102.4	98.2
[illegible]	[illegible]	[illegible]	[illegible]	[illegible]	[illegible]	[illegible]	[illegible]	[illegible]	[illegible]	[illegible]	[illegible]	[illegible]	[illegible]	38.4	80.2	86.9	84.2	92.4	98.0	140	102.2	98.0
[illegible]	[illegible]	[illegible]	[illegible]	[illegible]	[illegible]	[illegible]	[illegible]	[illegible]	[illegible]	[illegible]	[illegible]	[illegible]	[illegible]	38.2	81.2	87.6	85.2	92.6	99.3	140	103.8	99.3
[illegible]	[illegible]	[illegible]	[illegible]	[illegible]	[illegible]	[illegible]	[illegible]	[illegible]	[illegible]	[illegible]	[illegible]		[illegible]	37.9	79.1	85.5	84.1	92.1	98.0	140	102.3	98.0
[illegible]	[illegible]	[illegible]	[illegible]	[illegible]	[illegible]	[illegible]	[illegible]	[illegible]	[illegible]	[illegible]	[illegible]	[illegible]	[illegible]	37.3	78.8	85.2	84.4	92.6	97.3	140	101.6	97.3
[illegible]	[illegible]	[illegible]	[illegible]	[illegible]	[illegible]	[illegible]	[illegible]	[illegible]	[illegible]	[illegible]	[illegible]		-0.095	37.3	78.5	84.8	83.7	92.1	97.2	140	101.5	97.2
[illegible]	[illegible]	[illegible]	[illegible]	[illegible]	[illegible]	[illegible]	[illegible]	[illegible]	[illegible]	[illegible]	[illegible]	[illegible]	[illegible]	37.1	79.1	85.8	83.8	92.3	96.8	140	101.1	96.8
[illegible]	[illegible]	[illegible]	[illegible]	[illegible]	[illegible]	[illegible]	[illegible]	[illegible]	2163	[illegible]	[illegible]	[illegible]	[illegible]	36.9	78.3	86.1	83.9	92.4	96.2	150	99.7	96.2
[illegible]	[illegible]	[illegible]	[illegible]	[illegible]	[illegible]	[illegible]	[illegible]	[illegible]	[illegible]	[illegible]	[illegible]		[illegible]	38.1	67.7	73.3	73.4	80.1	82.7	140	85.3	83.7
[illegible]	[illegible]	[illegible]	[illegible]	[illegible]	[illegible]	[illegible]	[illegible]	[illegible]	[illegible]	[illegible]	[illegible]		-0.190	37.9	67.3	73.0	73.5	80.2	82.4	140	85.1	83.0
[illegible]	[illegible]	[illegible]	[illegible]	[illegible]	[illegible]	[illegible]	[illegible]	[illegible]	[illegible]	[illegible]	[illegible]	[illegible]	[illegible]	37.4	66.8	72.4	73.2	80.0	78.6	120	84.6	82.2
[illegible]	[illegible]	[illegible]	[illegible]	[illegible]	[illegible]	[illegible]	[illegible]	[illegible]	[illegible]	[illegible]	[illegible]	[illegible]	[illegible]	37.1	67.0	72.8	73.1	79.9	81.8	140	85.9	81.6
[illegible]	---	---	---	2.261	[illegible]	[illegible]	[illegible]	[illegible]	[illegible]	---	---	0	-0.248	36.2	67.5	73.7	73.9	81.6	80.3	130	85.1	81.7
[illegible]	[illegible]	[illegible]	[illegible]	[illegible]	[illegible]	1981	[illegible]	[illegible]	[illegible]	[illegible]	[illegible]	[illegible]	[illegible]	37.6	72.9	78.9	78.0	85.1	90.3	150	92.4	90.3
[illegible]	[illegible]	[illegible]	[illegible]	[illegible]	[illegible]	[illegible]	[illegible]	[illegible]	[illegible]	[illegible]	[illegible]	0	-0.267	37.5	71.8	78.0	78.[illegible]	85.3	88.3	140	91.3	89.1
[illegible]	[illegible]	[illegible]	[illegible]	[illegible]	[illegible]	1962	[illegible]	[illegible]	[illegible]	[illegible]	[illegible]	0	-0.263	37.0	70.5	76.8	77.7	84.8	87.2	140	90.5	88.3
[illegible]	[illegible]	[illegible]	[illegible]	[illegible]	1306	1963	[illegible]	[illegible]	[illegible]	[illegible]	[illegible]	0	-0.237	36.6	70.7	77.1	[illegible]	84.8	87.7	140	91.2	87.9
[illegible]	[illegible]	[illegible]	[illegible]	[illegible]	1314	1968	[illegible]	[illegible]	[illegible]	[illegible]	[illegible]	0	-0.226	36.4	71.0	[illegible]	78.5	86.1	88.0	150	90.[illegible]	88.0
[illegible]	---	---	---	[illegible]	[illegible]	[illegible]	[illegible]	[illegible]	1967	---	---	0	-0.096	36.1	71.4	78.0	78.7	86.5	87.5	140	91.1	87.9

Table A-5. 54-Element Coplanar Mixer Nozzle Test Matrix (Concluded).

Model No. 5
Config. 54-Element Coplanar Mixer
A_{FS} = 336 in.^{2} A_i = 11.30 in.^{2}, A_o = 23.496 in.^{2}

Point	Inner $(P_T/P_o)_i$	Inner T_{T_i} °R	Inner V_i ft/sec	Outer $(P_T/P_o)_o$	Outer T_{T_o} °R	Outer V_o ft/sec	Mass Averaged P_T/P_o	Mass Averaged T_T °R	Mass Averaged V ft/sec	V_o/V_i	W_o/W_i	V_{FS} ft/sec	Log R	10 Log_{10} $[F_s(T_o/T_{sm})^{\omega-1}]$	2400 ft Sideline 50° OASPL	50° PNL	90° OASPL	90° PNL	Peak OASPL	Peak θ	Peak PPNL	POASPL
26	[illegible]	[illegible]	[illegible]	[illegible]	[illegible]	[illegible]	2.857	1428	2100	1.612	1.825	279	-0.056	38.1	79.5	86.1	81.7	89.6	97.5	150	101.0	97.5
27	[illegible]	914	[illegible]	[illegible]	1733	2302	2.329	1528	1994	2.151	3.003	278	-0.201	36.0	74.2	79.8	77.9	85.4	92.2	150	94.6	92.2
28	[illegible]	907	[illegible]	[illegible]	[illegible]	[illegible]	3.049	1586	2292	2.383	3.938	278	-0.021	37.8	81.0	87.9	81.3	91.2	99.6	150	103.1	99.6
29	[illegible]	[illegible]	[illegible]	[illegible]	[illegible]	2593	3.091	1658	2358	2.004	4.518	281	-0.014	37.7	81.6	88.1	83.3	81.2	99.0	140	103.7	99.9
30	[illegible]	[illegible]	[illegible]	[illegible]	1738	2640	3.317	1695	2446	1.890	5.408	279	0.016	38.0	82.9	89.7	84.6	92.4	100.7	140	105.2	101.1
31	[illegible]	612	[illegible]	[illegible]	1623	[illegible]	2.844	1272	1991	1.930	1.877	282	-0.061	38.7	80.0	86.3	80.8	88.9	96.1	150	99.3	96.1
32	[illegible]	[illegible]	[illegible]	[illegible]	[illegible]	[illegible]	2.845	1284	2001	1.977	1.970	282	-0.061	38.6	80.0	86.3	80.9	89.0	96.1	150	99.2	96.1
33	[illegible]	[illegible]	[illegible]	[illegible]	[illegible]	[illegible]	2.812	1306	2009	2.081	2.164	282	-0.067	38.4	80.1	86.6	81.1	89.2	96.1	150	99.3	96.1
34	[illegible]	[illegible]	[illegible]	[illegible]	[illegible]	[illegible]	2.767	1333	2016	2.241	2.427	282	-0.076	38.2	79.9	86.3	80.5	88.5	96.1	150	99.5	96.1
35	[illegible]	619	[illegible]	[illegible]	[illegible]	[illegible]	2.723	1363	2025	2.486	2.751	282	-0.085	37.9	79.6	85.7	80.6	88.5	95.8	150	99.5	95.8
[illegible]	[illegible]	[illegible]	[illegible]	[illegible]	[illegible]	[illegible]	[illegible]	865	1237	2.453	3.649	370	-0.559	37.3	61.7	67.4	62.5	71.7	65.4	120	73.4	72.0
[illegible]	[illegible]	[illegible]	[illegible]	[illegible]	[illegible]	[illegible]	[illegible]	952	1341	1.493	1.870	369	-0.594	38.3	64.2	70.2	65.4	74.1	68.9	120	76.0	74.4
6	[illegible]	[illegible]	[illegible]	[illegible]	[illegible]	[illegible]	[illegible]	995	1221	1.081	2.201	368	0	36.8	61.2	66.8	61.5	70.8	63.0	120	69.4	69.3
10	[illegible]	964	[illegible]	[illegible]	[illegible]	[illegible]	[illegible]	1133	1646	1.505	3.035	365	-0.302	37.3	68.6	74.8	71.5	79.5	80.8	140	83.6	81.7
12	[illegible]	[illegible]	[illegible]	[illegible]	[illegible]	[illegible]	[illegible]	1136	1597	1.196	1.352	366	-0.407	37.1	70.0	77.1	70.6	78.3	78.5	130	83.2	80.5
[illegible]	[illegible]	[illegible]	[illegible]	[illegible]	[illegible]	[illegible]	[illegible]	1191	1707	1.298	1.299	367	-0.272	37.2	73.9	79.5	73.5	81.1	80.7	130	86.0	83.6
[illegible]	[illegible]	[illegible]	[illegible]	[illegible]	[illegible]	[illegible]	[illegible]	[illegible]	1767	1.583	1.744	367	-0.295	36.5	74.8	80.1	74.2	81.8	84.3	140	87.5	85.7
[illegible]	[illegible]	[illegible]	[illegible]	[illegible]	[illegible]	[illegible]	[illegible]	1318	1696	1.411	1.588	367	-0.458	36.0	73.2	78.5	72.5	80.0	82.0	140	84.9	83.3
[illegible]	[illegible]	[illegible]	[illegible]	[illegible]	[illegible]	[illegible]	[illegible]	[illegible]	2138	1.998	1.651	367	-0.072	37.4	80.5	86.8	80.7	89.5	95.1	150	98.0	95.1
[illegible]	[illegible]	[illegible]	[illegible]	[illegible]	[illegible]	[illegible]	[illegible]	[illegible]	1907	1.424	1.430	368	-0.182	36.9	75.5	81.3	76.9	84.6	89.1	150	90.8	89.1
[illegible]	[illegible]	[illegible]	[illegible]	[illegible]	[illegible]	[illegible]	[illegible]	[illegible]	1977	1.448	1.436	367	-0.125	37.4	77.6	83.7	78.5	86.9	90.9	150	93.0	90.9
[illegible]	[illegible]	[illegible]	[illegible]	[illegible]	[illegible]	[illegible]	[illegible]	[illegible]	2219	1.518	1.715	369	0.016	39.3	89.2	95.9	88.0	95.3	100.2	140	104.8	100.6
[illegible]	[illegible]	[illegible]	[illegible]	[illegible]	[illegible]	[illegible]	[illegible]	[illegible]	2132	1.516	1.883	368	-0.051	38.1	81.3	87.8	81.6	90.0	95.9	150	98.8	95.9
[illegible]	[illegible]	[illegible]	[illegible]	[illegible]	[illegible]	[illegible]	[illegible]	1583	2291	[illegible]	3.978	369	-0.021	37.9	81.1	87.8	82.9	91.2	97.0	140	101.7	97.4
[illegible]	[illegible]	[illegible]	[illegible]	[illegible]	[illegible]	[illegible]	[illegible]	1698	[illegible]	[illegible]	5.366	367	0.017	38.0	83.2	89.8	84.8	93.0	99.2	140	103.9	99.2

APPENDIX B

THE FLIGHT TRANSFORMATION PROGRAM

This computer program, developed by General Electric under Task 4 of the High Velocity Jet Noise Reduction program, transforms one-third octave band sound pressure levels measured in a free jet facility to those in flight. This appendix outlines the input instructions for using the program, a sample case and listing of the program. A narrative accompanies the listing to explain the major elements of the program.

DESCRIPTION OF FLTRANS INPUT

The input to the program required for computation is as follows:

SPIN, SPIDIN, SPOT and SPIDOT are used for identification of the input and output SPL arrays. A maximum of five integers must be used for defining SPIN and SPOT whereas any 12 alpha numeric description may be used for SPIDIN and SPIDOT.

IREFRC - Refraction correction option. IREFRC must be set to one of the following:

IREFRC = 3HYES - the flight transformed array will include the refraction correction.

IREFRC = 2HNO - the flight transformed array will not include the refraction correction.

IREFRC is initialized to 3HYES, as it is the recommended procedure.

ITURBC - Turbulence absorption correction option. ITURBC must be set to one of the following:

ITURBC = 3HYES - the flight transformed array will include the turbulence absorption correction.

ITURBC = 2HNO - the flight transformed array will not include the turbulence absorption correction.

ITURBC is initialized to 3HYES, as it is the recommended procedure.

IALPHA - The atmospheric attentuation option allows the application of air attenuation to the transformed array at the doppler shifted frequency. Two air attenuation models are available. IALPHA must be set to one of the following:

IALPHA = 3HSAE - This allows use of the extrapolated ARP 866A atmospheric attenuation corrections (Reference 13).

IALPHA = 3HSB - This allows use of the Shields and Bass atmospheric attenuation (Reference 19).

DIAMJT - Diameter of the free jet in inches. The diameter of the free jet used in the current study was 48 inches.

FLTVEL - The velocity of the free jet in ft/sec.

If FLTVEL in input as zero the corresponding SPL array will not be flight transformed. It will, however, be printed as a flight tranformed array. This option was developed to enhance the integration of static and free jet data.

TESTD - Input data arc distance in feet. TESTD is used in conjunction with IALPHA to determine air attenuation corrections. The program must have the input data on an arc. Sideline data can only be used if corrected to an arc.

SCFACT - Is the linear scale factor, which is defined as full scale nozzle diameter divided by the scale model diameter, used to obtain the measured scale model frequencies if the free jet data has been scaled before transformation. The data must always be scaled down to model size before the refraction and turbulence absorption corrections are applied.

IDOPS - Doppler shift option. IDOPS must be set to one of the following:

IDOPS = 3HYES - The flight transformed array will be Doppler shifted.

IDOPS = 2HNO - The flight transformed array will not be Doppler shifted.

IDOPS is initialized to 3HYES.

ANGLE - An array of angles, measured from the inlet, at which the input SPL's were measured. These angles must be multiples of ten. A maximum of 19 angles may be input. The angles must be in degrees.

NANG - Number of angles in the ANGLE array.

NFREQ - Number of frequencies in the input SPL array. Maximum value is 33 (50 Hz → 80 kHz).

TSPL - Is the input SPL array to be transformed. This array is dimensioned to be (19, 33), (Angle, Frequency). See Table B-1 for a sample input sheet.

TABLE B-1. SAMPLE INPUT SHEET

```
$INPUT
SPIN=____,____,____,____,____,
SPIDIN=12H______________________
SPOT=____,____,____,____,____,
SPIDOT=12H______________________
IREFRC=3HYES,
ITURBC=3HYES,
IALPHA=3HSAE,
IDOPS=3HYES,
DIAMJT=________,
TESTD=________,
FLTVEL=________,
SCFACT=________,
NFREQ=______,
NANG/ANGLE=______,______,______,______,______,______,______,______,______,
______,______,______,______,______,______,______,______,______,______,
TSPL(01,01)=______,______,______,______,______,______,______,______,______,
______,______,______,______,______,______,______,______,______,______,
TSPL(01,02)=______,______,______,______,______,______,______,______,______,
______,______,______,______,______,______,______,______,______,______,
  .
  .
  .
TSPL(01,33)=______,______,______,______,______,______,______,______,______,
______,______,______,______,______,______,______,______,______,______,
$
```

Sample Case

INPUT

```
2000 $INPUT
2010 SPIN=1,311,160,11,0,SPIDIN=12HT5SF32CAR2NB
2020 SPOT=1,311,160,11,0,SPIDOT=12HT5SF32CAR2PK
2072 IREFRC=3HYES,
2074 ITURBC=3HYES,
2076 IALPHA=3HSAE,
2080 DIAMJT=48.0,
2082 TESTD=160,
2090 FLTVEL=279,
2100 SCFACT=3.58,
2110 NFREQ=27,
2120 NANG/ANGLE=40,50,60,70,80,90,100,110,120,130,140,150,160,
2200 TSPL(01,01)= 84.48, 84.96, 85.30, 87.35, 88.49, 88.77, 90.68,
2210 TSPL(01,02)= 82.04, 84.45, 86.86, 88.16, 87.75, 89.37, 92.25,
2220 TSPL(01,03)= 83.14, 84.30, 85.46, 88.01, 88.84, 91.22, 92.60,
2230 TSPL(01,04)= 83.67, 85.46, 87.25, 88.04, 88.38, 89.74, 92.13,
2240 TSPL(01,05)= 84.25, 86.04, 87.83, 89.12, 89.21, 90.33, 92.71,
2250 TSPL(01,06)= 84.10, 86.01, 87.93, 89.22, 90.56, 91.68, 93.56,
2260 TSPL(01,07)= 85.87, 86.66, 87.45, 89.99, 91.08, 91.95, 95.08,
2270 TSPL(01,08)= 87.95, 88.49, 89.03, 90.82, 91.91, 93.02, 94.91,
2280 TSPL(01,09)= 87.78, 89.08, 90.37, 92.66, 94.25, 95.61, 96.75,
2290 TSPL(01,10)= 87.89, 89.31, 90.73, 92.02, 93.60, 94.47, 96.75,
2300 TSPL(01,11)= 88.44, 89.61, 90.78, 93.32, 93.40, 94.37, 96.55,
2310 TSPL(01,12)= 89.81, 91.23, 92.66, 93.94, 94.77, 95.49, 96.42,
2320 TSPL(01,13)= 90.30, 91.60, 92.91, 94.43, 95.77, 96.73, 97.67,
2330 TSPL(01,14)= 90.62, 91.43, 92.24, 94.51, 96.09, 97.06, 97.74,
2340 TSPL(01,15)= 91.50, 92.18, 92.87, 95.39, 96.82, 98.18, 99.12,
2350 TSPL(01,16)= 91.63, 92.70, 93.76, 95.28, 97.20, 98.32, 99.50,
2360 TSPL(01,17)= 93.39, 93.79, 94.20, 95.95, 96.87, 98.98,100.92,
2370 TSPL(01,18)= 95.96, 95.68, 95.39, 96.28, 98.45,100.56,102.25,
2380 TSPL(01,19)=100.14, 99.52, 98.90, 97.28, 97.68, 98.44,100.73,
2390 TSPL(01,20)=101.06,101.48,101.89,101.49, 99.63, 98.03, 99.93,
2400 TSPL(01,21)= 98.38, 99.91,101.44,102.35,100.12, 97.96, 99.82,
2410 TSPL(01,22)= 96.97, 97.87, 98.76,100.76,102.54,101.88,100.79,
2420 TSPL(01,23)= 96.38, 97.35, 98.31, 99.57,101.65,101.18, 99.95,
2430 TSPL(01,24)= 93.50, 94.72, 95.94, 97.90, 98.71, 98.55, 97.96,
[illegible] TSPL(01,25)= 87.82, 89.61, 91.40, 94.15, 94.35, 94.36, 95.10,
[illegible] TSPL(01,26)= 83.43, 85.38, 87.34, 90.47, 90.54, 90.20, 92.49,
[illegible] TSPL(01,27)= 81.24, 83.55, 85.87, 90.75, 88.60, 89.47, 89.10,
[illegible] TSPL(02,01)= 92.36, 96.48, 97.36,102.28,108.22,110.13,
[illegible] TSPL(02,02)= 94.41, 96.62,101.43,107.57,111.51,111.92,
[illegible] TSPL(02,03)= 94.01, 96.97,104.04,108.42,112.86,112.52,
[illegible] TSPL(02,04)= [illegible], 98.75,105.32,110.95,114.64,112.05,
[illegible] TSPL(02,05)= 94.87, 99.58,106.15,112.28,114.47,110.63,
[illegible] TSPL(02,06)= 94.97,100.18,106.25,113.13,114.31,109.97,
[illegible] TSPL(02,07)= [illegible],100.45,106.53,111.90,113.08,106.99,
[illegible] TSPL(02,08)= 97.32,101.28,105.86,110.48,111.91,104.57,
[illegible] TSPL(02,09)= [illegible],101.02,105.10,108.57,109.00,100.41,
[illegible] TSPL(02,10)= [illegible],102.39,104.21,106.54,105.26, 95.77,
[illegible] TSPL(02,11)= 98.82,102.19,104.02,105.34,101.31, 93.56,
[illegible] TSPL(02,12)= [illegible],103.31,103.89,103.71, 98.67, 90.68,
[illegible] TSPL(02,13)= [illegible],101.46,102.40,102.46, 95.92, 88.92,
[illegible] TSPL(02,14)= [illegible],102.39,101.49,100.03, 94.24, 86.74,
[illegible] TSPL(02,15)=101.29,101.77,102.12,100.16, 93.87, 86.87,
[illegible] TSPL(02,16)=[illegible],102.67,103.53,100.71, 95.30, 88.00,
[illegible] TSPL(02,17)=[illegible],101.95,105.38,103.64, 98.12, 91.16,
[illegible] TSPL(02,18)=104.33,106.29,107.19,105.98,101.09, 93.73,
[illegible] TSPL(02,19)=104.08,[illegible],106.83,105.88,101.97, 94.70,
[illegible] TSPL(02,20)=[illegible],103.39,104.27,103.01,101.55, 94.52,
[illegible] TSPL(02,21)=[illegible],101.30,103.09,100.99, 99.73, 92.48,
[illegible] TSPL(02,22)=101.06,102.22,103.11,100.08, 99.74, 92.57,
[illegible] TSPL(02,23)= 98.77, 99.57,100.26, 98.90, 97.27, 89.31,
[illegible] TSPL(02,24)= [illegible], [illegible], 97.78, 95.66, 94.43, 86.41,
```

```
2740 TSPL(08,25)= 94.75, 96.00, 95.28, 90.18, 90.55, 80.60,
2750 TSPL(08,26)= 91.52, 94.65, 92.96, 85.93, 86.10, 79.01,
2760 TSPL(08,27)= 88.40, 93.13, 89.84, 84.85, 79.89, 77.59,
2780 S
```

*

[illegible]

INPUT SPECTRUM

T5SF32CAR2NB
1 311 160 11 0

ACOUSTIC ANGLE FROM INLET

FREQ	40.	50.	60.	70.	80.	90.	100.	110.	120.	130.	140.	150.	160.
50	84.43	84.96	85.30	87.35	88.49	88.77	90.68	92.36	96.08	97.36	102.22	108.22	110.13
63	[illegible]	84.85	84.96	88.16	87.75	89.31	92.25	94.41	96.62	101.43	107.57	111.51	111.22
80	[illegible]	84.30	86.46	88.01	88.84	91.22	92.60	94.01	96.97	104.04	108.42	112.86	112.52
100	83.61	85.46	87.26	88.04	88.38	89.74	92.13	93.79	98.75	105.32	110.95	114.64	112.05
125	84.96	86.04	87.83	89.12	89.21	90.33	92.71	94.87	99.58	106.15	112.28	114.47	110.63
160	84.10	86.01	87.93	89.22	90.56	91.68	93.56	94.97	100.13	106.25	113.13	114.21	108.97
200	86.47	86.66	87.45	89.99	91.08	91.95	95.08	96.49	100.45	106.53	111.90	113.08	106.99
250	87.26	88.47	89.93	90.82	91.91	93.02	94.91	97.32	101.28	105.86	110.48	111.91	104.57
315	87.74	89.03	90.37	92.65	94.25	95.61	96.75	98.66	102.02	105.10	108.57	109.00	100.41
400	87.85	89.31	90.73	92.02	93.60	94.47	96.75	98.02	102.39	104.21	106.54	105.26	95.77
500	88.44	89.61	90.78	93.32	93.40	94.37	96.55	98.82	102.19	104.02	105.34	101.31	93.56
630	89.81	91.23	92.00	93.94	94.77	95.49	96.42	98.19	100.31	103.39	103.71	98.67	90.62
800	90.30	91.50	92.91	94.43	95.77	96.73	97.67	99.93	101.06	102.40	102.46	95.92	89.92
1000	90.62	91.43	92.24	94.51	96.09	97.06	97.74	99.91	102.39	101.49	100.03	94.04	86.74
1250	91.50	92.18	92.87	95.39	96.82	98.18	99.12	101.29	101.77	102.12	100.16	93.97	86.87
1600	91.63	92.70	93.76	95.28	97.20	98.32	99.50	102.43	102.67	103.53	100.71	95.30	88.00
2000	93.39	93.79	94.20	95.95	96.87	98.95	100.92	103.60	104.95	105.38	103.64	98.12	91.16
2500	95.96	95.68	95.39	96.28	98.45	100.55	102.25	104.33	106.29	107.19	105.98	101.09	93.72
3150	100.14	99.52	98.90	97.28	97.68	98.44	100.73	104.08	105.15	106.83	105.98	101.97	94.72
4000	101.06	101.48	101.89	101.49	99.63	98.03	99.93	102.04	103.39	104.27	103.31	101.55	94.52
5000	98.38	99.91	101.44	102.35	100.12	97.95	99.82	100.35	101.30	103.09	100.92	99.73	92.48
6300	96.97	97.87	98.76	100.76	102.54	101.88	100.79	101.66	102.22	103.11	100.08	99.74	92.57
8000	96.33	97.35	98.31	99.57	101.65	101.18	99.95	98.77	99.57	100.26	98.90	97.27	89.31
10000	93.50	94.72	95.94	97.90	98.71	98.55	97.96	97.65	98.09	97.78	95.66	94.03	86.41
12500	87.82	89.61	91.40	94.15	94.35	94.36	95.10	94.75	96.00	95.28	90.18	90.55	80.60
16000	83.43	85.38	87.34	90.47	90.54	90.20	92.49	91.52	94.65	92.96	85.93	86.10	79.01
20000	81.24	83.55	85.87	90.05	88.60	89.47	89.10	88.40	93.13	89.84	84.55	79.00	77.50
25000	0.	0.	0.	0.	0.	0.	0.	0.	0.	0.	0.	0.	0.

FLTTRANS PROGRAM

FLIGHT TRANSFORMATION SPECTRUM

T5SF32CAR2PK

1 311 160 11 0

ACOUSTIC ANGLE FROM INLET

FREQ	40.	50.	60.	70.	80.	90.	100.	110.	120.	130.	140.	150.	160.
50	86.25	85.90	85.27	89.32	89.47	88.71	89.31	89.60	92.70	96.27	102.40	108.62	112.41
63	89.25	88.89	88.27	90.08	88.70	89.37	90.96	91.84	92.16	97.69	102.15	110.22	114.39
80	86.95	88.36	89.77	90.26	89.96	91.22	90.86	90.71	96.53	102.65	108.23	113.21	113.84
100	88.44	88.58	88.76	90.37	89.60	89.84	91.08	91.69	98.01	104.16	110.41	114.37	114.69
125	88.88	89.81	90.63	91.46	90.45	90.40	91.98	93.15	98.69	104.42	111.58	114.96	115.64
160	89.46	90.39	91.21	91.58	91.83	91.84	92.77	93.11	99.89	105.93	111.81	115.39	114.45
200	89.31	90.37	91.33	92.38	92.38	92.15	94.51	95.22	100.96	105.46	110.58	114.40	112.20
250	91.07	91.03	90.86	93.24	93.25	93.27	94.62	96.32	102.47	105.66	109.75	112.63	109.23
315	93.15	92.86	92.46	95.11	95.64	95.93	96.65	98.17	100.51	101.75	104.13	104.86	100.25
400	92.98	93.46	93.82	94.53	95.06	94.87	95.66	95.85	102.23	104.17	106.22	104.88	102.67
500	93.08	93.70	94.21	95.89	94.94	94.87	96.36	98.02	100.30	103.90	104.34	101.87	99.38
630	93.62	94.02	94.29	96.58	96.41	96.12	96.30	97.41	101.16	102.45	103.02	98.88	96.89
800	94.98	95.65	96.21	97.18	97.55	97.53	97.76	99.30	102.86	101.89	100.93	97.52	94.83
1000	95.47	96.05	96.52	97.38	98.03	98.05	98.20	99.67	102.58	102.85	101.38	97.22	95.03
1250	95.77	95.91	95.92	98.41	98.96	99.43	99.86	101.36	103.84	104.62	102.03	98.66	96.17
1600	96.63	96.63	96.63	98.51	99.62	99.92	100.59	102.84	106.47	106.49	104.92	101.45	99.30
2000	96.74	97.25	97.64	99.42	99.61	100.93	102.38	104.35	107.79	108.29	107.25	104.42	101.87
2500	98.46	98.38	98.19	100.05	101.59	103.06	104.16	105.34	106.80	108.13	107.43	105.72	103.61
3150	100.93	100.28	99.49	100.61	100.84	101.44	102.86	105.13	105.64	106.27	105.42	106.34	104.56
4000	103.59	102.84	102.05	104.81	102.79	101.03	102.31	103.48	103.53	105.07	103.38	104.52	102.56
5000	104.53	104.87	105.15	106.14	103.53	100.96	102.27	101.92	105.39	106.13	103.58	105.69	103.81
6300	102.04	103.58	104.93	104.33	106.08	104.88	103.35	103.59	103.31	103.94	103.12	103.98	101.33
8000	101.24	101.87	102.36	103.64	105.19	104.13	102.54	100.84	101.93	101.51	99.89	100.77	98.57
10000	100.28	100.97	101.54	101.97	102.25	101.55	100.43	99.51	99.71	98.61	93.67	96.08	90.94
12500	96.79	97.74	98.56	98.22	97.89	97.36	97.33	96.12	99.57	97.49	90.63	92.84	90.55
16000	89.88	91.40	92.79	94.54	94.08	93.20	94.71	92.88	96.84	92.65	87.44	84.08	86.07
20000	84.50	86.17	87.74	94.89	92.53	92.47	90.66	88.23	98.61	94.42	89.21	85.85	87.84
25000	82.39	84.09	85.66	94.89	92.53	92.47	90.66	88.23	89.70	85.51	80.30	76.93	78.92

MODEL/FULL SIZE SCALE FACTOR
INPUT 3.580
CALC. 3.200

FREE JET VELOCITY (FT/SEC) 279.00

FREE JET DIAMETER (IN) 48.00

REFRACTION CORRECTION - YES TURBULANCE CORRECTION - YES ALPHA OPTION - SAE

```
900 #RUN *= 154"5ES/NWBTASK5/FLTRANC(BCD,NOGO)
9"0C
10000C THIS COMPUTER PROGRAM, DEVELOPED BY GENERAL ELECTRIC UNDER
10010C THE HIGH VELOCITY JET NOISE REDUCTION PROGRAM, TRANSFORMS
10020C MEASURED ONE-THIRD OCTAVE BAND SOUND PRESSURE LEVELS
10030C OBTAINED USING A FREE JET FACILITY TO THOSE IN FLIGHT.
10040C
10050       COMMON /BLKCON/ ABSORP(33,2),DOPCON(6),FREQ(33),
10060      & IALPHA,IDOPS,IDSHFT(6),IFREQ(33),ISB,NBCDI,
10070      & NBCDO,RPD,SPDSND,TESTD
10080       COMMON /BLKFEI/ IREFRC,ITURBC,NO,PI
10090       COMMON /COMFEI/ DIAMJT,EM,FP,LIE,NP,SPL1(10),SPLF(10),
10100      & THETD(10)
10110C
10120       DIMENSION ANGLE(19),ANGOT(19),FPAR(33),SPIDIN(2),
10130      & SPIDOT(2),SPIN(5),SPOT(5),SPLDS(19,33),SPLFLT(19,33),
10140      & TSPL(19,33)
10150C
10160       INTEGER SPIN,SPOT
10170C
10180 1000 FORMAT (1H1/1X,"FLTTRANS PROGRAM",
10190      & 40X,"INPUT SPECTRUM",//)
10200 1010 FORMAT (58X,2A6/49X,5(1X,I5)//
10210      & 52X,"ACOUSTIC ANGLE FROM INLET"//3X,"FREQ",1X,17(F7.0))
10220 1020 FORMAT (1X,I6,1X,17(F7.2))
10230 1100 FORMAT (1H1/1X,"FLTTRANS PROGRAM",
10240      & 31X,"FLIGHT TRANSFORMATION SPECTRUM"//)
10250 1110 FORMAT (1H0,20X,"MODEL/FULL SIZE SCALE FACTOR",5X,
10260      & "FREE JET VELOCITY (FT/SEC)",5X,
10270      & "FREE JET DIAMETER (IN)"/
10280      & 27X,"INPUT",6X,"CALC.",19X,F8.2,23X,F6.2/26X,F6.3,5X,F6.3//
10290      & 23X,"REFRACTION CORRECTION - ",A3,5X,
10300      & "TURBULANCE CORRECTION - ",A3,5X,"ALPHA OPTION - ",A3)
10310 8000 FORMAT (1H0,"ERROR READING NAMELIST INPUT")
10320 8200 FORMAT (1H0,"TESTD IS ZERO - ",
10330      & "NEEDED TO DETERMINE AIR ATTENUATION")
10340C
10350       NAMELIST /INPUT/ ANGLE,DIAMJT,FLTVEL,IALPHA,IDOPS,
10360      & IREFRC,ITURBC,NANG,NFREQ,
10370      & SCFACT,SPIDIN,SPIDOT,SPIN,SPOT,SPDSND,
10380      & TESTD,TSPL
10390C
10400C INITILAIZATION
10410  100 DO 102 I=1,19
10420       ANGOT(I)=0.0
10430  102 CONTINUE
10440C
10450C READ NAMELIST INPUT
10460  110 READ (NBCDI,INPUT,END=900,ERR=800)
10470       IF (TESTD.LE.0.0) GO TO 820
10480       NANGOT=NANG
10490       DO 120 I=1,NANG
10500       ANGOT(I)=ANGLE(I)
10510  120 CONTINUE
10520       DIST=TESTD/1000.0
10530C
10540C SET AIR ATTENUATION INDICATOR FOR SAE OR SHIELDS AND BASS, IABS
10550       IABS=1
10560       IF (IALPHA.EQ.ISB) IABS=2
10570C
10580C PRINT INPUT SPECTRUM
10590  140 WRITE (NBCDO,1000)
10600       WRITE (NBCDO,1010) SPIDIN,SPIN,(ANGLE(I),I=1,NANG)
10610       DO 150 J=1,NFREQ
10620       WRITE (NBCDO,1020) IFREQ(J),(TSPL(I,J),I=1,NANG)
10630  150 CONTINUE
10640C
```

A

Section A

Lines 10050-10160

This section contains the COMMON, DIMENSION, EQUIVALENCE, and TYPE statements. It should be noted that the labeled COMMON blocks /BLKFEI/ and /COMFEI/ are used by subroutine FIHEL which is the flight transformation subroutine. The common statement allows input and intermediate variables calculated in a specific subroutine to be used in other subroutines. The dimension statements defines the sizes of the arrays which are being input or calculated. The type statement defines certain variables as integers.

B

Section B

Lines 10180-10330

This section contains all of the format statements within this program. Formats 1000, 1010, and 1020 are used to print the input SPL array. Formats 1100, 1010, 1020, and 1110 are used to print the flight transformed array and input options. Formats 8000, and 8200, state various error conditions which will cause the program to stop.

NAMELIST Statement Lines 10350-10380

The NAMELIST statement, with NAMELIST name /INPUT/, contains the list of parameters which may be input to the FLTTRANS Program. See Section 1.0 for definitions of these parameters.

C

Section C

Lines 10400-10630

This section reads the NAMELIST input, initializes parameters and arrays, and prints the input array.

```
10650C CALCULATE SCALE FACTOR (SCALE) FROM INPUT SCALE FACTOR (SCFACT)
10660  160 SCFREQ=FREQ(1)*SCFACT
10670      DO 162 J=1,NFREQ
10680      IF (SCFREQ.LT.FREQ(J)) GO TO 164
10690  162 CONTINUE
10700      CNFREQ=FREQ(NFREQ)
10710      GO TO 168
10720  164 IF (J.GT.1) GO TO 166
10730      CNFREQ=FREQ(1)
10740      GO TO 168
10750  166 DEL1=SCFREQ-FREQ(J-1)
10760      DEL2=FREQ(J)-SCFREQ
10770      CNFREQ=FREQ(J-1)
10780      IF (DEL1.GT.DEL2) CNFREQ=FREQ(J)
10790  168 SCALE=CNFREQ/FREQ(1)
10800C
10810C CALCULATE MACH NUMBER AND FREQUENCY PARAMETERS
10820  180 EM=FLTVEL/SPDSND
10830      CONST=(PI*DIAMJT*SCALE)/(12.0*SPDSND)
10840      DO 190 J=1,NFREQ
10850  190 FPAR(J)=FREQ(J)*CONST
10860C
10870C TEST FOR ZERO SPL VALUES
10880      DO 260 I=1,NANG
10890      DO 250 J=1,NFREQ
10900      IF (TSPL(I,J).GT..001) GO TO 250
10910      IF (J.GE.NFREQ) GO TO 220
10920      JJ1=J+1
10930      DO 210 JJ=JJ1,NFREQ
10940      IF (TSPL(I,JJ).GT..001) GO TO 230
10950  210 CONTINUE
10960      IF (J.LE.1) GO TO 260
10970  220 IF (TSPL(I,J-1).LE..001) GO TO 260
10980      TSPL(I,J)=TSPL(I,J-1)
10990      GO TO 250
11000  230 IF (J.GT.1) GO TO 240
11010      TSPL(I,J)=TSPL(I,JJ)
11020      GO TO 250
11030  240 DIV=JJ-J+1
11040      TSPL(I,J)=TSPL(I,J-1)+(TSPL(I,JJ)-TSPL(I,J-1))/DIV
11050  250 CONTINUE
11060  260 CONTINUE
11070C
11080C TEST FOR MISSING ANGLES
11090      I=1
11100  265 IF (ANGOT(I+1)-ANGOT(I).LE.10.5) GO TO 285
11110      IA=NANGOT
11120      DO 275 IKNT=I+1,NANGOT
11130      ANGOT(IA+1)=ANGOT(IA)
11140      DO 270 J=1,NFREQ
11150      TSPL(IA+1,J)=TSPL(IA,J)
11160  270 CONTINUE
11170      IA=IA-1
11180  275 CONTINUE
11190      NANGOT=NANGOT+1
11200      ANGOT(I+1)=ANGOT(I)+10.0
11210      CONST=(ANGOT(I+2)-ANGOT(I+1))/(ANGOT(I+2)-ANGOT(I))
11220      DO 280 J=1,NFREQ
11230      TSPL(I+1,J)=TSPL(I+2,J)-CONST*(TSPL(I+2,J)-TSPL(I,J))
11240  280 CONTINUE
11250  285 I=I+1
11260      IF (I.LE.NANGOT-1) GO TO 265
11270C
11280C TEST FOR ZERO FLTVEL (NO TRANSFORMATION)
11290      IF (FLTVEL.GT..001) GO TO 300
11300      DO 290 J=1,NFREQ
11310      DO 290 I=1,NANGOT
11320      SPLDS(I,J)=TSPL(I,J)
11330  290 CONTINUE
11340      GO TO 586
```

D

Section D

Lines 10650-11340

This section contains calculations for the scale factor, Mach number and frequency parameters and uses linear interpolation to determine the SPL's at frequencies where the input SPL's were zero.

Scale factor

The input scale factor must be adjusted to account for even third-octave outer band shifts.

This is accomplished as follows:

$$S_F = 50.0 \times S_I$$

where S_I is the input scale factor and 50.0 is the frequency of the first third octave frequency band. Determine the third octave frequency which is closest to S_F. Let this be F. Then

$$S = F/50.0$$

when S is the adjusted scale factor and 50.0 is again the frequency of the first third octave frequency band.

Mach number

$$M = V/C$$

where M is the Mach number, V is the flight velocity, and C is the speed of sound for a 59° standard day.

Frequency parameter/constant

$$P = (\pi \times D \times S)/(12.0 \times 1116.0)$$

where D is the diameter of the jet in inches and S is the adjusted scale factor.

Thus,

$$FP_j = P \times F_j$$

where FP_j is the frequency parameter corresponding to third octave frequency band j and F_j is the frequency for band j.

Zero SPL values

Whenever possible, linear interpolation is used to evaluate an input SPL of zero. Zero SPL levels may occur due to correcting the measured data for the background noise on the free jet. The interpolation is done between frequencies for the given angle rather than between angles. If the zero SPL is not between two nonzero SPL's it will be set to the nearest nonzero SPL value.

Missing angles

Input angles must be even multiples of ten. No extrapolation will be done to establish spectra at angles on either end of the array. Because of test conditions an array sometimes does have a missing angle. The data for an array is completed by using linear interpolation to fill in the missing angle. The interpolation is done between angles using the angles on either side of the missing angle.

```
11350C
11360C SET THETD ARRAY FOR REAR QUADRANT ANGLES
11370  300 IR=NANGOT
11380      I=1
11390  310 IF (ANGOT(IR) LT 89 0) GO TO 320
11400      THETD(I)=180 0-ANGOT(IR)
11410      IR=IR-1
11420      I=I+1
11430      GO TO 310
11440  320 NP=I-1
11450      NA=IR+1
11460C
11470C FLIGHT TRANSFORMATION FOR REAR QUADRANT, ALL FREQUENCIES
11480      LIE=1
11490      DO 390 J=1,NFREQ
11500      FP=FPAR(J)
11510      ADDER=ABSORP(J,IABS)*DIST
11520C
11530C SET SPL1 ARRAY FROM TSPL, TAKE OUT AIR ATTENUATION (LOSSLESS)
11540  340 II=NANGOT+1
11550      DO 350 I=1,NP
11560      II=II-1
11570      SPL1(I)=TSPL(II,J)+ADDER
11580  350 CONTINUE
11590C
11600C CALCULATE FLIGHT TRANSFORMATION
11610      CALL FEIHE
11620C
11630C STORE SPLF IN SPLFLT ARRAY
11640      K=NP+1
11650      DO 370 I=NA,NANGOT
11660      K=K-1
11670      SPLFLT(I,J)=SPLF(K)
11680  370 CONTINUE
11690C
11700  390 CONTINUE
11710C
11720C SET THETD ARRAY FOR FORWARD QUADRANT ANGLES
11730      IR=NA
11740      I=1
11750  400 THETD(I)=180.0-ANGOT(IR)
11760      IF (IR.LE.1) GO TO 410
11770      IR=IR-1
11780      I=I+1
11790      GO TO 400
11800  410 NP=I
11810      NA=I
11820C
11830C FLIGHT TRANSFORMATION FOR FORWARD QUADRANT, ALL FREQUENCIES
11840      LIE=2
11850      DO 490 J=1,NFREQ
11860      FP=FPAR(J)
11870      ADDER=ABSORP(J,IABS)*DIST
11880C
11890C SET SPL1 ARRAY FROM TSPL, TAKE OUT AIR ATTENUATION (LOSSLESS)
11900  440 II=NA+1
11910      DO 450 I=1,NP
11920      II=II-1
11930      SPL1(I)=TSPL(II,J)+ADDER
11940  450 CONTINUE
11950C
11960C CALCULATE FLIGHT TRANSFORMATION
11970      CALL FEIHE
11980C
11990C STORE SPLF IN SPLFLT ARRAY
12000      K=NP+1
12010      DO 470 I=1,NP
12020      K=K-1
12030      SPLFLT(I,J)=SPLF(K)
12040  470 CONTINUE
12050C
12060  490 CONTINUE
12070C
```

E

Section E

Lines 11360-12060

This section prepares data for the flight transformation subroutine, FEIHE. Aft quadrant data are transformed slightly different from forward quadrant data. LIE is the indicator that tells FEIHE the quadrant from which the data were taken. It is set to one for the aft quadrant or to two for the forward quadrant.

Data for the aft quadrant angles (90° through 160°) are transformed first. Then the process is repeated for the forward quadrant angles (20° through 90°). The input angles are measured from the inlet. FEIHE requires them to be measured from the exhaust. To convert from inlet to exhaust reference each input angle is subtracted from 180°. The angles are sent to the FEIHE subroutine in the THETD array with NP containing the number of angles in the array. The corresponding SPL values, taken from the input TSPL array, are stored in the SPL1 array. The input SPL's are converted to "lossless" by adding back either SAE or Shields and Bass atmospheric attenuation. FEIHE transforms data for one frequency band at a time. Therefore, it is necessary to repeat the process of filling the SPL1 array for each input frequency. FP is set to the frequency parameter corresponding to that input frequency.

FEIHE stores the transformed SPL's in the SPLF array. Upon return from FEIHE the SPLF array is stored in the SPLFLT array which will eventually contain all flight transformed sound pressure levels.

```
12080C DOPPLER SHIFT
12090  498 IF (IDOPS.NE.NO) GO TO 510
12100      DO 500 I=1,NANGOT
12110      DO 500 J=1,NFREQ
12120      SPLDS(I,J)=SPLFLT(I,J)
12130  500 CONTINUE
12140      GO TO 580
12150  510 DO 570 I=1,NANGOT
12160      DOPFAC=1.0/(1.0-EM*COS(ANGOT(I)*RPD))
12170      DO 520 K=1,6
12180      IF (DOPFAC.GE.DOPCON(K)) GO TO 520
12190      IFLAG=IDSHFT(K)
12200      GO TO 530
12210  520 CONTINUE
12220      IFLAG=-3
12230  530 DO 570 J=1,NFREQ
12240      JJ=J+IFLAG
12250      IF (JJ.GE.1) GO TO 540
12260      SPLDS(I,J)=SPLFLT(I,1)-3.0*FLOAT(1-JJ)
12270      GO TO 550
12280  540 IF (JJ.LE.NFREQ) GO TO 560
12290      SPLDS(I,J)=SPLFLT(I,NFREQ)-3.0*FLOAT(JJ-NFREQ)
12300  550 IF (SPLDS(I,J).GT..001) GO TO 570
12310      SPLDS(I,J)=0.0
12320      GO TO 570
12330  560 SPLDS(I,J)=SPLFLT(I,JJ)
12340  570 CONTINUE
12350C
12360C PUT AIR ATTENUATION BACK IN
12370  580 DO 584 J=1,NFREQ
12380      ADDER=ABSORP(J,IABS)*DIST
12390      DO 584 I=1,NANGOT
12400      SPLDS(I,J)=SPLDS(I,J)-ADDER
12410  584 CONTINUE
12420C
12430C PRINT FLIGHT TRANSFORMED SPECTRUM, SPLDS
12440  586 WRITE (NBCDO,1100)
12450      WRITE (NBCDO,1010) SPIDOT,SPOT,(ANGOT(I),I=1,NANGOT)
12460      DO 590 J=1,NFREQ
12470      WRITE (NBCDO,1020) IFREQ(J),(SPLDS(I,J),I=1,NANGOT)
12480  590 CONTINUE
12490      WRITE (NBCDO,1110) FLTVEL,DIAMJT,SCFACT,SCALE,IREFRC,ITURBC,IALPHA
12500C
12510      GO TO 100
12520C
12530C ERROR RETURNS
12540  800 WRITE (NBCDO,8000)
12550      GO TO 900
12560  820 WRITE (NBCDO,8200)
12570      GO TO 900
12580C
12590  900 STOP
12600      END
20000C
20010C
20020C BLOCK DATA SUBROUTINE FOR FLTTRANS
20030C
20040      BLOCK DATA
20050C
20060      COMMON /BLKCON/ ABSORP(33,2),DOPCON(6),FREQ(33),
20070     & IALPHA,IDOPS,IDSHFT(6),IFREQ(33),ISB,NBCDI,
20080     & NBCDO,RPD,SPDSND,TESTD
20090      COMMON /BLKFEI/ IREFRC,ITURBC,NO,PI
```

F

Section F

Lines 12080-12510

The flight transformed array, stored in the SPLFLT array, may be Doppler shifted. The Doppler factor is calculated as:

$$D = 1.0/(1.0\text{-}M \times \cos A_i)$$

where M is the Mach number and A_i is the ith input angle.

The Doppler factor is compared with values tabulated in the DOPCON table. This then determines the Doppler shift which is tabulated in the corresponding IDSHFT table. These tables follow:

DOPCON	IDSHFT	
0.56	3	$D < 0.56$
0.71	2	$0.56 \le D < 0.71$
0.89	1	$0.71 \le D < 0.89$
1.12	0	$0.89 \le D < 1.12$
1.41	-1	$1.12 \le D < 1.41$
1.78	-2	$1.41 \le D < 1.78$
	-3	$1.78 \le D$

The Doppler shifted array is stored in the SPLDS array. Since the flight transformed array is "lossless" the standard day air attenuation are subtracted.

The flight transformed array is then printed out.

Control is returned to Section C to prepare to transform another array.

Error Returns - Lines 12530-12570

When an error is encountered in the program a comment is printed and the program terminates. The formats used for printing these statements may be found in Section B.

```
20100C
20110      DATA NBCDI  /05/
20120      DATA NBCDO  /06/
20130C
20140      DATA IALPHA /3HSAE/
20150      DATA IDOPS  /3HYES/
20160      DATA IREFRC /3HYES/
20170      DATA ISB    /2HSB/
20180      DATA ITURBC /3HYES/
20190      DATA NO     /2HNO/
20200C
20210      DATA DOPCON /0.56,0.71,0.89,1.12,1.41,1.78/
20220      DATA IDSHFT /3,2,1,0,-1,-2/
20230C
20240      DATA PI     /3.1415926/
20250      DATA RPD    /1.7453293E-2/
20260      DATA SPDSND /1116.0/
20270      DATA TESTD  /0.0/
20280C
20290C AIR ATTENUATION - SAE, 59 DEG.
20300      DATA (ABSORP(I,1),I=1,33) /
20310     & .071596, .090239, .114637, .143368, .179323, .229739,
20320     & .287470, .359806, .454133, .577982, .724422, .915994,
20330     & 1.16858, 1.46879, 1.84874, 2.38951, 3.03463, 3.97129,
20340     & 5.47439, 7.72822, 9.03521, 12.8734, 18.7629, 26.9699,
20350     & 38.9809, 58.6695, 84.5795, 121.555, 175.774, 256.393,
20360     & 363.185, 519.945, 752.157/
20370C
20380C AIR ATTENUATION - SHIELDS AND BASS, 59 DEG.
20390      DATA (ABSORP(I,2),I=1,33) /
20400     & .016864, .026557, .042256, .064760, .098255, .153155,
20410     & .223740, .317735, .440318, .590096, .745135, .917527,
20420     & 1.11392, 1.33211, 1.61641, 2.07011, 2.69266, 3.64337,
20430     & 5.17598, 7.68898, 11.3746, 17.3111, 26.9328, 40.7421,
20440     & 61.3409, 95.2370, 139.113, 198.203, 276.829, 376.470,
20450     & 485.966, 619.037, 789.283/
20460C
20470      DATA IFREQ /50,63,80,100,125,160,200,250,315,400,500,
20480     & 630,800,1000,1250,1600,2000,2500,3150,4000,5000,6300,
20490     & 8000,10000,12500,16000,20000,25000,31500,40000,50000,
20500     & 63000,80000/
20510      DATA FREQ /50.,63.,80.,100.,125.,160.,200.,250.,315.,
20520     & 400.,500.,630.,800.,1000.,1250.,1600.,2000.,2500.,3150.,
20530     & 4000.,5000.,6300.,8000.,10000.,12500.,16000.,20000.,
20540     & 25000.,31500.,40000.,50000.,63000.,80000./
20550C
20560      END
```

G

Section G

Lines 2011-2056

The DATA statements either initialize an input parameter, evaluate a constant, or evaluate a table. The following input parameters are initialized:

Input Parameter	Initialized to
NFREQ	0
TESTD	0.0
IALPHA	SAE
IDOPS	YES
IREFRC	YES
ITURBC	YES
SPDSND	1116.0

The following constants are assigned values

Constant	Set to	Definition
ISB	SB	IALPHA is tested against ISB to determine whether SAE or Shields and Bass (SB) air attenuation is requested
RPD	1.745329×10^{-2}	Radians per degree, used to convert angles from degrees to radians.
NBCDI	05	File code number for namelist input.
NBCDO	06	File code number for printed output.
NO	NO	Used to determine whether an option is set to YES or NO.
PI	3.1415926	π

The following tables are evaluated

Table	Definition
DOPCON	The Doppler factor is compared with this table to determine the Doppler shift
IDSHFT	This table corresponds to DOPCON and contains the number of frequency bands to Doppler shift the spectrum.
ABSORP(I,1)	SAE air attenuation table for a 59° standard day.
ABSORP(I,2)	Shields and Bass atmospheric attenuation table for a 59° standard day.
IFREQ	The one-third octave frequency bands in interger format. These are only used for printing.
FREQ	The one-third octave frequency bands used in the calculations.

```
900**RUN **;15475ES/NRBTASK5/FEIHEC(BCD,NOGO)
910C
200040C SUBROUTINE DERIVED FROM PROGRAM FEIHE
200050C ORIGINAL PROGRAM CAME FROM RAMANI MANI,
200060C RESEARCH LABS, SCHENECTADY
200070C
200080        SUBROUTINE FEIHE
200090C
200100        COMMON /BLKFEI/ IREFRC,ITURBC,NO,PI
200120        COMMON /COMFEI/ DIAMJT,EM,FP,LIE,NP,SPLI(10),SPLF(10),
200130       & THETD(10)
200140C
200150        DIMENSION A(10,10),AVERR(5),B(10),CORR(10),ERROR(10),
200160       & F(10,10),FI(10),FF(10,10),G(10),GF(10),GP(10),
200170       & IJVAL(10),IND(10),INDEX(10),SPL(10),SPLFTM(10,5),SPLP(10),
200180       & THET(10),W(10),X(10),Y(10),YY(10),Z(10)
200190C
200200        DATA CEM /1.0/
200210C
200220 IF (NP .GE. 6) GO TO 120
200230 WRITE (02,116)
200240 116 FORMAT (/35H PROGRAM REQUIRES AT LEAST 6 POINTS)
200250 GO TO 5000
200260  120 NSST=3-LIE
200262C
200264C CALCULATION OF REFRACTION CORRECTION
200270 DO 1737 MCASE=NSST,5
200280 MAX=MCASE+1
200290 TOPI2=(2./PI)**2
200300 EMM=CEM*EM
200310 THETO=ATAN(SQRT(2.*EMM+EMM**2))
200320 THETOD=THETO*180./PI
200330 DO 157 I=1,NP
200340 TH=THETD(I)*PI/180.
200350 CTH=COS(TH)
200360 QQ=(1.-EMM*CTH)**2
200370 STH=SIN(TH)
200380 CTH2=CTH*CTH
200390 XP=FP*STH
200400 YP=FP*SQRT(ABS(CTH2-(1.-EMM*CTH)**2))
200410 SCHUB=.26*EMM*(30.7*FP-4.35)
200420 SCHUB1=41.67*EMM
200430 IF(SCHUB.GT.SCHUB1)SCHUB=SCHUB1
200432        CORR(I)=0
200434        IF (IREFRC.EQ.NO) GO TO 562
200440 IF (FP.GT.3.) GO TO 462
200450 CALL BESLJY(XP,FJOX,FJ1X,FYOX,FY1X)
200460 IF (THETD(I).GT.THETOD) GO TO 150
200470 CALL BESLI(YP,FIOY,FI1Y)
200480 RBOTO=YP*FI1Y*FJOX+XP*FIOY*QQ*FJ1X
200490 AIBOTO=YP*FI1Y*FYOX+XP*FIOY*QQ*FY1X
200500 GO TO 153
200510 150 CALL BESLJ(YP,FJOY,FJ1Y)
200520 RBOTO =YP*FJ1Y*FJOX-XP*FJOY*QQ*FJ1X
200530 AIBOTO=YP*FJ1Y*FYOX-XP*FJOY*QQ*FY1X
200540 153 CRR=TOPI2/(RBOTO**2+AIBOTO**2)
200550 CORR(I)=-4.34295*ALOG(CRR)
```

H

Section H

Lines 200220 through 200250 is text to determine if the inlet and exhaust arc data to be transformed have at least six points, if not the computation will be terminated.

Lines 200260 through 200660 contain the routine to calculate the refraction correction as a function of angle and frequency to be applied to the input sound pressure levels. LIE is set equal to 2 for the forward quadrant computation and equal to 1 for the aft quadrant computation. MAX is the level of singularity at which the fitting of input data is initiated. Specifically MAX equal to 1, 2 or 3 corresponds to monopole, dipole or quadrupole source types, respectively. The equations used to calculate the refraction correction are summarized on pages 267 and 268 of Reference 6.

HONEYWELL PAGE PRINTING SYSTEM- P1188-02

```
200560 GO TO 157
200570 462 IF (LIE EQ 2) GO TO 467
200580 IF(ABS(THETD(I)-20.) LT.1.) CORR(I)=SCHUB
200590 IF(ABS(THETD(I)-30 ) LT 1 ) CORR(I)=SCHUB 2
200600 IF(ABS(THETD(I)-40 ) LT 1 ) CORR(I)=SCHUB 4
200610 IF(ABS(THETD(I)-50 ) LT 1 ) CORR(I)=SCHUB 6
200620 IF(ABS(THETD(I)-60.) LT 1 ) CORR(I)=SCHUB/8
200630 IF((THETD(I)-60 ) GT 5 ) CORR(I)=0 0
200640 GO TO 562
200650 467 CORR(I)=4 34295*ALOG(QQ)
200660  562 CONTINUE
```

Lines 20[illegible] through [illegible] data [illegible] [illegible] the refraction correction, CORR(I), which is a function of frequency, angle, and free jet Mach Number.

```
200662C
200664C CALCULATION OF TURBULENCE ABSORPTION CORRECTION
200666        IF (ITURBC EQ.NO) GO TO 157
200672        TAC90=2 0*(EMM .25)**2*FP/72
200682  564 IF (TAC90 GT 3 ) TAC90=3.
200690 IF (LIE EQ.2) GO TO 578
200700 TAC=TAC90+2 *(1 5-THETD(I)/60 )
200712        IF (TAC GT 3 ) TAC=3
200720 CORR(I)=CORR(I)+TAC
200730 GO TO 157
200740 578 TAC=TAC90*(2.8-THETD(I)/50 )
200750 IF (TAC LT 0 ) TAC=0.
200760 CORR(I)=CORR(I)+TAC
```

Section I

Lines 200664 through 2[illegible] calculate the turbulence absorption correction. This correction is a function of frequency and angle. In line 200720 and 200760 this correction is added to the refraction correction.

```
200770 157 CONTINUE
200780 DO 170 I=1,NP
200790 THET(I)=THETD(I)*PI/180.
200800 SPL(I)=SPL1(I)+CORR(I)
200810 170 CONTINUE
```

Section J

In lines 200780 through 200810, the input sound pressure levels, SPL1(I) are corrected for turbulence absorption and refraction. The output of this section is SPL(I).

```
200820 SPMIN=SPL(1)
200830 DO 188 I=1,NP
200840 IF (SPL(I) LT.SPMIN) SPMIN=SPL(I)
200850 188 CONTINUE
200860 DO 220 I=1,NP
200870 XX=.1*(SPL(I)-SPMIN)
200880 G(I)=10 **XX
200890 220 CONTINUE
```

Section K

This section, lines 200820 through 200890, determines the minimum sound pressure level in a given set; determines the delta's relative to this value for the remaining levels and then linearizes these levels.

```
200900 APB=2*(MAX-1)+1
200910 IEX=4*(MAX-1)
200920 C=GAMF(APB)*2.**IEX
200930 DO 248 I=1,MAX
200940 AA=2*(MAX-I)+1
200950 BB=2*(I-1)+1
200960 TA=4*(MAX-I)+1
200970 TB=4*(I-1)+1
200980 TERM=GAMF(TA)*GAMF(TB)/(C*GAMF(AA)*GAMF(BB))
200990 YY(I)=SQRT(TERM)
201000 248 CONTINUE
```

Section L

This section, lines 200900 through 201000 calculates the normalization constants, N_S using the expression

$$N_S^2 = 2/\pi \int_0^{\pi/2} \cos^{2i} \theta \sin^{2h} \theta \, d\theta.$$

are the exponent of the singularity type being considered. This i and h integral was evaluated using Equation 858.534 from Reference 15.

```
201010 DO 400 I=1,NP
201020 TH=THET(I)
201030 Q=ABS(THETD(I)-90.)
201040 IF (Q .GT. 1.) GO TO 580
201050 F(MAX,I)=1./YY(MAX)
201060 MAX1=MAX-1
201070 DO 570 J=1,MAX1
201080 F(J,I)=0.
201090 570 CONTINUE
201100 GO TO 400
201110 580 CTH2=COS(TH)**2
201120 STH2=SIN(TH)**2
201130 DO 620 J=1,MAX
201140 F(J,I)=CTH2**(MAX-J)*STH2**(J-1)/YY(J)
201150 620 CONTINUE
201160 400 CONTINUE
```

Section M

This section, lines 201010 through 201160, calculates the normalized F array which is a function of singularity type. For example, this array for the quadrupole fitting level may be written as follows

$\mathrm{Cos}^4 160/N_1$	$\mathrm{Cos}^2 160\ \mathrm{Sin}^2 160/N_2$	$\mathrm{Sin}^4 160/N_3$
$\mathrm{Cos}^4 150/N_1$	$\mathrm{Cos}^2 150\ \mathrm{Sin}^2 150/N_2$	$\mathrm{Sin}^4 150/N_3$
$\mathrm{Cos}^4 140/N_1$	$\mathrm{Cos}^2 140\ \mathrm{Sin}^2 140/N_2$	$\mathrm{Sin}^4 140/N_3$
$\mathrm{Cos}^4 130/N_1$	$\mathrm{Cos}^2 130\ \mathrm{Sin}^2 130/N_2$	$\mathrm{Sin}^4 130/N_3$
$\mathrm{Cos}^4 120/N_1$	$\mathrm{Cos}^2 120\ \mathrm{Sin}^2 120/N_2$	$\mathrm{Sin}^4 120/N_3$
$\mathrm{Cos}^4 110/N_1$	$\mathrm{Cos}^2 110\ \mathrm{Sin}^2 110/N_2$	$\mathrm{Sin}^4 110/N_3$
$\mathrm{Cos}^4 100/N_1$	$\mathrm{Cos}^2 100\ \mathrm{Sin}^2 100/N_2$	$\mathrm{Sin}^4 100/N_3$
$\mathrm{Cos}^4 90/N_1$	$\mathrm{Cos}^2 90\ \mathrm{Sin}^2 90/N_2$	$\mathrm{Sin}^4 90/N_3$

Similar generalized expressions may be written for the forward quadrant and also for the various singularities considered.

```
201170 DO 1030 I=1,MAX
201180 IJVAL(I)=I
201190 1030 CONTINUE
201200 DO 1160 I=1,NP
201210 B(I)=G(I)
201220 1160 CONTINUE
201230 DO 1250 I=1,NP
201240 DO 1240 J=1,MAX
201250 A(I,J)=F(J,I)
201260 1240 CONTINUE
201270 1250 CONTINUE
201280 CALL NNLS(A,10,NP,MAX,B,X,RNORM,W,Z,INDEX,MODE)
201290 DO 2140 J=1,MAX
201300 Y(J)=X(J)/YY(J)
201310 2140 CONTINUE
201320 DO 2400 I=1,MAX1
201330 DO 2390 J=1,I
201340 JJ1=MAX+J-I
201350 FF(I,J)=1.E+06
201360 DO 2310 JJ=J,JJ1
201370 T1=MAX+1-I
201380 T2=JJ-J+1
201390 T3=T1-T2+1.
201400 TERM=Y(JJ)*GAMF(T2)*GAMF(T3)/GAMF(T1)
201410 IF (TERM .LT. FF(I,J)) FF(I,J)=TERM
201420 IF (ABS(FF(I,J)) .LE. 1.0E-06) FF(I,J)=0.
201430 2310 CONTINUE
201440 DO 2380 JJ=J,JJ1
201450 T1=MAX+1-I
201460 T2=JJ-J+1
201470 T3=T1-T2+1.
201480 TERM=GAMF(T1)/(GAMF(T2)*GAMF(T3))
201490 Y(JJ)=Y(JJ)-FF(I,J)*TERM
201500 2380 CONTINUE
201510 2390 CONTINUE
201520 2400 CONTINUE
201530 DO 2430 J=1,MAX
201540 FF(MAX,J)=Y(J)
201550 2430 CONTINUE
201560 DO 2680 I=1,NP
201570 GF(I)=0.
201580 GP(I)=0.
201590 CTH2=COS(THET(I))**2
201600 STH2=SIN(THET(I))**2
201610 CAF=1./(1.+EM*COS(THET(I)))**2
201620 DO 2670 J=1,MAX
201630 JJ=IJVAL(J)
201640 GP(I)=GP(I)+X(JJ)*F(JJ,I)
201650 CAFJ=CAF**J
201660 IF (ABS(THETD(I)-90.) .GT. 1.) GO TO 2658
201670 GF(I)=GF(I)+FF(J,J)
201680 GO TO 2670
201690 2658 SUM=0.
201700 DO 2665 JJ=1,J
201710 SUM=SUM+CAFJ*FF(J,JJ)*CTH2**(J-JJ)*STH2**(JJ-1)
201720 2665 CONTINUE
201730 GF(I)=GF(I)+SUM
201740 2670 CONTINUE
201750 2680 CONTINUE
```

N

Section N

This section, lines 201170 through 201270, sets the F array required for the least squares fitting routine. Also the B array is defined as the linearized values, G(I) relative to the minimum SPL level. The G array would be written as follows:

G(160)
G(150)
G(140)
G(130)
G(120)
G(110)
G(100)
G(90)

O

Section O

This section calls line 201280 the "NNLS" subroutine for calculating coefficients of the singularity level being considered. In general this subroutine solves the problem of finding a nonnegative vector $\bar{X}$, given matrix $\bar{A}$ and vector b such that the error $|| \bar{A}\bar{X} - \bar{b} ||$ is minimized in the least squares sense.

P

Section P

This section, lines 201290 through 201520, is the recombination procedure and test to determine the least singular distribution. The generalized recombination procedure is described in Reference 6 and an example is also presented.

Q

Section Q

This section of the program, lines 201530 through 201750, calculates the linearized static and flight mean square pressure levels. GF(I) is the linearized levels inflight. GP(I) are the predicted linearized levels.

```
201760 DO 2730 I=1,NP
201770 IF (GP(I) .LE. 0.) GP(I)=1.0E-20
201780 IF (GF(I) .LE. 0.) GF(I)=1.0E-20
201790 SPLP(I)=SPMIN+4.34295*ALOG(GP(I))
201800 SPLP(I)=SPLP(I)-CORR(I)
201812        SPLFTM(I,MCASE)=SPL(I)+4.34295*ALOG(GF(I)/GP(I))
201820 IF (LIE.EQ.1.AND.I.EQ.NP)GO TO 2730
201830 ERROR(I)=ABS(SPLP(I)-SPL1(I))
201840 2730 CONTINUE
201850 IF (LIE.EQ.1) NP1=NP-1
201860 IF (LIE.EQ.2) NP1=NP
201870 FNP1=NP1
201880 ESUM=0.0
201890 EMAX=ERROR(1)
201900 DO 1906 I=1,NP1
201910 ESUM=ESUM+ERROR(I)
201920 IF (ERROR(I).GT.EMAX) EMAX=ERROR(I)
201930 1906 CONTINUE
201941        AVERR(MCASE)=ESUM/FNP1
201952        TERR=AVERR(MCASE)+EMAX
201962        IF (AVERR(MCASE).LT.1.9) GO TO 1739
201970 1737 CONTINUE
201981 1739 AVMIN=1000.0
201982        DO 1800 M=NSST,MAX-1
201983        IF (AVERR(M).GE.AVMIN) GO TO 1800
201984        MMIN=M
201985        AVMIN=AVERR(M)
201986        IF (M.GE.MAX+1) GO TO 1800
201987        IF (AVERR(M).LT.AVERR(M+1)) GO TO 1810
201988 1800 CONTINUE
201989 1810 DO 1820 I=1,NP
201990        SPLF(I)=SPLFTM(I,MMIN)
201992 1820 CONTINUE
201994 5000 RETURN
202000 END
210000C
210010C
210020 FUNCTION GAMF(X)
210030 N=X-.9
210040 IF (N.EQ.0) N=1
210050 ANS=1.
210060 DO 60 I=1,N
210070 FI=I
210080 ANS=ANS*FI
210090 60 CONTINUE
210100 GAMF=ANS
210110 RETURN
210120 END
```

R

Section R

This section of the program, lines 201760 through 201994, converts the [illegible] to [illegible] sound pressure level. Also the flight sound pressure levels are calculated. The predicted and measured sound pressure levels are compared to [illegible] error in decibels. The average error is calculated by summing up the individual errors and dividing by the total number of points. This error is then tested to determine if it is less than 1.9 dB. If the error is greater than 1.9 dB the calculation is repeated for the next singularity level. If the error diverges from the previous value, the singularity distribution which has the minimum error will be used to calculate the dynamic effect.

S

Section S

This section, lines 210030 through 210100, evaluates the Gamma function in integer form only and uses the relationship $\Gamma(n) = (n-1)!$. This relationship is established in Reference 15.

HONEYWELL PAGE PRINTING SYSTEM- P1188-02

```
220000C
220010C
220020 *      SUBROUTINE NNLS  (A,MDA,M,N,B,X,RNORM,W,ZZ,INDEX,MODE)
220030 *       C.L.LAWSON AND R.J.HANSON, JET PROPULSION LABORATORY, 1973 JUNE 15
220040 *       TO APPEAR IN 'SOLVING LEAST SQUARES PROBLEMS', PRENTICE-HALL, 1974
220050 *
220060 *           **********   NONNEGATIVE LEAST SQUARES   **********
220070 *
220080 *      GIVEN AN M BY N MATRIX, A, AND AN M-VECTOR, B,  COMPUTE AN
220090 *      N-VECTOR, X, WHICH SOLVES THE LEAST SQUARES PROBLEM
220100 *
220110 *                       A * X = B  SUBJECT TO X .GE. 0
220120 *
220130 *      A(),MDA,M,N      MDA IS THE FIRST DIMENSIONING PARAMETER FOR THE
220140 *                       ARRAY, A().   ON ENTRY A() CONTAINS THE M BY N
220150 *                       MATRIX, A.           ON EXIT A() CONTAINS
220160 *                       THE PRODUCT MATRIX, Q*A , WHERE Q IS AN
220170 *                       M BY M ORTHOGONAL MATRIX GENERATED IMPLICITLY BY
220180 *                       THIS SUBROUTINE.
220190 *      B()     ON ENTRY B() CONTAINS THE M-VECTOR, B.   ON EXIT B() CON-
220200 *              TAINS Q*B.
220210 *      X()     ON ENTRY X() NEED NOT BE INITIALIZED.  ON EXIT X() WILL
220220 *             CONTAIN THE SOLUTION VECTOR.
220230 *      RNORM   ON EXIT RNORM CONTAINS THE EUCLIDEAN NORM OF THE
220240 *              RESIDUAL VECTOR.
220250 *      W()     AN N-ARRAY OF WORKING SPACE.  ON EXIT W() WILL CONTAIN
220260 *              THE DUAL SOLUTION VECTOR.   W WILL SATISFY W(I) = 0.
220270 *              FOR ALL I IN SET P  AND W(I) .LE. 0. FOR ALL I IN SET Z
220280 *      ZZ()     AN M-ARRAY OF WORKING SPACE.
220290 *      INDEX()       AN INTEGER WORKING ARRAY OF LENGTH AT LEAST N.
220300 *                    ON EXIT THE CONTENTS OF THIS ARRAY DEFINE THE SETS
220310 *                    P AND Z AS FOLLOWS..
220320 *
220330 *                    INDEX(1)    THRU INDEX(NSETP) = SET P.
220340 *                    INDEX(IZ1) THRU INDEX(IZ2)    = SET Z.
220350 *                    IZ1 = NSETP + 1 = NPP1
220360 *                    IZ2 = N
220370 *      MODE    THIS IS A SUCCESS-FAILURE FLAG WITH THE FOLLOWING
220380 *              MEANINGS.
220390 *              1      THE SOLUTION HAS BEEN COMPUTED SUCCESSFULLY.
220400 *              2      THE DIMENSIONS OF THE PROBLEM ARE BAD.
220410 *                     EITHER M .LE. 0 OR N .LE. 0.
220420 *             3    ITERATION COUNT EXCEEDED.  MORE THAN 3*N ITERATIONS.
220430 *
220440        SUBROUTINE NNLS (A,MDA,M,N,B,X,RNORM,W,ZZ,INDEX,MODE)
220450        DIMENSION A(MDA,N), B(M), X(N), W(N), ZZ(M)
220460        INTEGER INDEX(N)
220470        ZERO=0.
220480        ONE=1.
220490        TWO=2.
220500        FACTOR=0.01
220510 *
220520        MODE=1
220530        IF (M.GT.0.AND.N.GT.0) GO TO 10
220540        MODE=2
220550        RETURN
220560     10 ITER=0
```

Section T

Lines 220020 through 252070 contains the subroutine from Reference 16 which determines the coefficients of the singularities which are used to predict the relative normalized mean square pressures in a given one-third octave band. In general, the program solves the problem of finding a non-negative vector $\bar{X}$, given matrix A and vector $\bar{b}$ such that the error $\| A \bar{X} - \bar{b} \|$ is minimized in the least squares sense.

```
      ITMAX=3*N
*
*                  INITIALIZE THE ARRAYS INDEX() AND X().
*
         DO 20 I=1,N
         X(I)=ZERO
   20    INDEX(I)=I
*
      IZ2=N
      IZ1=1
      NSETP=0
      NPP1=1
*                            ******  MAIN LOOP BEGINS HERE  ******
   30 CONTINUE
*                  QUIT IF ALL COEFFICIENTS ARE ALREADY IN THE SOLUTION.
*                       OR IF M COLS OF A HAVE BEEN TRIANGULARIZED.
*
      IF (IZ1.GT.IZ2.OR.NSETP.GE.M) GO TO 350
*
*        COMPUTE COMPONENTS OF THE DUAL (NEGATIVE GRADIENT) VECTOR W().
*
         DO 50 IZ=IZ1,IZ2
         J=INDEX(IZ)
         SM=ZERO
            DO 40 L=NPP1,M
   40       SM=SM+A(L,J)*B(L)
   50    W(J)=SM
*                                  FIND LARGEST POSITIVE W(J).
   60 WMAX=ZERO
         DO 70 IZ=IZ1,IZ2
         J=INDEX(IZ)
         IF (W(J).LE.WMAX) GO TO 70
         WMAX=W(J)
         IZMAX=IZ
   70    CONTINUE
*             IF WMAX .LE. 0. GO TO TERMINATION.
*             THIS INDICATES SATISFACTION OF THE KUHN-TUCKER CONDITIONS.
      IF (WMAX) 350,350,80
   80 IZ=IZMAX
      J=INDEX(IZ)
*     THE SIGN OF W(J) IS OK FOR J TO BE MOVED TO SET P.
*     BEGIN THE TRANSFORMATION AND CHECK NEW DIAGONAL ELEMENT TO AVOID
*    NEAR LINEAR DEPENDENCE.
      ASAVE=A(NPP1,J)
      CALL H12 (1,NPP1,NPP1+1,M,A(1,J),1,UP,DUMMY,1,1,0)
      UNORM=ZERO
      IF (NSETP.EQ.0) GO TO 100
         DO 90 L=1,NSETP
   90    UNORM=UNORM+A(L,J)**2
  100 UNORM=SQRT(UNORM)
      IF (DIFF(UNORM+ABS(A(NPP1,J))*FACTOR,UNORM)) 130,130,110
*     COL J IS SUFFICIENTLY INDEPENDENT.  COPY B INTO ZZ, UPDATE ZZ AND
*   > SOLVE FOR ZTEST ( = PROPOSED NEW VALUE FOR X(J) ).
  110    DO 120 L=1,M
  120    ZZ(L)=B(L)
      CALL H12 (2,NPP1,NPP1+1,M,A(1,J),1,UP,ZZ,1,1,1)
      ZTEST=ZZ(NPP1)/A(NPP1,J)
```

```
*                                       SEE IF ZTEST IS POSITIVE
*     REJECT J AS A CANDIDATE TO BE MOVED FROM SET Z TO SET P.
*      RESTORE A(NPP1,J), SET W(J)=0., AND LOOP BACK TO TEST DUAL
       IF (ZTEST) 130,130,140
*      COEFFS AGAIN.
   130 A(NPP1,J)=ASAVE
       W(J)=ZERO
       GO TO 60
*      THE INDEX  J=INDEX(IZ)  HAS BEEN SELECTED TO BE MOVED FROM
*      SET Z TO SET P.    UPDATE B,  UPDATE INDICES,  APPLY HOUSEHOLDER
*      TRANSFORMATIONS TO COLS IN NEW SET Z,  ZERO SUBDIAGONAL ELTS IN
*      COL J,  SET W(J)=0.
   140     DO 150 L=1,M
   150     B(L)=ZZ(L)
       INDEX(IZ)=INDEX(IZ1)
       INDEX(IZ1)=J
       IZ1=IZ1+1
       NSETP=NPP1
       NPP1=NPP1+1
       IF (IZ1.GT.IZ2) GO TO 170
           DO 160 JZ=IZ1,IZ2
           JJ=INDEX(JZ)
   160     CALL H12 (2,NSETP,NPP1,M,A(1,J),1,UP,A(1,JJ),1,MDA,1)
   170 CONTINUE
       IF (NSETP.EQ.M) GO TO 190
           DO 180 L=NPP1,M
   180       A(L,J)=ZERO
   190 CONTINUE
       W(J)=ZERO
*                                  SOLVE THE TRIANGULAR SYSTEM.
*                                  STORE THE SOLUTION TEMPORARILY IN ZZ().
       ASSIGN 200 TO NEXT
       GO TO 400
   200 CONTINUE
*                        ******  SECONDARY LOOP BEGINS HERE ******
*                           ITERATION COUNTER.
   210 ITER=ITER+1
       IF (ITER.LE.ITMAX) GO TO 220
       MODE=3
       PRINT 440
       GO TO 350
   220 CONTINUE
*                     SEE IF ALL NEW CONSTRAINED COEFFS ARE FEASIBLE.
*                                    IF NOT COMPUTE ALPHA.
       ALPHA=TWO
           DO 240 IP=1,NSETP
           L=INDEX(IP)
           IF (ZZ(IP)) 230,230,240
   230     T=-X(L)/(ZZ(IP)-X(L))
           IF (ALPHA.LE.T) GO TO 240
           ALPHA=T
           JJ=IP
   240     CONTINUE
*           IF ALL NEW CONSTRAINED COEFFS ARE FEASIBLE THEN ALPHA WILL
*           STILL = 2.    IF SO EXIT FROM SECONDARY LOOP TO MAIN LOOP.
       IF (ALPHA.EQ.TWO) GO TO 330
*           OTHERWISE USE ALPHA WHICH WILL BE BETWEEN 0. AND 1. TO
```

```
*        INTERPOLATE BETWEEN THE OLD X AND THE NEW ZZ.
             DO 250 IP=1,NSETP
             L=INDEX(IP)
  250        X(L)=X(L)+ALPHA*(ZZ(IP)-X(L))
*        MODIFY A AND B AND THE INDEX ARRAYS TO MOVE COEFFICIENT I
*          FROM SET P TO SET Z
        I=INDEX(JJ)
  260   X(I)=ZERO
        IF (JJ.EQ.NSETP) GO TO 290
        JJ=JJ+1
            DO 280 J=JJ,NSETP
            II=INDEX(J)
            INDEX(J-1)=II
            CALL G1 (A(J-1,II),A(J,II),CC,SS,A(J-1,II))
            A(J,II)=ZERO
                DO 270 L=1,N
                IF (L.NE.II) CALL G2 (CC,SS,A(J-1,L),A(J,L))
  270           CONTINUE
  280       CALL G2 (CC,SS,B(J-1),B(J))
  290   NPP1=NSETP
        NSETP=NSETP-1
        IZ1=IZ1-1
        INDEX(IZ1)=I
*          SEE IF THE REMAINING COEFFS IN SET P ARE FEASIBLE.  THEY SHOULD
*          BE BECAUSE OF THE WAY ALPHA WAS DETERMINED.
*          IF ANY ARE INFEASIBLE IT IS DUE TO ROUND-OFF ERROR.  ANY
*          THAT ARE NONPOSITIVE WILL BE SET TO ZERO
*          AND MOVED FROM SET P TO SET Z
            DO 300 JJ=1,NSETP
            I=INDEX(JJ)
            IF (X(I)) 260,260,300
  300       CONTINUE
*           COPY B( ) INTO ZZ( ).  THEN SOLVE AGAIN AND LOOP BACK.
            DO 310 I=1,M
  310       ZZ(I)=B(I)
        ASSIGN 320 TO NEXT
        GO TO 400
  320   CONTINUE
        GO TO 210
*                      ******  END OF SECONDARY LOOP  ******
*
  330       DO 340 IP=1,NSETP
            I=INDEX(IP)
  340       X(I)=ZZ(IP)
*          ALL NEW COEFFS ARE POSITIVE.  LOOP BACK TO BEGINNING.
        GO TO 30
*                        ******  END OF MAIN LOOP  ******
*                        COME TO HERE FOR TERMINATION.
*                    COMPUTE THE NORM OF THE FINAL RESIDUAL VECTOR
  350   SM=ZERO
        IF (NPP1.GT.M) GO TO 370
            DO 360 I=NPP1,M
  360       SM=SM+B(I)**2
        GO TO 390
  370       DO 380 J=1,N
  380       W(J)=ZERO
  390   RNORM=SQRT(SM)
```

```
             RETURN
      *      THE FOLLOWING BLOCK OF CODE IS USED AS AN INTERNAL SUBROUTINE
      *      TO SOLVE THE TRIANGULAR SYSTEM, PUTTING THE SOLUTION IN ZZ().
        400      DO 430 L=1,NSETP
                 IP=NSETP+1-L
                 IF (L.EQ.1) GO TO 420
                     DO 410 II=1,IP
        410          ZZ(II)=ZZ(II)-A(II,JJ)*ZZ(IP+1)
        420      JJ=INDEX(IP)
        430      ZZ(IP)=ZZ(IP)/A(IP,JJ)
             GO TO NEXT, (200,320)
        440 FORMAT (35H0 NNLS QUITTING ON ITERATION COUNT.)
        999 RETURN;END
      C
      C
      *      SUBROUTINE H12 (MODE,LPIVOT,L1,M,U,IUE,UP,C,ICE,ICV,NCV)
      *      C.L.LAWSON AND R.J.HANSON, JET PROPULSION LABORATORY, 1973 JUN 12
      *      TO APPEAR IN 'SOLVING LEAST SQUARES PROBLEMS', PRENTICE-HALL, 1974
      *      CONSTRUCTION AND/OR APPLICATION OF A SINGLE
      *      HOUSEHOLDER TRANSFORMATION..      Q = I + U*(U**T)/B
      *      MODE    = 1 OR 2   TO SELECT ALGORITHM  H1  OR  H2 .
      *      LPIVOT IS THE INDEX OF THE PIVOT ELEMENT.
      *      L1,M   IF L1 .LE. M   THE TRANSFORMATION WILL BE CONSTRUCTED TO
      *             ZERO ELEMENTS INDEXED FROM L1 THROUGH M.   IF L1 GT. M
      *             THE SUBROUTINE DOES AN IDENTITY TRANSFORMATION.
      *      U(),IUE,UP    ON ENTRY TO H1 U() CONTAINS THE PIVOT VECTOR.
      *                    IUE IS THE STORAGE INCREMENT BETWEEN ELEMENTS.
      *                                ON EXIT FROM H1 U() AND UP
      *                    CONTAIN QUANTITIES DEFINING THE VECTOR U OF THE
      *                    HOUSEHOLDER TRANSFORMATION.   ON ENTRY TO H2 U()
      *                    AND UP SHOULD CONTAIN QUANTITIES PREVIOUSLY COMPUTED
      *                    BY H1   THESE WILL NOT BE MODIFIED BY H2.
      *      C()    ON ENTRY TO H1 OR H2 C() CONTAINS A MATRIX WHICH WILL BE
      *             REGARDED AS A SET OF VECTORS TO WHICH THE HOUSEHOLDER
      *             TRANSFORMATION IS TO BE APPLIED.  ON EXIT C() CONTAINS THE
      *             SET OF TRANSFORMED VECTORS.
      *     ICE    STORAGE INCREMENT BETWEEN ELEMENTS OF VECTORS IN C().
      *      ICV    STORAGE INCREMENT BETWEEN VECTORS IN C().
      *      NCV    NUMBER OF VECTORS IN C() TO BE TRANSFORMED. IF NCV .LE. 0
      *             NO OPERATIONS WILL BE DONE ON C().
             SUBROUTINE H12 (MODE,LPIVOT,L1,M,U,IUE,UP,C,ICE,ICV,NCV)
             DIMENSION U(IUE,M), C(1)
             DOUBLE PRECISION SM,B
             ONE=1
             IF (0.GE.LPIVOT.OR.LPIVOT.GE.L1.OR.L1.GT.M) RETURN
             CL=ABS(U(1,LPIVOT))
             IF (MODE.EQ.2) GO TO 60
      *                           ****** CONSTRUCT THE TRANSFORMATION. ******
                 DO 10 J=L1,M
         10      CL=AMAX1(ABS(U(1,J)),CL)
             IF (CL) 130,130,20
         20 CLINV=ONE/CL
             SM=(DBLE(U(1,LPIVOT))*CLINV)**2
                 DO 30 J=L1,M
         30      SM=SM+(DBLE(U(1,J))*CLINV)**2
      *                              CONVERT DBLE. PREC. SM TO SNGL. PREC. SM1
             SM1=SM
```

```
      CL=CL*SQRT(SM1)
      IF (U(1,LPIVOT)) 50,50,40
   40 CL=-CL
   50 UP=U(1,LPIVOT)-CL
      U(1,LPIVOT)=CL
      GO TO 70
*            ****** APPLY THE TRANSFORMATION  I+U*(U**T)/B  TO C. ******
   60 IF (CL) 130,130,70
   70 IF (NCV.LE.0) RETURN
      B=DBLE(UP)*U(1,LPIVOT)
*                       B  MUST BE NONPOSITIVE HERE.  IF B = 0., RETURN.
      IF (B) 80,130,130
   80 B=ONE/B
      I2=1-ICV+ICE*(LPIVOT-1)
      INCR=ICE*(L1-LPIVOT)
          DO 120 J=1,NCV
          I2=I2+ICV
          I3=I2+INCR
          I4=I3
          SM=C(I2)*DBLE(UP)
              DO 90 I=L1,M
              SM=SM+C(I3)*DBLE(U(1,I))
   90         I3=I3+ICE
          IF (SM) 100,120,100
  100     SM=SM*B
          C(I2)=C(I2)+SM*DBLE(UP)
              DO 110 I=L1,M
              C(I4)=C(I4)+SM*DBLE(U(1,I))
  110         I4=I4+ICE
  120     CONTINUE
  130 RETURN
      END
C
C
      SUBROUTINE G1 (A,B,COS,SIN,SIG)
*     C.L.LAWSON AND R.J.HANSON, JET PROPULSION LABORATORY, 1973 JUN 12
*     TO APPEAR IN 'SOLVING LEAST SQUARES PROBLEMS', PRENTICE-HALL, 1974
*     COMPUTE ORTHOGONAL ROTATION MATRIX.
*     COMPUTE.. MATRIX   (C, S) SO THAT (C, S)(A) = (SQRT(A**2+B**2))
*                        (-S,C)         (-S,C)(B)   (   0           )
*     COMPUTE SIG = SQRT(A**2+B**2)
*        SIG IS COMPUTED LAST TO ALLOW FOR THE POSSIBILITY THAT
*        SIG MAY BE IN THE SAME LOCATION AS A OR B .
      ZERO=0
      ONE=1.
      IF (ABS(A).LE.ABS(B)) GO TO 10
      XR=B/A
      YR=SQRT(ONE+XR**2)
      COS=SIGN(ONE/YR,A)
      SIN=COS*XR
      SIG=ABS(A)*YR
      RETURN
   10 IF (B) 20,30,20
   20 XR=A/B
      YR=SQRT(ONE+XR**2)
      SIN=SIGN(ONE/YR,B)
      COS=SIN*XR
```

```
240250       SIG=ABS(B)*YR
240260       RETURN
240270    30 SIG=ZERO
240280       COS=ZERO
240290       SIN=ONE
240300       RETURN
240310       END
251000C
251010C
251020       SUBROUTINE G2    (COS,SIN,X,Y)
251030 *     C.L.LAWSON AND R.J.HANSON, JET PROPULSION LABORATORY, 1972 DEC 15
251040 *     TO APPEAR IN 'SOLVING LEAST SQUARES PROBLEMS', PRENTICE-HALL, 1974
251050 *          APPLY THE ROTATION COMPUTED BY G1 TO (X,Y).
251060       XR=COS*X+SIN*Y
251070       Y=-SIN*X+COS*Y
251080       X=XR
251090       RETURN
251100       END
252000C
252010C
252020       FUNCTION DIFF(X,Y)
252030 *    C.L.LAWSON AND R.J.HANSON, JET PROPULSION LABORATORY, 1973 JUNE 7
252040 *     TO APPEAR IN 'SOLVING LEAST SQUARES PROBLEMS', PRENTICE-HALL, 1974
252050       DIFF=X-Y
252060       RETURN
252070       END
260000C
260010C
260020 SUBROUTINE BESLI (X,BI0,BI1)
260030 T=X/3.75
260040 IF (X .GT. 3.75) GO TO 200
260050 T2=T**2
260060 A2=3.5156229
260070 A4=3.0899424
260080 A6=1.2067492
260090 A8=.2659732
260100 A10=.0360768
260110 A12=.0045813
260120 ABI=(((((A12*T2+A10)*T2+A8)*T2+A6)*T2+A4)*T2+A2)*T2+1.
260130 BI0=ABI
260140 B2=.87890594
260150 B4=.51498869
260160 B6=.15084934
260170 B8=.02658733
260180 B10=.00301532
260190 B12=.00032411
260200 BBI=(((((B12*T2+B10)*T2+B8)*T2+B6)*T2+B4)*T2+B2)*T2+.5
260210 BI1=BBI*X
260220 GO TO 830
260230 200 TN=1./T
260240 C0=.39894228
260250 C1=.01328592
260260 C2=.00225319
260270 C3=-.00157565
260280 C4=.00916281
260290 C5=-.02057706
260300 C6=.02635537
```

Section U

Lines 260020 through 260510 is a subroutine used to evaluate the modified Bessel functions, $I_0(X)$ and $I_1(X)$, of the first kind and argument X.

HONEYWELL PAGE PRINTING SYSTEM- P1186-02

```
260310 C7=-.01647633
260320 C8=.00392377
260330 CBI=((((((((C8*TN+C7)*TN+C6)*TN+C5)*TN+C4)*TN+C3)*TN+C2)*TN+C1
260340 &)*TN+C0
260350 BI0=CBI/SQRT(X)
260360 BI0=BI0*EXP(X)
260370 D0=.39894228
260380 D1=-.03988024
260390 D2=-.00362018
260400 D3=.00163801
260410 D4=-.01031555
260420 D5=.02282967
260430 D6=-.02895312
260440 D7=.01787654
260450 D8=-.00420059
260460 DBI=((((((((D8*TN+D7)*TN+D6)*TN+D5)*TN+D4)*TN+D3)*TN+D2)*TN+D1)*
260470 & TN+D0
260480 BI1=DBI/SQRT(X)
260490 BI1=BI1*EXP(X)
260500 830 RETURN
260510 END
270000C
270010C
270020 SUBROUTINE BESLJY (X,BJ0,BJ1,BY0,BY1)
270030 PI=3.1415926
270040 IF (X .GT. 3.) GO TO 395
270050 X32=(X/3.)**2
270060 A2=-2.2499997
270070 A4=1.2656208
270080 A6=-.3163866
270090 A8=.0444479
270100 A10=-.0039444
270110 A12=.00021
270120 BJ0=(((((A12*X32+A10)*X32+A8)*X32+A6)*X32+A4)*X32+A2)*X32+1.
270130 Y=(2./PI)*ALOG(X/2.)*BJ0
270140 Y0=.36746691
270150 Y2=.60559366
270160 Y4=-.74350384
270170 Y6=.25300117
270180 Y8=-.04261214
270190 Y10=.00427916
270200 Y12=-.00024846
270210 BY0=(((((Y12*X32+Y10)*X32+Y8)*X32+Y6)*X32+Y4)*X32+Y2)*X32+Y0+Y
270220 H0=.5
270230 H2=-.56249985
270240 H4=.21093573
270250 H6=-.03954289
270260 H8=.00443319
270270 H10=-.00031761
270280 H12=.1109E-04
270290 H1X=(((((H12*X32+H10)*X32+H8)*X32+H6)*X32+H4)*X32+H2)*X32+H0
270300 BJ1=H1X*X
270310 D=(2./PI)*X*ALOG(X/2.)*BJ1
270320 D0=-.6366198
270330 D2=.2212091
270340 D4=2.1682709
270350 D6=-1.3164827
```

U

V

Section V

Lines 270020 through 280590 contain two subroutines used to evaluate the Bessel functions of the first and second kind, $J_0(X)$, $J_1(X)$, $Y_0(X)$ and $Y_1(X)$ of argument X. The results of Items U and V are used to aid in the calculation of the refraction corrections described in *Item H.*

```
      D8=.3123951
      D10=-.0400976
      D12=.0027873
      Y1X=(((((D12*X32+D10)*X32+D8)*X32+D6)*X32+D4)*X32+D2)*X32+D0+D
      BY1=Y1X/X
      GO TO 760
  395 X3=3./X
      C0=.79788456
      C1=-.77E-06
      C2=-.0055274
      C3=-.00009512
      C4=.00137237
      C5=-.00072805
      C6=.00014476
      F0=(((((C6*X3+C5)*X3+C4)*X3+C3)*X3+C2)*X3+C1)*X3+C0
      T0=-.78539816
      T1=-.04166397
      T2=-.3954E-04
      T3=.00262573
      T4=-.00054125
      T5=-.00029333
      T6=.00013558
      THETA0=((((((T6*X3+T5)*X3+T4)*X3+T3)*X3+T2)*X3+T1)*X3+T0+X
      BJ0=(1./SQRT(X))*F0*COS(THETA0)
      BY0=(1./SQRT(X))*F0*SIN(THETA0)
      E0=.79788456
      E1=.156E-05
      E2=.01659667
      E3=.00017105
      E4=-.00249511
      E5=.00113653
      E6=-.0002033
      F1=((((((E6*X3+E5)*X3+E4)*X3+E3)*X3+E2)*X3+E1)*X3+E0
      G0=-2.35619449
      G1=.12499612
      G2=.565E-04
      G3=-.00637879
      G4=.00074348
      G5=.00079824
      G6=-.00029166
      THETA1=((((((G6*X3+G5)*X3+G4)*X3+G3)*X3+G2)*X3+G1)*X3+G0+X
      BJ1=(1./SQRT(X))*F1*COS(THETA1)
      BY1=(1./SQRT(X))*F1*SIN(THETA1)
  760 RETURN
      END
C
C
      SUBROUTINE BESLJ (X,BJ0,BJ1)
      PI=3.1415926
      IF (X .GT. 3.) GO TO 395
      X32=(X/3.)**2
      A2=-2.2499997
      A4=1.2656208
      A6=-.3163866
      A8=.0444479
      A10=-.0039444
      A12=.00021
```

```
      BJ0=(((((A12*X32+A10)*X32+A8)*X32+A6)*X32+A4)*X32+A2)*X32+1.
      H0=.5
      H2=-.56249985
      H4=.21093573
      H6=-.03954289
      H8=.00443319
      H10=-.00031761
      H12=.1109E-04
      H1X=(((((H12*X32+H10)*X32+H8)*X32+H6)*X32+H4)*X32+H2)*X32+H0
      BJ1=H1X*X
      GO TO 760
  395 X3=3./X
      C0=.79788456
      C1=-.77E-06
      C2=-.0055274
      C3=-.00009512
      C4=.00137237
      C5=-.00072805
      C6=.00014476
      F0=(((((C6*X3+C5)*X3+C4)*X3+C3)*X3+C2)*X3+C1)*X3+C0
      T0=-.78539816
      T1=-.04166397
      T2=-.3954E-04
      T3=.00262573
      T4=-.00054125
      T5=-.00029333
      T6=.00013553
      THETA0=(((((T6*X3+T5)*X3+T4)*X3+T3)*X3+T2)*X3+T1)*X3+T0+X
      BJ0=(1./SQRT(X))*F0*COS(THETA0)
      E0=.79788456
      E1=.156E-05
      E2=.01659667
      E3=.00017105
      E4=-.00249511
      E5=.00113653
      E6=-.0002033
      F1=(((((E6*X3+E5)*X3+E4)*X3+E3)*X3+E2)*X3+E1)*X3+E0
      G0=-2.35619449
      G1=.12499612
      G2=.565E-04
      G3=-.00637879
      G4=.00074348
      G5=.00079824
      G6=-.00029166
      THETA1=(((((G6*X3+G5)*X3+G4)*X3+G3)*X3+G2)*X3+G1)*X3+G0+X
      BJ1=(1./SQRT(X))*F1*COS(THETA1)
  760 RETURN
      END
```

V

GLOSSARY OF TERMS

II, IA, IR	-	Indices used to denote a specific angle in a given array.
ANGOT	-	Angle array for the flight transformed data.
NCBDI	-	Input file code number.
INPUT	-	Namelist name for the input parameters.
END	-	Used to signal that all namelist input parameters have been read.
ERR	-	Used to signal an error was encountered while reading the input data.
TESTD	-	Input parameter.
NANGOT	-	The number of angles in the ANGOT array.
NANG	-	Input parameter.
ANGLE	-	Input parameter.
DIST	-	TESTD divided by 1000 and is used for calculating the atmospheric absorption correction.
IABS	-	Air attenuation indicator which either chooses the SAE model or the Shields and Bass Model.
IALPHA	-	Input parameter.
ISB	-	Constant used to identify the Shields and Bass air attenuation model.
NBCDO	-	Output file code number.
SPIDIN	-	Input parameter.
SPIN	-	Input parameter.
J,JJ,JJ1,	-	Are indices used to denote a specific frequency in a given array.
NFREQ	-	Input parameter.
IFREQ	-	Integer list of one-third octave band center frequencies.
TSPL	-	Input parameter.

SCFREQ	- Scale model frequency to the nearest one-third octave band.
FREQ	- Array of one-third octave band center frequencies.
SCFACT	- Input parameter.
CNFREQ	- Frequency variable used to calculate the frequency shift corresponding to a scale factor which would result in a integer number of third octave band shifts.
DEL1, DEL2	- Are used to determine which one-third octave band center frequency is closer.
SCALE	- New scale factor which would allow an integer number of third octave band shifts.
EM	- Free jet Mach number.
FLTVEL	- Input parameter.
SPDSND	- Speed of sound, 1116 ft/sec, assuming a 59° Standard Day.
CONST	- Intermediate variable name.
PI	- 3.141659
DIAMJT	- Input parameter.
FPAR	- Frequency parameter array.
IKNT	- Index used to adjust the input data arrays to allow insertion of a missing angle.
SPLDS	- Output data array of the FLIGHT transformation program. This is the answer.
THETD	- Angle array used for calculations in the transformation process. These angles are measured from the exhaust.
NP	- Number of angles in the THETD array.
NA	- An index which identifies the 90° angle in the ANGOT array.
LIE	- Index to identify either the forward quadrant, LIE = 2, or the aft quadrant LIE = 1.
FP	- The frequency parameter πf/SPDSND DIAMJT.
ADDER	- Air attenuation in decibels applied to a given frequency.

ABSORP	-	Air attenuation array. This array defines the amount of air attenuation which should be applied to a given one-third octave band.
SPL1	-	Input SPL array to the flight transformation after being corrected for air attenuation.
FEIHE	-	Name of the main subroutine for the flight transformation. The subroutine corrects the input data for refraction turbulence absorption and dynamic effect.
K	-	An index which defines a specific angle in the SPLF array.
SPLFLT	-	Is the flight transformed array before doppler shift.
IDOPS	-	Input parameter.
DOPFAC	-	Doppler factor used to determine the number of frequency bands the SPLFLT array has to be shifted.
COS	-	Library subroutine to calculate the cosine of an angle.
RPD	-	Constant used to convert angles from degrees to radians.
DOPCON	-	An array to which the doppler factor, DOPFAC, is compared to determine the number of frequency shifts.
IFLAG	-	The number of frequency bands that specific parts of the SPLFLT array are shifted by.
IDSHFT	-	The table used to determine IFLAG.
FLOAT	-	Instrinic function to change from integer to real numbers.
SPIDOT	-	Input parameter.
SPOT	-	Input parameter.
IREFRC	-	Input parameter.
ITURBC	-	Input parameter.
NSFT,MCASE	-	Are indices which define the level of singularity.
TOPI2	-	Constant, TOPI2 $(2/\pi)^2$.
THETO	-	The critical angle θ_c.
THETOD	-	The critical angle in degrees.

TH	-	Is a specific angle of the input angle array in radians.
XP	-	FP sin θ
XP	-	FP $(\lvert \text{Cos}^2\theta - (1\text{-M Cos } \theta)^2 \rvert)^{1/2}$
SCHUB	-	Refraction correction in dB in the aft quadrant if FP>3 (before the shape factor is applied).
SCHUB1	-	Is the maximum refraction correction for FP>3 before the shape factor is applied. Note: that if SCHUB is greater than SCHUB1 then SCHUB1 is used.
BESLJ, BESLYJ, BELI,	-	Subroutines for the evaluation of Bessel functions.
RBOTO	-	Real part of the denominator term in the solution of the sound pressure for the plug flow model.
AIBOTO	-	Imaginary part of the denominator term in the solution of the sound pressure for the plug flow model.
CORR(I)	-	Is used to denote either the refraction correction or the refraction correction plus the turbulence absorption correction in decibels.
TAC 90	-	Turbulence absorption correction at 90°.
TAC	-	Turbulence absorption correction at the other acoustic angles.
SPL(I)	-	Input sound pressure levels corrected for refraction and turbulence absorption.
SPMIN	-	The minimum sound pressure level at a given frequency and in a given quadrant.
G(I)	-	The linearized delta mean square pressure levels.
F(J,I)	-	The array established as a function of singularity type.
XX	-	Intermediate variable used in the calculation of the mean square pressure.
APB, IEX, C, AA, BB, TA, TB, TERM	-	Intermediate variables used in the calculation of the normalization constants.
YY(I)	-	Normalization constants N_S

B(I)	-	Input array for the NNLS subroutine.
A(I,J)	-	Input array for the NNLS subroutine.
X(J)	-	The output from the NNSL routine.
NNLS	-	Subroutine for calculating coefficients of the singularities, refer to reference 16 for details.
Y(J)	-	The coefficients of the singularities from the NNLS routine divided by the appropriate normalization constants
T1, T2, T3	-	Are intermediate variables used in the recombination procedure.
Y(JJ)	-	Are the coefficients of the singularities after the recombination procedure.
CAF	-	The square of the doppler factor, $(1/(1+M \cos \theta_E)^2$
GP(I)	-	Predicted relative mean square pressure levels.
CAFJ,SUM	-	Intermediate variables used for correcting the measured relative mean square pressures for dynamic effects
GF(I)	-	Relative mean square pressure levels corrected for dynamic effects.
SPLP	-	Predicted sound pressure levels.
SPLF, SPLFTM	-	Are the input sound pressure levels corrected for refraction turbulence absorption and dynamic effects.
ERROR(I)	-	Difference between the predicted and measured sound pressure level at a specific angle and frequency.
AVERR	-	Average error for a specific one-third octave band directivity pattern.
GAMF(x)	-	Gamma Function.

LIST OF SYMBOLS

Symbol	
A	- Nozzle Exhaust Area, ft^2.
AR	- Suppressor Area Ratio, Determined by the Total Nozzle Area, Excluding any Plug, to the flow area of the nozzle.
C_{fg}, C_{f_g}	- Thrust Coefficient.
D, d	- Diameter, Ft.
EPNL	- Effective Perceived Noise Level, EPNdB.
F_s	- Ideal Gross Thrust, lbs_f,
M	- Jet Mach Number or Freestream (External) Mach Number.
OASPL	- Overall Sound Pressure Level dB.
P	- Pressure, lbs_f/in^2,
PNL	- Perceived Noise Level, PNdB.
R_r	- Radius Ratio Determined by the Ratio of the Inner Radius to the Outer Radius for the Particular Flow Passage.
r/r_o	- Normalized Radial Position When Referring to Tertiary Plume Surveys.
SPL	- One-Third Octave Sound Pressure Level, dB.
T	- Temperature, ° R.
U_{max}	- Velocity at Tertiary Nozzle Exit Plane, ft/sec.
$\overline{U}$	- Mean Velocity When Referring to Tertiary Flow Plume ft/sec
U'	- Turbulent Velocity when referring to Tertiary Flow Plume, ft/sec.
V	- Jet Velocity, ft/sec.
W	- Weight Flow Rate, lbs_m/sec.
X	- Axial Distance, ft.

LIST OF SYMBOLS (Concluded)

Symbol

β - Shock Cell Noise Parameter - $\sqrt{M^2 1}$.

θ_i - Acoustic Angle Relative to Inlet Axis, degrees.

ω - Jet Density Exponent.

Subscript

1 - Tertiary Exit Flow Plane.

2 - Tertiary Flow Plane at Nozzle Exit Plane.

FS - Tertiary Flow (Freestream) Conditions or Full Scale Conditions

i - Inner Stream or Bypass Flow (Usually Cold).

m,ma,mix - Mass Averaged Conditions.

o - Outer Stream, Tertiary or Ambient Conditions.

s - Static Conditions.

T - Total or Tertiary Flow Conditions.

Superscript

o - Outer Stream

i - Inner or Bypass Stream (Usually Cold).

AD-A094 297 GENERAL ELECTRIC CO CINCINNATI OH AIRCRAFT ENGINE GROUP F/G 20/1
HIGH VELOCITY JET NOISE SOURCE LOCATION AND REDUCTION. TASK 5. --ETC(U)
JAN 79 N BAUMGARDT, J F BRAUSCH, W S CLAPPER DOT-OS-30034
UNCLASSIFIED R78AE6628 FAA-RD-76-79-5 NL

3 OF 3
AD
A094297

END
DATE
FILMED
3-81
DTIC

REFERENCES

1. Stringas, E.J. and Kazin, S.B., "Supersonic Transport Noise Reduction Technology Program - Phase II," General Electric Company, FAA-SS-73-29-1, September 1975.

2. Atvars, J., et al., "SST Technology Follow-On Program - Phase II," Boeing Company, FAA-SS-73-11, March 1975.

3. Clapper, W.S., et al., "High Velocity Jet Noise Source Location and Reduction: Task 3 - Experimental Investigation of Suppression Principles; Volume III - Suppressor Concepts Optimization," General Electric Company, FAA-RD-76-79, III - III, to be Published.

4. ANON, "Evaluation of Jet Noise Suppression Potential," ICAO Committee on Airport Noise (CAN), French Working Paper Prepared for Working Group E, April 1977.

5. Brausch, J.F., "Flight Velocity Influence on Jet Noise of Conical Ejector, Annular Plug and Segmented Suppressor Nozzles," NASA CR-120961, August 1972.

6. Clapper, W.S., et al., "High Velocity Jet Noise Source Location and Reduction: Task 4 - Development/Evaluation of Techniques for In-flight Investigation," General Electric Company, FAA-RD-76-79, IV, February 22, 1977.

7. Williams, J., "Aeroacoustic Requirements for Model Noise Experiments in Subsonic Wind Tunnels," Appendix 4, AGARD Advisory Report No. 105, August 1977.

8. Plumblee, Harry E., et al., "Effects of Forward Velocity on Turbulent Jet Mixing Noise," Lockheed-Georgia Company, NASA CR-2702, July 1976.

9. Knott, P.R., "Free Jet Acoustic Investigation of High-Radius-Ratio Coannular Plug Nozzles," NASA Contract NAS3-20619, to be Published.

10. Clapper, W.S., et al., "High Velocity Jet Noise Source Location and Reduction: Task 3 - Experimental Investigation of Suppression Principles; Volume II - Parametric Testing and Source Measurements," General Electric Company, FAA-RD-76-79, III - II, to be Published.

11. Task 1 Supplement - Certification of the General Electric Jet Noise Anechoic Test Facility, Report No. FAA-RD-76-79, February 1977.

12. Knott, P.R. and Mossey, P., "Parametric Laser Velocimeter Studies of High-Velocity, High-Temperature, Turbulent Jets," "Chapter III of Vol. II AFAPL-TR-76-68 Supersonic Jet Exhaust Noise Investigation," Knott, P.R., Editor (July 1976).

13. ANON, "Standard Values of Atmospheric Absorption as a Function of Temperature and Humidity," Society of Automotive Engineers, ARP-866A, March 1975.

14. Knott, P.R., Blozy, J.T. and Staid, P.S.; "Acoustic and Performance Investigation of Coannular Plug Nozzles," NASA-Lewis Research Center/ General Electric Company; NASA Contract NAS3-19777, to be Published.

15. Dwight, "Tables of Integrals and Other Mathematical Data" Fourth Edition, MacMillan, 1963.

16. Hanson, R.J. and Lawson, C.L., "Solving Least Squares Problems," Prentice-Hall, 1974.

17. Stringas, E.J., "High Velocity Jet Noise Source Location and Reduction: Task 6 - Noise Abatement Nozzle Design Guide," General Electric Company, FAA-RD-76-79, VI, to be Published.

18. ANON, "Design Integration and Noise Study for a Large STOL Augmentor Wing Transport - Task I," Prepared Under Contract NAS2-6344, The Boeing Company, Report No. D6-60139.

19. Shields, F.D. and Bass, H.E., "Atmospheric Absorption of High Frequency Noise and Application to Fractional - Octave Bands," University of Mississippi, NASA CR-2760, June 1977.

20. Hay, J.A., "Lateral Noise Propagation," British Aircraft Corporation Limited," Acoustics Report 526, April 21, 1977.